The timescales of andesite generation at Mount Ruapehu, New Zealand

Thesis

The Timescales of Andesite Generation at Mount Ruapehu, New Zealand

A thesis presented for the degree of Doctor of Philosophy

by

Robert David Hughes

BSc (Hons.) Leicester, 1995

Department of Earth Sciences
The Open University
Milton Keynes, U.K.

March 1999

For any one who has ever had the pleasure of MK...,

It had meant that Crowley had been allowed to develop Manchester, while Aziraphale had a free hand in the whole of Shropshire. Crowley took Glasgow, Aziraphale had Edinburgh (neither claimed any responsibility for Milton Keynes[1], although both reported it as a success)

[1]Note for Americans and other aliens: Milton Keynes is a new city approximately halfway between London and Birmingham. It was built to be modern, efficient, healthy, and, all in all, a pleasant place to live. Many Britons find this amusing.

from Good Omens, Terry Pratchett & Neil Gaiman.

Abstract

Intermediate composition arc volcanoes present some of the most serious natural hazards because of their tendency towards violent, explosive eruptions. Very little is known about the long term processes which produce such magmas and the timescales over which they operate. U-series systematics have considerable potential for helping to understand these timescales, although very few studies to date have examined individual volcanoes in detail. A detailed series of ^{230}Th-^{238}U and ^{226}Ra-^{230}Th analyses are presented in conjunction with major and trace elements and Sr, Nd and Pb isotopes for lavas sampled from coherent stratigraphic sequences on Mount Ruapehu. This andesitic volcano lies at the southern end of the Taupo Volcanic Zone (TVZ) in the centre of North Island, New Zealand. Volcanic activity at Ruapehu is related to the subduction of the Pacific Plate beneath the Indian Plate along the Hikurangi Trough.

Major element trends are dominated by shallow level crystallisation and assimilation processes. Modelling of crystallisation trends suggests that the magmas were hydrous and may have elevated fO_2. Trace element patterns show high LILE/HFSE ratios characteristic of arc lavas. AFC models of isotope data suggest that 50% crystallisation and 10-15% assimilation can explain the observed trends. The assimilant is likely to have been dominated by partial melts of local Torlesse basement. Major element extrapolations suggest that the mantle wedge beneath the TVZ was relatively fertile. Modelling of the trace element budgets in relatively primitive lavas suggests that a three component model is required for magma generation. Partial melts of sediments were added to the mantle wedge at a relatively shallow level, and the modified mantle was then fluxed by fluids derived from subducted oceanic crust at greater depth. 10-90% of many LILE and other elements are derived from fluids and sediments rather than the wedge.

U-Th analyses show 1-14% U excess and ($^{230}Th/^{232}Th$) ratios in the range 0.75-0.85. Data for the coherent stratigraphic sequences fall on linear trends on an equiline diagram. Crystallisation and alteration are ruled out as causes of the observed U/Th variation and although the lavas have been affected by assimilation, links between U/Th and indices of assimilation are difficult to demonstrate. Crustal melts with similar U/Th ratios to the parental basalts and relatively low U and Th abundances are the most likely candidate for the assimilant. It is argued that the U-Th systematics reflect addition of hydrous fluids to the mantle wedge. Whole rock pseudo-isochron ages are derived for the different stratigraphic sequences, and compared with data on eruption ages to estimate combined transit and residence times (CTRTs). Rocks from older sequences dated at ~80 ka and ~130 ka have very short CTRTs « 40 ka, whereas younger sequences have longer CTRTs on the order of 40-80 ka. It is inferred that the magmas of the younger sequences spent a longer period of time ponded at the base of the crust and underwent limited chemical modification.

A detailed model of the behaviour of U-Th-Ra systematics during crustal magmatic processes is also presented. This allows crystallisation, assimilation and replenishment processes to be combined with a time factor to predict magma evolution curves. Whilst detailed systematic studies of individual volcanic centres are required to test the model, the lack of age constraints and complex sub-volcanic history of Ruapehu magmas do not permit the detailed application of this model here.

Acknowledgements

During the course of three (and a bit...) years, many people have had a hand in shaping the near endless saga which has become this thesis, and of course in the fashioning of my approach to geochemistry. At the top of the list of course are my supervisors, Chris for ideas, encouragement and rapid reading of drafts, and Nick for an endless torrent of slander and abuse guaranteed to liven the dullest occasion. Thanks also to my examiners for reading the mighty tome at the end of it all...

A huge thanks to all those who gave me the opportunity to work in New Zealand and great hospitality while I was there; Ian Smith and Richard Price for organising everything and letting me have access to samples and data, John, Eloise and JR for companionship in the field, and John Gamble for generously furnishing me with samples and data.

In the lab, which has become my life and home over the last few years (at times it has felt to literally be my home, usually sometime between 3 a.m. and 5 a.m.), thanks must go to the Clog for maintaining the machines despite our best efforts to break them, for innumerable discussions on techniques and guidance in just how the 'Lada' 262 actually worked. Immense gratitude as well to Mabs for guidance, jokes, chocolate and forbearance in the face of yet more melted teflon; to Jessica (before the desertion..:)) for guidance and cookie competitions; to Dave Peate for help with chemistry and numerous U-series discussions; to Dave Wright who changed the programs all the time to keep us on our toes.

Thanks must be given to the downstairs crew; John Holbrook for fixing the money, John Watson for XRF advice and analyses, Kay for the odd section or two, Brian for supreme cutting ability, Mike for the barbeques...

On the marginally more social side, one must of course thank the stalwart members of the august company of Friday drinkers, Simon T for being the first in most weeks, Rhino for advice on the best beer, Antipodean Bruce for taking over the running of the bar and providing a superb selection of beverages to ensure that almost no writing was ever achieved on a Friday night. Thinking back to all those early mornings, it would be impossible not to mention Glyn for putting the coffee on and for being a loud-mouthed, brash Yankee with an amazing ability to insult even more people than myself, and Helen for being small, Scottish and generally completely barking. A mention as well for my associates in Maths; Louise, who should also be mentioned in conjunction with the lab (but sadly space is limited), for being far too nice a person (we'll teach you eventually to be nasty to people...), Georg for being German and Christophe for not being there most of the time.

Finally, there are others who must be mentioned who either don't fit in to the above categories, or fit into to many to mention in one case. Principally my fellow member of the Early Morning Club, general companion in mass spectrometry and geochemistry, co-founder of the OUMAS and alter-ego, thanks must go to Pete for sharing endless foul thoughts and insults, coffee, an office, and rarely some geochemical discussion.

Apologies to all of those who I have managed to forget from the acknowledgements, and to all those who I have managed to insult or offend in the time I have been at the OU. OK – I'll just apologise to the whole department to make it easier.

And almost finally, thanks to my parents for making sure I was still in the land of the sane from time to time – not all that often though it has to be said. And definitely finally, I must thank Sam for looking after me all the time, letting me escape Milton Keynes from time to time, a holiday to Greece, and of course for many, many others things.

Contents

List of Figures

List of Tables

Firstly and most importantly,

Quid quid latin dictum sit altum viditur

unattributed.

Chapter 1

Introduction

1.1 Magmatism in Arc Environments

Destructive plate margins have long held a fascination for geologists because of the abundant seismic and volcanic events which occur in these regions. That such areas were of great geological importance was clear long before plate tectonic concepts were put forward by workers such as Vine and Wilson (Vine and Matthews, 1963; Vine, 1966; Wilson, 1965; Wilson, 1966).

The advent of plate tectonic theory presented a framework by which it was possible to understand the geological processes which were responsible for the generation of modern arc volcanics. Such processes have been the focus of considerable interdisciplinary research over the past three decades. This has led to huge leaps in our understanding of the igneous, sedimentary and metamorphic processes leading to arc volcanism.

The importance of understanding subduction zone processes cannot be overstated. At the present day, for much of the Phanerozoic and quite possibly during the Proterozoic and Archaean, subduction zones have been a major mechanism for chemical replenishment of the Earth's mantle and possibly crustal growth. There has been considerable debate over the importance of arc magmatism as a major mechanism of crustal growth (e.g. summaries and discussions of Rudnick, 1995; Taylor and McLennan, 1995), and it may be that Phanerozoic arc magmatism has had little effect other than effectively diluting the 'continental' signature (Foden, 1997). Such an argument cannot be resolved until mass fluxes within subduction zones are understood better. Destructive plate margins also

represent the most geologically hazardous regions on Earth, hosting frequent major earthquakes and volcanic eruptions. As the areas inhabited by humans progressively expand, it becomes increasingly important to understand both the short and long term processes which are responsible for controlling volcanicity and seismicity in such active tectonic environments.

This thesis looks in detail at the timescales of petrogenetic processes in recent New Zealand arc volcanics using ^{238}U-^{230}Th-^{226}Ra systematics. The principle aims of the work are to address some of the contentious areas in our understanding of subduction zone processes using a wide range of geochemical data and ideas from other fields. In addition this study will look at the timescales of eruption and duration of volcanism at a persistently active continental arc volcano.

1.1.1 Mechanisms of Magma Generation in Arcs

Since the recognition that plate tectonic processes were responsible for the generation of subduction-related arc basalts, numerous ideas and theories have been put forward to explain the voluminous magmatism seen at destructive plate margins. Early work concentrated on looking at whether the more evolved andesitic compositions which dominate in continental arc settings, represented a primary magma type. It was suggested on the basis of experimental studies that it was possible to generate andesites by melting subducting oceanic crust (e.g. Green and Ringwood, 1968). This idea was supported by early thermal models which suggested that it was relatively easy to melt the subducting slab (e.g. McKenzie, 1969; Oxburgh and Turcotte, 1970). With further investigation of magmatism in arc settings, it has become accepted that in most locations the primary magmas feeding arc volcanisms are basaltic rather than andesitic (e.g. Arculus and Johnson, 1978; McBirney, 1978; Arculus, 1981; Gill, 1981).

Increasingly, it has become widely accepted that many arc basalts result from partial melting of the mantle wedge, particularly those with high magnesium contents (e.g. Perfit et al., 1980; Arculus and Johnson, 1981). There has been more debate, however, over the origin of abundant high alumina basalts (HAB). Some authors suggested that these

magmas were derived as a result of crystallisation and crystal accumulation processes affecting high magnesium basalts (Perfit et al., 1980; Crawford et al., 1987). Other studies have suggested that HAB compositions can be explained by slab melting (e.g. Brophy and Marsh, 1986).

One of the most significant steps forward in understanding petrogenetic and tectonic processes occurring in subduction zones has been the idea of induced convection. It is thought that the drag resulting from a cold, dense lithospheric slab sinking into the mantle can induce convection in the overlying asthenospheric mantle, pulling material downwards parallel with the subducting slab (e.g. McKenzie, 1969; Andrews and Sleep, 1974; Toksöz and Hsui, 1978; Hsui and Toksöz, 1981). A consequence of material in the asthenospheric wedge being pulled down with the slab, is that fresh mantle material has to be drawn into the wedge to compensate for the loss of mass.

The role of water in generating subduction related magmas was considered during the early development of the field (e.g. Kushiro and Yoder, 1969; Nicholls, 1974). One of the important physical effects of subducting a cold lithospheric plate into the mantle is to reduce the temperature of the mantle wedge, which makes generating mantle melts in subduction zones more difficult than at mid-ocean ridges. In order to explain melting in such environments, and the frequent presence of hydrous phases in arc lavas, many authors began to stress the importance of water in promoting melting of the mantle wedge overlying the subducting slab (Boettcher, 1977; Pearce, 1982; Tatsumi et al., 1986). It was initially proposed that amphibole was the primary agent of water transport in the subducting slab, and that pressure controlled breakdown of these phases was responsible for the apparent consistent distance of arc volcanoes above the descending plate (Tatsumi, 1989). More recently it has become clear that whilst amphibole is important, there are many other hydrous phases, such as lawsonite, phengite and clinozoisite, which are stable to considerable depth (Poli and Schmidt, 1995; Liu et al., 1996; Schmidt and Poli, 1998). These may not only be important for promoting behind-arc volcanism, but may also contribute to mass transfer at much greater depths in the mantle.

The mechanism by which fluid infiltration of the mantle wedge promotes melting has been the subject of considerable debate. Dehydration of the subducting slab and incorporation of the resulting hydrous fluids into the mantle are likely to amphibolitise the wedge (e.g. Tatsumi et al., 1986; Davies and Stevenson, 1992). The temperature of the mantle wedge near to the subducting slab tends to be rather low because of the presence of the cold oceanic crust, and therefore the mantle remains below the amphibole saturated solidus. One model suggests a process can then occur, whereby induced convection drags the amphibolitised material downwards, parallel to the slab, and dehydration reactions allow fluids to subsequently percolate back upwards. This process allows the zone of amphibitolisation to traverse the wedge, and thereby reaching the warmer central areas and crossing the amphibole saturated solidus (Tatsumi, 1989; Davies and Stevenson, 1992). It has also been suggested that melting can occur primarily in response to adiabatic decompression (Plank and Langmuir, 1988). In this model, the role of fluid infiltration and amphibitolisation of the wedge is to promote instability, upwelling and diapirism. More recent models suggest that a component of both may occur (e.g. Pearce and Parkinson, 1993). A further recent development has been the suggestion that hydraulic fracturing is important in moving hydrous fluids through the mantle (Davies and Rowland, 1997). This idea is supported by certain seismic evidence (Davies and Rowland, 1997), and it helps to overcome apparent difficulties with porous flow of water in an olivine rich medium (Watson and Brenan, 1987).

With the development of detailed thermal models of subduction zones it has been convincingly demonstrated that in most arcs, the subducting oceanic crust cannot melt (Peacock, 1990; Peacock, 1991; Davies and Stevenson, 1992; Peacock, 1993). The exceptions to this are where hot, young oceanic crust is subducted, which tends to lead to the formation of unusual high-Mg andesites which have been termed adakites (Kay, 1978; Defant and Drummond, 1990).

1.1.2 Mass Fluxes in Subduction Zones

With the development of analytical techniques which allow for easy determination of trace element abundances for large numbers of samples, it has become possible to

quantify the trace element systematics of arc lavas. It is well established that arc lavas show characteristic enrichments of large cations of low charge (the large ion lithophile elements or LILE), and other elements such as U, Th and light rare earth elements (LREE) relative to MORB (Jakeš and Gill, 1970; Jakeš and White, 1972; Saunders and Tarney, 1979; Pearce, 1982). In contrast, arc lavas often show depletions in cations of high charge (high field strength elements or HFSE), such as Nb, Ta, Hf and Zr relative to the LILE, and in some cases relative to MORB (e.g. Pearce, 1982).

Given that hydrous fluids appeared to play an important role in arc magma genesis, it was a logical step to suggest that these fluids could also be the agents of mass transfer between the subducting slab and the mantle wedge (e.g. Best, 1975; Hawkesworth et al., 1979; Saunders and Tarney, 1979; Pearce, 1982). It has long been suggested in addition, however, that on the basis of isotopic evidence, it is necessary to invoke the involvement of subducted sediments in subduction zone magma genesis (e.g. Armstrong, 1968; Armstrong, 1971; Kay et al., 1978; Kay, 1980; Sun, 1980; Hole et al., 1984). With the development of analytical techniques to measure ^{10}Be, the role of subducted sediment has become undeniable (Brown et al., 1982; Tera et al., 1986). This is a cosmogenic isotope which forms by spallation of oxygen and nitrogen in the atmosphere and only exists in surficial sediments on the subducting slab. The short half-life of ^{10}Be (~1.5 Ma) means that its presence in young arc lavas, but not those of other tectonic settings, requires some kind of recent sedimentary input into the mantle wedge (Tera et al., 1986).

The mechanism of sediment addition is also an issue which is as yet not fully resolved. Initial ideas were centred around the sediment component being tectonically incorporated fragments (e.g. Armstrong, 1971). Experiments on the partitioning behaviour of various elements into hydrous fluids have shown that some elements which are often enriched in arc magmas, such as Th, are essentially immobile which rules out hydrous fluids as the main method of adding a sediment component (e.g. Keppler and Wyllie, 1990; Brenan et al., 1995; Keppler, 1996). Recently, as the first experimental studies into sediment melting have been undertaken, it has become clear that it may be possible to melt sediments within the thermal regime of most subduction zones (Plank and Langmuir, 1992;

Nichols et al., 1994; Nichols et al., 1996; Plank and Johnson, 1997). Several studies which have examined U-series systematics in arc lavas have also required that partial melts are the main agents of mass transfer from subducted sediments to the mantle wedge (e.g. Elliott et al., 1997; Turner et al., 1997a).

1.1.3 Timescales of Magmatic Processes in Subduction Zones

There are two ways in which it is possible to examine in detail the timescales of magmatic processes in subduction zones, namely U-series systematics and ^{10}Be. As has already been mentioned in Section 1.1.2, ^{10}Be has a half-life of ~1.5 Ma and is uniquely generated on the surface of the Earth. The abundance of ^{10}Be in subducted sediments will be sufficiently low after ~5-6 half-lives (7-9 Ma) to be undetectable (Morris et al., 1990). From the presence of ^{10}Be in young arc lavas, it can be inferred that the processes of sediment subduction, incorporation into the wedge, melt generation and melt transport combined take less than 9 Ma.

The theory of U-Th-Ra isotope systematics is discussed at more length in Chapter 2, and the application of U-series data in subduction zones is summarised in Chapter 5. A brief overview is given here in order to show the importance of studying and understanding U-series data.

As with ^{10}Be there has also been extensive interest in the use of U-series systematics to constrain magmatic timescales. Unlike ^{10}Be, U-series techniques look primarily at the time since the last chemical fractionation of various isotopes from one another. Although there are a number of isotopes from the ^{235}U, ^{238}U and ^{232}Th decay chains which can be used, the main systems presently used in looking at arc volcanics are ^{230}Th-^{238}U and ^{226}Ra-^{230}Th. As with ^{10}Be, the timescales over which these isotopes are useful is determined by their half-lives, which means that ^{230}Th-^{238}U is effective over ~300-350 ka, and ^{226}Ra-^{230}Th can be used on a timescale of ~8 ka (e.g. Condomines et al., 1988).

The principal interest in U-Th systematics in arcs has been the discovery that some arcs show very large U excesses over Th. This has been interpreted as reflecting the

fluxing of the mantle wedge by hydrous slab-derived fluids (Gill and Williams, 1990; McDermott and Hawkesworth, 1991; Condomines and Sigmarsson, 1993; Hawkesworth et al., 1997b; Hawkesworth et al., 1997a). The fact that disequilibria are still present implies that the time since the last fractionation of U from Th is less than 300 ka. Several studies have shown that in many cases the time since this fractionation event and eruption is of the order of 20-50 ka (Sigmarsson et al., 1990; Elliott et al., 1997; Turner et al., 1997a). The presence of excess of Ra over Th in some arc rocks makes interpretation of the timescales more difficult as very little is known about the behaviour of Ra. If Ra excesses also reflect a fractionation process induced by fluid fluxing of the mantle wedge, then this implies a very short time (< 8 ka) between the last fractionation event and eruption (e.g. Condomines et al., 1988; Chabaux and Allègre, 1994; Chabaux et al., 1999). Other studies have suggested that Ra-Th and U-Th systematics are decoupled and that Ra excesses reflect melting rather than slab-derived fluids (e.g. Elliott et al., 1997; Turner et al., 1997a).

The interpretation of U-series systematics can be further complicated by crustal level magmatic processes. Several models have looked at possible effects of such processes on U-Th-Ra systematics (Condomines et al., 1982; Pyle, 1992), and the issue will be considered at length in Chapter 2. In general, such issues are likely to be of more concern in continental arc lavas rather than in intra-oceanic arc settings, although the identification of evidence for long magma chamber residence times in the Lesser Antilles suggests that understanding these processes is important for all environments (Heath et al., 1998b).

Recently, there have been advances in the application of U-series data to looking at crustal residence and transit times. As mentioned above, long magma chamber residence times, on the order of 50 ka, have been obtained from mineral isochrons in the Lesser Antilles (Heath et al., 1998b). Similarly, long transport and residence times have been inferred from Kamchatka (Turner et al., 1998) and Santorini (Zellmer, 1998). In contrast, however, zero age lava-cumulate isochrons from Raoul imply short magma chamber residence times in the Kermadec arc (Turner et al., 1997a).

Finally, it has recently been demonstrated that it is possible to place estimates on the timing of sediment infiltration of the mantle wedge by identifying particular sediment signatures in erupted lavas (Turner and Hawkesworth, 1997; Turner et al., 1997a). In this instance, it appears that it takes on the order of 4 Ma for distinctive signatures from the Louisville Ridge to appear in erupted lavas.

1.2 New Zealand

The geological background of New Zealand is described in detail in Chapter 3, but it is briefly reviewed here in order to examine the main reasons for studying the U-series systematics of volcanic rocks from North Island.

New Zealand lies at the boundary between the Pacific and Indian Plates. Throughout most of South Island this boundary is manifest as the Alpine transform fault system. In North Island however this boundary turns into a convergent margin and the Pacific plate subducts beneath eastern New Zealand. New Zealand itself is a fragment of continental crust, although to the north and south, the plate boundary becomes wholly intra-oceanic (see Figure 1.1).

In the centre of North Island, the Taupo Volcanic Zone (TVZ) has been the main centre of subduction related volcanism over the last 2 Ma. In broad terms it is continuous with the intra-oceanic arc volcanics of the Tonga and Kermadec arcs to the north. This setting makes the TVZ an ideal location to make a detailed study of the U-series systematics of continental arc volcanoes. To date there has been relatively little U-series work done on such volcanic centres because of the intrinsic greater complexities than observed in intra-oceanic arcs (although see Newman et al., 1986; Sigmarsson et al., 1990; Volpe and Hammond, 1991; Volpe, 1992; Sigmarsson et al., 1998). As detailed studies have been made of lavas from the Tonga and Kermadec arcs (Regelous et al., 1997; Turner et al., 1997a), by working on New Zealand volcanics it is possible to make comparisons across the continental-oceanic divide. This presents the possibility of increasing the understanding of processes both within the upper mantle source and at a crustal level.

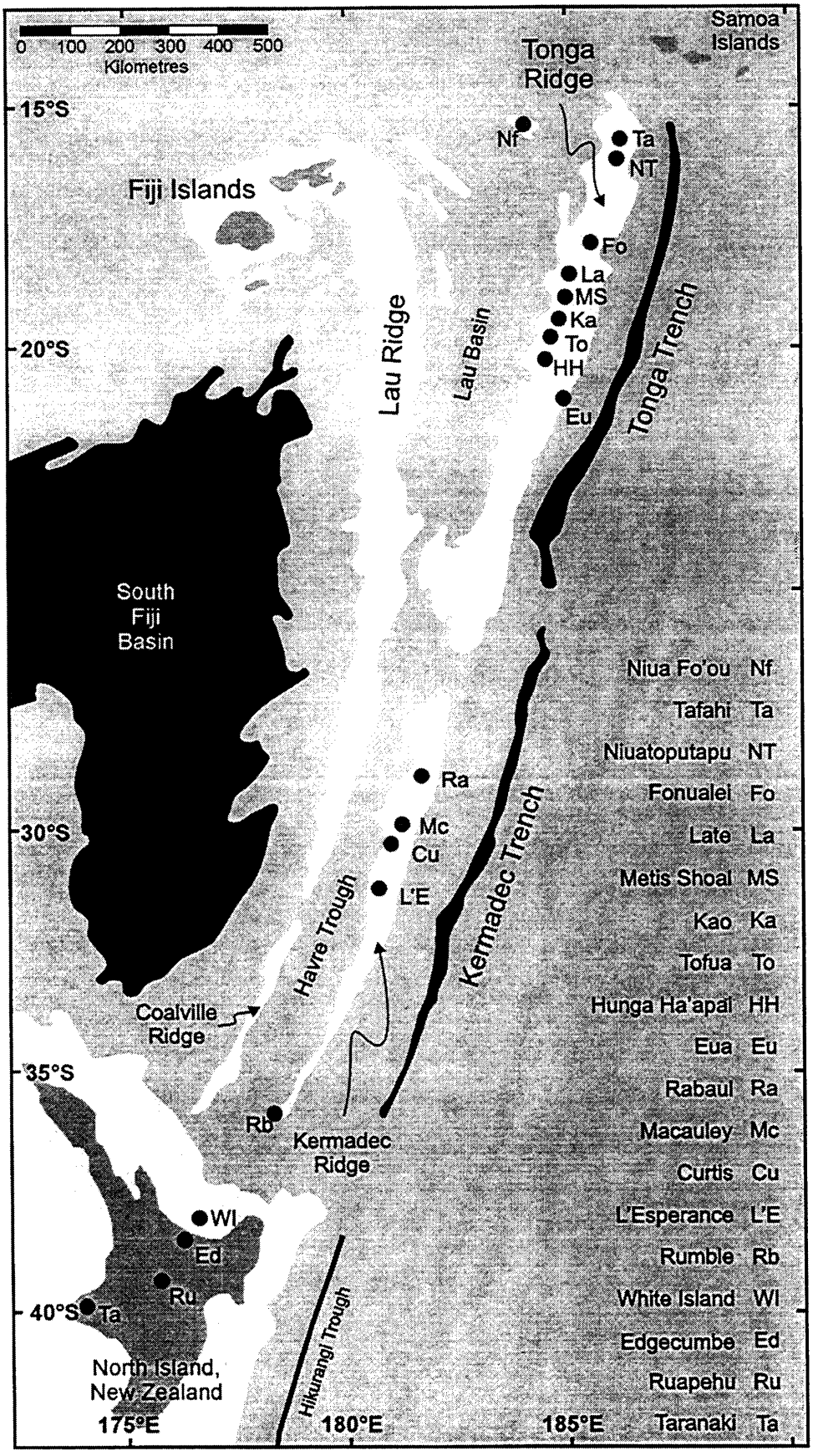

Figure 1.1: Map showing the distribution of volcanism along the New Zealand-Kermadec-Tonga arc system. Adapted after Ewart et al. (1977). Subduction of the Pacific Plate westwards beneath the Indian Plate is occurring along the Tonga and Kermadec Trenches and the Hikurangi Trough.

The largest of the andesitic arc volcanoes in New Zealand, Mount Ruapehu, is the site of the main focus of this thesis. Detailed sampling of sequences with clear relative stratigraphies has been carried out and are combined with material from historic eruptions to provide a suite of samples which covers the past 150 ka of volcanic activity at Ruapehu. Other volcanoes, Edgecumbe, White Island and Taranaki have also been examined to provide further comparisons.

1.3 Thesis Objectives

The principal objectives of this work are to look in detail at the timescales of magmatic processes in a continental subduction zone environment; an area which to date has received less attention than similar work in intra-oceanic environments. This thesis aims to address the timescales of both crustal level processes and melt generation in the mantle wedge. The principal areas which will be addressed are outlined below.

1 To make detailed theoretical considerations of the potential effects of crustal level magmatic processes on U-series systematics.

2 To constrain the processes and conditions involved in the crustal level differentiation of mantle-derived magmas in New Zealand.

3 To show how U-series data may be used to constrain and improve resolution of stratigraphy in a complex, composite volcanic setting.

4 To constrain transit and residence times following melt generation, and to place these times in a tectonic framework to aid understanding of the complexities of continental arc volcanism.

5 To constrain mass fluxes from the subducting slab beneath New Zealand and to evaluate the effects of subduction geometry on these fluxes.

1.4 Thesis Structure

The layout of this thesis is designed to guide the reader in a logical development of concepts and ideas. These build up a discussion of the behaviour of short-lived isotopes in magma chambers and the application of U-series systematics in determining the rates

and timescales of magma generation and differentiation in a complex continental arc environment.

Chapter 1 introduces the background to the current understanding of the petrogenetic processes which occur at subduction zones. It illustrates some of the areas where our understanding is poor and briefly explains the logic behind this study and the goals of the thesis.

Chapter 2 presents an introduction to the principles of radioactivity and short-lived isotope theory. The main part of the chapter discusses theoretical modelling of the effects of magma chamber processes on U-series systematics. A model is developed which permits the combination of crystallisation, assimilation, replenishment and radioactive decay to predict the effect of these processes on the behaviour of U-Th-Ra isotopes.

Chapter 3 details the tectonic setting and background geology of North Island, New Zealand. The stratigraphy, history and sampling of the volcanic centres studied in this thesis are summarised, concentrating on Mount Ruapehu, the principle volcano investigated during the project.

Chapter 4 examines the major element, trace element and radiogenic isotope data obtained for a suite of Ruapehu samples during this study in conjunction with published databases. The discussion centres around the differentiation processes occurring within crustal magma chambers, which have played a major role in controlling the chemical evolution of Ruapehu samples. Major element trends are used to constrain the conditions of crystallisation, and radiogenic isotope signatures are used to investigate the degree of assimilation of local basement rocks.

Chapter 5 presents U-Th-Ra data for Ruapehu volcanics and discusses how these data may be used to help determine the timescales of magma generation and differentiation processes. The data is used to derive an interpretation of the nature of magma transport, storage and eruption at Ruapehu and how these processes have varied over the last 150 ka.

Chapter 6 makes comparisons with data obtained for volcanic centres along- and across-arc from Ruapehu, and with published data sets for the intra-oceanic continuation of the subduction zone to the north of New Zealand in the Kermadec and Tonga arcs. These comparisons are used to help understand the importance of both tectonic parameters and source processes in the generation of arc magmas.

Chapter 7 summarises what has been learned from this study. Finally, consideration is given to what sort of investigation needs to be made in the future to help further constrain the rates and controls of magma generation and differentiation processes in arc environments.

None of the chapters presented in this thesis are presently in the form of journal manuscripts, although it is intended that at least three papers will be forthcoming from this work. These will be:

The effects of magma replenishment processes on ^{238}U-^{230}Th *disequilibrium in arc* magmas. R.D. Hughes and C.J. Hawkesworth, accepted for publicaton in Geochimica et Cosmochimica Acta. (Based on Chapter 2)

The magmatic evolution of a composite andesite volcano: Evidence from U-Th-Ra isotopes. (Based on Chapter 5)

U-series systematics in young arc lavas from New Zealand: Subcrustal processes and the timescales of magma generation. (Based on Chapter 6)

Something that supervisors ought to bear in mind...,

Non anti septem dies proxima, Sqviri

The motto of the Guild of Plumbers and Dunnykindivers

from 'The concife and possibly even accuratte Mapp' and 'Discworld Companion' – Terry Pratchett & Stephen Briggs.

Chapter 2

Modelling the Behaviour of Short-Lived Isotopes During Magma Chamber Processes

2.1 Introduction

The volcanic centres for which new analyses of U-Th-Ra isotopes are presented in this study are all built on continental crust, and universally show evidence for having spent some unconstrained period of time evolving in a crustal magma chamber. This chapter introduces the principles of radioactivity and short-lived isotope theory, and presents modelling which investigates how various magma chamber processes such as crystallisation, assimilation and replenishment can affect U-series isotope systematics. The chapter presented herein is based on a paper accepted for publication in Geochimica et Cosmochimica Acta, which has been lengthened to include a discussion on assimilation and the effect of magma chamber processes on Ra-Th systematics.

The use of U-series systematics to investigate the timescales of magmatic processes is potentially an extremely powerful tool. In order to make the best use of analytical data, it is necessary to understand how magma chamber processes can affect the systematics, as a number of case studies have demonstrated how short-lived isotope systematics can be disturbed by such mechanisms. Some of the first U-series mineral separate analyses demonstrated that an apparent Th isotopic heterogeneity existed between the mineral phases and the groundmass which was taken to result some kind of post-crystallisation process affecting melt composition (Taddeucci et al., 1967; Allègre, 1968). A number of subsequent studies have used whole rock data to try and constrain various magmatic processes (e.g. Capaldi et al., 1976; Condomines et al., 1982;

Condomines et al., 1995), and the potential importance of magma chamber processes such as assimilation has been emphasised by several authors (Bennett et al., 1982; Condomines et al., 1988; Villemant and Fléhoc, 1989; Villemant et al., 1993).

Of all the tectonic environments studied with U-series techniques, arc lavas are perhaps the most likely to show the effects of magma chamber processes given the frequent evidence for complex pre-eruption histories commonly displayed (e.g. Gill, 1981). Consequently it is not surprising that a number of studies of subduction related lavas have identified possible disturbances of U-Th-Ra systematics whilst the magma is resident in the crust; e.g. Mount Shasta (Newman et al., 1986; Volpe, 1992), Vesuvius (Capaldi et al., 1982), Santorini (Pyle et al., 1988), Mount St. Helens (Volpe and Hammond, 1991), Nevado del Ruiz (Schaeffer et al., 1993).

2.2 Radioactivity and Short-Lived Isotopes

In this section, radioactivity and its application in short-lived isotope systematics is examined. The background and development of the specialised field of short-lived isotopes is summarised from several sources (Faure, 1986; Dickin, 1997 and references therein), and some of the principal tenets and current state of knowledge of short-lived isotopes are set out.

2.2.1 The History of Radioactivity and Isotope Geoscience

Whilst the principles of radioactivity are important in many branches of science and have led to a fundamental revision of our concepts of Earth history, these ideas only began to develop towards the end of the last century.

The discovery of radioactivity followed from pioneering work by Roentgen and Becquerel who identified the effects caused by particles emitted from uranium salts as a result of radioactive decay. Shortly after these discoveries, Pierre and Marie Curie found that thorium and radium also emitted similar particles. The growing evidence for radioactive decay led Rutherford and Soddy to investigate the nature of the emitted particles, and to quantify the physical processes in operation.

As investigations probed deeper into the nature of radioactivity, evidence accumulated that atomic masses were not integer values. This led to Soddy suggesting that many elements had more than one isotope, which was confirmed with the discovery of the neutron by Chadwick. By now, all the theory was in place to allow geologists and others to begin to use isotopes as a tool to investigate the formation and history of the Earth. The invention of the mass spectrograph by Thomson and Aston, and subsequent developments by the likes of Dempster, Bainbridge and Nier, gave geologists the equipment to begin to use isotope geochemistry in a routine fashion.

The potential uses of radioactive decay in investigating geological problems was appreciated almost immediately after the discovery of radioactivity. Work by Strutt and Joly between 1905 and 1909 looked at the importance of radioactivity as a heat source, and around the same time, Rutherford and Boltwood had realised the possibilities for geochronology that had been opened up by the discovery of radioactivity. By measuring the amount of helium accumulated in uranium bearing minerals, Rutherford suggested that the age of the Earth might be around 500 Ma. This early estimate using radioactivity was superseded by progressively older ages as new, more rigorous and accurate ways of using radioactivity to date rocks were employed.

2.2.2 Radioactive Decay

The early work of Rutherford and Soddy led to the first quantification of radioactive decay. Whilst a number of different types of radioactive decay can occur in different isotopes, two principle mechanisms are of interest in order to understand short-lived isotope systematics; the alpha (α) and beta (β^-) decay paths. The studies of Rutherford and Soddy enabled them to suggest that regardless of the mechanism, the rate of decay (number of atoms of a particular isotope undergoing radioactive decay per unit time) was proportional to the number of atoms of the parent isotope present. This relationship is shown in Equation 2.1 where N represents the number of atoms of a given isotope present.

$$-\frac{dN}{dt} \propto N \tag{2.1}$$

This proportionality can be converted into an equality by addition of a constant, known as the decay constant, which is given the symbol λ.

$$-\frac{dN}{dt} = \lambda N \tag{2.2}$$

If Equation 2.2 is rearranged and integrated,

$$-\int \frac{1}{N} dN = \lambda \int dt \tag{2.3}$$

which can be solved, and the constant of integration found for the condition $t = 0$ to give Equation 2.4 where N_0 is the number of atoms at time $t = 0$.

$$-\ln N = \lambda t - \ln N_0 \tag{2.4}$$

This can then be rearranged to give Equation 2.5.

$$N = N_0 e^{-\lambda t} \tag{2.5}$$

The concept of half-life ($t_{1/2}$) is fundamental to radioactivity, and is defined as the time taken for half the atoms present to decay. It follows that at $t_{1/2}$ the number of atoms present can be written as $N_0/2$. This can be substituted into Equation 2.5 and rearranged to give Equation 2.6.

$$t_{1/2} = \frac{\ln 2}{\lambda} \tag{2.6}$$

Thus every radioactive isotope is uniquely characterised by both its half-life and its decay constant, which is a measure of the number of atoms which will on average decay per year.

2.2.3 Short-Lived Isotope Systematics

Of all the isotopes that have been studied in geological systems, ^{238}U, ^{232}Th and to a lesser extent ^{235}U are perhaps uniquely important. These isotopes are the principal heat producing elements in the Earth, are extremely versatile for U-Pb and Pb-Pb dating of rocks and minerals and have proved powerful tracers for geochemical reservoirs. In addition to these uses, there has been increasing interest in some of the intermediate radioactive daughter products in the decay chains of these isotopes.

The parent isotopes, ^{238}U, ^{235}U and ^{232}Th have very long half-lives (4.47 Ga, 704 Ma and 14.01 Ga respectively), and each has a long decay chain which lead to the

stable daughter isotopes, ^{206}Pb, ^{207}Pb and ^{208}Pb respectively. The intermediate products in each of the decay chains have much shorter half-lives than their parent isotope, and within these intermediate isotopes there are a number of sub-systems where the half-life of the parent is significantly long with respect to that of the daughter. The decay chains for the three systems are illustrated in Figure 2.1.

Under normal circumstances in such a system, the rate at which the short-lived daughter decays is controlled by the rate of decay of the parent, i.e. the rate at which the daughter isotope is produced. The rate of decay of a radioactive isotope is expressed as activity, which is the number of atoms of a given isotope decaying in a unit time. Activity is calculated as the product of the number of atoms present, and the decay constant of the isotope of interest as given by Equation 2.7, where X represents the isotope of interest, N_x is the number of atoms of isotope X, and λ_x is the decay constant of X. Conventionally in short-lived isotope systematics, activity is denoted by parentheses, whereas concentrations of a given isotope are indicated by square brackets to distinguish between the two properties. This convention is followed throughout this thesis when referring to short-lived isotope systematics (this is summarised in Appendix A for reference).

$$(X) = N_x \lambda_x \tag{2.7}$$

Under normal circumstances where the decay of the daughter is controlled by the rate at which it is produced, the ratio of parent activity to daughter activity is unity, and the system is said to be in secular equilibrium. However, if a process can fractionate the parent and daughter isotopes, the system becomes disturbed and is said to be in disequilibrium. Two such circumstances can be envisaged; firstly where the abundance of the parent is increased relative to the daughter (parent excess), and secondly where the opposite situation is true (daughter excess).

In the first instance, because the abundance of the parent increases, its activity also increases. This means that more atoms of the parent than the daughter decay in a given time, with the effect that the abundance of the daughter increases such that the activities of parent and daughter move towards equality. The system is therefore returned to secular equilibrium through a processes known as daughter ingrowth. In the case of daughter

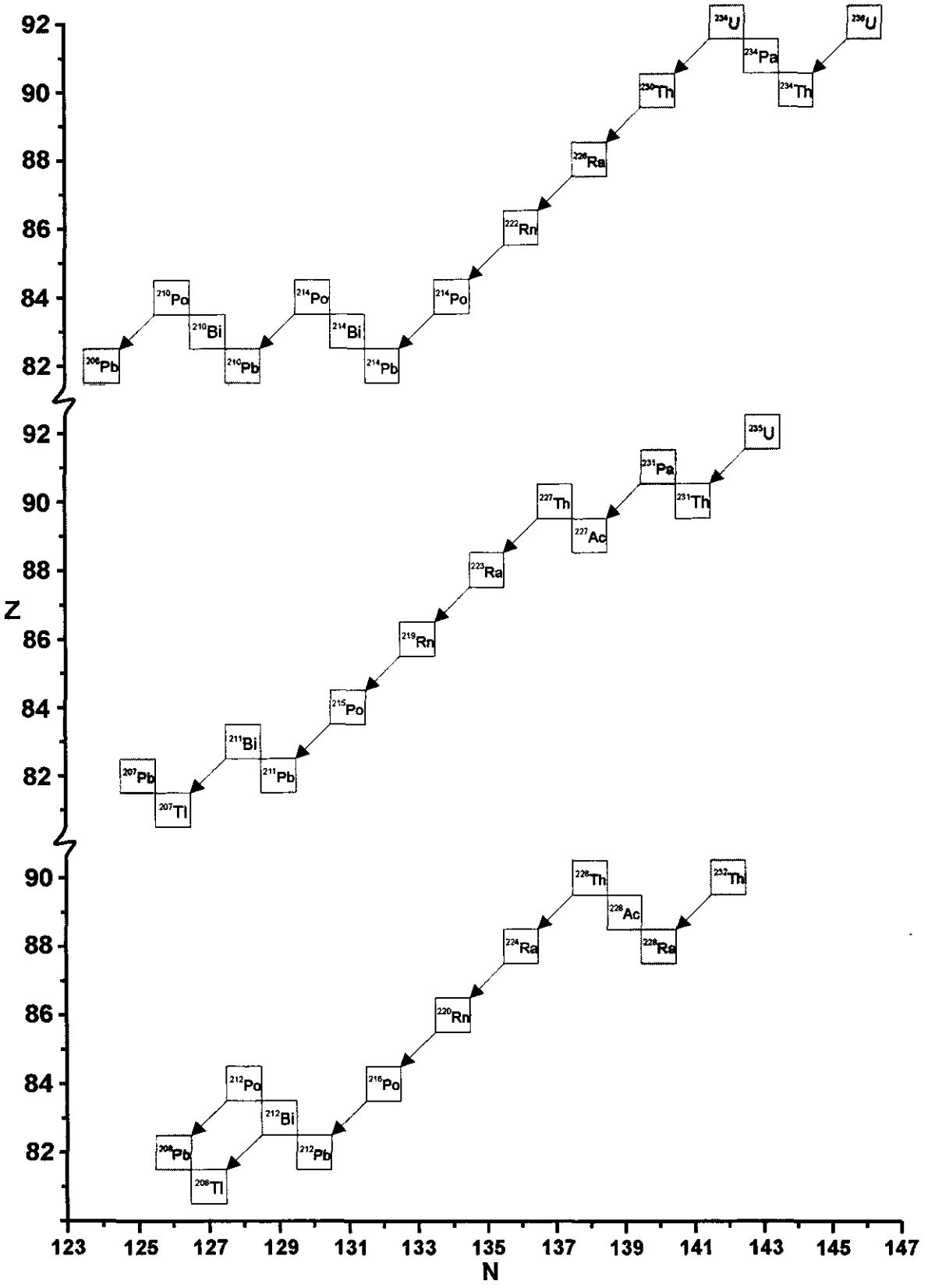

Figure 2.1: Diagram showing the decay chains of the three main long-lived radioactive nuclides discussed in this study. The parent and short-lived daughter isotopes of interest in this work are shaded. Redrawn after Dickin (1997).

excess, the activity of the daughter isotope increases relative to the parent, and therefore a greater number of atoms of the daughter decay compared to the parent in a given time. This has the effect of reducing the abundance of the daughter until the system returns to secular equilibrium. This is referred to as the daughter isotope being unsupported.

These features of the three decay chains illustrated in Figure 2.1, have been known almost as long as radioactivity itself, and the first mathematical solution of the differential equations controlling the parent and daughter decay was provided by Bateman (1910). This is given by Equation 2.8, where $(D)_t$ is the activity of the daughter after time t, $(D)_{init}$ is the initial activity of the daughter isotope, (P) is the activity of the parent (assumed to be invariant on the timescales considered), and λ_D is the decay constant of the daughter isotope.

$$(D)_t = (D)_{init} e^{-\lambda_D t} + (P)\left(1 - e^{-\lambda_D t}\right) \quad (2.8)$$

One of the fundamental features of short-lived isotope systematics, is that the time taken for a perturbed system to return to secular equilibrium (within the limits of analytical techniques) either through daughter ingrowth, or decay of an unsupported daughter, is approximately 5 half-lives of the daughter isotope. It is this property that makes short-lived isotopes so useful in geological studies of rapid processes, because it means that such systems are sensitive to timescales ranging from < 100 years in the case of ^{228}Ra-^{232}Th to < 1.5 Ma in the case of ^{234}U-^{238}U. The principal systems of interest in this study and in the majority of igneous systems are ^{230}Th-^{238}U (useful over timescales < 350 ka) and ^{226}Ra-^{230}Th (useful over timescales < 8 ka).

2.2.4 Analysis of Short-Lived Isotopes

The full details of the chemical and analytical procedures followed in this study are given in Appendix D. The purpose of this section is briefly to outline the developments in analytical techniques which have taken place in recent years, which present the possibility of using short-lived isotopes to look at geological processes which were previously obscured due to the limitations of analytical precision.

The analysis of U and Th concentrations by mass spectrometry using isotope dilution techniques is long established (e.g. Allègre and Condomines, 1976). However, analysis of low abundance isotopes such as ^{230}Th and ^{226}Ra is much more difficult. Initially, alpha and gamma spectrometry were employed to analyse these isotopes (e.g. Allègre and Condomines, 1976; Capaldi et al., 1976), but the low abundances of these isotopes in natural samples means that long counting times are generally required. Even when counting for a week or so, the typical precision on most samples is 5-10% 2σ, with better precision generally only achieved on samples with high abundances of U and Th.

More recently, thermal ionisation mass spectrometry techniques (TIMS) have been developed to analyse for very low abundance isotopes. These were initially perfected for use with carbonate samples which have higher abundances of isotopes such as ^{230}Th and ^{234}U than igneous systems (Chen et al., 1986; Edwards et al., 1987). The principal difficulty in TIMS analysis of short-lived isotopes is low abundance sensitivity. For any ion peak measured by mass spectrometry, there is a tail on the low mass side of the peak, produced as a result of collisions reducing the energy of ions. If a very low abundance isotope (e.g. ^{230}Th) has a mass slightly lower than that of a larger peak (e.g. ^{232}Th), this tail on the low mass side of the large peak can swamp the signal from the low abundance isotope.

These difficulties have been overcome to allow the analysis of short-lived isotopes in igneous systems (e.g. Goldstein et al., 1989), by the use of various techniques such as peak interpolation (McDermott et al., 1993) or the use of energy filters (van Calsteren and Schwieters, 1995). The use of mass spectrometry has allowed typical precisions to be reduced to 0.5-1% (2σ) even in samples with low abundances of Th and U.

The analysis of Ra isotopes using mass spectrometry has also been a very recent advance. In the past few years, methods for TIMS analysis of ^{226}Ra in igneous rocks have been developed (Volpe et al., 1991; Cohen and O'Nions, 1991; Cohen et al., 1992), although the extremely low abundance of ^{228}Ra in typical igneous systems has meant that to date successful analyses of this isotope have only been obtained by counting techniques.

2.2.5 U-Th and Ra-Th as a Dating System

The earliest uses of ^{230}Th-^{238}U systematics in igneous systems were as a dating tool for very young rocks. It was appreciated that where crystallisation of various phases had occurred simultaneously, it was possible to use U-Th systematics in a similar fashion to a conventional isochron system (e.g. Cerrai et al., 1965; Kigoshi, 1967; Taddeucci et al., 1967; Allègre and Condomines, 1976).

The equivalent of a normal isochron diagram in the ^{230}Th-^{238}U system normalises both axes to ^{232}Th and uses isotope activities rather than isotopic abundances, so that (^{238}U/^{232}Th) is plotted on the x-axis and (^{230}Th/^{232}Th) on the y-axis. This diagram has subsequently become known as the equiline diagram (Allègre and Condomines, 1976) because a line passing through the origin with a gradient of 1 (known as the equiline) represents the locus of compositions in secular equilibrium. On such a diagram, instantaneous fractionation of U and Th has a horizontal vector, whereas radioactive decay produces a vertical vector as illustrated in Figure 2.2a.

The use of this plot as an isochron diagram is illustrated in Figure 2.2b. Fractionation of U and Th during the crystallisation of a phase, moves the composition of the mineral horizontally on the equiline diagram away from the liquid composition. A number of cogenetic phases will lie on a horizontal line at the time of crystallisation. Following crystallisation, radioactive decay drives the Th isotopic composition of each coexisting phase towards secular equilibrium, increasing the (^{230}Th/^{232}Th) ratio of samples in U excess, and decreasing the (^{230}Th/^{232}Th) composition of phases in Th excess. The effect of this is to cause the initially horizontal line to rotate about the point at which it crosses the equiline, such that after ~5 half lifes of ^{230}Th, a best fit line through the array of mineral compositions approaches the equiline.

The mathematical treatment of the isochron diagram uses the Bateman equation (Equation 2.8) which is normalised, in the case of the ^{230}Th-^{238}U system to ^{232}Th which can be considered to be stable over the timescales of interest. This gives Equation 2.9, which has the mathematical form of a straight line, as with other isochron equations.

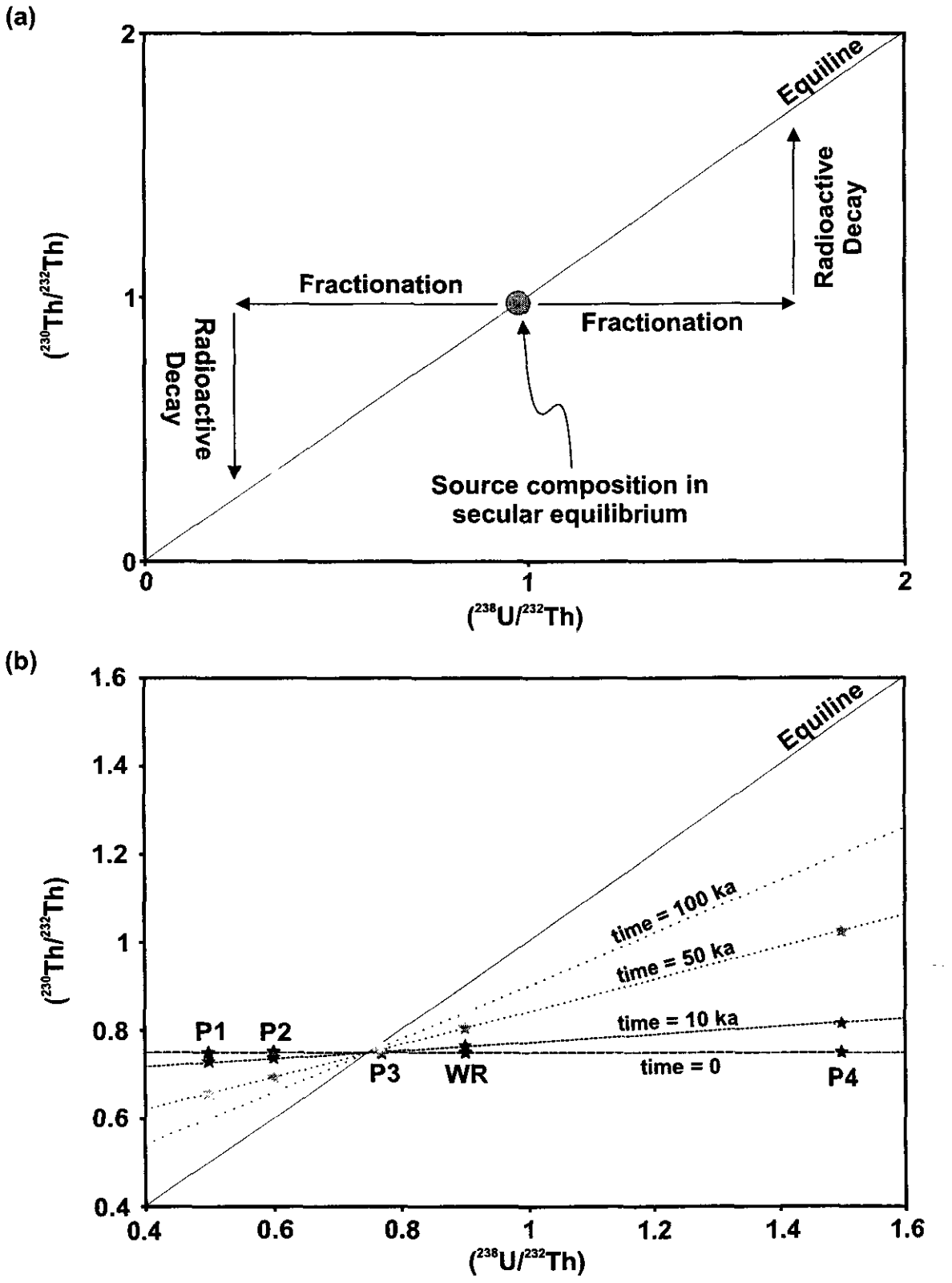

Figure 2.2:

(a) - Equiline diagram showing the simplest model for the behaviour of U-Th systematics during magmatic processes. Simple, instantaneous fractionation of U and Th produces horizontal movement, whereas radioactive decay produces vertical movement. After Allègre and Condomines (1976).

(b) - The application of ^{230}Th-^{238}U disequilibrium as a dating system using mineral isochrons after Allègre (1968) and Allègre and Condomines (1976).

$$\left(\frac{^{230}Th}{^{232}Th}\right)_t = \left\{\left(\frac{^{230}Th}{^{232}Th}\right)_{init} e^{-\lambda_{230}t}\right\} + \left\{\left(\frac{^{238}U}{^{232}Th}\right)\left\{1 - e^{-\lambda_{230}t}\right\}\right\} \quad (2.9)$$

Thus, a suite of cogenetic samples define a straight line whose gradient is a function of their age. The expression for the gradient can be rearranged to give the time since U-Th fractionation as given by Equation 2.10, where m is the gradient of the line.

$$t = -\frac{\ln m}{\lambda_{230}} \quad (2.10)$$

The evolving cogenetic compositions rotate about a constant point on the equiline, the (^{230}Th/^{232}Th) ratio of which represents the Th isotopic composition of the magma and newly formed crystals at the time of crystallisation. This composition can also be calculated from the point at which a line passing through cogenetic data intercepts the y-axis, using Equation 2.11 where I denotes the intercept with the y-axis

$$\left(\frac{^{230}Th}{^{232}Th}\right)_{init} = \frac{I}{e^{-\lambda_{230}t}} \quad (2.11)$$

Initial work using ^{230}Th-^{238}U systematics demonstrated that it was possible to get dates which corresponded with those from other systems reasonably well (Kigoshi, 1967), but other work also showed that the system could be more complex in some circumstances (Taddeucci et al., 1967; Allègre, 1968) where data for mineral separates and glass appeared to relate to two different events. A number of studies have subsequently used the U-Th system as a means of dating crystallisation, although such efforts have not always been without difficulty (e.g. Allègre and Condomines, 1976; Condomines and Allègre, 1980; Condomines et al., 1982; Volpe and Hammond, 1991; Volpe, 1992; Peate et al., 1996; Condomines, 1997; Heath et al., 1998b).

A similar isochron technique can be used with ^{226}Ra-^{230}Th and disequilibria. In this instance, there is no long-lived Ra isotope available to normalise to, so the most common solution adopted has been to normalise to Ba concentrations, which should have very similar partitioning behaviour to Ra in most systems (Williams et al., 1986). The equivalent Bateman equation used with ^{226}Ra-^{230}Th is given by equation 2.12.

$$\left\{\frac{(^{226}Ra)}{[Ba]}\right\}_t = \left\{\left\{\frac{(^{226}Ra)}{[Ba]}\right\}_{init} e^{-\lambda_{226}t}\right\} + \left\{\frac{(^{230}Th)}{[Ba]}\left\{1 - e^{-\lambda_{226}t}\right\}\right\} \quad (2.12)$$

The application of ^{226}Ra-^{230}Th systematics as a geochronological tool has been fairly limited to date because of difficulties in making precise measurements. However several studies have shown the potential of the system (e.g. Volpe and Hammond, 1991; Volpe, 1992; Reagan et al., 1992; Schaeffer et al., 1993; Black et al., 1998; Evans, 1999).

2.2.6 U-Th-Ra Disequilibria During Melting and Subduction Zone Processes.

Shortly after the first application of the U-Th dating system to igneous rocks, a number of studies began to make use of U-Th and Ra-Th systematics to examine the timescales of processes which were producing U-Th-Ra disequilibrium in primary liquids (e.g. Allègre and Condomines, 1976; Capaldi et al., 1976; Condomines et al., 1982).

A considerable amount of ^{230}Th-^{238}U data is now available, and it is possible to identify key differences between MORB/OIB magmas and subduction related melts. The former are always in secular equilibrium or show Th excess. This has been attributed to small degrees of partial melting in the presence of residual garnet (Chabaux and Allègre, 1994 and references therein), and more recently it has been suggested that under certain circumstances, residual clinopyroxene can also produce Th excesses (Wood et al., 1998). In order to produce the observed range of U-Th compositions through simple melting models, it is necessary to invoke unrealistically small degrees of melting. A number of studies have used more complex models of dynamic melting processes to explain the range of U-Th isotope ratios obtained from MORB and OIB (e.g. McKenzie, 1985b; Spiegelman and McKenzie, 1987; Spiegelman and Elliott, 1993).

Subduction related magmas are much more variable in both ($^{238}U/^{232}Th$) and ($^{230}Th/^{232}Th$) composition. A large number of arc samples analysed to date tend to plot in or fairly close to secular equilibrium, and can show Th or U excess. However a number of samples show large U excesses, most commonly from highly depleted (with respect to MORB) intra-oceanic arcs such as the Tonga and Mariana arc (Elliott et al., 1997; Turner and Hawkesworth, 1997; Turner et al., 1997a; Regelous et al., 1997). The unique occurrence of U excesses in arc magmas is generally thought to be related to the presence

of oxidising fluids during melt generation, which can mobilise U preferentially to Th (e.g. Keppler and Wyllie, 1990; Brenan et al., 1995; Keppler, 1996). The interpretation of U-series systematics in arc lavas will be discussed in more depth in subsequent chapters.

The relative lack of ^{226}Ra-^{230}Th data means that less is known about the behaviour of these systematics during magmatic processes. Various authors have attempted to link ^{226}Ra-^{230}Th disequilibria to melting processes (e.g. Chabaux and Allègre, 1994; Iwamori, 1994), implying that in many cases, melt generation can occur over very short timescales (e.g. < 8 ka). However, there have been a number of examples where ^{230}Th-^{238}U analyses plot in secular equilibrium, whereas the same samples show ^{226}Ra-^{230}Th disequilibrium (e.g. Hémond et al., 1994). As Ra is generally believed to have a similar chemistry to Ba, a number of possibilities can be proposed for the decoupling of Ra-Th and U-Th disequilibria, such as disturbance of Ra-Th systematics in the presence of fluids or preferential incorporation of Ra over Th into minerals such as plagioclase which can show a preference for Ba under certain conditions.

2.3 Models for U-Th-Ra Systematics in Magma Chambers

Several authors have produced models which describe the effects of magma chamber processes on U-Th-Ra systematics. Mainly qualitative models have been described for a wide range of processes such as replenishment and assimilation by Allègre, Condomines and co-workers in a series of studies (Allègre and Condomines, 1976; Condomines and Allègre, 1980; Allègre and Condomines, 1982). A comprehensive series of quantitative models for the generation and evolution of coexisting ^{226}Ra-^{230}Th and ^{228}Ra-^{232}Th disequilibria have been described with particular reference to lavas from Etna and Stromboli (Capaldi et al., 1976). More recently, a model has been proposed to relate short-lived isotope disequilibria to magma residence time in steady-state systems (Pyle et al., 1991; Pyle, 1992; Pyle, 1994), although the applicability of the model to the systems evaluated by Pyle has been called into question (Condomines, 1994).

The published models are limited for a number of reasons. Firstly the equations given by Capaldi et al. (1976) refer only to radium isotopes and in addition require that

both ^{228}Ra-^{232}Th and ^{226}Ra-^{230}Th disequilibria are present. Although the model presented by Pyle (1992) is more general in nature, the author acknowledges that where a ^{228}Ra-^{232}Th disequilibrium can be measured, the model allows greater constraints to be placed on the derived residence time. However, ^{228}Ra-^{232}Th disequilibrium have only been reported for a few systems, viz. Stromboli and Etna (Capaldi et al., 1976), Oldoinyo Lengai (Williams et al., 1986; Pyle et al., 1991) and Sakurajima (Black, 1997), and such models are of limited use in systems where ^{228}Ra-^{232}Th disequilibria have not been measured. Secondly, the equations given by Capaldi et al. (1976) have a mathematical limitation in that they do not have unique solutions. Thirdly, the more recent model of Pyle is specifically designed to address the issue of the behaviour of short-lived isotopes in shallow, steady-state magma chambers. In this case, steady-state is defined as having a constant mass influx balanced by a constant mass outflux. The existence of such magma chambers has been demonstrated on short timescales of a few tens or hundreds of years (Wadge, 1980; Wadge, 1982). However, it is difficult to demonstrate their existence on timescales of thousands to tens of thousands of years, i.e. those to which ^{226}Ra-^{230}Th and ^{230}Th-^{238}U systematics are most applicable, particularly given that many volcanoes apparently go through long periods of quiescence during their evolution.

In essence, despite valuable work in previous studies, there is still a need for a model which can be used to investigate and quantify the effects of various processes on short-lived isotopes under a wide range of conditions, from systems which are closed to new magmatic input and only undergo assimilation-fractional crystallisation (AFC) type processes, to steady-state magma chambers which are continually refilled with fresh magma.

The modelling presented here allow the effects of magma chamber processes for the full range of conditions described above to be combined with the effects of time and radioactive decay by using aspects of models of periodically refilled chambers (O'Hara, 1977; O'Hara and Mathews, 1981; Albarède, 1985), AFC processes (Allègre and Minster, 1978; DePaolo, 1981) and short-lived isotope theory.

2.4 Modelling Magma Chamber Processes

This section describes the modelling undertaken as part of this work, and discusses its implications for understanding the time information that short-lived isotopes can provide. The details of the models are discussed and then results of modelling replenishment, crystallisation and assimilation are considered in turn. The effects of these processes on combined U-Th and Ra-Th systematics are considered, and finally the application of the modelling to real systems is discussed with particular reference to how the model may be tested. Throughout this section, the discussion will be illustrated principally with examples of ^{230}Th-^{238}U disequilibria in U excess, as this is the main situation of interest in arc magmas. However, the model is equally applicable to any initial composition which is out of secular equilibrium in either the ^{230}Th-^{238}U or the ^{226}Ra-^{230}Th system.

2.4.1 Methodology

The methodology used here to model the behaviour of short-lived isotopes in magma chambers is based on an iterative approach to approximate the effects of the different processes. There are several advantages to such an approach; firstly, it negates the requirement of having a steady-state system and allows periodic chamber replenishment to be modelled. Secondly, it is a simple task to combine the effects of several processes which affect the isotopes of interest differently. Thirdly, it is easy to model the effects of adding a timescale to such magma chamber processes and finally, if sufficient data are available for any given volcanic system, it is possible to tailor the model to fit the known constraints, even if the parameters vary through time.

Two computer programs were used to evaluate the effects of magma chamber processes, one for ^{230}Th-^{238}U and one for ^{226}Ra-^{230}Th disequilibria, the systems of relevance to this study. The general outline of these programs is shown in Figure 2.3 (the source code for the programs is given in Appendix F).

Essentially, the calculation is broken down into a series of mixing cycles. Each cycle contains a chamber evolution step where the effects of radioactive decay,

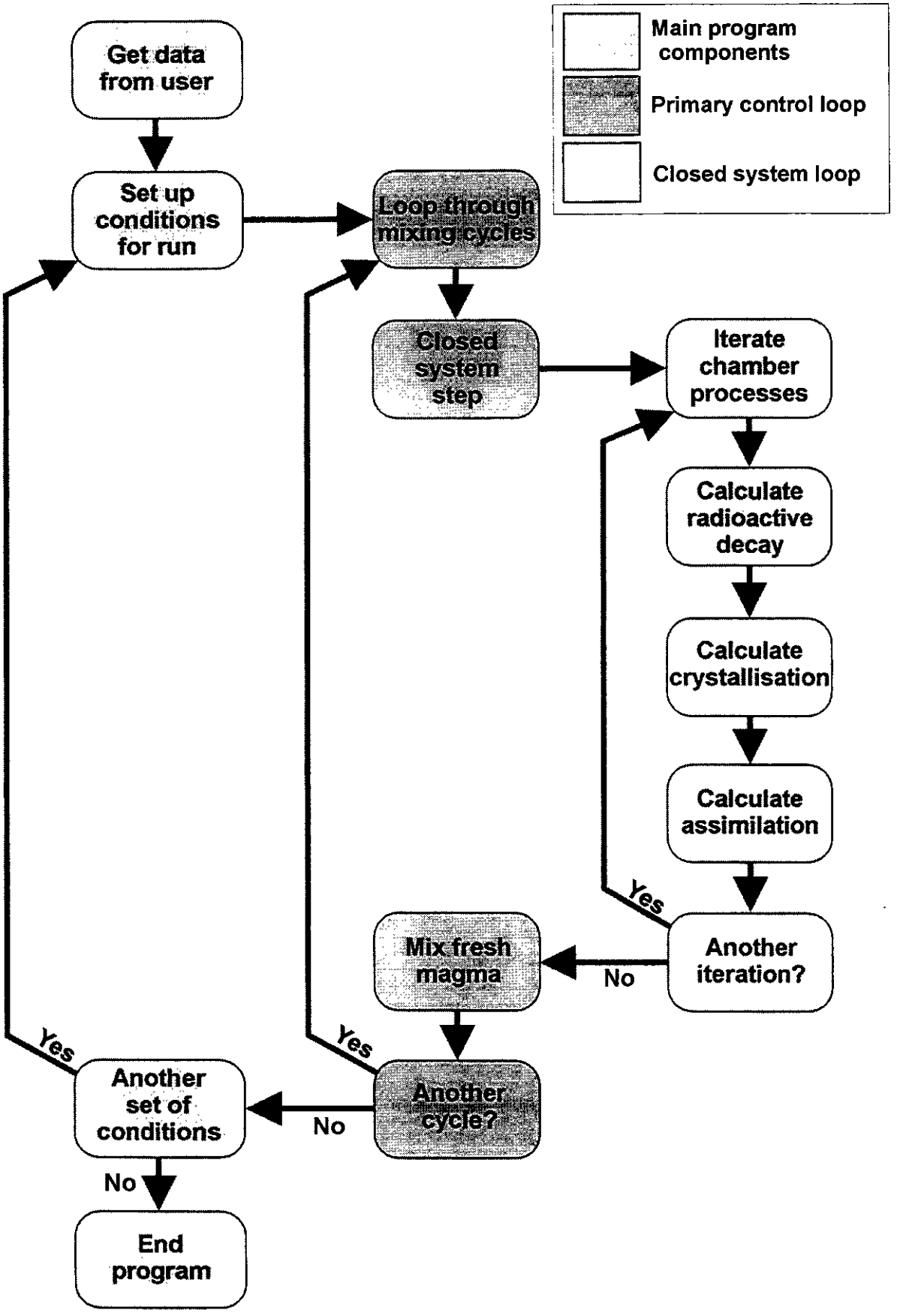

Figure 2.3: Flow chart showing the organisation of the computer program used iteratively to model the behaviour of short-lived isotopes in replenished magma chambers. The code for the program is given in Appendix F, and a discussion of the methodology is given in the text.

assimilation and crystallisation are calculated, and a replenishment step where magma chamber refilling is dealt with. The chamber evolution step is further broken down into a series of iterations of short time period. This allows the effects of radioactive decay, crystallisation and assimilation to be calculated consecutively for these very short time intervals, permitting continuous operation of these processes to be approximated. In practice, 10-20 iterations within each chamber evolution step was found to give a reasonable approximation for most refilling frequencies. In general, the number of iterations required to give a good approximation increases with increasing refilling frequency.

In the chamber evolution step, the effects of radioactive decay on ($^{230}Th/^{232}Th$) are calculated using Equation 2.8 given in Section 2.2.3. The change in concentration of the isotopes of interest due to crystallisation is then calculated using the standard Rayleigh fractional crystallisation equation (see Appendix E). Assimilation is calculated as a simple mixing relationship for each of the elements. It is then necessary to convert the isotope abundances into activity ratios so that the effects of radioactive decay can be calculated for the next iteration, which is done using constant relationships defined by the ratios of the decay constants of the isotopes of interest (see Appendix E). The effects of the replenishment step are calculated using mixing equations given in Appendix E in the same way as for assimilation.

The model has been designed to give as much flexibility as possible, but it is still useful to put certain limitations in place. The calculations assume that a mass balance is maintained, and the mass of fresh magma in each refilling event is such that the mass of assimilant and fresh magma in each mixing cycle is equal to the mass of magma crystallised and erupted. However, as it is potentially of interest to use this modelling to constrain the volume of a given magmatic system, the model uses volume rather than mass throughout. In order to do this, the mass balance is maintained by assuming that the density of all the components is constant in a similar fashion to previous models (Pyle, 1992; Pyle, 1994; Condomines, 1994).

This assumption is certainly reasonable for the slight variations in density that are likely to exist between crystallising magma and fresh magma except perhaps in the case of highly evolved systems mixing with basalt. The density of the assimilant is more problematic and highly dependant on the source rock of the assimilant and the nature of the melting process, so there is no easy way to handle this aspect of the model. It is therefore only possible to provide relatively crude estimates of absolute volumes using this model, although in practice as will be demonstrated, it is the ratio of various volumes which are critical in controlling the behaviour of short-lived isotopes.

A further assumption which is made is that mixing with injections of fresh magma is instantaneous. The dynamics of magma mixing are in reality much more complex than this (e.g. Sparks and Marshall, 1986; Snyder and Tait, 1998), however on the timescales for which ^{230}Th-^{238}U data are applicable (i.e. > 5-10 ka), it is unlikely that non-instantaneous mixing has a significant effect in most cases. The effects of non-instantaneous mixing are probably more relevant to the ^{226}Ra-^{230}Th system, and the effects will be discussed subsequently.

In a real magmatic system, many of the processes discussed here are linked by thermal constraints. Crystallisation is in practice controlled by the temperature of parental magmas and the time available to cool, amongst other factors, and it has long been suggested that assimilation occurs in response to the release of latent heat during crystallisation (Bowen, 1928). However for this model it is reasonable to allow the parameters to be independent of one another, and therefore the viability of the chosen conditions for a real system must be independently supported.

2.4.2 Replenishment

There is abundant field and geochemical evidence for periodic mingling of basic and evolved magma and this has led to the development of models for so called RTF (periodically Replenished, periodically Tapped, continuously Fractionated) magma chambers (O'Hara, 1977; O'Hara and Mathews, 1981; Albarède, 1985). One of the principal points that came from these studies is that, if the conditions remain constant, the

composition of the magma chamber approaches a steady-state, even though crystallisation is ongoing (O'Hara and Mathews, 1981). This will be discussed with reference to short-lived isotopes.

The simplest model considered here is for a magma chamber that does not assimilate local crust and which is not undergoing crystallisation. The only processes affecting the U-Th systematics are radioactive decay, and replenishment by a magma with the same U and Th concentrations and Th isotopic composition as the original magma in the chamber. The effects of replenishment on ^{226}Ra-^{230}Th disequilibria in the simplified system discussed here is exactly the same as for ^{230}Th-^{238}U systematics.

The principal effect of magma chamber replenishment is to modify the degree of disequilibrium. The modelling here assumes that the fresh magma has the same U/Th ratio and therefore (^{238}U/^{232}Th) ratio as the original magma in the chamber and the same (^{230}Th/^{232}Th) ratio as the original magma when it was emplaced. However because the original magma was emplaced a significant length of time ago, its (^{230}Th/^{232}Th) ratio has changed in response to radioactive decay. The effects of magma replenishment are demonstrated graphically on an equiline diagram in Figure 2.4a. Each injection of fresh magma changes the Th isotopic composition of the magma chamber such that the (^{230}Th/^{238}U) ratio moves further from unity towards the value of the fresh magma.

When describing magma chamber evolution, some authors have used a diagram which plots (^{230}Th/^{232}Th) against $e^{\lambda t}$ (e.g. Condomines and Allègre, 1980). Throughout the subsequent discussion, a similar diagram will be used which has time as a linear scale on the x-axis, so that magma chamber events do not become compressed at one end of the scale. The effects of replenishment on such a diagram have been shown by previous authors (Condomines and Allègre, 1980; Condomines et al., 1982) and are illustrated on a linear scale in Figure 2.4b.

The effects of replenishment are illustrated for a range of reinjection frequencies and for variable ratios of input volume to chamber volume in Figures 2.5a and 2.5b respectively. In both diagrams the other conditions are summarised in the figure captions and have been chosen to be applicable to typical continental arc volcanoes which are the

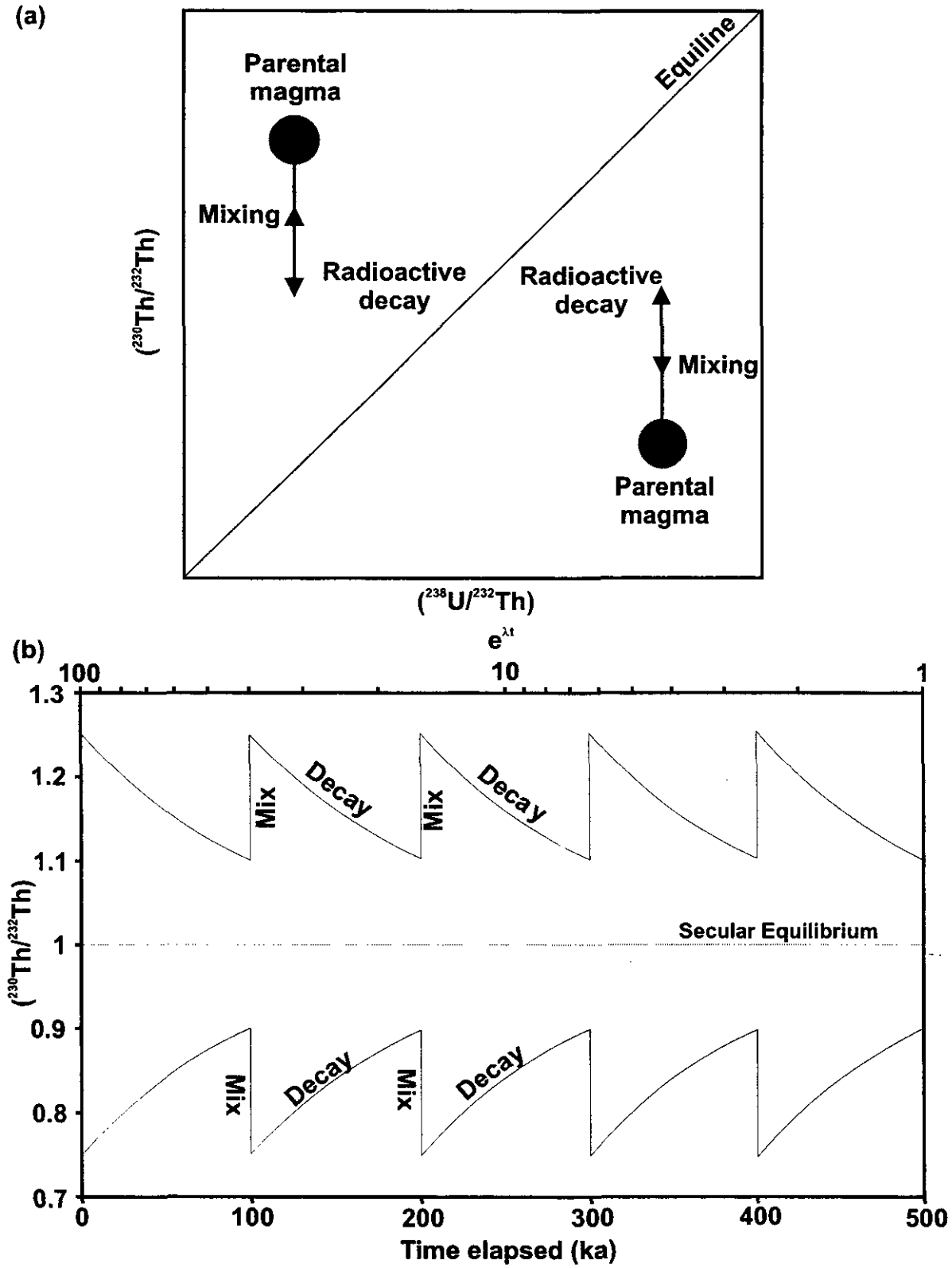

Figure 2.4:

(a) - Illustration of the effects of magma chamber replenishment on an equiline diagram. Injections of fresh magma move the composition of the magma in the chamber away from the equiline and further out of equilibrium.

(b) - Magma chamber replenishment events on a Th isotope evolution diagram, after Condomines & Allègre (1980) and Condomines et al. (1982). The diagram is drawn assuming a system with ($^{238}U/^{232}Th$) = 1.0, hence a ($^{230}Th/^{232}Th$) ratio of 1.0 represents secular equilibrium.

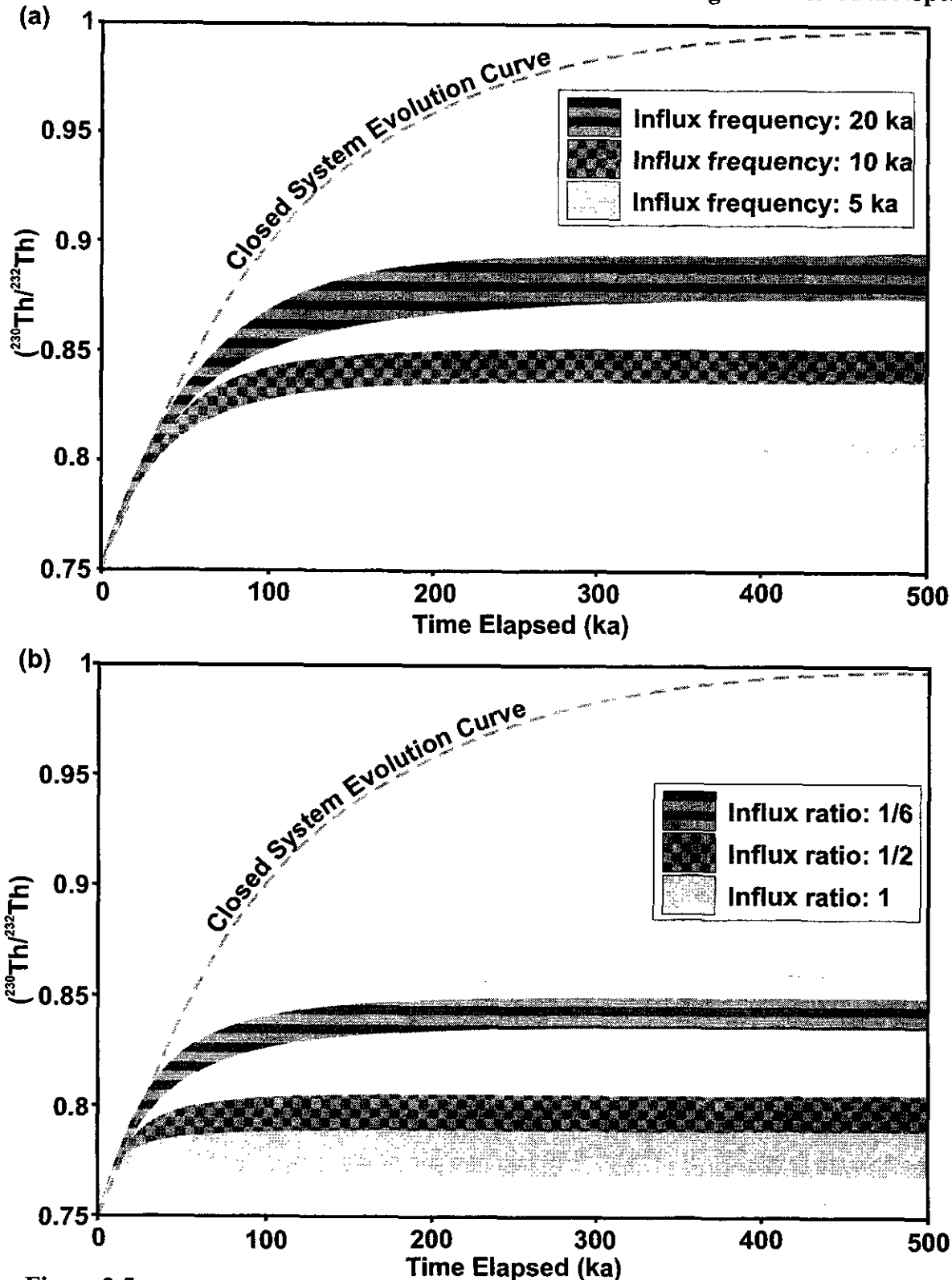

Figure 2.5:

(a) - Variation of ($^{230}Th/^{232}Th$) in a replenished magma chamber with varying refilling frequencies and no crystallisation or assimilation. All other conditions are constant and as follows: ($^{230}Th/^{232}Th)_{init}$: 0.75, ($^{238}U/^{232}Th$): 1.0, [Th]: 1 μg g^{-1}, Chamber volume: 30 km^3, Input volume: 5 km^3.

(b) - Variation of ($^{230}Th/^{232}Th$) in a replenished magma chamber with varying influx ratios (defined as ratio of influx volume to chamber volume) and no crystallisation or assimilation. All other conditions are constant and as follows: ($^{230}Th/^{232}Th)_{init}$: 0.75, ($^{238}U/^{232}Th$): 1.0, [Th]: 1 μg g^{-1}, Chamber volume: 30 km^3, Refilling period: 10 ka (defined as the time between replenishment events).

primary interest of this study. The results of this modelling are consistent with previous qualitative descriptions (Allègre and Condomines, 1976; Condomines and Allègre, 1980; Condomines et al., 1982).

Repeated replenishment events cause the chemical composition of a system to approach a steady-state (O'Hara, 1977; O'Hara and Mathews, 1981). In the system modelled here, radioactive decay acts similarly to crystallisation in the O'Hara model, and moves the Th isotopic composition of the chamber away from that of the initial parental magma. This means that the system evolves towards a steady-state ($^{230}Th/^{232}Th$) ratio different from that of the replenishing magma, even if crystallisation is not occurring. This steady-state is evident in Figure 2.5 where the range in ($^{230}Th/^{232}Th$) values through which the system oscillates (shown by the different fields) becomes constant.

The effects of changing the model conditions are largely intuitive; e.g. if the frequency of replenishment is increased there is less time between each mixing event for the system to evolve towards secular equilibrium through radioactive decay. Thus the ($^{230}Th/^{232}Th$) ratio of the system is maintained further from the equiline and closer to the input composition. Similarly, if the ratio of input volume to chamber volume is increased, then the ($^{230}Th/^{232}Th$) composition of the input magma has a greater effect on the chamber composition during each mixing event and the system reaches a steady-state with a Th isotopic composition closer to that of the input magma and further away from secular equilibrium.

In practical terms, it is as important to consider the time taken to approach a steady-state as the actual ($^{230}Th/^{232}Th$) composition of the system. Increasing the frequency of replenishment events and increasing the ratio of input volume to chamber volume both have the effect of decreasing the time it takes to approach a steady-state Th isotopic composition. With frequent injections and/or large input volumes, it is perfectly feasible to reach a steady-state Th isotopic composition within a few thousand years. In other systems where conditions are less favourable, it may take a few hundred thousand years to reach a constant ($^{230}Th/^{232}Th$) ratio. In these cases the more important effect in terms of

interpreting real systems is that the system can still deviate considerably from a closed-system evolution curve in a much shorter time.

2.4.3 Crystallisation

The behaviour of U-Th systematics during fractional crystallisation is an important consideration, although the limited partition coefficient data can make it difficult to interpret real systems. The simplest system is one in which both U and Th are treated as highly incompatible elements with the same partition coefficients. For the model presented here the bulk distribution coefficients used are $\overline{D}_U^{cryst/liq} = \overline{D}_{Th}^{cryst/liq} = 0.05$ which have been estimated from the data summarised in Tables 2.1 and 2.2 as typical of much of the published data for partitioning of U and Th into the major rock forming phases (e.g. olivine, pyroxene and plagioclase). Throughout this thesis, the symbols used to denote partition coefficients follow the conventions given by Beattie et al. (1993), which are summarised in Appendix A.

In this instance, illustrated in Figure 2.6, increasing the amount of crystallisation which occurs between each replenishment event, results in the steady-state ($^{230}Th/^{232}Th$) composition of the system moving closer to secular equilibrium and further away from the input composition. This is because the effect of crystallisation in each chamber evolution step is to increase the Th abundance in the magma and therefore for a given ratio of input volume to chamber volume, each new input has a smaller effect on the ($^{230}Th/^{232}Th$) ratio. Changing the partition coefficient has only a small effect on the evolution of the Th isotopic composition of the chamber as long as U and Th remain highly incompatible. In this example, and others used throughout the chapter where crystallisation occurs, the concentrations of U and Th in the magma chamber provide a useful means of checking if the model parameters are viable for a real system. In the examples used in this section, the Th concentrations are $\leq 20\ \mu g\ g^{-1}$ and the U abundances are $\leq 6.5\ \mu g\ g^{-1}$ (in most models these concentrations remain significantly lower, $\leq 10\ \mu g\ g^{-1}$ for Th and $\leq 2.5\ \mu g\ g^{-1}$ for U), which are reasonable for sequences where basalts evolve towards intermediate, andesitic to dacitic compositions.

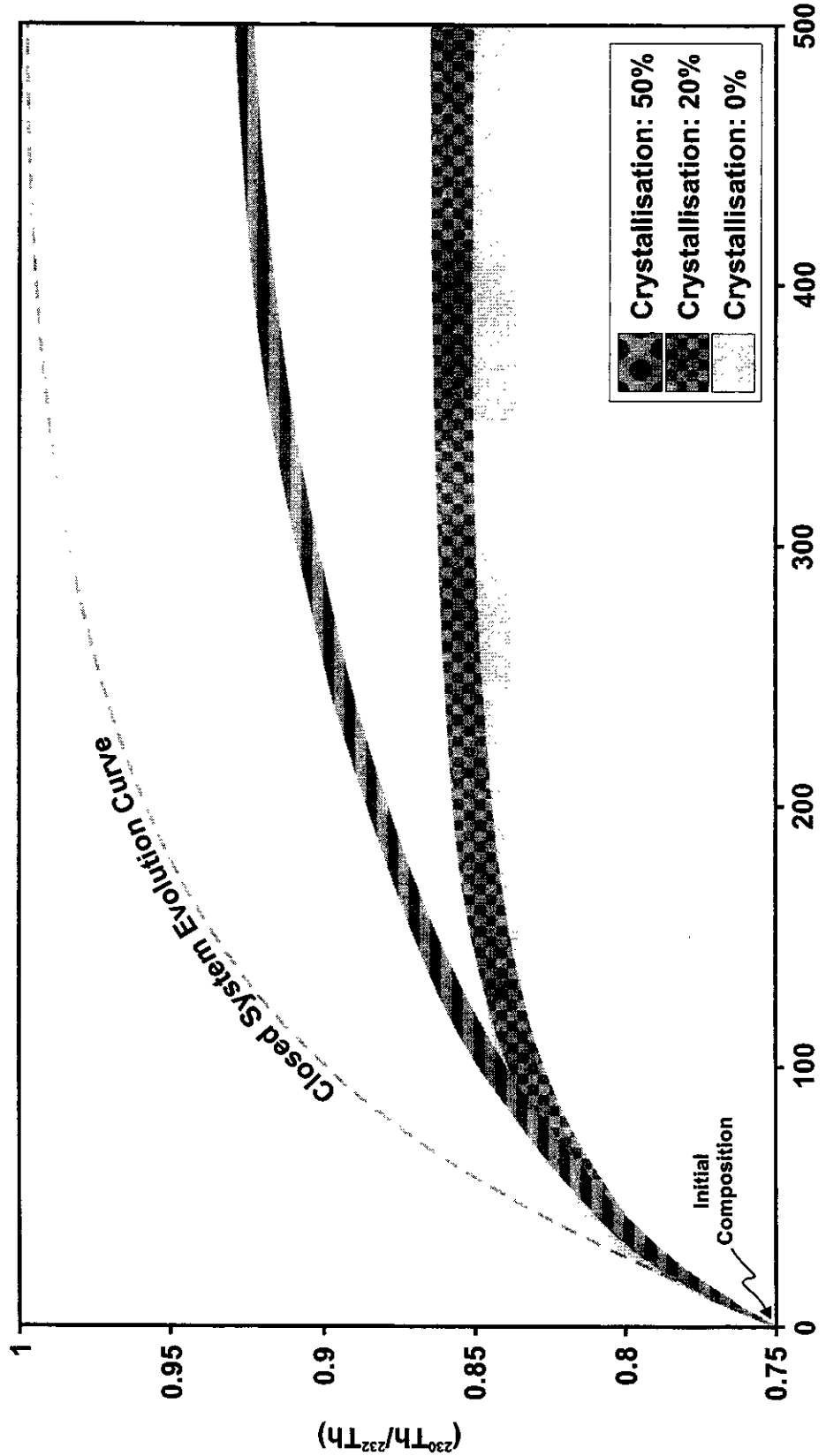

Figure 2.6: Variation of ($^{230}Th/^{232}Th$) in a replenished magma chamber with varying degrees of crystallisation ($D_U = D_{Th} = 0.05$). The closed system evolution curve is valid for any partition coefficient and any degree of crystallisation, provided that $D_U = D_{Th}$. Other model parameters are: $(^{230}Th/^{232}Th)_{init}$: 0.75, ($^{238}U/^{232}Th$): 1.0, [Th]: 1 μg g^{-1}, Refilling period: 10 ka, Chamber volume: 30 km^3, Eruption volume: 5 km^3

The previous situation is probably reasonable for many relatively primitive basalt→basaltic andesite→andesite sequences, where both elements remain highly incompatible in all of the phases crystallising. If the partition coefficients of U and Th are different but both elements are still highly incompatible, the effect on the overall systematics is generally very limited. Even if there is an order of magnitude difference between the bulk partition coefficients, e.g. $\overline{D}_U^{cryst/liq} = 0.05$ and $\overline{D}_{Th}^{cryst/liq} = 0.005$, then 40-50% fractional crystallisation per iteration will only produce a 2-3% shift in the ($^{238}U/^{232}Th$) composition of the magma. It is only if U and/or Th starts to become less incompatible that a significant shift in the ($^{238}U/^{232}Th$) ratio can be achieved with smaller degrees of crystallisation, e.g. $\overline{D}_U^{cryst/liq} = 0.5$ and $\overline{D}_{Th}^{cryst/liq} = 0.05$ will produce a 5% shift in ($^{238}U/^{232}Th$) with only 10% crystallisation.

The above discussion has illustrated that whilst fractional crystallisation can exert a control on the ($^{230}Th/^{232}Th$) ratio of a replenished system, ($^{238}U/^{232}Th$) ratios are only affected to a significant degree if the extent of crystallisation is large or if U and/or Th become reasonably compatible. Whilst constraining the partition coefficients of U and Th in different minerals is difficult, there is a reasonable database of data from both experimental studies and glass/mineral pairs, which is summarised in Tables 2.1 and 2.2.

Generally, major rock forming phases such as pyroxene, olivine and plagioclase have very low partition coefficients for U and Th, and fractionation between these elements can only become significant at very small degrees of partial melting, or high degrees of fractional crystallisation. Some of the data for major phases is quite variable particularly when obtained from real rocks, and some of the estimates of partition coefficients suggest that U and Th are quite compatible even in phases such as plagioclase. However, these high values are likely to reflect the presence of inclusions of melt or minor phases (e.g. Bourdon et al., 1994; Heath et al., 1998b).

Mineral	Rock Type	Ref.	D_{Th}	D_U	$K_{D\ U/Th}$
plagioclase	andestite→dacite	1	0.022-0.106	0.023-0.049	0.386-1.236
plagioclase	olivine basalt→ andesite→dacite	2	0.025-0.137	0.029-0.148	0.834-0.926
plagioclase	andesite	3	0.056	0.057	1.021
plagioclase	andesite	4	0.090	0.099	1.102
plagioclase	basalt→andesite	5	0.045-0.102	0.051-0.127	0.703-2.021
feldspar (sanidine + plag)	phonolite	6	0.052	0.051	0.984
plag (phenocryst)	alkali basalt trachyte	7	0.029-0.948	0.036-0.949	0.967-1.228
plag (groundmass)	alkali basalt	7	0.719	0.705	0.980
plagioclase	basaltic andesite	8	0.085-0.143	0.074-0.114	0.798-0.866
pyroxene	andesite→dacite	1	0.021-0.141	0.020-0.146	0.942-1.069
pyroxene	olivine basalt→ andesite→dacite	2	0.062-0.181	0.065-0.215	0.852-0.954
pyroxene	andesite	3	0.119	0.112	0.941
pyroxene	basalt→andesite	5	0.056-0.854	0.056-0.621	0.440-1.043
pyroxene	phonolite	6	0.123	0.054	0.438
pyroxene	alkali basalt trachyte	7	0.053-0.086	0.050-0.080	0.925-0.95
pyroxene (groundmass)	alkali basalt	7	0.480	0.479	0.998
pyroxene	basaltic andesite	8	0.085-0.143	0.074-0.114	0.798-0.866
pyroxene	phonotephrite	9	0.059-0.096	0.082-0.109	1.115-1.430
amphibole	dacite	1	0.031	0.011	0.363
amphibole	phonolite	6	0.023-0.254	0.010-0.103	0.389-0.407
olivine	olivine basalt	2	0.030	0.027	0.897
olivine	basaltic andesite	8	0.156-0.196	0.129-0.132	0.676-0.822
olivine	phonotephrite	9	0.024	0.027	1.116
magnetic sep.	dacite	1	0.099	0.094	0.946
magnetic sep.	dacite	2	0.032-0.058	0.076-0.112	1.913-2.344
magnetic sep. (phenocryst)	andesite	4	0.140-0.333	0.138-0.266	0.799-1.526
magnetic sep. (groundmass)	andesite	4	0.299-1.014	0.409-0.588	0.579-1.340
magnetic sep.	andesite	3	0.291	0.307	1.057
magnetic sep.	basalt→andesite	5	0.068-0.199	0.077-0.341	0.945-1.714
magnetic sep.	phonolite	6	0.063-0.254	0.028-0.301	0.407-1.259
magnetic sep. (phenocryst)	alkali basalt	7	0.082-0.582	0.098-1.355	0.850-2.721
magnetic sep. (groundmass)	alkali-basalt	7	0.460-2.210	0.841-2.509	0.798-2.533
magnetic sep.	basaltic andesite	8	0.394-0.878	0.381-0.883	0.967-1.006
magnetic sep.	phonotephrite	9	0.062-1.334	0.093-0.131	0.763-1.505
apatite	andesite	5	3.268	2.401	0.731
apatite	phonolite	6	2.504-2.741	1.225-1.269	0.463-0.489
sphene	phonolite	6	2.432-15.74	1.186-5.876	0.373-0.485
haüyne	phonolite	6	0.010-0.017	0.009-0.022	0.932-1.339
leucite	phonotephrite	9	0.032-0.115	0.103-0.214	1.090-3.190

Table 2.1: Partition coefficients for various mineral-groundmass pairs determined as part of U-series dating studies. Where groundmass determinations were not available in the literature, whole rock data were used, which makes the partition coefficients listed maximum values. References are: (1) - Volpe, 1992; (2) - Volpe and Hammond, 1991; (3) - Schaeffer et al., 1993; (4) - Condomines and Allègre, 1980; (5) - Allègre and Condomines, 1976; (6) - Bourdon et al., 1994; (7) - Condomines et al., 1982; (8) - Heath et al., 1998b; (9) - Black et al., 1998.

Mineral	Rock Type	Ref.	D_{Th}	D_U	$K_{D\ U/Th}$
clinopyroxene	basalt	1	0.014	0.0127	0.91
clinopyroxene	basalt	2	0.008-0.036	0.004-0.0146	0.5-0.41
clinopyroxene	basalt	3	0.0014-0.01	0.00007-0.0038	0.05-0.38
clinopyroxene	basalt→andesite	4	0.03	0.04	1.3
olivine	basalt→andesite	5	0.022-0.039	0.04-0.081	1.8-2.1
olivine	chondrule	6	0.000052-0.0063	0.00018-0.0070	3.5-1.1
orthopyroxene	basalt→andesite	5	0.01	0.0013-0.023	0.13-2.3
orthopyroxene	chondrule	6	0.00011-0.058	0.000059-0.079	0.54-1.4
plagioclase	basalt→andesite	5	0.13-0.19	0.051-0.034	0.39-0.18
plagioclase	basalt→andesite	4	0.01	0.01	1
garnet	basalt	7	0.0010-0.0032	0.00918-0.00179	0.01-0.56
garnet	basalt	1	0.00137	0.00588	4.3
garnet	basalt	8	0.0017	0.015	8.8
sphene*	trachyte	9	17.1	9.9	0.58
magnetite*	hawaiite	10	0.1	0.11	1.1
magnetite*	mugearite	10	0.13	0.16	1.2
magnetite*	trachyte	9	0.06	0.12	2
amphibole	andesite	11	0.017	0.008	0.47
amphibole	basalt→andesite	4	0.5	0.1	0.2
amphibole*	hawaiite	10	0.02	0.03	1.5
amphibole*	mugearite	10	0.01	0.02	2
zircon	leucosome	12	22.1	254	11.5
apatite	leucosome	12	41	43.7	1.1
apatite	pantellerite	13	1.6	2.6	1.6

Table 2.2: Selection of typical partition coefficients for U and Th determined by mainly by experimental techniques. Samples marked by a asterisk have been determined from rock samples. Data taken from a larger database of partition coefficients obtained from the GERM homepage (http://www-ep.es.llnl.gov/germ). References are: (1) – Hauri et al., 1994; (2) – LaTourrette and Burnett, 1992; (3) – Lundstrom et al., 1994; (4) – Dostal et al., 1983; (5) – Dunn and Sen, 1994; (6) – Kennedy et al., 1993; (7) – Beattie, 1993; (8) – LaTourrette et al., 1993; (9) – Luhr et al., 1984; (10) – Lemarchand et al., 1987; (11) – Brenan et al., 1995; (12) – Bea et al., 1994; (13) – Mahood and Stimac, 1990.

Where phenocryst and groundmass phases have been analysed separately (Condomines and Allègre, 1980; Condomines et al., 1982), there is some suggestion that the groundmass phases generally have higher partition coefficients, although whether this is a crystallisation feature or just represents imperfect separation between the crystal phases and groundmass glass remains uncertain.

Certain accessory phases commonly present in igneous rocks, such as apatite, sphene or zircon are able to take large tetravalent cations such as U and Th into their crystal lattice relatively easily, and so they have high partition coefficients. The most common minor phases in volcanic rocks are Fe-Ti oxides (Gill, 1981), which have quite variable but relatively small partition coefficients. Whilst magnetite has proved to be a

useful mineral in producing mineral isochrons, because it tends to fractionate U from Th, it is unlikely that fractional crystallisation of Fe-Ti oxides will have much effect on the whole rock U/Th ratios.

In most volcanic systems, it is unlikely that crystallisation of accessory phases in which U and Th are compatible is extensive enough to cause significant fractionation. In andesites and more primitive rocks, these minor phases generally make up less than 1% of the crystallising assemblage (Gill, 1981), unless the composition of the magma is unusual. However, in more evolved compositions where crystallisation of accessory phases can become more important, it is useful to consider the effects of such crystallisation. A rough calculation (using typical values from Tables 2.1 and 2.2) in a system with a crystallising assemblage made up of 50% plagioclase ($D_U^{plag} = D_{Th}^{plag} = 0.05$), 35% pyroxene ($D_U^{pyx} = D_{Th}^{pyx} = 0.05$), 10% olivine ($D_U^{ol} = D_{Th}^{ol} = 0.01$) and 5% apatite ($D_U^{ap} = 2.4, D_{Th}^{ap} = 3.25$) shows that the presence of apatite raises the bulk partition coefficients by a factor of ~3.5 for U and ~4.5 for Th ($\overline{D}_U^{cryst/liq} = 0.164$, $\overline{D}_{Th}^{cryst/liq} = 0.206$). Whilst both elements are still incompatible, the difference in partition coefficient is sufficient that 20% fractional crystallisation of such an assemblage will produce a detectable (~2%) shift in ($^{238}U/^{232}Th$) ratio. When such a shift is multiplied over numerous injections, it can become more significant. It is also worth noting that the effect of phases such as zircon will be significantly more extreme because of their much higher partition coefficients, but they only tend to crystallise in high-Si magmas.

It is clear that the presence of certain accessory phases in the crystallising assemblage, even in small quantities, can have an identifiable effect on U-Th systematics. This is modelled for both replenished and non-replenished systems and for two different pairs of partition coefficients which approximate the effects of accessory phase fractional crystallisation. These models are illustrated on three diagrams; an equiline diagram (Figure 2.7a), a Th isotope evolution diagram (Figure 2.7b) and a diagram showing the variation of degree of disequilibrium, ($^{230}Th/^{238}U$) ratio, with time (Figure 2.7c) hereafter termed a disequilibrium evolution diagram. The curves illustrated on the equiline diagram represent the 200 ka time periods shown in the other plots.

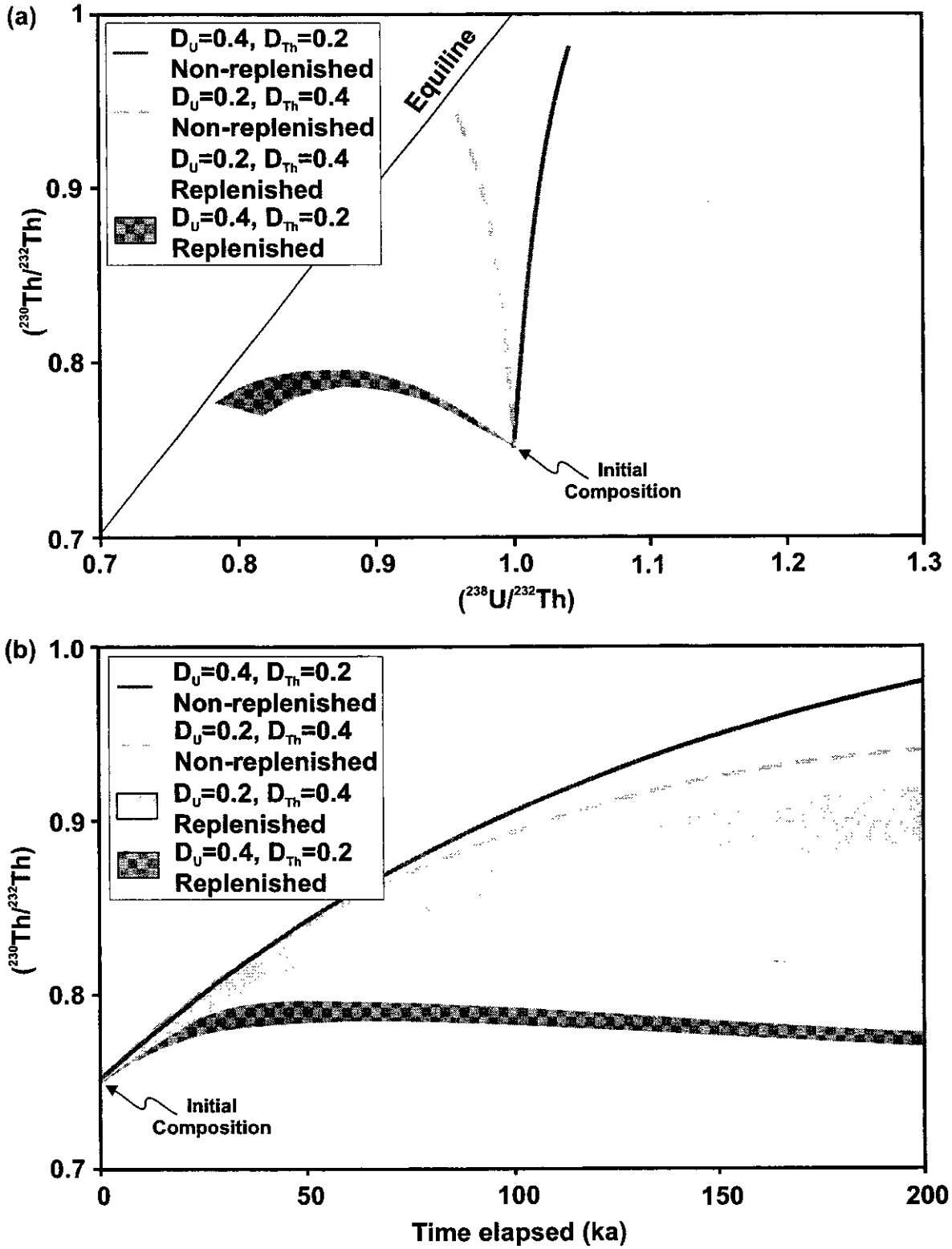

Figure 2.7:

(a) - Variation of U-series systematics on an equiline diagram with different crystallisation conditions. Other than indicated in the key, the model conditions are as follows: $(^{230}Th/^{232}Th)_{init}$: 0.75, $(^{238}U/^{232}Th)_{init}$: 1.0, $[Th]_{init}$: 1 μg g^{-1}, Chamber volume: 30 km^3, Input volume: 11 km^3, Refilling period: 10 ka, f_{cryst}: 0.2.

(b) - Variation of $(^{230}Th/^{232}Th)$ ratio with time. All conditions where not indicated in the key are the same as for (a).

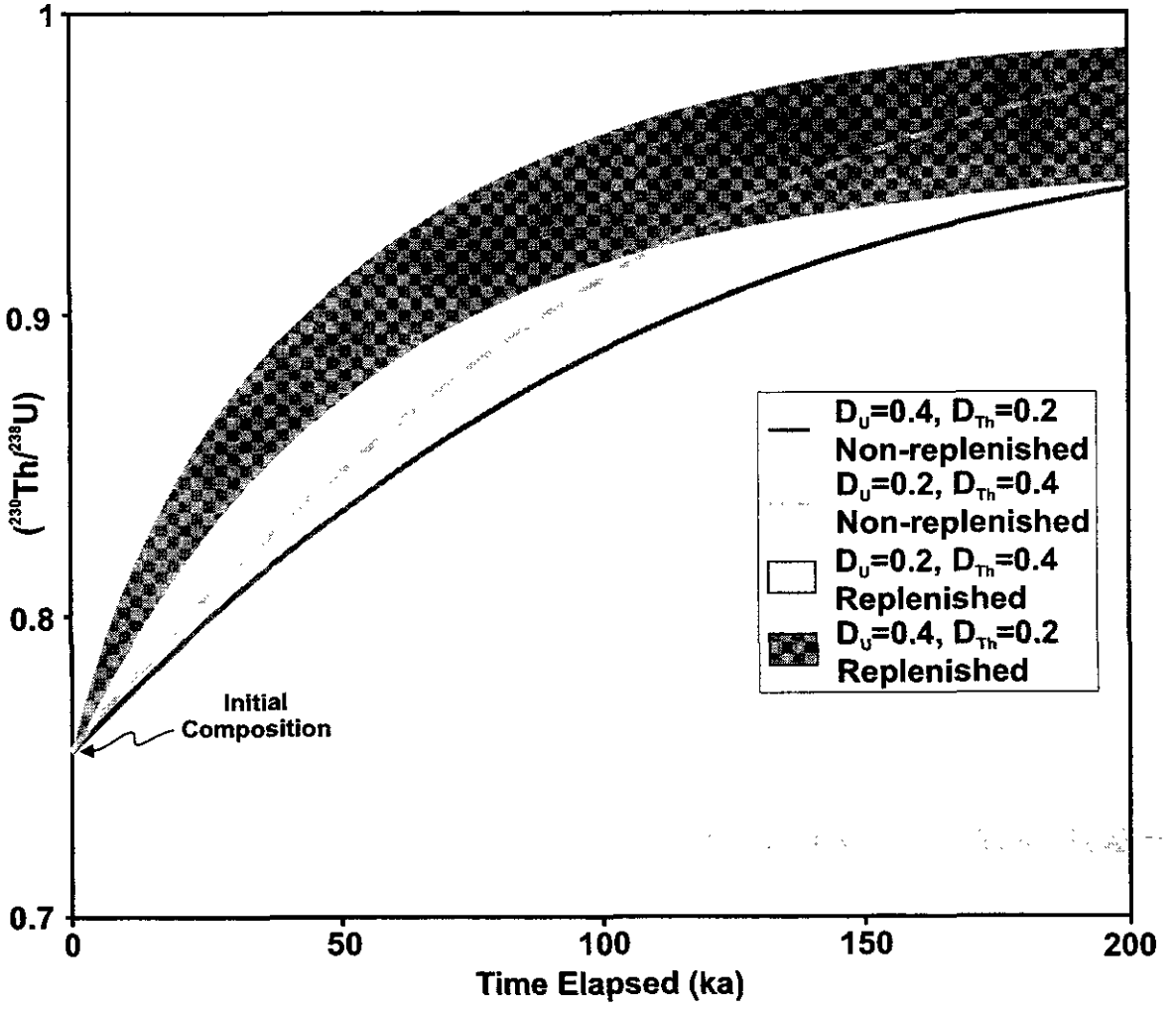

Figure 2.7 (cont):

(c) - Disequilibrium evolution diagram for various crystallisation conditions, showing the change in ($^{230}Th/^{238}U$) ratio through time. All conditions not shown in the key are the same as for Figure 2.7a.

Even in a non-replenished system, with only 20% crystallisation, it is apparent that the differences in partition coefficient are sufficient to produce a detectable difference on an equiline diagram (Figure 2.7a). The resulting differences in ($^{230}Th/^{232}Th$) ratio over time are very small, however, because the shift in ($^{238}U/^{232}Th$) ratio are not large enough to greatly affect the change in ($^{230}Th/^{232}Th$) ratio through radioactive decay (Figure 2.7b). Similarly, only very small differences in ($^{230}Th/^{238}U$) ratio are observed between the two non-replenished systems (Figure 2.7c).

The effects of multiple replenishment events is more extreme, producing shifts of ~20% in ($^{238}U/^{232}Th$) after 20 replenishment events. With U more compatible than Th, the composition of the system moves rapidly towards the equiline, and thus whilst the ($^{230}Th/^{232}Th$) ratio of the system stays almost constant in this example, the system approaches a steady-state ($^{230}Th/^{238}U$) ratio very close to secular equilibrium. In the replenished system with Th more compatible than U, the composition of the magma in the chamber moves subparallel to the equiline. Mixing in each replenishment event occurs almost along the reverse vector to combined radioactive decay and fractional crystallisation, producing a locus of compositions close to a straight line. The system approaches a steady-state ($^{230}Th/^{232}Th$) value after 150-200 ka and the value is similar to that in the non-replenished models. However, the latter approaches a steady-state ($^{230}Th/^{238}U$) composition after just 50 ka.

The effects of crystallisation on Ra-Th disequilibrium are essentially the same as for the ^{230}Th-^{238}U system. It is generally thought that Ra has a very similar partitioning behaviour to Ba (Williams et al., 1986), and therefore by comparing $\overline{D}_{Ba}$ and $\overline{D}_{Th}$ for a given crystallising assemblage, it is possible to estimate the degree of fractionation Ra and Th will undergo. A range of partition coefficients for Ba in different minerals and rock types is given in Table 2.3, which shows that in pyroxene, olivine and garnet, Ba is highly incompatible. In plagioclase, amphibole and apatite, Ba can become relatively compatible, and by inference these phases also ought to have something of a preference for Ra. In biotite, and particularly alkali feldspar, Ba becomes highly compatible which implies that these phases have the ability to produce significant fractionation of Ra and Th. It is in

systems where abundant crystallisation of alkali feldspar has occurred that large fractionations of Ra and Th are observed (Reagan et al., 1992; Evans, 1999).

Phase	Rock Type	Ref.	D_{Ba}
clinopyroxene	basalt	1	0.0058
clinopyroxene	basalt	2	0.00068
olivine	andesite	3	0.000043-0.0082
olivine	basalt→andesite	4	0.0000013-0.000032
orthopyroxene	basanite	5	0.02
orthopyroxene*	rhyolite	6	0.063-0.084
plagioclase	basalt→andesite	7	0.38-1.45
plagioclase	rhyolite	8	1.07-18.38
plagioclase*	andesite	6	0.56
garnet	basalt	1	0.0007
K-feldspar*	rhyolite	6	1.7-20.9
K-feldspar*	peralkaline rhyolite	6	3.5-18.9
K-feldspar	rhyolite	9	22
K-feldspar	rhyolite	10	1-44
amphibole	andesite	11	0.12
amphibole	basanite	12	0.46
amphibole*	rhyolite	6	0.16-4.5
biotite	basanite	13	3.68
biotite*	rhyolite	6	6.4
apatite*	pantellerite	14	0.45
apatite*	trachyte	15	< 0.3

Table 2.3: Partition coefficients for Ba in a range of minerals in different rock types. Where the phase is marked by an asterisk, the partition coefficient has been determined mineral/matrix comparisons in rock samples, otherwise the coefficients have been determined by experimental studies. Data are taken from a larger compilation obtained from the GERM homepage (http://www-ep.es.llnl.gov/germ). References are: (1) – Hauri et al., 1994; (2) – Hart and Dunn, 1993; (3) – Kennedy et al., 1993; (4) – Beattie, 1994; (5) – Green et al., 1993; (6) – Ewart and Griffin, 1994; (7) – Dunn and Sen, 1994; (8) – Icenhower and London, 1996; (9) – Leeman and Phelps, 1981; (10) – Stix and Gorton, 1990; (11) – Brenan et al., 1995; (12) – Adam et al., 1993; (13) – LaTourrette et al., 1995; (14) – Mahood and Stimac, 1990; (15) – Luhr et al., 1984.

2.4.4 Assimilation

The assimilation of local crust by basaltic magmas has long been considered a major petrogenetic process following the suggestion of Bowen (1928) that melting of the crust would occur in response to the release of latent heat during crystallisation. More recently, considerable effort has been devoted to identifying the processes which have a significant effect on the systematics of various radiogenic and stable isotopes. The link between crystallisation and assimilation led some authors to put forward numerical models for the behaviour of trace elements and isotope systematics during so called AFC or combined assimilation and fractional crystallisation (Allègre and Minster, 1978; DePaolo, 1981).

Most of the U-series studies of igneous systems which have been undertaken so far have concentrated on rocks where assimilation is inferred to have been a very minor process, if it operated at all. Consideration of AFC processes with short-lived isotopes is more complex than with conventional isotopes, because it is necessary to consider a time element in addition to the normal factors involved with AFC modelling.

The model outlined in this chapter deals with assimilation in a slightly different way to that of DePaolo (1981). The formulation of the published model allows the use of any value for the ratio of the mass of crust assimilated to the mass crystallised (r). Most commonly however, the AFC equations have been applied to systems where the mass of magma crystallised is greater than the mass of crust assimilated and thus $(r) < 1$. Conventionally therefore, AFC curves have been plotted for various amounts of mass of liquid remaining (F). Because the model presented here is designed to have a constant volume after each mixing event, this approach is not directly applicable. However it is possible to calculate the effective value of r and F for a given chamber evolution step and check that the same results are obtained using this model as in the model of DePaolo (1981).

Thus, if a non-replenished system with a volume of 30 km^3, $(^{238}U/^{232}Th) = 1.0$, $(^{230}Th/^{232}Th) = 0.75$ and $[Th] = 1\ \mu g\ g^{-1}$ undergoes 20% crystallisation and assimilates 2 km^3 of upper continental crust, assumed to be in secular equilibrium with $[U] = 2.8\ \mu g\ g^{-1}$, $[Th] = 10.7\ \mu g\ g^{-1}$ (Taylor and McLennan, 1995), then the calculated parameters in terms of the DePaolo model are $r = 0.355$ and $F = 0.879$. If the time for a chamber evolution step is set to 1 year, i.e. effectively instantaneous, it is possible to check the model used here against that of DePaolo. This modelling yields $[U] = 0.5828\ \mu g\ g^{-1}$, $[Th] = 1.934\ \mu g\ g^{-1}$ and $(^{230}Th/^{232}Th) = 0.7683$ in the liquid, which compares with values obtained using the DePaolo model of $[U] = 0.5823\ \mu g\ g^{-1}$, $[Th] = 1.9329\ \mu g\ g^{-1}$ and $(^{230}Th/^{232}Th) = 0.7683$, demonstrating that the model developed here produces reasonable estimates for continuous AFC using an iterative approach.

Whilst the discussion throughout this section concentrates on assimilation of local basement rocks by crystallising magmas, this is in essence a specific type of magma

mixing, where there is an implied link between the two magmas. However, the modelling described below could equally apply to the modelling of general magma mixing, where no genetic connection between the components is implied. As mentioned earlier, non-instantaneous mixing may be an important consideration in some systems, particularly where ^{226}Ra-^{230}Th data is being used. The assimilation modelling undertaken here can also be thought of as demonstrating the effects on mixing trends of such a process.

2.4.4.1 Non-replenished Systems

The system modelled here is similar to that used in the above comparison. Two different assimilants have been used, both estimates of bulk upper continental crust composition (Taylor and McLennan, 1981; Taylor and McLennan, 1995), and both assumed to be in U-Th isotope equilibrium. They have been chosen simply because they provide compositions with higher and lower ($^{230}Th/^{232}Th$) ratios than the primary magma composition used, and thus allow the model to be illustrated for two different generalised possibilities.

Figure 2.8 presents the results of modelling AFC processes in non-replenished magma chambers for a range of timescales. In each of the diagrams, the path followed by the magma in the chamber in response to continuing assimilation and fractional crystallisation is indicated by the filled symbols. In each case, instantaneous AFC curves calculated using published models (DePaolo, 1981) are shown for reference. The principal effect of adding time to the AFC equations is to produce magma evolution curves which do not trend towards the assimilant composition because of the additional effect of radioactive decay.

However, if the fractionating system were sampled by eruption at various time intervals, these samples would then evolve through simple radioactive decay and move vertically towards the equiline. The results of such a situation are illustrated in Figure 2.8 by the open symbols, which are the present day compositions of the rocks erupted from the chamber at the different time increments. The interesting feature which is immediately observed is that a series of such samples in fact falls on a straight line, and if a reference

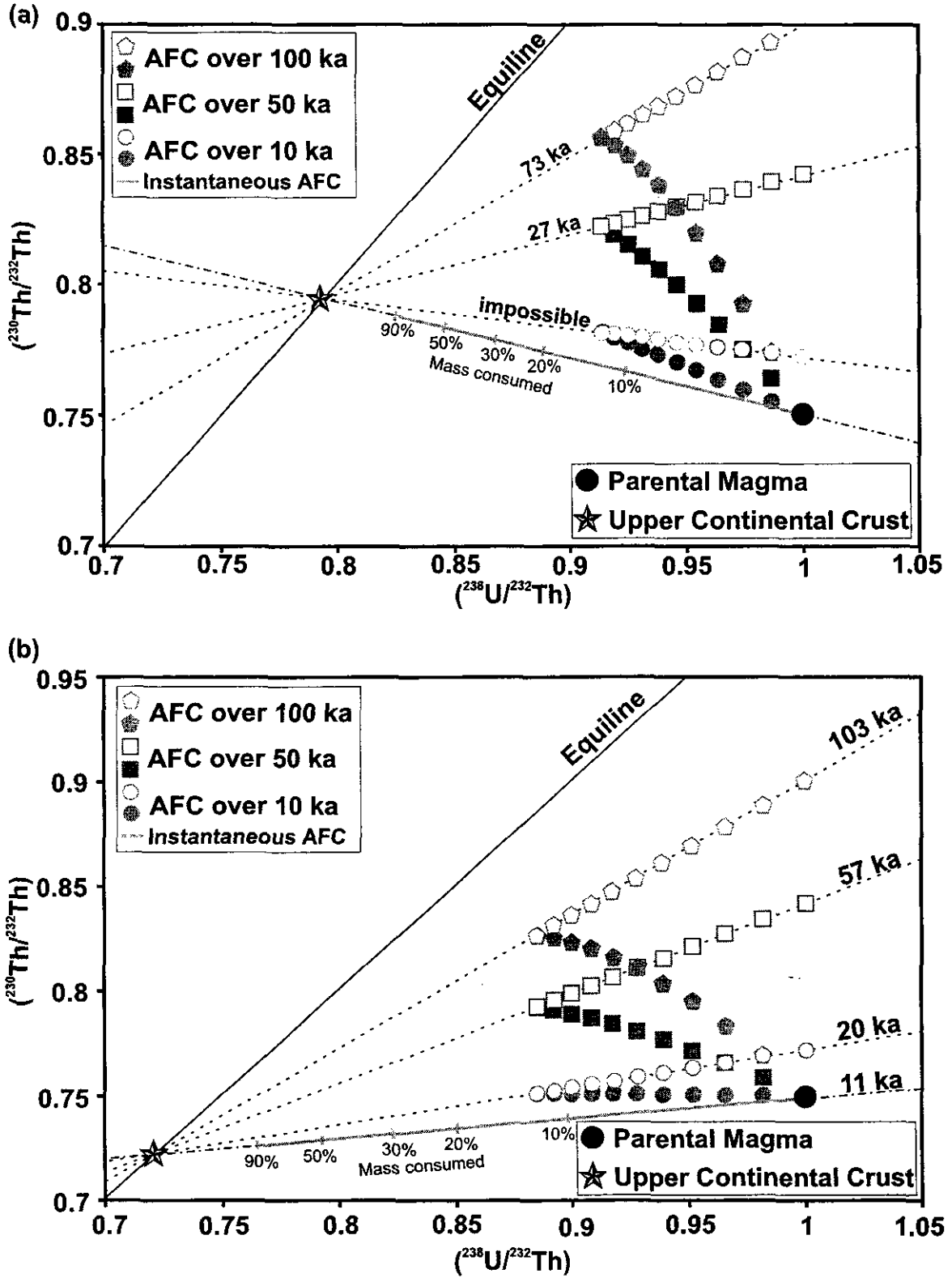

Figure 2.8: Combined assimilation-fractional crystallisation (AFC) models for ^{230}Th-^{238}U disequilibrium in non-replenished systems. For each model, the filled symbols represent a magmatic system evolving with time, and the open symbols show an age corrected line assuming the system is sampled through time. The filled symbols are at time intervals of 1000, 5000 and 10000 years for the 10 ka, 50 ka and 100 ka curves respectively. Upper continental crust in (a) is taken from Taylor & McLennan (1995) and in (b) from Taylor and McLennan (1981). The instantaneous AFC curves are calculated using the equations of DePaolo (1981). The model conditions are as follows: $(^{230}Th/^{232}Th)_{init}$: 0.75, $(^{238}U/^{232}Th)_{init}$: 1.0, $[Th]_{init}$: 1 μg g^{-1}, Chamber volume: 30 km^3, Assimilant volume: 2 km^3, $D_{Th} = D_U = 0.05$, f_{cryst}: 0.2

line is fitted through the points, it always crosses the equiline at the composition of the assimilant. Also shown in Figure 2.8 are the ages which would be obtained if these lines were treated as isochrons. These ages clearly have little meaning without good constraints on the amount and composition of the assimilant, and demonstrate the care which must be taken in interpreting such trends in real data.

2.4.4.2 Replenished Systems

The effects of AFC in replenished systems are shown in Figure 2.9 for a range of crystallisation conditions. In the case of no crystallisation and crystallisation with $\overline{D}_U^{cryst/liq} = \overline{D}_{Th}^{cryst/liq} = 0.05$ the evolution is relatively simple, with crystallisation in the latter case effectively reducing the influence of the assimilant because the elemental abundances of U and Th in the chamber are higher than with crystallisation absent. In both cases, the replenishment vector is almost opposite the vector followed during AFC without replenishment, and thus narrow trends are produced.

Where similar models to those used to demonstrate possible effects of accessory phase crystallisation are used, the evolution of the system on an equiline diagram is considerably more complex. When Th is more compatible than U, there is a contest between crystallisation and assimilation trying to move the system in opposite directions on the equiline diagram. This contest is initially won by the assimilation process, but as the concentration of U and Th in the chamber begins to increase, crystallisation begins to dominate more. In the opposite case where U is more compatible than Th, the combined effect of crystallisation and assimilation is sufficient in this instance to pull the system across the equiline.

The different models also have very different trends on a Th isotope evolution diagram and a disequilibrium evolution diagram (Figures 2.9b and 2.9c respectively). Both the model without crystallisation and the model with $\overline{D}_U^{cryst/liq} = \overline{D}_{Th}^{cryst/liq} = 0.05$ show little variation in ($^{230}Th/^{232}Th$), whereas the other two models show greater variation, but in opposite directions, with ($^{230}Th/^{232}Th$) increasing in the model where the bulk partition coefficient of Th is greater than the bulk partition coefficient of U. These latter two models

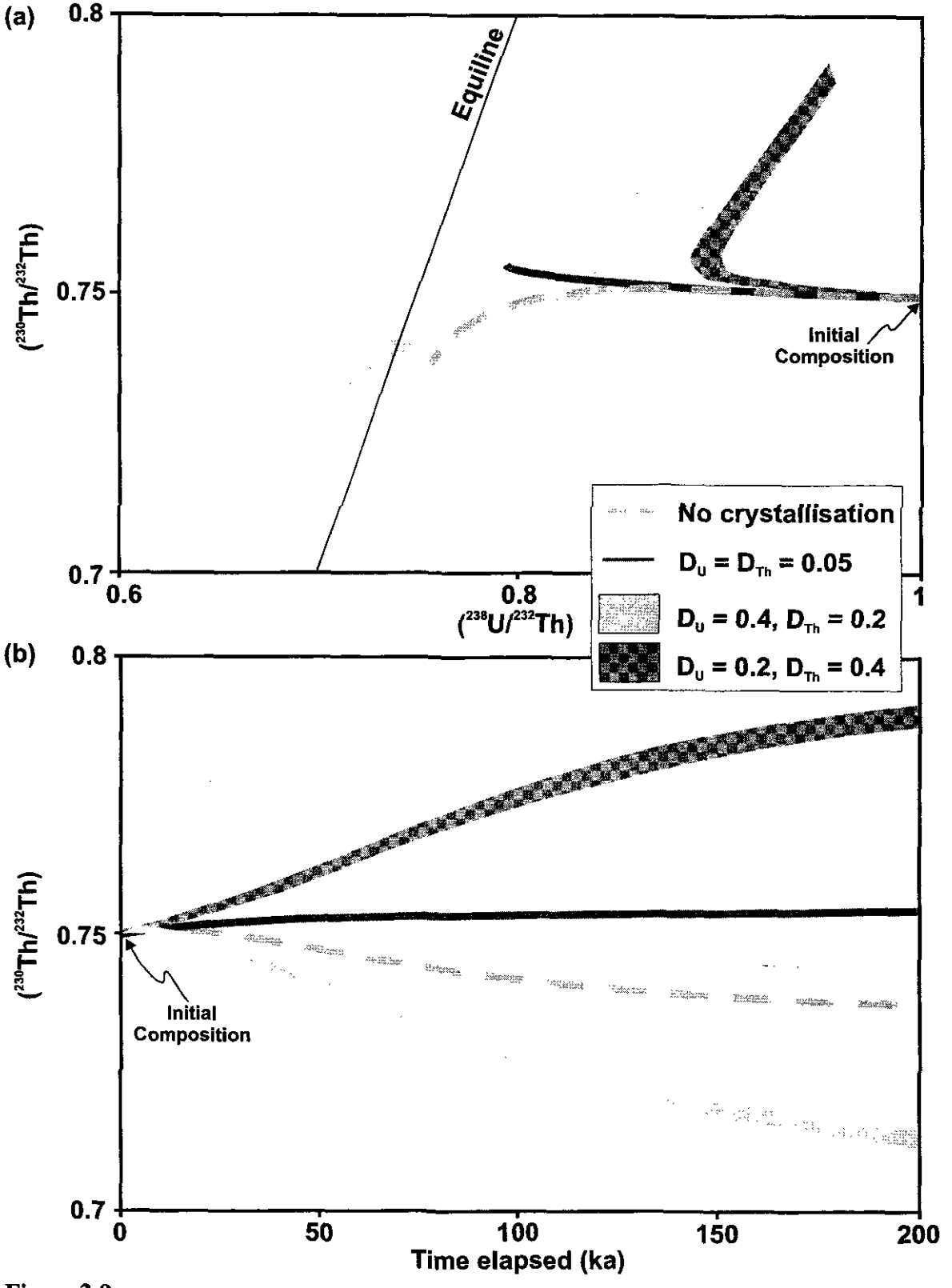

Figure 2.9:

(a) - The combined effects of crystallisation and assimilation in a replenished magma chamber. All model conditions not in the key are as follows: $(^{230}Th/^{232}Th)_{init}$: 0.75, $(^{238}U/^{232}Th)_{init}$: 1.0, $[Th]_{init}$: 1 μg g^{-1}, $f_{cry's}$: 0.2, Chamber volume, 30 km^3, Input volume: 9 km^3, Assimilation volume: 2 km^3, $[Th]_{assim}$: 10.5 μg g^{-1}, $[U]_{assim}$: 2.5 μg g^{-1}. The assimilant was assumed to be in secular equilibrium. The assimilant composition used was upper continental crust after Taylor & McLennan (1981) - see text for a full discussion.

(b) - The combined effects of crystallisation and assimilation on a Th isotope evolution diagram. All model conditions and data sources are as for (a).

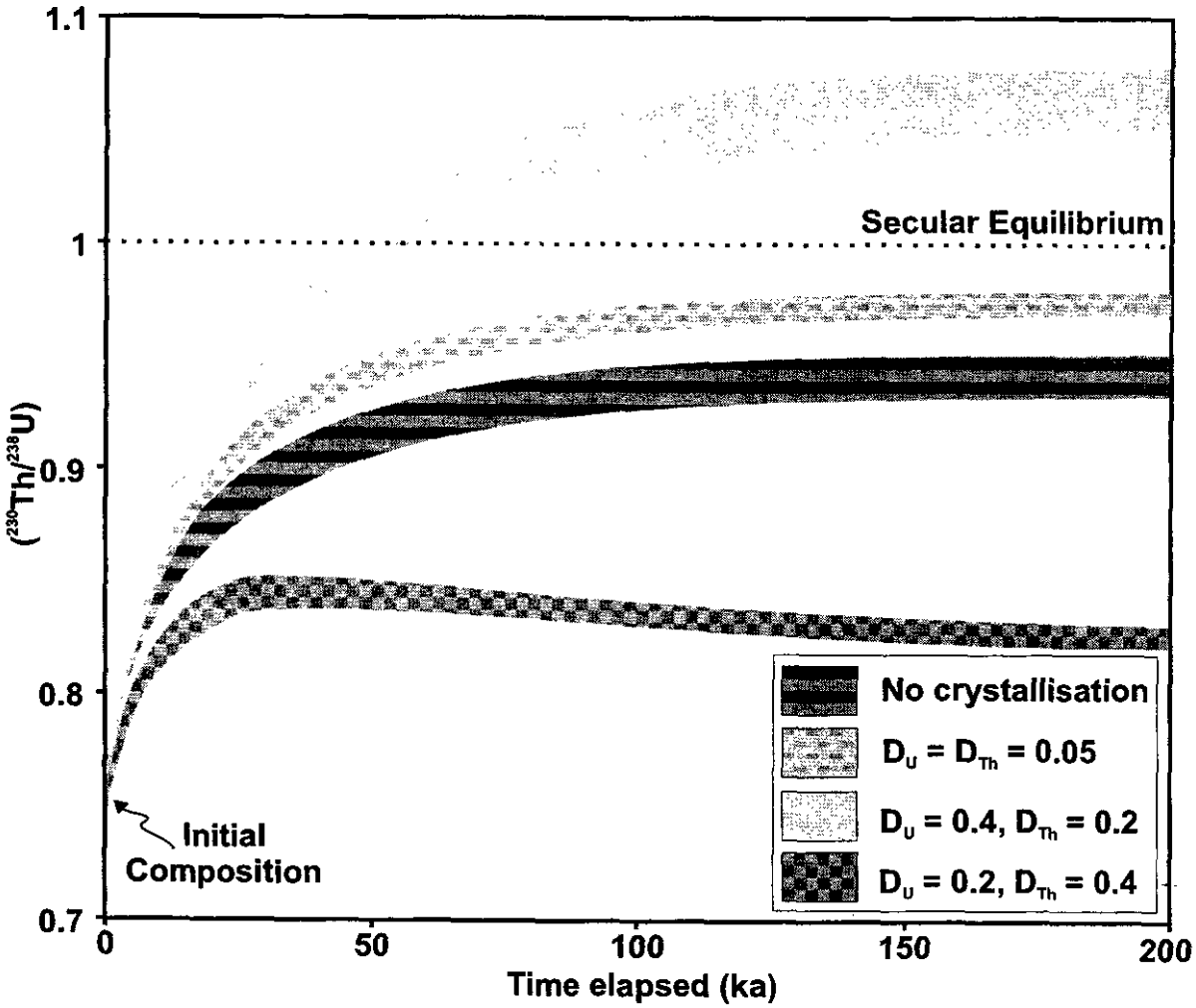

Figure 2.9 (cont.):

(c) - The effects of AFC on U-Th disequilibrium in a replenished magma chamber. All conditions not indicated in the key are the same as for Figure 2.9a.

approach a steady-state ($^{230}Th/^{232}Th$) composition more slowly than the first two, and the Th isotopic ratios are still evolving after 200 ka. On the disequilibrium evolution diagram, the models without crystallisation and with equal bulk partition coefficients for both U and Th again show very similar trends, approaching steady-state ($^{230}Th/^{238}U$) ratios after ~100 ka, with values close to secular equilibrium. In the model where $\overline{D}_U^{cryst/liq} < \overline{D}_{Th}^{cryst/liq}$ the degree of disequilibrium initially decreases and then begins slowly to increase again, approaching a steady-state ($^{230}Th/^{238}U$) composition after ~150 ka. The final model rapidly moves towards secular equilibrium, but crosses the equiline as seen in Figure 2.9a, and approaches a steady-state ($^{230}Th/^{238}U$) composition again after ~150 ka.

2.4.4.3 Assimilant Composition: in Secular Equilibrium?

The discussion so far has assumed that the assimilant is in secular equilibrium. If bulk assimilation of local basement occurs, then this is reasonable. However, many studies have demonstrated that bulk assimilation isn't sufficient to generate the observed geochemical signatures, and that partial melts of the basement are more reasonable contaminants (e.g. Graham and Hackett, 1987; Preston et al., 1998). In this instance, it is possible that the assimilant will not be in secular equilibrium, dependant on the mineralogy of the residue and the degree of melting. Using conventional melting models, it would be expected that U and Th would partition readily into the melt, and the generation of an assimilant in disequilibrium would require both a residual accessory phase with a preference for either U and/or Th and a small degree of melting. However recent work looking primarily at the generation of crustal melt granites requires further discussion.

There have been a wide range of studies which have investigated partial melting of continental crust. Recently, it has been appreciated that the behaviour of U and Th (and also Y and the REE) during crustal melting is highly dependant on the mineralogy of the source rocks (e.g. Bea, 1996; Ayres and Harris, 1997). It has been shown that in granites and crustal protoliths the U and Th budgets are controlled by certain accessory phases, such as monazite, allanite, xenotime, zircon and Th-silicates, which can frequently contain > 70% of the total U and Th despite forming only a tiny fraction of the whole assemblage (Bea, 1996).

These accessory phases are unusual because U, Th and REE's form essential structural components (ESC's) of the mineral lattices. During melting and crystallisation, the behaviour of these elements does not follow Henry's Law, and thus standard models which depend on partition coefficients are not applicable (Bea, 1996; Ayres and Harris, 1997). The principle controls on the behaviour of U and Th during melting are therefore dependant on the dissolution kinetics of the minor phases and their physical location, commonly either as inclusions or around the boundaries of other phases (Bea, 1996). Various studies have demonstrated that melting a protolith which contains very small abundances of accessory phases with U and Th as ESC's can readily fractionate these elements (Rapp and Watson, 1986; Bea, 1996). It is therefore possible that assimilants produced by partial melting of local basement can be in U-Th disequilibrium.

The lack of data for Ra in different phases means that it is almost impossible to make any predictions about its behaviour during melting. The best predictions about the chemical behaviour of Ra suggest that it should be similar to Ba, although it does have a somewhat larger ionic radius. Except in unusual circumstances (e.g. melting of a protolith containing barite or another Ba phase), it is unlikely that the Ba budget of a protolith is dominated by phases in which it is an ESC, and thus Ba and therefore Ra should follow normal melting models. However, as the behaviour of Th may well be controlled as described above, it may well still be relatively easy to produce assimilants which are not in secular equilibrium.

If the contaminant is out of secular equilibrium two end-member cases can be envisaged. In one case, if partial melts of the host rock are continually generated and mixed rapidly, it isn't necessary to account for the effects of radioactive decay on the ($^{230}Th/^{232}Th$) ratio of the assimilant, whereas the ($^{230}Th/^{232}Th$) composition of the magmatic system will be evolving towards secular equilibrium. The second end-member assumes that partial melting occurs once, and that the resulting melt is mixed slowly into the magma system over time. In this case, it is important to take into account the effects of radioactive decay on the ($^{230}Th/^{232}Th$) ratios of both the contaminant and the magma system.

The degree to which the choice of end-member model affects the U-Th systematics of the evolving magma body is dependant on the degree of disequilibrium in the assimilant, although the difference is generally limited unless the disequilibrium in the assimilant is fairly extreme. A larger U-Th disequilibrium in the contaminant will produce a greater difference between the evolution paths followed using the two methods. In the example illustrated in Figure 2.10a, the assimilant has an initial ($^{230}Th/^{238}U$) ratio of ~0.9, and at any given time the evolution curves produced using the two models have < 1% variation in ($^{230}Th/^{232}Th$) ratio.

The main difference is observed when post-eruptive radioactive decay is allowed for in a similar fashion to that used in Figure 2.8. This is illustrated in Figure 2.10b, which shows that the resulting linear correlation does not pass through the composition of the assimilant when continuous melting and mixing is assumed. In contrast, if the contaminant is allowed to evolve through radioactive decay, the resulting linear trend passes through the composition of the assimilant at the end of the evolution period.

2.4.5 Combined ^{230}Th-^{238}U and ^{226}Ra-^{230}Th Systematics

The combination of two short-lived isotope schemes which operate over different timescales, presents the possibility of quite different behaviour depending on the timescales of the processes previously discussed and the initial composition of the magma in each of the short-lived isotope systems. A question of considerable interest is whether it is possible to maintain a magma in both U-Th and Ra-Th disequilibrium over long periods of time through crustal processes, or whether if both systems are in disequilibrium it either implies a very short melting and transfer time, or decoupling between the systems.

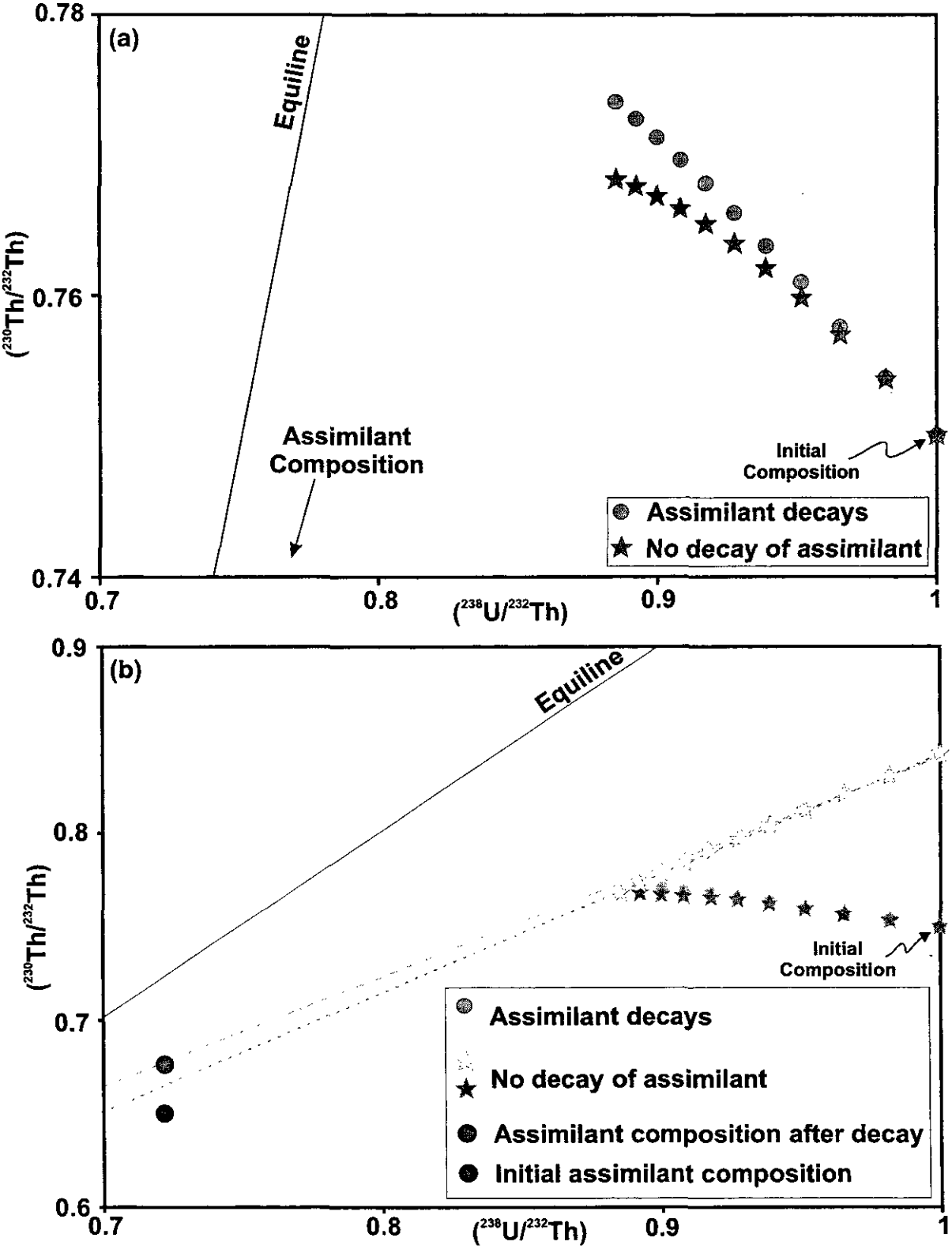

Figure 2.10:

(a) - Equiline diagram showing the effects of crustal assimilation, with a contaminant which is out of secular equilibrium. Two models are shown as described in the text. The shaded field represents a 1% variation about the lower curve for reference. The assimilant composition is calculated from the upper continental crust composition of Taylor and McClennan (1981), assuming a $(^{230}Th/^{232}Th)$ ratio of 0.65. The model conditions are: $(^{230}Th/^{232}Th)_{init}$: 0.75, $(^{238}U/^{232}Th)_{init}$: 1.0, $[Th]_{init}$: 1 $\mu g\ g^{-1}$, f_{cryst}: 0.2: $D_U=D_{Th}=0.05$, Chamber volume: $30km^3$, Assimilant volume: $2km^3$.

(b) - Equiline diagram showing curves corrected for radioactive decay as in Figure 2.8 and described in the text. All model conditions as for (a).

The majority of studies which have looked at ^{230}Th-^{238}U disequilibria have attributed both U- and Th- excesses to processes occurring in mantle sources at the time of melt generation (e.g. Condomines et al., 1988; Chabaux and Allègre, 1994). The origin of ^{226}Ra-^{230}Th disequilibria is less clearly established. Some authors have linked ^{226}Ra-^{230}Th disequilibria to melting conditions and source processes, particularly in primitive systems where limited fractional crystallisation of plagioclase has occurred (Chabaux and Allègre, 1994), or where mixing of different components in the source is inferred to have occurred (Clark et al., 1998). However, other studies have required crustal level processes in order to explain the behaviour of ^{226}Ra-^{230}Th, or differences between ^{230}Th-^{238}U and ^{226}Ra-^{230}Th systematics (e.g. Reagan et al., 1992; Condomines et al., 1995; Black et al., 1998).

Given the uncertainty regarding the source of Ra-Th disequilibrium in many cases, this discussion will be illustrated with two relatively simple examples. The first of these looks at a non-replenished system, which is assumed to have a crystallising assemblage made up from 50% olivine and pyroxene, and 50% plagioclase. The bulk partition coefficients are assumed to be equal for Ra and Ba ($\overline{D}_{Ra}^{cryst/liq} = \overline{D}_{Ba}^{cryst/liq} = 0.25$), and the system is assumed to undergo 50% fractional crystallisation over a range of different timescales. The system has the same initial U-Th disequilibrium as used in previous models, but is assumed to be in Ra-Th equilibrium.

The results of the modelling are shown on a Ra equiline diagram in Figure 2.11a and a plot of ($^{230}Th/^{238}U$) vs ($^{226}Ra/^{230}Th$) in Figure 2.11b. On the equiline diagram, the model which was run for a 1 ka duration shows as expected only a small change in (^{226}Ra)/[Ba] because of the short time period, but an increase in (^{230}Th)/[Ba] as a result of plagioclase fractional crystallisation. The other two models both show progressively greater changes in (^{226}Ra)/[Ba] with increasing model duration. Both models clearly move towards a trend which is parallel to the equiline but in ^{230}Th excess. In Figure 2.11b, this is seen clearly, where the model which was run for a 20 ka duration approaches a steady-state ($^{226}Ra/^{230}Th$) composition close to equilibrium with ~2% ^{230}Th excess, but the degree of U-Th disequilibrium decreases with radioactive decay, moving the trend horizontally, parallel to the ^{226}Ra-^{230}Th equiline. The shortest model shows almost no increase in

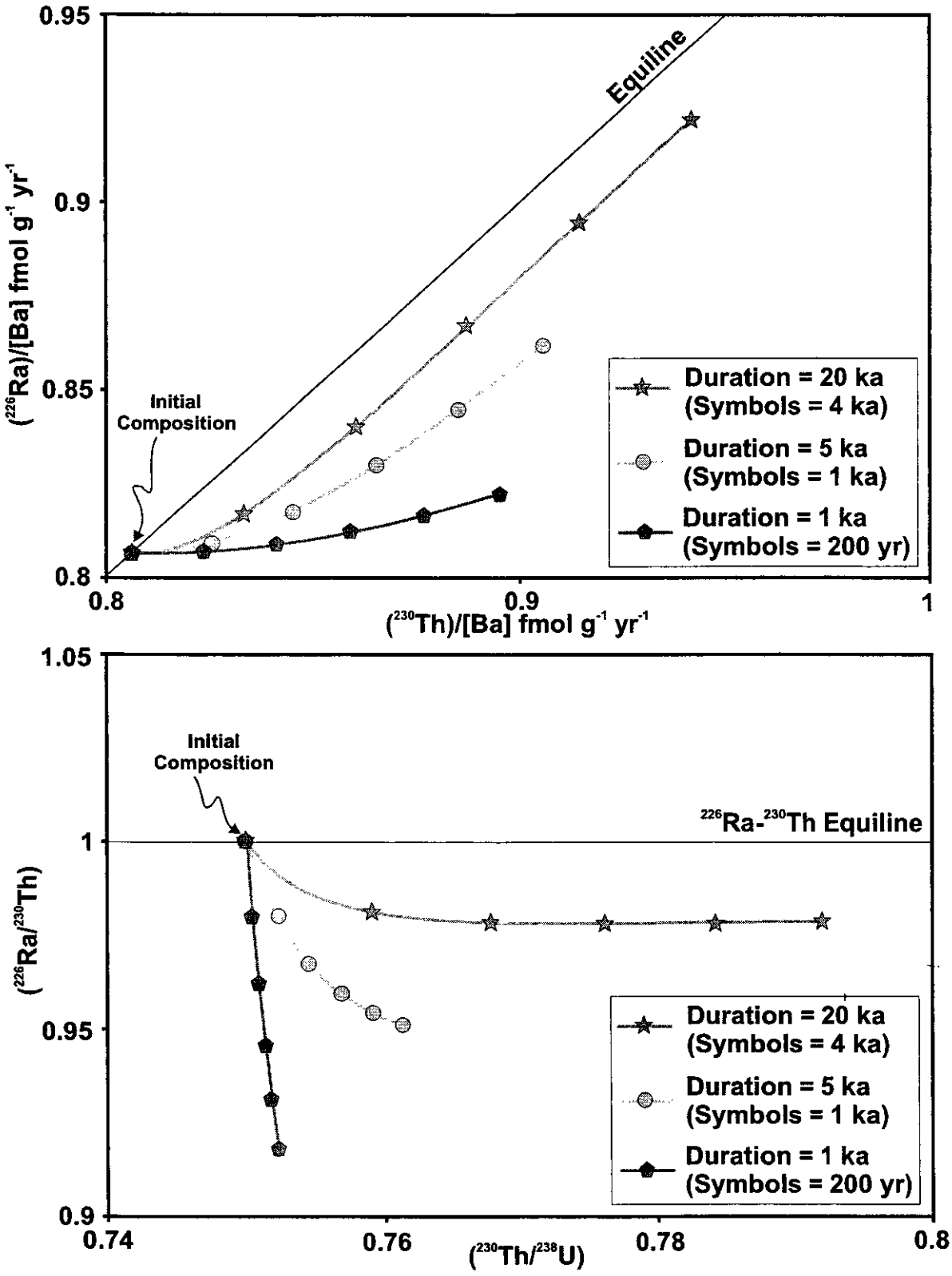

Figure 2.11:

(a) - Ra-Th equiline diagram demonstrating the effects of fractional crystallisation in a non-replenished system on ^{226}Ra-^{230}Th disequilibrium for a range of model durations. The duration of each model is indicated in the key. The model conditions are: $(^{230}Th/^{232}Th)_{init}$: 0.75, $(^{238}U/^{232}Th)$: 1.0, $[Th]_{init}$: 1 μg g^{-1}, $[Ba]_{init}$: 200 μg g^{-1}, $[Ra]_{init}$: 85 fg g^{-1}, f_{cryst}: 0.5, $D_{Ra}=D_{Ba}=0.25$, $D_U=D_{Th}=0.05$.

(b) - Diagram showing the evolution of Ra-Th and U-Th disequilbria during fractional crystallisation in a non-replenished system for a range of model durations. Model conditions are as for (a).

($^{230}Th/^{238}U$) because of the short time period but shows a progressive increase in the degree of ^{230}Th excess over ^{226}Ra with time.

The second example looks at a replenished system, which has an initial Ra excess. The reason for the different choice of source composition compared with the previous model is to illustrate a second possible model for Ra-Th disequilibrium. In the previous model, it is assumed that the primary magma is in Ra-Th equilibrium can be attributed entirely to crustal level processes. In the model described below, it is assumed that the primary magma is in Ra excess, either as a result of melting processes or addition of Ra (and Ba) by a fluid phase during melt generation. The model was run over a range of timescales using similar conditions to the example described above, and the results are shown in Figure 2.12. Plagioclase fractionation drives all the modelled trends towards the equiline in Figure 2.12a, and all eventually cross into ^{230}Th excess. The trends show varying degrees of (^{226}Ra)/[Ba] decrease prior to crossing the equiline, with the biggest decrease in the sample with the longest iteration length. Once in ^{230}Th excess, the trends show very similar behaviour to the model described above, and start to approach parallelism with the equiline. In Figure 2.12b, the behaviour is again similar to that described Figure 2.11b. The trends for iteration lengths of 250 years and 1 ka show distinct ^{230}Th excesses but only limited variation in ($^{230}Th/^{238}U$) and an iteration length of 5 ka produces a trend which is almost in Ra-Th equilibrium following its initial drop in (^{226}Ra)/[Ba]. Replenishment has relatively small effects, because of the significant increases in [^{226}Ra] due to radioactive decay.

It has been demonstrated in previous sections that provided a magmatic system can be maintained over tens of thousands of years, it is relatively easy to produce a steady-state U-Th disequilibrium which can be sustained indefinitely if the physical conditions remain constant. However if such models are coupled to Ra-Th data, additional constraints are available. In order to maintain coexisting Ra-Th and U-Th disequilibria over a long period of time in the simple systems modelled here, would require either frequent replenishment events and/or high input volume to chamber volume ratios. This would result in constant U-Th systematics with compositions close to that of the

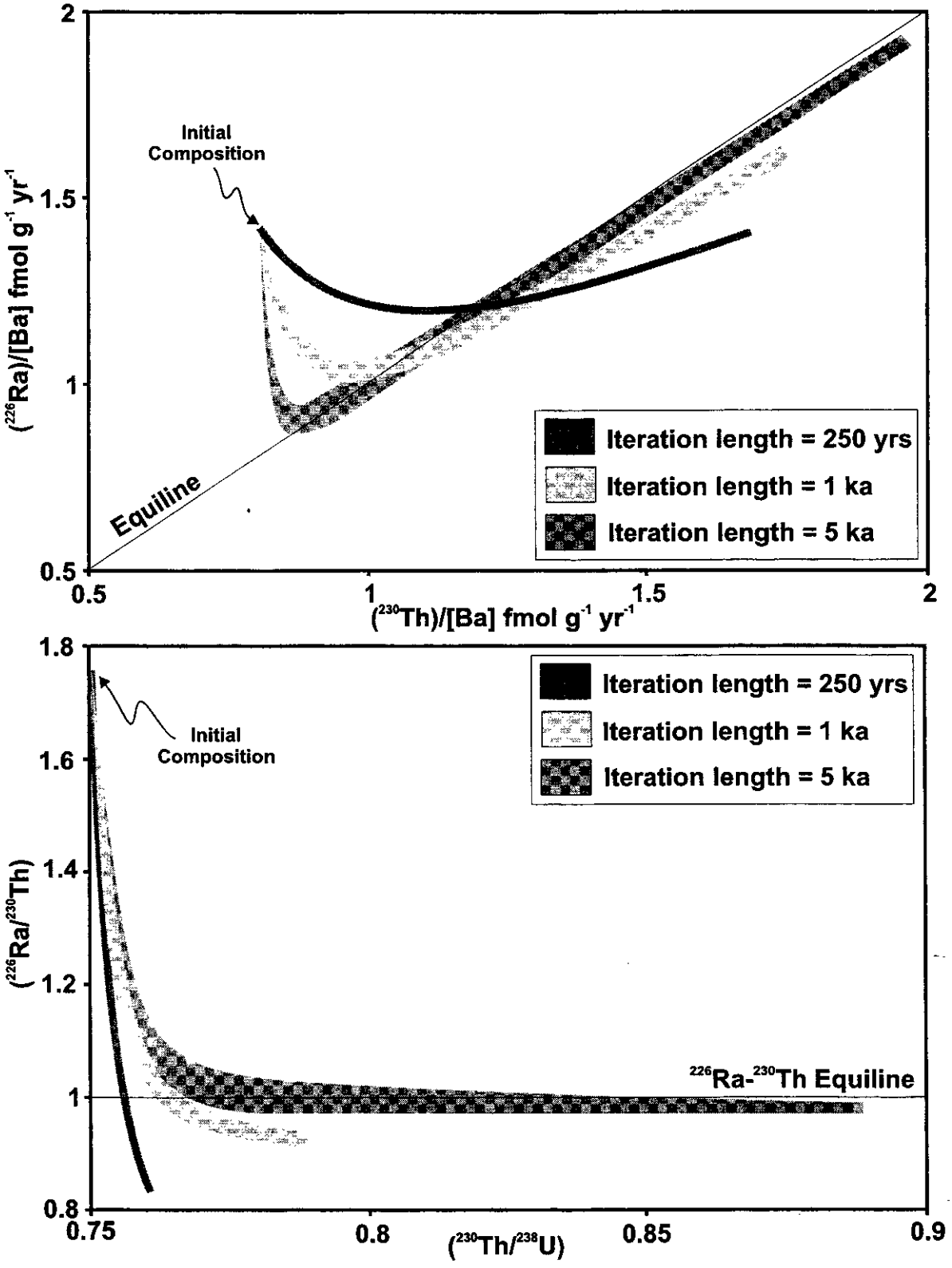

Figure 2.12:

(a) - Radium equiline diagram showing the effects of magma chamber replenishment for a range of replenishment periods. In each case the model was run for 20 replenishment events. The model conditions were: $(^{230}Th/^{232}Th)_{init}$: 0.75, $(^{238}U/^{232}Th)_{init}$: 1.0, $[Th]_{init}$: 1 μg g^{-1}, $[Ba]_{init}$: 200 μg g^{-1}, $[Ra]_{init}$: 150 fg g^{-1}, f_{cryst}: 0.2, $D_{Ba}=D_{Ra}=0.25$, $D_{Th}=D_{U}=0.05$.

(b) - Diagram showing the evolution of Ra-Th and U-Th disequilibria in a replenished system, for a range of replenishment periods. Model conditions are as for (a).

replenishing magma. If a phase in which Ba was highly compatible, e.g. alkali feldspar, was crystallising over a long time period in either a replenished or non-replenished system, it would be easier to maintain both the short-lived isotope systems discussed here in disequilibrium. Equally, it is possible that AFC processes could have a similar effect, however the ^{226}Ra compositions of potential assimilants are essentially unknown at this time.

2.4.6 Testing the Model on Real Systems

It has been demonstrated that it is possible to generate a wide range of different evolution paths for complex magmatic systems. It is important that this theoretical work is related to real systems so that future studies can use the ideas presented here to help constrain the complex petrogenetic processes occurring in crustal magma chambers. At the current time, published data sets do not have enough high-precision short-lived isotope data with good stratigraphic and independent chronological control that is necessary to test the effectiveness of the model.

On the whole, the full potential of short-lived isotope data as a tool to interpret the timescales of crustal petrogenetic processes has not yet been realised for several reasons. Many of the features predicted by the model used here, are relatively small variations which would have been very difficult to detect with the alpha counting techniques employed in early studies. With the advent of mass spectrometric techniques, it has become possible to obtain the high precision data necessary to identify and constrain the processes discussed above. However much of effort to date in the use of short-lived isotopes have either concentrated on regional studies with only a small number of samples from any given centre, or have lacked the required stratigraphic control as discussed below.

In order make full use of this modelling, it will be necessary to study volcanic centres where extensive exposure of lava sequences define clear relative stratigraphies, so that variations through time can be identified with confidence. In addition, if these studies

are combined with other high-precision chronological techniques, it will enable further constraints to be placed on the rates of magmatic processes in crustal magma chambers.

Such constraints are important because at the current time there are radically different estimates for the timescales of crustal level magmatic processes. Constraints on the basis of Sr isotopes and U-series systematics suggest that crustal residence times may in some cases be on the order of tens of thousands to hundreds of thousands of years (Halliday et al., 1989; Christensen and DePaolo, 1993; Heath et al., 1998b). In contrast, thermodynamic models, and studies of crystal size distributions argue for short timescale magmatic processes (e.g. Marsh, 1988; Higgins, 1996; Marsh, 1998; Edwards and Russell, 1998). Short-lived isotope systematics have the power to resolve between such models, but require detailed, high-precision studies.

2.5 Summary

Modelling the effects of magma chamber processes on short-lived isotope systematics shows that the evolution of the U-Th and Ra-Th disequilibrium can potentially be very complex. Replenishment processes can maintain the ($^{230}Th/^{238}U$) and ($^{226}Ra/^{230}Th$) compositions in disequilibrium for long periods of time in excess of 5 half-lives of the daughter isotope, and if sufficient refilling events occur, a steady-state composition is approached. The time taken to obtain a steady-state system is highly dependant on the physical conditions, but it is relatively easy to reach such a situation within a few tens of thousands of years.

Extensive crystallisation will generally increase the time it takes for a system to reach a steady-state composition, where the elements of interest remain incompatible. Small amounts of accessory phases can change the bulk partition coefficients of U and Th sufficiently that shifts in ($^{238}U/^{232}Th$) can occur. Both Ba and Ra are moderately compatible in a number of phases such as plagioclase, which can readily fractionate ^{226}Ra and ^{230}Th. If either alkali feldspar or biotite are present in the crystallising assemblage, this fractionation can be much greater, as Ba and Ra are both compatible in these phases.

The effects of AFC or magma mixing processes are also important to take account of. If such processes are non-instantaneous, then curves are produced which do not trend directly towards the mixing/assimilating composition. Whether an assimilant is in equilibrium or not is poorly constrained, however in general, it makes little difference to the behaviour of the systematics.

Combined U-Th and Ra-Th systematics suggest that even with relatively favourable model conditions, it is difficult to sustain disequilibrium in both systems except where there are high volume and/or high frequency refilling events, which result in a U-Th composition close to that of the replenishing magma.

A phrase familiar to PhD students?,

Moneta Svpervacanea, Magister?

The motto of the Beggars Guild

from 'The concife and possibly even accuratte Mapp' and 'Discworld Companion' – Terry Pratchett & Stephen Briggs.

Chapter 3

Tectonic Setting, Geology and Volcanic History of Mount Ruapehu and the Taupo Volcanic Zone

3.1 Introduction

Magmatic processes affecting the petrogenesis of arc lavas are strongly dependent on the local geology, regional tectonics and the structure of the subducting slab (e.g. Gill, 1981; Jarrard, 1986). This chapter outlines the tectonic setting and history of the North Island of New Zealand, establishing the development and nature of subduction occurring along the Hikurangi Margin. The geology, tectonics and volcanism of the Taupo Volcanic Zone are discussed. Finally the areas of study are considered in more detail, and the sampling strategy used for this project is described.

3.2 Plate Tectonic Setting of North Island

3.2.1 The Hikurangi Margin

The North Island of New Zealand lies at the southern end of the Tonga-Kermadec arc system, where the Indian Plate to the west overrides the subducting Pacific Plate (figure 3.1). Offshore to the east of North Island, west-directed subduction of the Pacific Plate underneath the continental crust of North Island continues south from the Kermadec Trench into the Hikurangi Trough, although there appears to be a slight offset of ~20-25 km between these features on the basis of bathymetry (1980). This offset is also marked by gravitational differences (Hatherton and Syms, 1975).

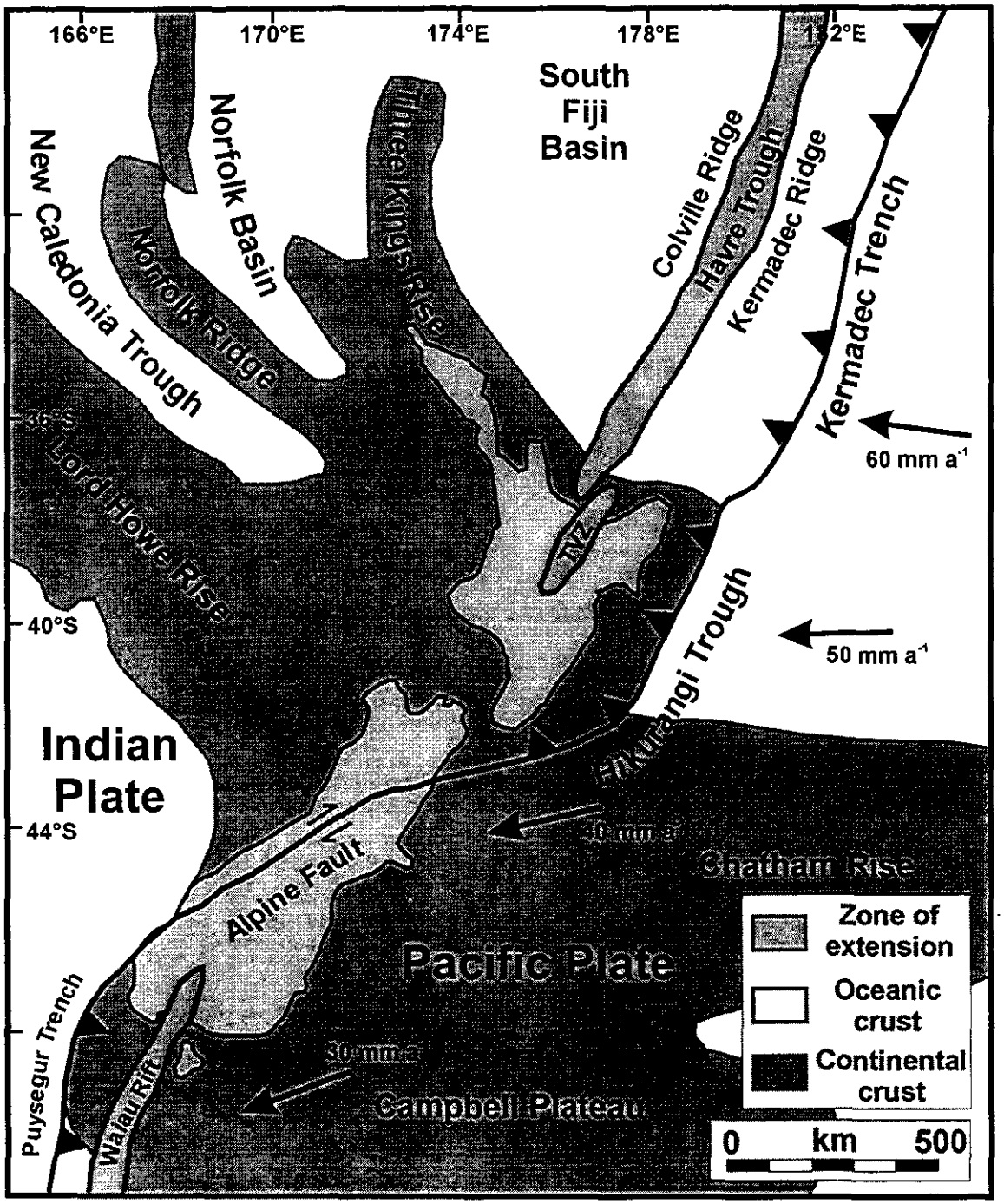

Figure 3.1: The tectonic setting of New Zealand after Cole & Lewis (1981). The arrows indicate the direction and rate of motion of the Pacific Plate relative to the Indian Plate. The boundary between oceanic and continental crust at the southern end of the Kermadec Ridge has been drawn to coincide with the northern extremity of the Taupo Volcanic Zone, consistent with more recent data from Wright (1992).

As the site of subduction progresses southwards, convergence becomes increasingly oblique, grading into the dextral, transpressional Alpine fault system in South Island (Walcott, 1998). The location of this transition may be in part related to the difficulty in subducting the Chatham rise, an area of buoyant, submarine continental crust east of South Island (Cole and Lewis, 1981). To the south of New Zealand, subduction resumes, but with reversed polarity so that the Indian plate descends beneath the Pacific plate along the Puysegur Trench (Christoffel, 1971; Cole and Lewis, 1981). The rate of convergence of the Pacific Plate relative to the Indian Plate along the Hikurangi margin at present is ~60 mm a^{-1}, faster than it has been at any time during the Cenozoic (Walcott, 1987).

3.2.2 Tectonics of the Taupo Volcanic Zone

The Taupo Volcanic Zone (TVZ), a region of late Cenozoic volcanism, lies 200 km behind the Hikurangi Trough in the north, and the trench-volcanism gap increases southwards to some 270 km at Mt. Ruapehu (Cole and Lewis, 1981). The axis of volcanism lies ~80-100 km above the subducting Pacific Plate, where the plate bends downwards to an angle of ~50° (Adams and Ware, 1977; Reyners, 1980).

To the east of the TVZ, the tectonic regime is dominated by compression and lateral shear as a result of oblique plate convergence. Incipient thrusting is recorded in seismic profiles across the sedimentary wedge off the east coast of North Island (Davey et al., 1986), and uplift and shear are seen in the North Island Shear Belt, the surface expression of which is the Axial Greywacke Ranges (Cole, 1990).

The TVZ itself however is an area bounded by NNE-SSW oriented extensional faulting, identified from field evidence, earthquake focal mechanisms, and seismic profiles (Reyners, 1980). This faulting has produced a rift-like structure, the crust of which may well be notably thinner (~15 km) than that either to the east or west (see discussion in Section 3.3.4).

The tectonic nature of the TVZ is equivocal and it has been the subject of considerable debate. Extension in the TVZ is offset to the southeast of the Havre Trough

back-arc system in the Kermadec arc system to the north, possibly along the line of the Vening-Meinesz fracture zone (Wright, 1992; Wright, 1993), whilst the Hikurangi Trough and arc related volcanism are offset to the northwest of the volcanic arc in the Kermadec system (Hatherton and Syms, 1975). Despite these offsets, the alignment of the TVZ with the Hikurangi Trough and the presence of arc-like volcanics, often in close conjunction with extensional faulting (e.g. Cole, 1990), suggests that the extension is subduction-related, and therefore the TVZ must be regarded as a region where back-arc extension and subduction related magma generation coincide.

One factor that has made the tectonic interpretation of the TVZ difficult is the presence of calc-alkaline andesites typical of continental arcs erupted within the area of apparent back-arc rifting. It has been suggested that on careful examination of other arc systems which have active back-arc regions, such as the Tonga and Mariana arcs (Taylor and Karner, 1983), it is apparent not only that extension occurs within the volcanic arc, but active arc volcanism can occur within back-arc regions (Wright, 1992).

Geodetic strain measurements suggest that the rate of extension is ~12 mm a^{-1} at the Bay of Plenty Coast (Walcott, 1987). Moreover, estimates on the basis of the rate of migration of andesite volcanism suggest an average extension of ~20 mm a^{-1} over at least 2 Ma period (e.g. Stern, 1987), although this rate has been questioned by some authors (Wilson et al., 1995) because the andesite migration is backed up by poor age constraints. These rates of migration are consistent with a progressive decrease in back-arc extension rate southwards in the Tonga-Kermadec-New Zealand arc system, from high extension rates of ~160 mm a^{-1} in the northern part of the Lau Basin, intermediate rates of 80-60 mm a^{-1} in the southern Lau Basin and Havre Trough, to slower extension in the TVZ.

3.2.3 The Structure of the Subduction Zone

Whilst the Tonga-Kermadec-Hikurangi subduction systems are almost continuous, the structure of the subduction zone is very different in the Hikurangi system

as a result of the increasing obliquity of convergence and subduction beneath continental crust.

The Pacific Plate descends beneath the Indian Plate along the Hikurangi Trough and seismic refraction studies show a persistent décollement feature proceeding at a very shallow angle of ~3° westwards beneath a wedge of deforming Miocene-Pleistocene sediments (Reyners, 1980; Davey et al., 1986). At a depth of 14 km, ~150 km inshore of the Hikurangi Trough, the décollement steepens as it intersects a zone of increased seismic activity beneath the eastern coast of North Island (Davey et al., 1986). A second bend and steepening of the descending slab can be identified from subcrustal earthquakes beneath the Taupo Volcanic Zone at a depth of ~70-80 km where the slab begins to descend at ~50° (Adams and Ware, 1977; Reyners, 1980). The structure of the slab beneath North Island is illustrated in Figure 3.2, which is discussed further in Section 3.3.4.

3.2.4 Tectonic Evolution of North Island

The complexity of the tectonic evolution of New Zealand during the Tertiary and Quaternary is due in part to the close proximity of the instantaneous pole of rotation of the Indian and Pacific plates (Chase, 1978; Minster and Jordan, 1978; Stock and Molnar, 1982). This has resulted in North Island being located at the transition between destructive and conservative plate motions, where old Cretaceous oceanic crust is subducted beneath continental lithosphere (Walcott, 1987). Consequently, convergence along the Hikurangi Margin is variably oblique to the strike of the trough system, with the angle of coincidence and rate of convergence decreasing southward as the margin gradually switches into a transform fault (Figure 3.1).

Plate reconstructions for the period since magnetic anomaly 18, ~43 Ma ago, suggest that the Hikurangi Margin has developed through clockwise rotation and straightening of the subduction zone (Walcott, 1987). For the period 43-21 Ma, the instantaneous pole of rotation for the system and the rate of rotation were approximately constant (Stock and Molnar, 1982). Estimates of rotation poles and rates for magnetic anomaly 5, (~9.8 Ma) suggest that there was an increase in the rate of rotation from

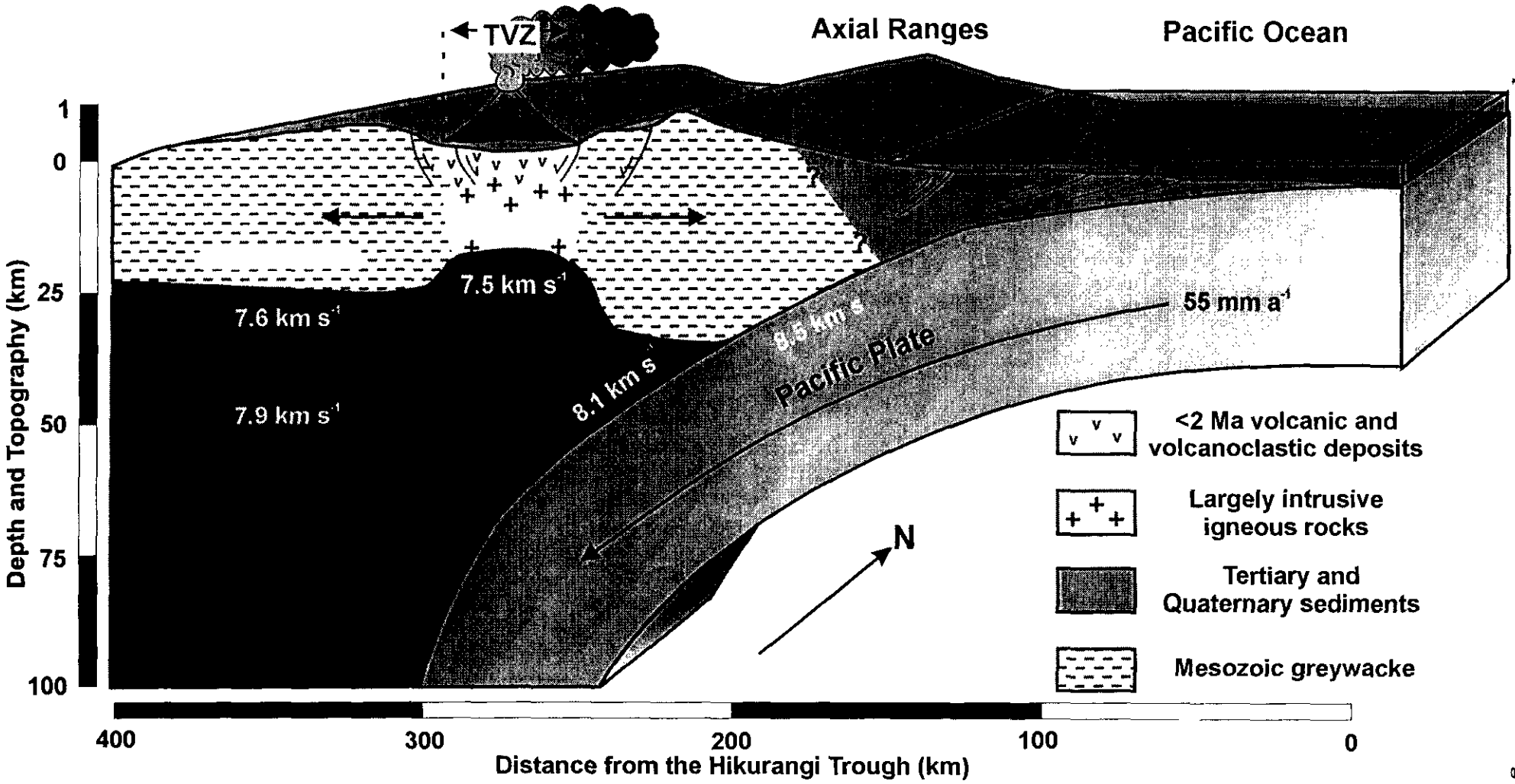

Figure 3.2: Schematic cross-section showing the structure of the Taupo Volcanic Zone and the subducting Pacific Plate, modified after Stern & Davey (1987). Vertical exageration is x 1.5 for the portion of the diagram below sea level and x 15 for the subaerial portion of the diagram.

~15-25 mm a^{-1} to ~40-50 mm a^{-1}, and the direction of plate motion has also changed by ~20-30° (Stock and Molnar, 1982), consistent with a shift in the Euler pole of rotation some 12° to the southwest to its present day position. This effectively moved the pole further along strike, away from the subduction zone and increased the convergence rate (Wright and Walcott, 1986). These authors suggest that this shift may be linked to the opening of the Lau Basin and Havre Trough in the Tonga-Kermadec system at around 4 Ma ago (Malhoff et al., 1982), the onset of extension and volcanism in the Taupo Volcanic Zone, occurring ≥ 2 Ma ago (Wilson et al., 1995) and the growth of the Southern Alps in South Island sometime after ~6 Ma (Walcott, 1998).

The clockwise rotation of the Hikurangi subduction system over the past 40 Ma (Walcott, 1987) can be identified by the presence of areas of onshore calc-alkaline volcanics, and two offshore rises, the Colville Ridge and Three Kings Rise (Figure 3.1). The earliest subduction related volcanism identified onshore are basaltic andesites and andesites along the western edge of the Northland Peninsula, which have been called the Waitakere arc (Ballance, 1976), and were active 25-15 Ma ago (Cole and Lewis, 1981). Volcanism spread to the eastern side of the Northland peninsula ~18 Ma ago, producing a series of andesite-dacite centres which were partially coeval with the earlier Waitakere arc (Ballance, 1976). Following an apparent break in major volcanism between 15-6 Ma, andesititc and voluminous rhyolitic magmatism began in the Hauraki-Coromandel Volcanic Region, which has been related to extensional faulting (Cole and Lewis, 1981). The exact nature and timing of the switch between volcanism in the Hauraki-Coromandel area and the Taupo Volcanic Zone, which began to see volcanic activity ~2 Ma ago (Wilson et al., 1995), is contentious and is discussed further below (see Sections 3.3.1 and 3.3.2).

3.3 The Volcanism and Geology of the Taupo Volcanic Zone

3.3.1 The Taupo Volcanic Zone

It has long been recognised that historical and late Cenozoic volcanism and hydrothermal activity in North Island is largely confined to a region extending southwest

from the Bay of Plenty (Hochstetter, 1864), which subsequently became known as the Taupo Volcanic Zone (TVZ) by modern authors (Healy, 1962). The onshore part of this region runs from an apex at Ruapehu in the south to a broader ~40 km wide boundary with the Bay of Plenty coast. Offshore, this region encompasses the highly active White Island, and it has recently been suggested that volcanism continues to the edge of continental crust and the boundary with the Kermadec-Havre Trough system (Wright, 1992; Wright, 1993).

In the past several authors (Stern, 1987; Stern and Davey, 1987; Cole, 1990) have called a larger area of volcanism encompassing a wider timespan the Central Volcanic Region (CVR) (Figure 3.3). This region encompassed the earlier and now extinct volcanism in the Hauraki-Coromandel area. It has been proposed that the CVR represents a continuum of activity formed by the rotation of the locus of active volcanism possibly for some 20 Ma (Cole, 1986; Cole, 1990). In this model, the TVZ represents the present position of the rotating region of activity. More recently, it has been suggested that this definition is based on very weak chronology, and the apparent rotation is because the TVZ overprints part of the older Hauraki-Coromandel system Wilson et al., 1995), active < 6 Ma ago (Cole and Lewis, 1981).

The terminology preferred by Wilson et al. (1995) is to call the region that was active between 2 Ma and the Whakamaru group eruptions at ~0.34 Ma the old TVZ, and the smaller, currently active (since 0.34 Ma) area the young TVZ. The old TVZ encompasses a wider region to the west, but its eastern margin coincides with that of the young TVZ. To resolve this argument requires a much larger database of accurate age determinations, but in this study the terminology of Wilson et al. (1995) is preferred.

3.3.2 Volcanic History

It has long been recognised that there is an apparent spatial split in the nature and style of volcanism in the TVZ, with silicic rhyolitic eruptions, associated with minor small volume basalt activity, dominating the central areas of the TVZ, and andesite-dacite volcanism being prevalent at the northern and southern extremities (Figure 3.3). Some researchers have developed this idea further, suggesting that andesite-dacite arc style

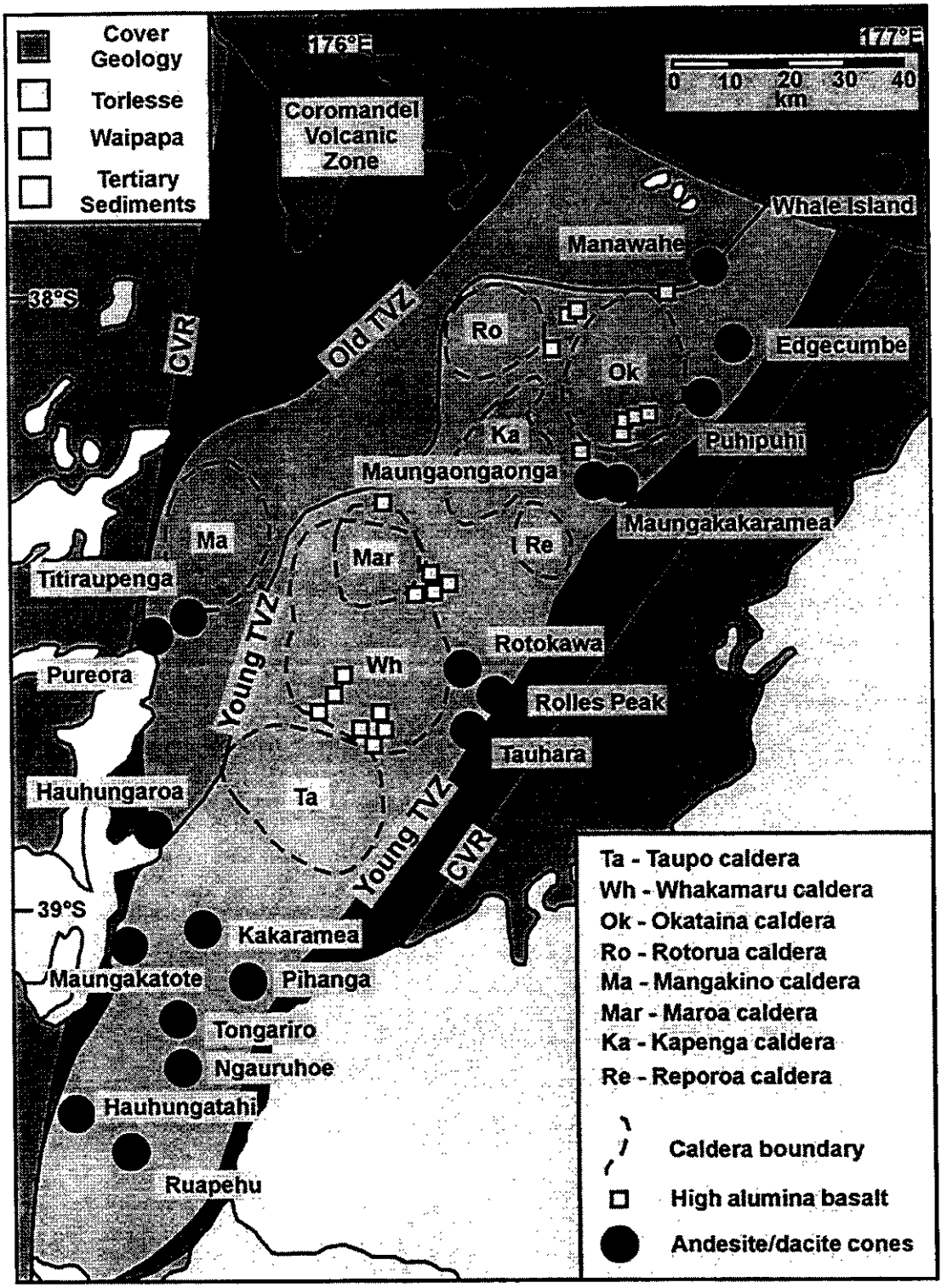

Figure 3.3: Map showing the distribution of volcanic centres in the TVZ modified after Graham et al. (1995). Also shown is the distinction between old and young TVZ regions as discussed by Wilson et al. (1995).

volcanism is currently restricted to the eastern margins of the TVZ, whilst rhyolite calderas were forming behind the active arc (e.g. Cole, 1990).

Wilson and co-workers (Wilson et al., 1995) have pointed out that this separation is may be incorrect or at least significantly more complex (Wright, 1992), because the eastern boundary of the TVZ has seen extensive rhyolite activity at Okataina and Reparoa Calderas. There is also evidence from boreholes of andesitic material beneath the TVZ, although the temporal relationship between the overlying rhyolites and these andesites is uncertain (Browne et al., 1992). It is more likely that small volume andesite activity has been hidden and swamped by voluminous rhyolitic eruptions (Wilson et al., 1995).

The earliest volcanism identified in the TVZ was a series of andesite volcanoes in the Hauhungaroa Range, erupted ~2 Ma ago, which form the western boundary of known activity (Wilson et al., 1995). Along the almost linear eastern edge of the TVZ, andesite-dacite volcanism has been present throughout the Holocene, and for at least 0.34 Ma, with limited age data suggesting that the andesite volcanoes at Rolles Peak and Rotokawa, were active as early as 0.71 Ma ago (Browne et al., 1992; Wilson et al., 1995). At the southern end of the TVZ, andesite-dacite volcanism has been widespread in the Tongariro Volcanic Centre, producing four andesite massifs, Kakaramea-Tihia, Pihanga, Tongariro and Ruapehu, the latter having formed the southern apex of volcanic activity in the TVZ for at least 250 ka, and possibly for significantly longer (Graham and Hackett, 1987).

Throughout much of the volcanic history of the TVZ there have been numerous large rhyolite eruptions from at least eight calderas. The earliest rhyolitic activity identified occurred from the Mangakino caldera ~1.6 Ma ago. Most of the deposits exposed at the surface are ≤ 0.34 Ma old, because a series of large ignimbrite eruptions from the Whakamaru caldera covered much of the earlier material. In the last 2 ka, both Taupo and Okataina have been active, with Taupo producing one of the largest ignimbrite eruptions known in 181 AD (Wilson et al., 1980).

3.3.3 Underlying Geology: Meta-Sedimentary or Volcanic?

Geochemical and geophysical investigations of the TVZ have been hampered by a poor knowledge of the underlying basement geology. To the west of the TVZ the basement is formed from rocks of the Waipapa Group of the Caples Terrane, whilst to the east the uplifted basement of the Axial Greywacke Ranges is formed from greywackes of the Torlesse Terrane (Korsch and Wellman, 1988). Lithologically, the Waipapa and Torlesse rocks are similar, although they may be distinguished on the basis of chemistry (e.g. Graham and Hackett, 1987; Graham et al., 1992). The Waipapa Group is believed to have been derived in part from the Permian Brook Street arc (Frost and Coombs, 1989) and it was laid down as turbidites in the Triassic and early Jurassic (Graham et al., 1992). The Torlesse terrane is mainly made up of deposits derived from plutonic rocks which are considered to have formed the roots of a magmatic arc (MacKinnon, 1983), and they were laid down in an accretionary prism throughout much of the Mesozoic, until the mid-Cretaceous (Korsch and Wellman, 1988).

The exact location and nature of the boundary between these two terranes is uncertain, but must occur somewhere beneath the TVZ. Numerous boreholes have been drilled into the TVZ as a result of extensive exploitation of the area for hydrothermal power schemes. Several of these have penetrated thick (> 2 km) overlying volcanic sequences and reached metasedimentary basement. Drill cores from Kawerau near the Bay of Plenty coast show that the area is underlain by Waipapa-like lithologies (Reid, 1983), whilst further south, cores drilled at Rotokawa near the eastern margin of the TVZ reach rocks of Torlesse affinities (Browne et al., 1992). At the southern apex of the TVZ, the presence of xenoliths of Torlesse-like metasedimentary xenoliths in the lavas of the Tongariro Volcanic Centre strongly argues for the presence of underlying metasedimentary basement of Torlesse affinity (Graham and Hackett, 1987; Graham et al., 1988).

Seismic velocities beneath the TVZ are equivocal in terms of the lithologies present, although it has been suggested that dense plutonic rocks at depths of 1.8-2.7 km could produce the observed seismic velocities (Stern and Davey, 1987). Studies of the shallow crust with resistivity measurements have been used to suggest that the much of the

uppermost 5 km of the TVZ is made up from volcanic and volcaniclastic material (Bibby et al., 1998).

The debate over the underlying basement of the TVZ remains unresolved, because most of the firm evidence for Torlesse related basement occurs close to the margins of the TVZ. Thus, some authors suggest, mainly on the basis of geophysical considerations, that much of the central TVZ may have been sufficiently extended and rifted for much of the underlying crust to be made up from intrusive igneous rocks (Stern, 1987; Soengkono, 1995). This view is at least partially supported by the presence in a borehole at Ngatamariki of a diorite pluton at depth (Browne et al., 1992), meta-igneous granulite xenoliths in lavas of the Tongariro Volcanic Centre (Graham et al., 1990), and dioritic xenoliths in rhyolite erupted from the Taupo Caldera (Brown et al., 1998). Calculations of the heat source required to produce the observed thermal flux at the surface are compatible with numerous large plutons cooling at depth in the TVZ (Stern, 1985; Stern, 1987).

3.3.4 Crustal and Mantle Structure Beneath the TVZ

Seismic refraction and reflection profiles have been used to investigate the crustal and mantle structure beneath North Island (Haines, 1979; Stern and Davey, 1987). These authors suggest that the crust under the Taupo Volcanic Zone is extremely thin, with a thickness of ~15 km, and low P-wave velocities ranging between 3.0 km s^{-1} and 6.1 km s^{-1}. Although such velocities are equivocal in terms of the associated lithologies, they are attributed to the crust in this region being dominated by dioritic to granitic intrusive rocks on the basis of heat flow arguments (Stern, 1987). The mantle beneath the Taupo Volcanic Zone is likewise identified as having a very low P-wave velocity, 7.4-7.5 km s^{-1}. The crustal thickness and mantle velocities are similar to values for other areas of active extensional tectonics such as the Basin and Range and Kenya Rift, and they have been linked to hot, low density mantle material, upwelling isostatically to compensate for the thin crust (Stern and Davey, 1987).

The crust to the west of the Taupo Volcanic Zone is also somewhat thinner than normal crust, ~20-25 km thick (Stern and Davey, 1987), and it is underlain by low P-wave

velocity mantle, of 7.6-7.9 km s^{-1} (Haines, 1979). The crust underneath the Axial Greywacke Ranges, forming the eastern part of North Island appears to be of normal thickness, although few data exist for this region (Stern and Davey, 1985).

More recently, the seismic interpretation has been called into question, and it has been suggested that in some cases, mafic gabbros and granulites can have seismic velocities of the same order as the anomalous mantle inferred to underlie the TVZ (Hochstein, 1995; Wilson et al., 1995). In this model, the reflectors previously interpreted as the crust-mantle boundary represent the top of a dense, mafic rich cumulate residue, underlain at some unknown depth by the true crust-mantle boundary (Hochstein, 1995).

3.4 Areas of Study

This thesis investigates lavas from a number of different volcanic centres in New Zealand. The majority of samples are from Ruapehu and they will be used to constrain the nature and timing of crustal and subcrustal petrogenetic processes. Comparisons will also be made with samples from Edgcumbe and White Island, smaller andesite-dacite volcanoes which lie along the arc to the north, and with Taranaki, a large, chemically distinct volcano lying directly across the arc from Ruapehu.

3.4.1 Mount Ruapehu

Mount Ruapehu is the highest mountain in North Island (2797m), lying at the end of a series of andesite massifs collectively known as the Tongariro Volcanic Centre (ToVC), and it currently forms the southern apex of volcanic activity in the TVZ. Most eruptive activity has taken place from a series of central vents aligned along a NNE-SSW lineament, parallel with the strike of extensional deformation in the TVZ. Early activity may have been aligned with NW-SE trends associated with the Hauraki-Coromandel system (Cole, 1990). In addition however, there are a number of parasitic flank vents associated with the most recent phase of effusive activity, two of which are of interest to this study; Rangataua and Saddle Cone. Four small eruptive centres, Hauhungatahi, Pukeonake, Pukekaikiore and Ohakune, near the main Ruapehu cone may be also be related satellite vents (Graham and Hackett, 1987; Hackett and Houghton, 1989).

The main edifice comprises almost entirely lavas, auto-breccias and minor pyroclastics, which are often deeply cut by streams and rivers draining the permanent summit glaciers. The present day topography of the cone has been predominantly fashioned by the effects of fluvial and ice erosion during the last glaciation. The local climate has also played a major role in the recent (< 10 ka) development of the terrain, with the lower slopes of the western side of the volcano being covered by forest and low scrub, whilst the east side forms a rain shadow and remains largely devoid of vegetation and is known as the Rangipo Desert.

3.4.1.1 Volcanism

Ruapehu has been extremely active throughout the recorded history of North Island, with at least 50 periods of small-scale eruptive activity since 1861 (Houghton et al., 1987; Hackett and Houghton, 1989; Simkin and Siebert, 1994). Most of the recorded activity has been small explosive phreatic eruptions through the crater lake that is inferred to have been almost continually present in the western summit crater at least since 1879 (Christenson and Wood, 1993).

Two purely magmatic events took place in 1861 and 1945. In the latter eruptive episode, dome building occurred, which completely displaced the waters of Crater Lake into the Whangaehu Valley (Hackett and Houghton, 1989). Eruptions in June 1996 also seem to have completely dispersed Crater Lake for a short time, although poor weather made observation difficult. The most dangerous feature of the historic eruptions has been numerous large lahars in five drainage systems around the volcano; the Whangaehu, Whakapapaiti, Whakapapanui, Mangaturuturu and Mangatoetoenui rivers (see Figure 3.6) (Houghton et al., 1987).

Interpreting the nature of prehistorical activity is more difficult, because only major events tend to be preserved, with periods of frequent but small scale activity such as that ongoing during historical times being unidentifiable in earlier sequences. Various styles of volcanism can be identified from the Holocene eruptives of the Whakapapa Formation which are: Strombolian eruptions from summit and flank vents, aa and block

lava flows from summit and flank vents, at least one major sub-plinian eruption, minor cone collapse features and two major lahar events in the last 1000 years (Houghton et al., 1987).

Field evidence from this study and others (Graham and Hackett, 1987; Hackett and Houghton, 1989) suggests that these eruptive styles have probably been prevalent throughout the history of Ruapehu, with older sequences comprising mostly lava and auto-breccia with occasional major laharic units and minor pyroclastics, ash layers and intrusive bodies (Hackett and Houghton, 1989). A large lahar deposit on the northwestern flank of Ruapehu, the Murimotu Lahar Formation, is inferred to reflect a series of three or more sector collapses relating to dome formation during the Whakapapa eruptions (Hackett and Houghton, 1989), and it is likely that major collapses have occurred at other times throughout the volcanic history of Ruapehu.

3.4.1.2 Stratigraphy and Chronology

The stratigraphy of Ruapehu is constrained at two levels. Firstly, a well known stratigraphy and timescale exists for tephras and ash on the distal ring plain (Cronin et al., 1996; Cronin et al., 1996; Cronin and Neall, 1997; Cronin et al., 1997; Donoghue et al., 1997). Secondly, the chronology of the lavas of the main edifice is much less well known (Graham and Hackett, 1987). The available stratigraphic and chronological data are combined in Figure 3.4.

The ring plain stratigraphy is based around the presence of a number of well characterised marker horizons produced by major eruptions at the Taupo and Okataina centres. These horizons have been dated mainly by ^{14}C and K-Ar methods and provide a stratigraphy back as far as ~75 ka (Topping, 1973; Topping and Kohn, 1973; Froggatt and Lowe, 1990; Wilson, 1993). The extremely poor preservation of tephra and ash on the main cone of Ruapehu due to high surface run off and erosion by streams and lahars (Hackett and Houghton, 1989), make any correlation between the ring plain deposits and the lavas on the main edifice extremely difficult.

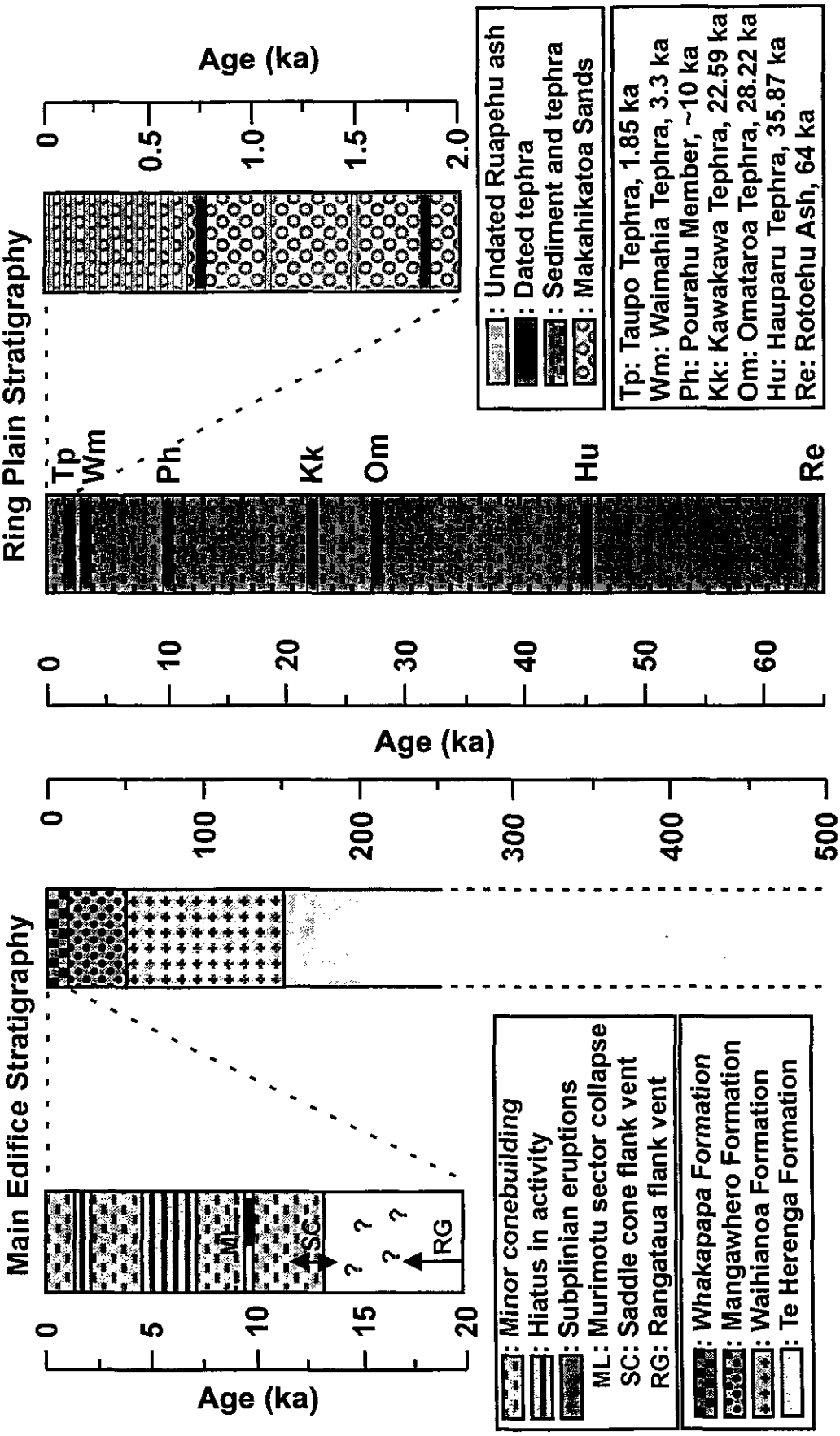

Figure 3.4: Compilation of Ruapehu stratigraphy on the main edifice and the eastern ring plain. Dates are based on ^{14}C ages, K-Ar ages, tephrastratigraphy and estimates on the basis of degree of glaciation. *Data from Graham & Hackett* (1987), Hackett & Houghton (1989), Donoghue et al. (1997) and Cronin & Neall (1997).

At least four cone building episodes can be recognised on Ruapehu based on field evidence and petrology (Graham and Hackett, 1987). These are called the Te Herenga, Waihianoa, Mangawhero and Whakapapa Formations, from oldest to youngest respectively (Figure 3.5). Almost no accurate chronological data exist for the main edifice of Ruapehu. Although a K-Ar date for a lava from the Te Herenga Formation indicates that the upper part of the oldest sequence has an age of ~230 ka (Stipp, 1968). It has been suggested, although somewhat tenuously, that activity may have been recurrent since ~500 ka ago, the time at which the satellite vent of Hauhungatahi is thought to have been formed (Graham and Hackett, 1987). Two other K-Ar dates of 24 and 36 ka exist for the Mangawhero Formation, although these have large errors (Stipp, 1968). The Whakapapa Formation began erupting ≤ 15 ka ago, as it shows no evidence for the glacial dissection and erosion evident in the older formations. Some of the Whakapapa lavas have recently been identified as overlying the Taupo Pumice erupted at 181 AD (R.C. Price, pers. comm.), although their relationship to the older Whakapapa lavas is still uncertain.

3.4.1.3 Sampling

A suite of samples was collected from the Tukino area on the eastern flanks of Ruapehu during February 1996 (see Figure 3.6). This region is cut by two of the main lahar paths active during historic activity, the Whangaehu River and Mangatoetoenui Stream, as well as numerous more minor watercourses draining the small summit glaciers. These rivers and streams, many of which were carved out during the last glaciation, afford excellent exposure of continuous sequences of thick andesite lavas (Figure 3.7).

Two sequences were sampled in detail from the Whangaehu and Ohinepango valleys. These sequences give an excellent opportunity to examine the geochemical evolution and crustal processes occurring during major cone building episodes on andesite volcanoes. In addition, material from a number of other flows was also collected, including young carapace and valley filling flows. These flows are thought to represent some of the youngest activity on the eastern side of Ruapehu. Two samples were collected from the Waihianoa valley, which spatially appears to be part of the same sequence as that sampled in the Whangaehu valley. Throughout this thesis, the coherent samples taken from vertical

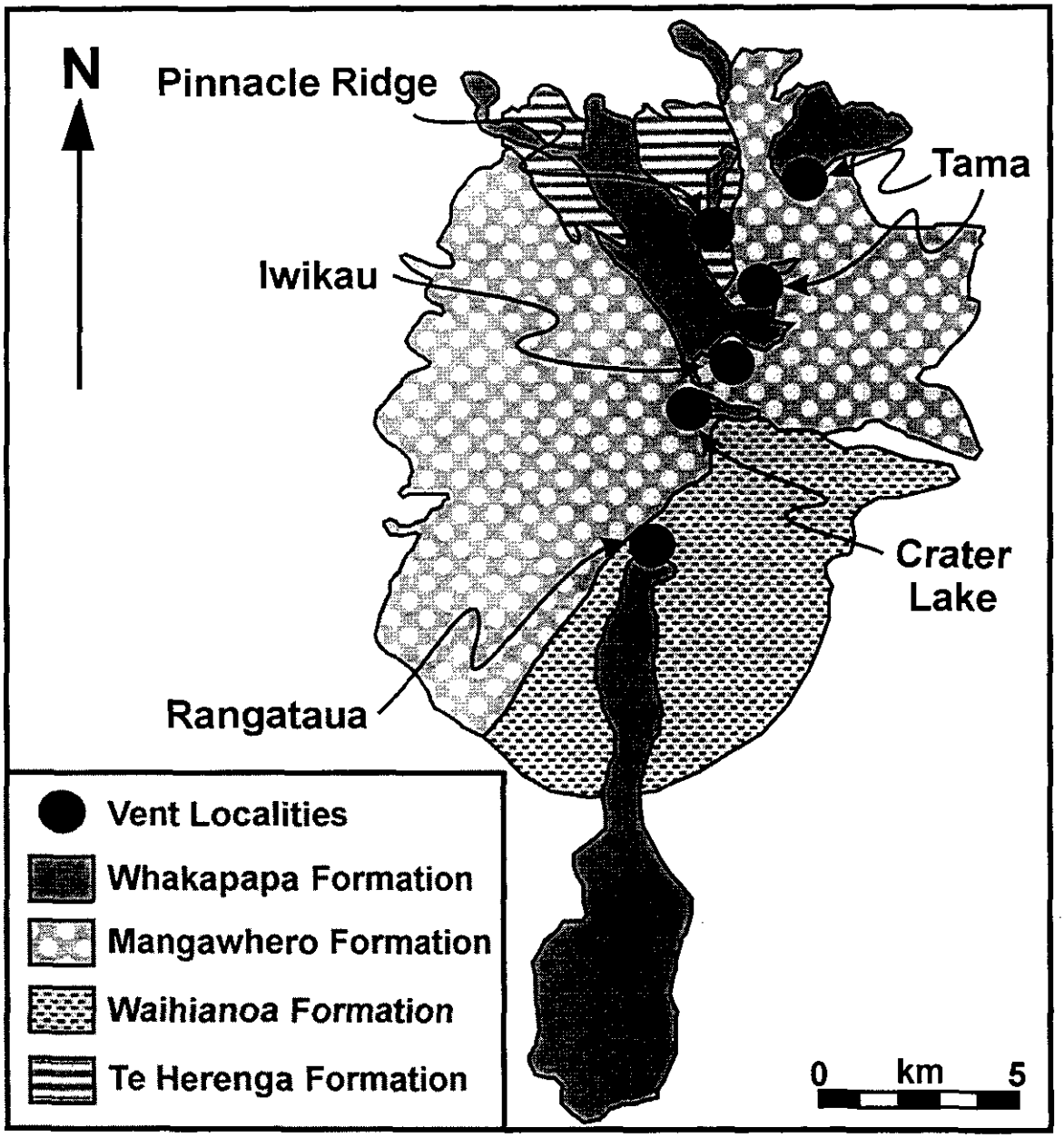

Figure 3.5: Stratigraphy of the main edifice of Ruapehu showing the four main stratigraphic divisions and localities of vents during eruption of the Whakapapa Formation. Modified after Hackett & Houghton (1989).

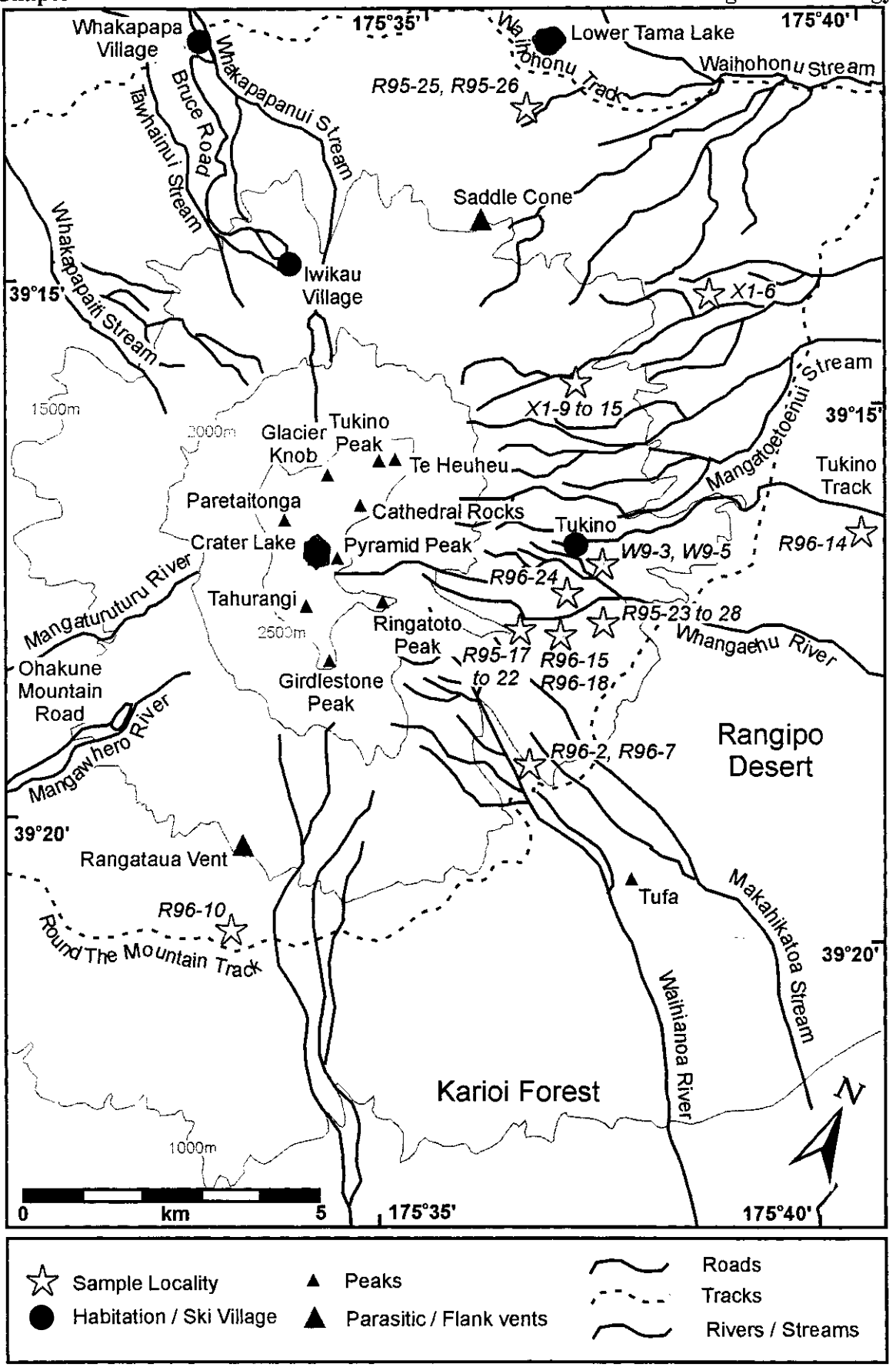

Figure 3.6: Schematic map of Ruapehu, showing the main geographic features and sample localities. Redrawn from Land Information New Zealand 1:50000 maps 260-T20 and 260-S20.

a)

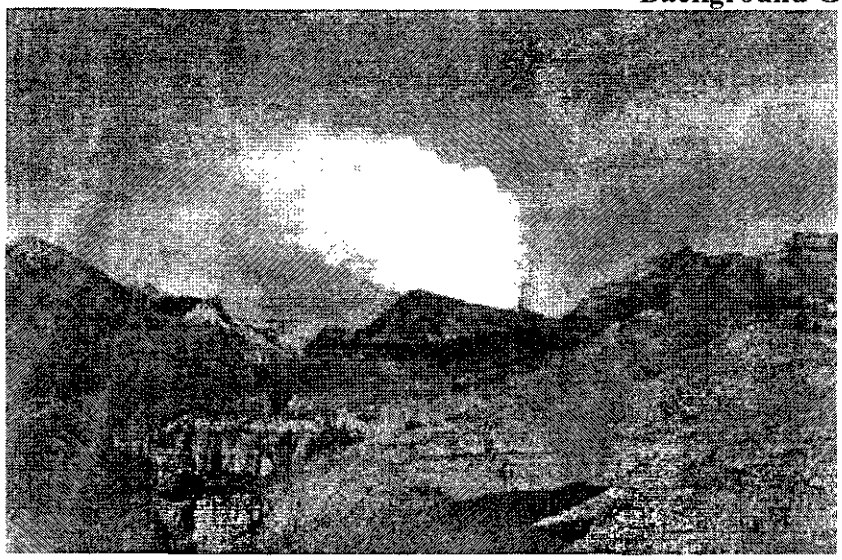

b)

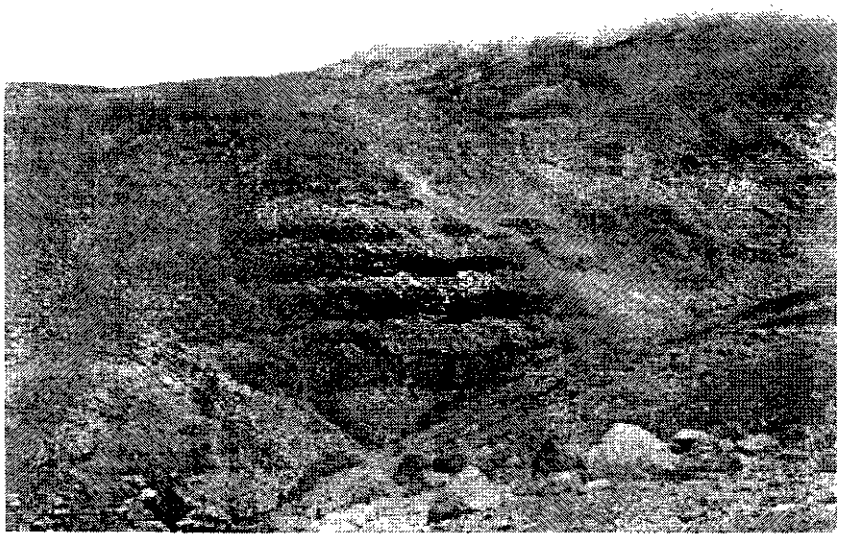

c)

Figure 3.7:

a) Large steam plume rising above Crater Lake in February 1996.

b) The Ohinepango section, Northeast Ruapehu. The mounds in the foreground are covered in ash, pumice and bombs from numerous small eruptions over recent centuries.

c) The proximal end of the Whangaehu section, Eastern Ruapehu, immediately below Girdlestone Peak. The pale, triangular body near the base of the section is a small intrusion, overlain by numerous lavas and interbedded pyroclastics.

sections are referred to as the Whangaehu, Waihianoa and Ohinepango sequences. These groupings have no formal stratigraphic significance, but form continuous exposures from which relative stratigraphy can be deduced. Recent lavas, representing the only samples known to be of the same age as the Whakapapa Formation, were sampled from the Rangataua and Saddle Cone parasitic vents on the southern and northern flanks of the volcano respectively. It is not clear how the activity at the main vent is related to the parasitic eruptions, and this will be assessed in this study. The sampling localities are shown in Figure 3.7.

At each locality ~0.5-1 kg of lava was collected, with weathered surfaces being removed as far as possible in the field. Specimens were selected on basis of freshness, with any showing signs of alteration rejected in the field. Each specimen was double wrapped and labelled on a weathered surface of the specimen and separately in the bag to avoid any possible mismatching of samples.

In addition to material collected in 1996, this study also makes use of further material collected in 1995 by Professor Richard Price (University of Waikato) and Dr Ian Smith (University of Auckland) from the Whangaehu sequence (samples prefixed R95 on Figure 3.6), and small samples of tephra from historic eruptions (sampled in the summit region, and from other collections), from Dr John Gamble (Victoria University of Wellington).

3.4.2 Edgecumbe and White Island: Along-arc Comparisons

At the northern end of the TVZ, two volcanoes have been active in the last 10 ka, Edgecumbe and White Island (see Figures 1.1 and 3.3). Edgecumbe is a small polygenetic cone located near the Bay of Plenty coast, which is made up from andesites, dacites and associated pyroclastic deposits. There are believed to have been two main eruptive episodes at ~6 ka and ~4 ka, and activity continued at least until ~3 ka ago (Carroll et al., 1997).

White Island is situated 50 km north of the North Island of New Zealand in the Bay of Plenty. The volcano has been characterised by minor explosive and phreatic

eruptions throughout the last 200 years (Simkin and Siebert, 1994). The island has a vigorous hydrothermal and fumarole system (Giggenbach, 1987; Le Cloarec et al., 1992), driven by small volumes of magma at shallow depths beneath the volcanic edifice (Le Cloarec et al., 1992). The volcano comprises lavas and bombs, dominantly calc-alkaline and basaltic andesite to andesite in composition. A few very unusual compositions have been erupted as bombs from recent eruptions. The bombs are highly peralkaline and chlorine rich, and are believed to represent melts of local lake sediments and/or hydrothermally altered tuffs (Wood and Browne, 1996).

Aliquots of sample powder for two lavas from each of these volcanoes were supplied by Dr John Gamble.

3.4.3 Taranaki (Mt. Egmont): Across-arc Comparisons

Taranaki lies ~140 km to the west of the TVZ (see Figure 1.1), and is the most recent of a series of volcanic edifices which have formed along a broadly north-south trend, where eruptive activity has migrated south with time (Neall et al., 1986). These cones are collectively known as the Taranaki Volcanoes, and they have been active for at least 1.75 Ma (Stewart et al., 1996). The four volcanoes are: Paritutu (1.75 Ma), Kaitake (0.5 Ma), Pouakai (0.25 Ma) and Taranaki (< 120 ka). In some publications, Taranaki is referred to as Egmont, although the volcano is now more commonly called by its Maori name, Taranaki, which will be used throughout this thesis. The present volcano is ~180 km above the descending Pacific Plate (Adams and Ware, 1977), and despite its position it is inferred to be related to subduction (Price et al., 1992; Stewart et al., 1996) on the basis of geochemical signatures.

The earliest activity at the present cone is known only from volcaniclastic sediments deposited around the edifice (Neall et al., 1986; Stewart et al., 1996). This activity is thought to have commenced sometime before ~115 ka (Alloway et al., 1992). The current volcanic edifice is formed from pyroclastics, scoria and lava flows, and it is believed to have been built within the last 10 ka (Downey et al., 1994; Stewart et al., 1996). The lavas forming the main cone of Taranaki form a series of high K_2O, basaltic to

andesitic flows. These lavas differ from those of the TVZ by the frequent occurrence of amphibole phenocrysts.

Powders for a number of samples collected in 1989 and 1990 were obtained for analysis from Prof. Richard Price.

3.5 Summary

Westward subduction of the Pacific Plate under New Zealand has given rise to a series of volcanically active regions over the past 20 Ma. The youngest of these regions is the Taupo Volcanic Zone which has been active for ~2 Ma. The TVZ is also an area of extension which is thought to be related to the propagation of back-arc spreading from the Havre Trough to the north. The crustal thickness and composition beneath the TVZ is equivocal. Although fragments of Torlesse and Waipapa basement may be present at shallow levels in the TVZ, at deeper levels it may well be that much of the crust is of igneous origin.

Ruapehu, the main site of study for this thesis, is located at the southern apex of the TVZ and has been active for up to 500 ka. Throughout recorded history, Ruapehu has been active, with minor phreatic and phreatomagmatic activity, most recently in 1995 and 1996. A suite of samples has been gathered from coherent stratigraphic sequences for detailed geochemical analysis. Samples have also been analysed from Edgecumbe, White Island and Taranaki to provide comparisons within New Zealand.

Well there is room for one profound statement...,

Faber est qvisqve fortvnae svae

The motto of the Duke of Sto Helit

from 'The concife and possibly even accuratte Mapp' and 'Discworld Companion' – Terry Pratchett & Stephen Briggs.

Chapter 4

Petrography and Geochemistry of Ruapehu Lavas

4.1 Introduction

This chapter will review the published petrographic and geochemical data for Ruapehu lavas and incorporate and compare various data obtained as part of this study. Despite considerable work on both the andesitic and rhyolitic systems of the Taupo Volcanic Zone (TVZ), and many recent advances in our understanding of how subduction results in magma generation, there are still considerable uncertainties and problems in explaining the complex nature of volcanism at Mount Ruapehu and throughout the TVZ. The data will be examined in terms of identifying the processes and conditions involved in the differentiation of Ruapehu magmas, in order to provide a framework for understanding the time information that the U-series data presented in Chapter 5 can yield.

The samples analysed as part of this study were selected for their applicability to U-series work, and therefore only represent a limited part of the stratigraphic and compositional range of Ruapehu lavas. The detailed petrological and geochemical complexities of Ruapehu eruptives are being examined in ongoing work by R.C. Price and coworkers, and therefore this chapter presents a broad look at the general differentiation processes involved in generating Ruapehu eruptives.

4.2 Petrography

The petrography of Ruapehu lavas has been looked at in varying detail by several studies (Clark, 1960a; Clark, 1960b; Ewart and Stipp, 1968; Cole, 1978; Cole, 1979; Graham and Hackett, 1987; Gamble et al., 1990; Graham et al., 1995). A petrographic classification scheme for Ruapehu lavas was put forward by Cole (1978), and an improved

scheme employing both petrographic and geochemical characteristics was subsequently outlined by Graham and Hackett (1987). This classification system has subsequently been expanded upon to cover all the andesites and dacites from the TVZ (Patterson and Graham, 1988; Graham and Worthington, 1988; Cole and Graham, 1989; Graham et al., 1995), which is summarised in Table 4.1. The significance of these different andesite types is a matter open to some conjecture but for the most part, it is probably reasonable to argue that the distinct characteristics are linked to differences in the pre-eruption differentiation of these magmas (e.g. Graham and Hackett, 1987). However, it is also possible that there are subtle differences, for example in volatile contents, in the parental melts at different locations within the TVZ, or that the apparent geographic limits of certain types is simply a function of limited exposure and sampling.

Type	Phase assemblage	Locality	Reference
1	plag > pyx ± ol + op	Ubiquitous	a, b
2	plag >> pyx + op	Ubiquitous	a, b
3	pyx + ol >> plag + op	Ubiquitous	a, b
4	pyx >> plag + hbl ± ol + op	Ruapehu, Ngatamariki	a, b
5	ol + pyx >> plag (gm) + op	Hauhungatahi, Ohakune, Pukekaikiore, Waimarino	a, b
6	plag >> ol + pyx + op	Ruapehu, Pukeonake	a, b
7	plag > ol + pyx + op	Central ToVC	b, c
8	plag >> ol + pyx + op	Rolles Peak	b, d
9	ol + pyx > plag + op	White Island	b, e

Table 4.1: Types of andesite and dacite from the Taupo Volcanic Zone. Abbreviations are: plag = plagioclase, pyx = clino- and orthopyroxene, ol = olivine, hbl = hornblende, op = opaques, gm = groundmass, ToVC = Tongariro Volcanic Centre. References are: a = Graham and Hackett (1987), b = Graham et al. (1995), c = Patterson and Graham (1988), d = Graham and Worthington (1988), e = Cole and Graham (1989).

The petrographic details of individual samples used in this study are summarised in Appendix B. Samples from the minor eruptions this century were not studied in thin section in view of the very small amounts of material available, and a number of samples from the Whangaehu and Ohinepango sequences were available only as powders, and so no petrographic information is presented for these samples. The majority of samples available as thin section or hand specimens used in this study appear to be type 1-3 andesites based on the ubiquitous presence of plagioclase, clinopyroxene and orthopyroxene phenocrysts (Graham and Hackett, 1987).

All the samples examined in thin section have similar phenocryst petrography but with subtle differences in the proportions of phenocrysts present, and in the degree of crystallinity of their groundmasses. This is probably the result of differences in residence time and/or physical conditions in very shallow magma storage areas immediately beneath the volcano, or to variations in eruptive processes. Differences in the eruptive history of certain flows is apparent in the field, where evidence of either sub-glacial eruption, or flows which have come into contact with either water or ice, can be identified in the form of fine grained glassy flows exhibiting multiple scales of columnar jointing due to extremely rapid cooling.

The normal phenocryst phases present in order of decreasing proportions are; plagioclase, clinopyroxene and orthopyroxene, with microphenocrysts of titanomagnetite and patches of ilmenite. The groundmass comprises plagioclase microlites, pyroxene and opaque Fe-Ti oxides. Flow aligned, trachytic texture is common in the groundmass of many samples and in some cases (e.g. R96-14) phenocrysts also show a degree of alignment. Phenocrysts of forsteritic olivine (Fo_{94}-Fo_{74}) have been reported in a few Ruapehu lavas spanning the entire range of whole rock compositions, although they are most abundant in the more primitive compositions (Graham and Hackett, 1987; Gamble et al., 1990). Highly resorbed hornblende has also been found in one sample (Graham and Hackett, 1987). Neither of these phases has been identified in any of the samples available as thin sections in this study.

Plagioclase phenocrysts have two general forms in the samples studied. Large euhedral to subhedral crystals up to 5 mm in size commonly have cores which are filled with inclusions of glass, pyroxene and rarely magnetite, and these cores are mantled by thin rims of inclusion free plagioclase. The second form of plagioclase phenocrysts occurs more often as smaller, commonly subhedral crystals < 2 mm in size, although sometimes as larger crystals, and these show complex twinning and oscillatory zoning textures. In some cases these zoned crystals are overgrown by thin rims, which are often more sodic (Graham and Hackett, 1987). Plagioclase phenocrysts often show evidence for extremely complex growth histories in addition to the zoning and inclusions previously mentioned.

Many of the larger crystals are clearly formed from multiple fragments which have combined and grown together, with growth twins overprinting different zoning patterns and irregular internal boundaries.

It is clear from visual inspection that many of the plagioclase crystals have been out of equilibrium with their host melt at some time. Some studies elsewhere have tried to assess such disequilibrium by comparing the Ca# $(100*Ca/(Ca+Na))$ of phenocryst rims with whole rock Ca# values, and used the lack of correlation to suggest that many of the crystals are not in equilibrium with their host magmas (e.g. Heath et al., 1998a). However, the highly porphyritic nature of the Ruapehu samples makes it unlikely that the whole rock composition is a true reflection of the liquid composition at the time of eruption, and therefore such a comparison is not valid in this instance.

Reported compositions for plagioclase phenocrysts from microprobe analyses are An_{89}-An_{40} (Graham and Hackett, 1987). Several studies have used experimental data to derive empirical relationships between plagioclase compositions and P-T-X parameters (Grove et al., 1992; Panjasawatwong et al., 1995). In general, the effect of increasing Ca# and Al# $(100*Al/(Al+Si))$ in the melt is to increase the An content of plagioclase, whereas increasing pressure tends to reduce the An content. The presence of H_2O in the melt tends to increase the An content of plagioclase, although the effect is less systematic than those considered above, particularly in water under-saturated melts (Baker and Eggler, 1987; Panjasawatwong et al., 1995).

Despite this caveat it is possible to make qualitative statements about the composition and physical parameters of the crystallising magmas at Ruapehu; in general, the more calcic plagioclase compositions are consistent with high An contents observed in other arc magmas, which some authors have suggested is related to the raised water contents of the magmas (e.g. Sisson and Grove, 1993a). There is evidence, discussed in Section 4.3.4, which suggests that the magmas erupted at Ruapehu are generally water-under saturated, and therefore it is likely that the high An contents, reflect both relatively shallow crystallisation of plagioclase and elevated H_2O contents. The lower An contents are most likely a result of differentiation affecting the Al# and Ca# of the melt, and the

experimental data of Panjasawatwong (1995) imply that the lowest An contents are produced from a melt with Ca# and Al# of 45-55 and 20-24 respectively, consistent with whole rock major element abundances.

Clinopyroxene is universally present, and usually subordinate to plagioclase as a phenocryst phase, although in some cases it is approximately equal in abundance. Phenocrysts are usually similar in size to those of plagioclase, and in some samples, the larger crystals are often altered (X1-9, W9-3, R96-2). Orthopyroxene is normally less abundant than clinopyroxene except in the most evolved rocks, and it is commonly found as small phenocrysts (1-3 mm). The lower abundance and smaller typical size of orthopyroxene is consistent with gradual replacement of clinopyroxene by orthopyroxene as the main pyroxene phase in the crystallising assemblage with increasing differentiation (Graham and Hackett, 1987). This change probably either occurs because olivine becomes unstable and undergoes reaction to orthopyroxene at some stage during crystallisation, or simply because orthopyroxene enters the crystallising assemblage later (Grove and Kinzler, 1986; Myers and Johnston, 1996). The conditions under which this transition occurs, and whether reaction between olivine and liquid occurs depends largely on magma composition and whether equilibrium or fractional crystallisation is occurring (Grove and Kinzler, 1986).

Minor phases present as phenocrysts are titanomagnetite and occasionally apatite. Titanomagnetite occurs as anhedral to subhedral microphenocrysts and occasionally as inclusions in pyroxene. In some samples, titanomagnetite is found clustered around the grain boundaries of plagioclase and pyroxene (e.g. X1-9). Apatite has been reported as microphenocrysts and a groundmass phase in andesites and dacites (Graham and Hackett, 1987), although its presence has not been identified in any of the samples examined in this study.

Glomerocrysts are common in many lavas, indicating potentially complex growth histories for some crystals. These occur as anorthosite, pyroxenite (often with abundant interstitial and phenocryst titanomagnetite) and gabbroic compositions. One sample (R96-2) contains a fragment of an apparently layered (pyroxenite-anorthite) glomerocryst.

Whether these glomerocrysts represent true cumulate fragments or just aggregations of free crystals is uncertain, although the presence of layered glomerocrysts suggests that at least some of these crystal masses may be of cumulate origin.

Ruapehu lavas often contain small xenoliths of various compositions (Graham and Hackett, 1987). In the samples examined in this study, the only xenoliths present are predominantly quartzofeldspathic and appear to be of sedimentary origin, although meta-igneous granulite xenoliths have also been reported in lavas from Ruapehu (Graham and Hackett, 1987; Graham et al., 1990).

4.3 Major and Trace Element Geochemistry

The samples described in Section 4.2 were analysed for major and trace element abundances by XRF spectrometry at the Open University. Most of the samples were also analysed for rare earth element (REE) concentrations by INAA at the Open University (data for these analyses is presented in Appendix C, and full analytical details for both techniques are given in Appendix D). The samples investigated in detail for this study are limited in terms of stratigraphic range because they were selected specifically for U-series analysis. Therefore comparisons with more extensive databases for Ruapehu lavas will be used to show that the sample suite used in this study is characteristic of much of the compositional range observed in the eruptives from Ruapehu.

4.3.1 Classification

The samples analysed in this study have a range of SiO_2 concentrations of ~54-64 wt% and MgO abundances are ~2-7 wt%. These data cover much of the total variation observed in a large compilation of Ruapehu data by Graham (1994) which shows ranges of ~53-67 wt% SiO_2 and ~1-9 wt% MgO. This indicates that despite the limited number of samples analysed in this study, their major element compositions span much of the observed range in Ruapehu eruptives.

Three classification diagrams will be used to show the general nature of the lavas erupted at Ruapehu and to put them in the context of other arc lavas. In order to

discriminate between calc-alkaline and tholeiitic compositions, Figures 4.1 and 4.2 show both the compilation of Graham (1994) and the data for the samples from this study respectively on the AFM diagram of Irvine and Baragar (Irvine and Baragar, 1971) and the SiO_2 vs FeO(T) / MgO diagram of Miyashiro (Miyashiro, 1974).

On both diagrams, almost all samples can be classified as calc-alkaline, the interpretation of which in terms of crystallisation conditions will be discussed in some detail in Section 4.3.4. If the data for the four main stratigraphic groups are examined in detail, there appears to be little temporal evolution or variation, with samples from the Waihianoa, Mangawhero and Whakapapa Formations covering a very similar range on both diagrams, except for the absence of samples of more primitive compositions in the most recent Whakapapa Formation. The oldest identifiable rocks from Ruapehu, in the Te Herenga Formation, do appear to be slightly different with lower levels of SiO_2 and alkali enrichment at a given MgO or FeO(T) / MgO composition. This may represent a real difference in process or possibly a sampling artifact as the Te Herenga Formation has very limited surface exposure. For the main purpose of this study, however, rocks of Te Herenga affinity are of little significance because they are too old for U-series techniques to be applicable.

The samples studied in this work are typical of previous analyses of Ruapehu lavas. The samples produce an almost flat trend on an AFM diagram, and a broad positive correlation on a plot of FeO(T) / MgO vs SiO_2, which trends roughly parallel to the boundary between calc-alkaline and tholeiitic compositions. The sample suite analysed for this study doesn't contain any examples of the most extreme enrichments of SiO_2 and alkalis that have been identified from other studies; such compositions are likely to have undergone the largest degrees of crustal assimilation and are the least likely to preserve source features.

Intermediate arc rocks are commonly also classified on the basis of SiO_2 and K_2O concentrations (e.g. Gill, 1981; Le Maitre, 1989), and data for Ruapehu lavas are shown plotted on the discrimination diagram of Le Maitre (Le Maitre, 1989) in Figure 4.3. As with the calc-alkaline vs tholeiitic discrimination plots, the ranges spanned by the main

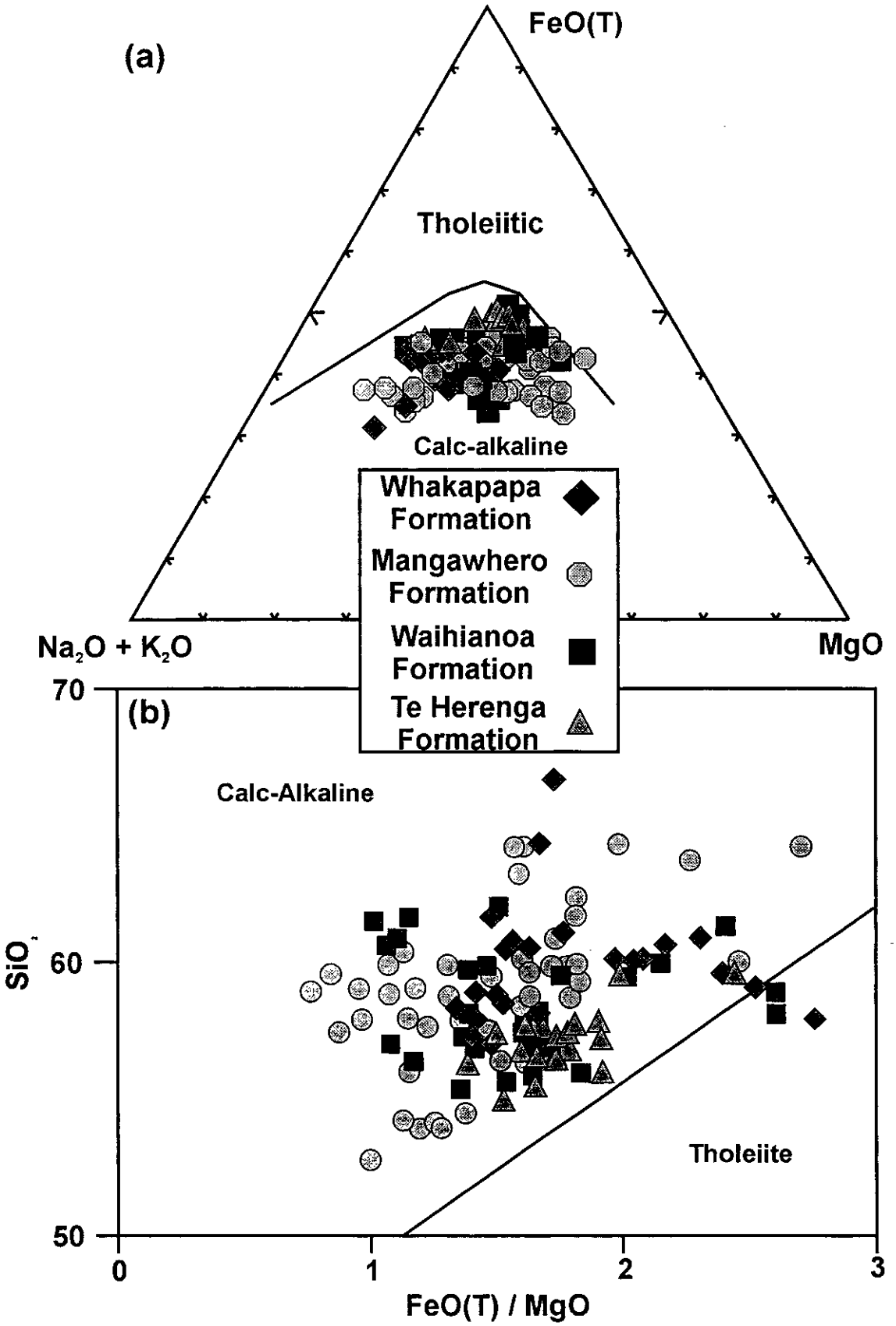

Figure 4.1:

(a) - AFM diagram of Irvine and Barager (1971), see text for full discussion. FeO(T) is calculated as FeO + 0.8998 * Fe_2O_3. Data is from the compilation of Graham (1994). All oxides are expressed in wt%.

(b) - FeO(T)/MgO vs SiO_2 discrimination plot for calc-alkaline and tholeiitic rocks after Miyashiro (1974). Calculation of FeO(T) and data sources are the same as for (a). All oxides are expressed in wt%.

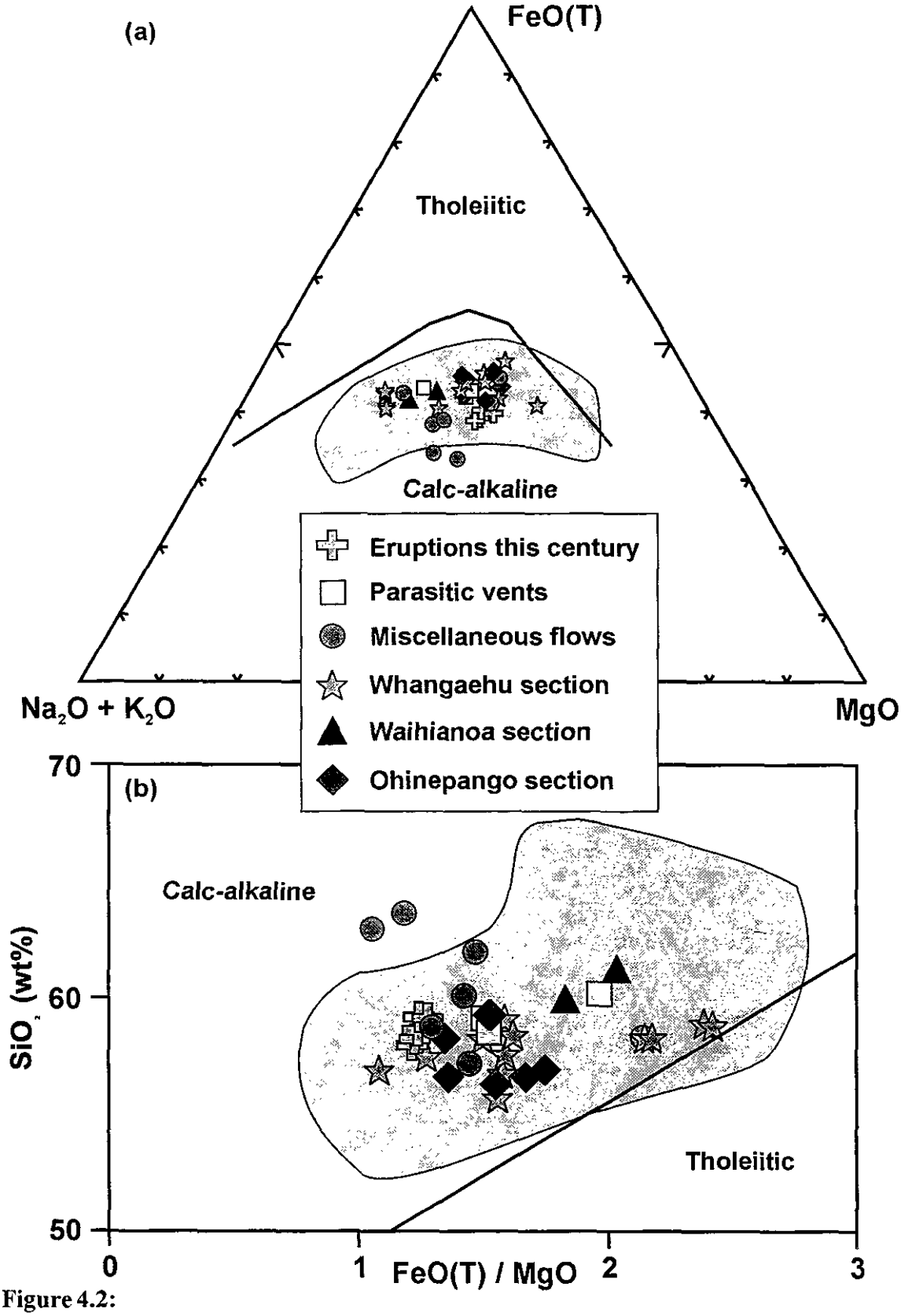

Figure 4.2:

(a) - Samples used in this study plotted on an AFM discrimination diagram after Irvine and Barager (1971). The shaded field represents the data for Ruapehu lavas from the compilation of Graham (1994). FeO(T) is calculated as FeO + 0.8998 * Fe_2O_3. All oxides are expressed as wt%.

(b) - Samples used in this study plotted on and FeO(T) / MgO vs SiO_2 discrimination diagram after Miyashiro (1974). Shaded field and calculation of FeO(T) is the same as for (a). All oxides expressed as wt%.

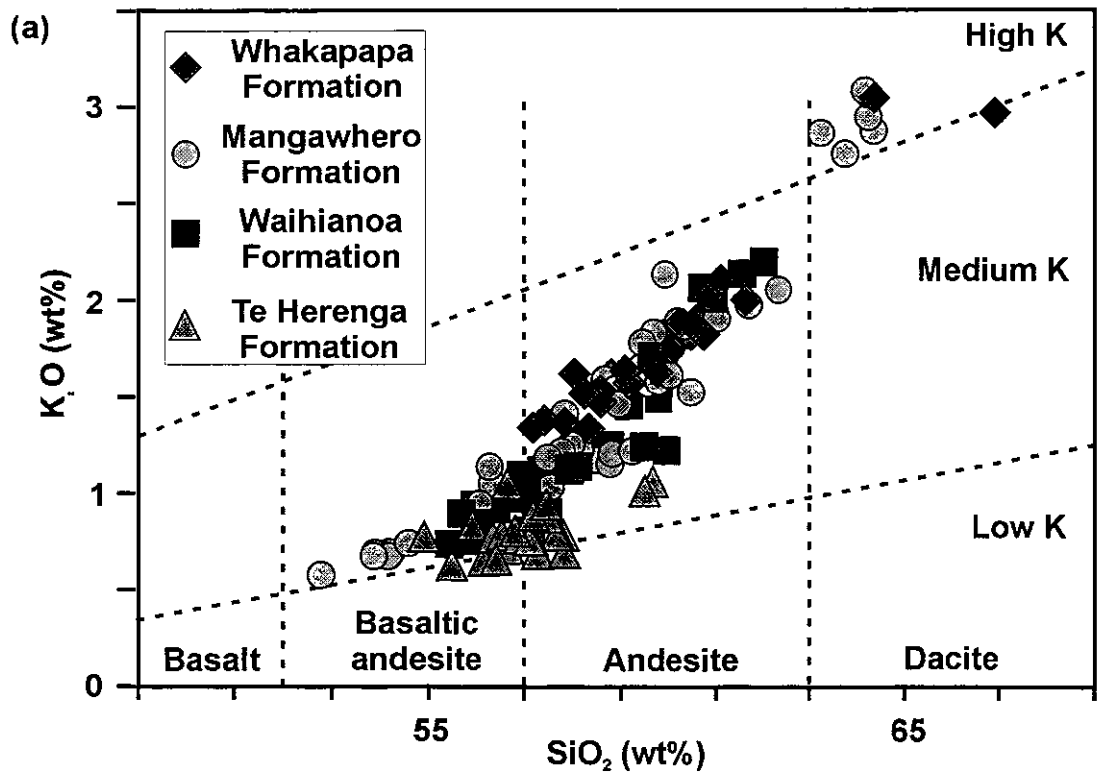

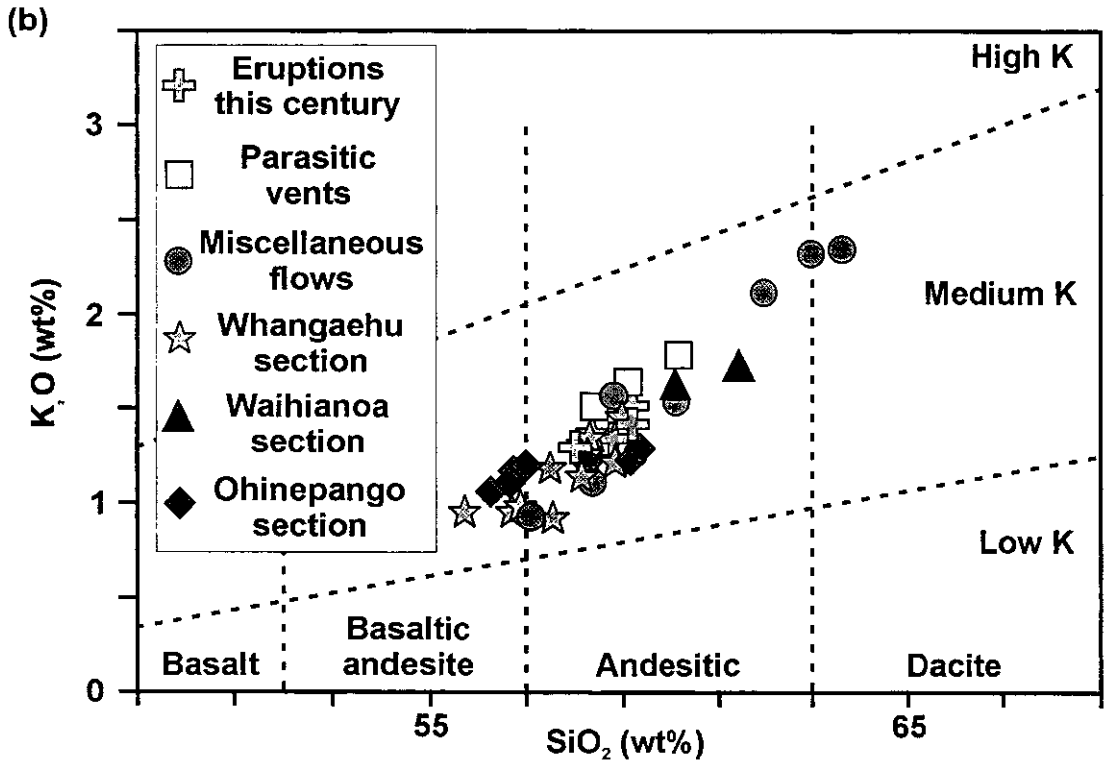

Figure 4.3:

(a) - Data for Ruapehu lavas from the compilation of Graham (1994) plotted on an SiO_2 vs K_2O discrimination diagram with fields after Le Maitre (1989).

(b) - Data for samples used in this study plotted on an SiO_2 vs K_2O discrimination diagram after Le Maitre (1989).

stratigraphic groupings are very similar for the younger three Formations. The lavas are largely basaltic andesites and andesites and mostly fall within the medium-K field, although there is a progressive rise into the high-K field in the more evolved compositions which are dacitic in terms of their SiO_2 contents. The Te Herenga lavas have slightly different characteristics, consistent with the differences noted above, and trend along the boundary between the low- and medium-K fields. The data for the samples used in this study are predominantly andesites with a few dacites and basaltic andesites, and all show consistent increases of K_2O with increasing SiO_2.

4.3.2 Major Element Variations

A number of studies have looked at the major element chemistry and petrogenesis of both Ruapehu lavas and TVZ andesites as a whole. There has been a gradual evolution of ideas about the nature of these intermediate volcanics, particularly with a view to establishing the nature of the magmatic source and its relation to the subducting Pacific Plate. Early work suggested that the andesitic magmas were either generated through contamination of mantle derived basalts by continental crust, or were primary, mantle derived andesites (Ewart and Stipp, 1968). Subsequent studies suggested that the andesites were generated by melting of the downgoing slab and associated amphibolitised sediments (Ewart et al., 1977; Cole, 1978; Cole, 1979; Cole, 1981; Cole et al., 1983). Recent studies have essentially gone full circle, and suggest that andesites are the result of differentiation and contamination of mantle derived basalts (Graham and Hackett, 1987; Cole, 1990; Wilson et al., 1995; Graham et al., 1995). In this section existing data for Ruapehu lavas will be reviewed, and new data from this study presented.

The discussion of major element variations will concentrate on using both SiO_2 and MgO as the common variables, as both of these oxides show reasonably large ranges in Ruapehu lavas. The two have been used in conjunction because MgO is more likely to respond to fractional crystallisation influences, particularly growth and removal of the mafic phases such as olivine and clinopyroxene, whereas SiO_2 is likely to be sensitive to fractional crystallisation of non-silicate phases such as titanomagnetite, and to assimilation of local basement.

4.3.2.1 Major Element Variations with MgO

The variations of major elements with MgO for samples used in this study and for the compilation of Graham (Graham, 1994) are shown in Figures 4.4 and 4.5 respectively. Overall there is considerable scatter, which can be apportioned both to the presence of numerous different magma batches with variable pre-eruptive histories (Price et al., 1998), and to differences in phenocryst incorporation. Despite these variables, distinct trends are present representing in effect an average compositional history for a typical magma batch at Ruapehu.

Both CaO and FeO(T) are compatible throughout the range of MgO compositions and show systematically lower abundances with decreasing MgO content. The samples with the lowest MgO concentrations used in this study have higher CaO and Al_2O_3 values than expected although FeO(T) abundances fall within the anticipated trend, which is probably due to incorporation of high proportions of plagioclase relative to mafics, a feature which will discussed in greater detail later.

The main observations in the plots of SiO_2, Al_2O_3, K_2O and Na_2O are the negative correlations with MgO content. The samples mentioned above which probably have higher proportions of plagioclase than normal have lower concentrations of SiO_2 and K_2O than expected from the observed correlations. This has the effect of producing apparent inflections in the trends, although these do not reflect a change in the phases present in the crystallising assemblage. When a larger database is considered (Figure 4.5), these features disappear because the volume of information obscures the subtle shifts observed.

The concentrations of TiO_2 show very little systematic variation across the range of MgO compositions. The samples from this study show almost no correlation, although it is worth noting that the samples erupted in minor events this century have both very low TiO_2 concentrations and are some of the most primitive rocks, in terms of MgO content, used in the subsequent discussions. The larger database of Graham (1994) shows a very poor positive correlation of TiO_2 with MgO. Incorporation of titanomagnetite phenocrysts to differing degrees cannot be responsible for the variation, because the proportions present would have $\leq 0.25\%$ of the TiO_2 budget of a typical lava. It is more probable that variable

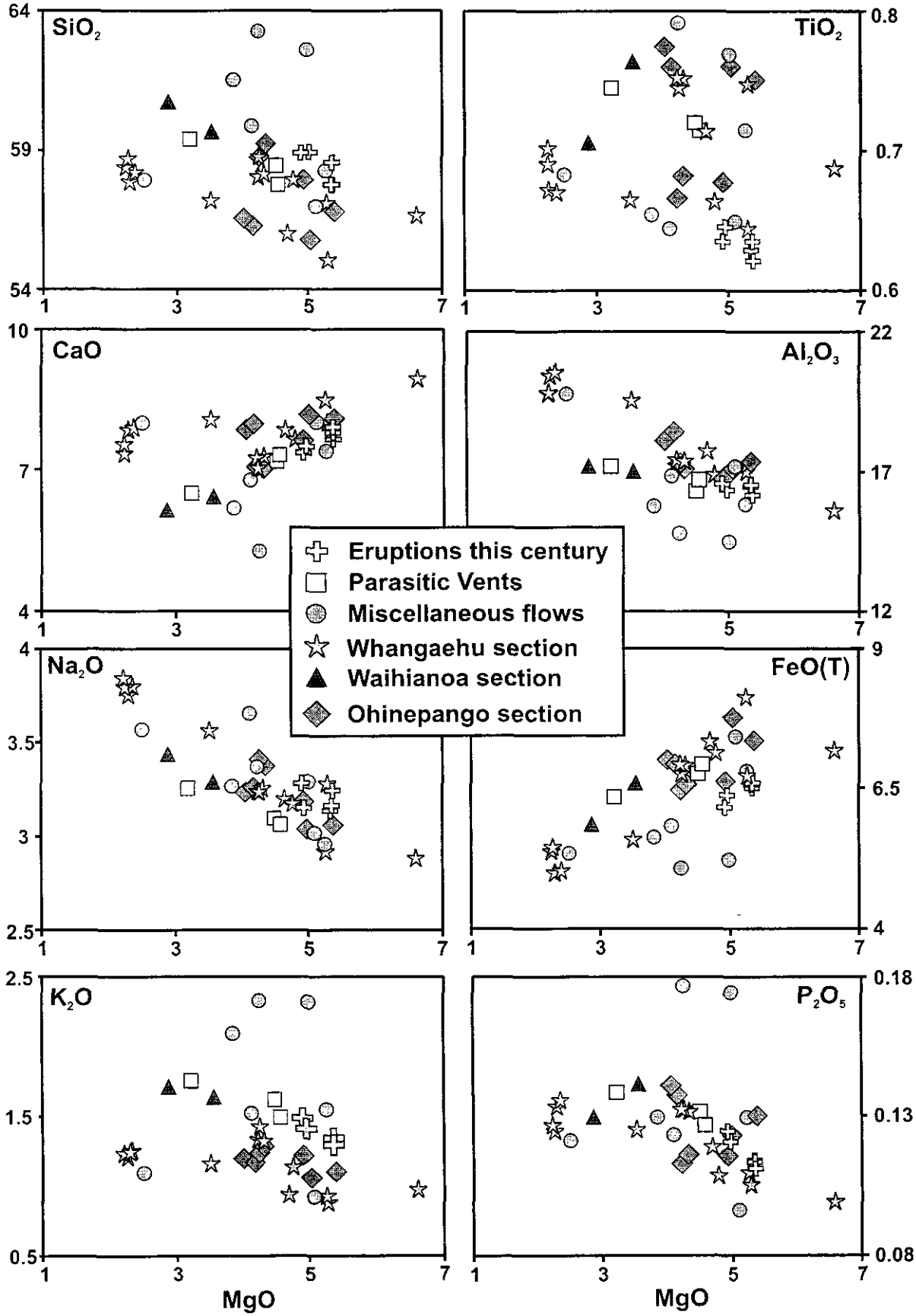

Figure 4.4: Variation of major elements with MgO content for Ruapehu samples analysed in this study. All axes are in wt% oxide. FeO(T) is calculated as $0.8998*Fe_2O_3$.

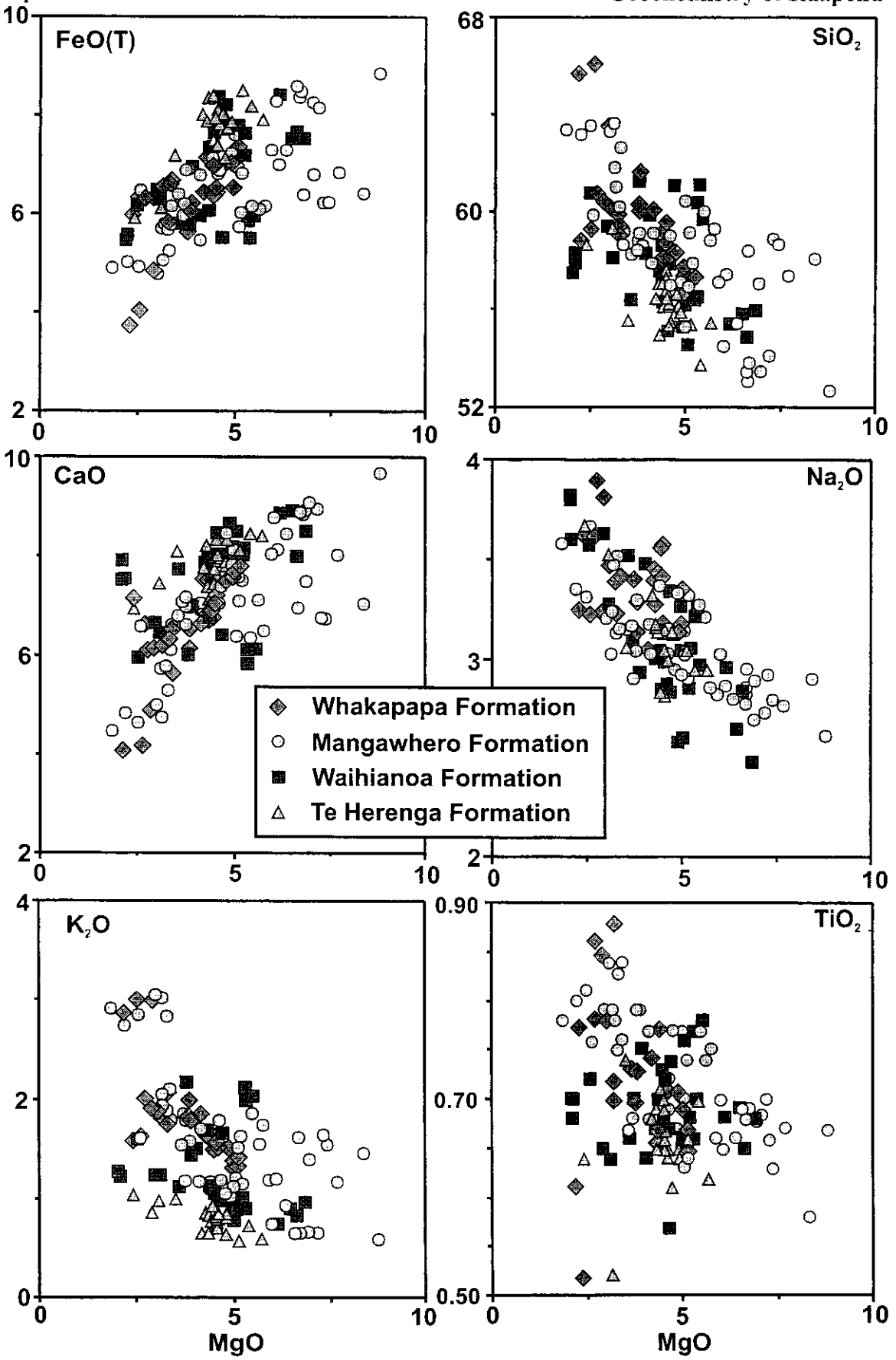

Figure 4.5: Major element variation diagrams showing the general nature of the geochemistry of Ruapehu lavas using data from Graham (1994). All axes are expressed as oxide wt%. FeO(T) is calculated as FeO + 0.8998 * Fe_2O_3.

degrees of fractional crystallisation and assimilation are responsible, particularly since the high density of magnetite is likely to make it more prone to crystal settling than other phases. There is considerable difference between the behaviour of FeO(T) and TiO_2 during magma evolution. This most likely results from FeO(T) abundances being strongly influenced by olivine crystallisation, whereas relatively small amounts of titanomagnetite and ilmenite fractional crystallisation can exert a much stronger control on TiO_2 than FeO(T) because of the difference in the relative abundance of these phases.

Whilst apatite is reported as a rare accessory phase in the more evolved lavas (e.g. Graham and Hackett, 1987), it never crystallises in sufficient quantities to affect the behaviour of P_2O_5 which remains incompatible in the samples analysed in this study. Data from the compilation of Graham (1994) has not been plotted because it is older and is of relatively poor quality. The most evolved lavas used in this study appear to have lower P_2O_5, suggesting compatibility, but this may be an effect of preferential incorporation of plagioclase over mafic phenocrysts as mentioned above, and the lower proportions of mafic phenocrysts present has had the effect of lowering MgO concentrations.

4.3.2.2 Major Element Variations with SiO_2

Variations of major element oxide abundances with SiO_2 are important because of the sensitivity to crystallisation of non-silicate phases and assimilation of silicic crustal melts. The variations observed in lavas used in this study are shown in Figure 4.6. A comparison between the samples analysed in this work and the larger data set of Graham and Hackett (1987) is made in Figure 4.7, where the fields for the different andesite types discussed in Section 4.2 are illustrated.

Variations of FeO(T) and CaO with SiO_2 produce very tight trends which show persistent decrease of Fe and Ca concentrations with increasing SiO_2. It is interesting to note that the samples with low MgO contents which showed anomalous CaO abundances in Figure 4.4, fall within the main trend when CaO is plotted against SiO_2, however these samples form a distinct group on a plot of FeO(T) against SiO_2. It can also be seen from Figure 4.7 that these samples consistently fall within the field of type 2 plagioclase

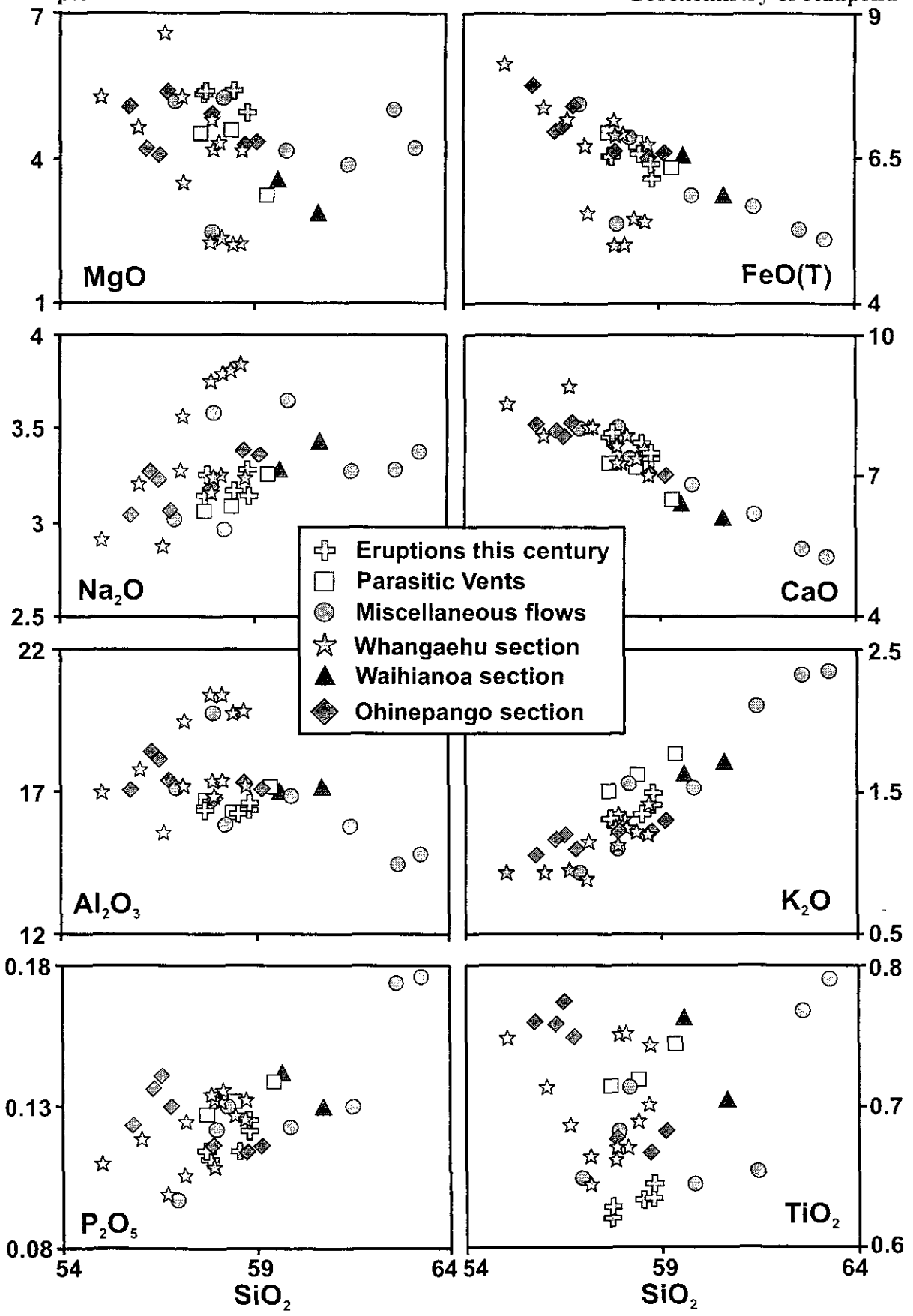

Figure 4.6: Variation of major elements with SiO_2 content for Ruapehu samples analysed in this study. All axes are expressed as oxide wt%. FeO(T) is calculated as 0.8998 * Fe_2O_3.

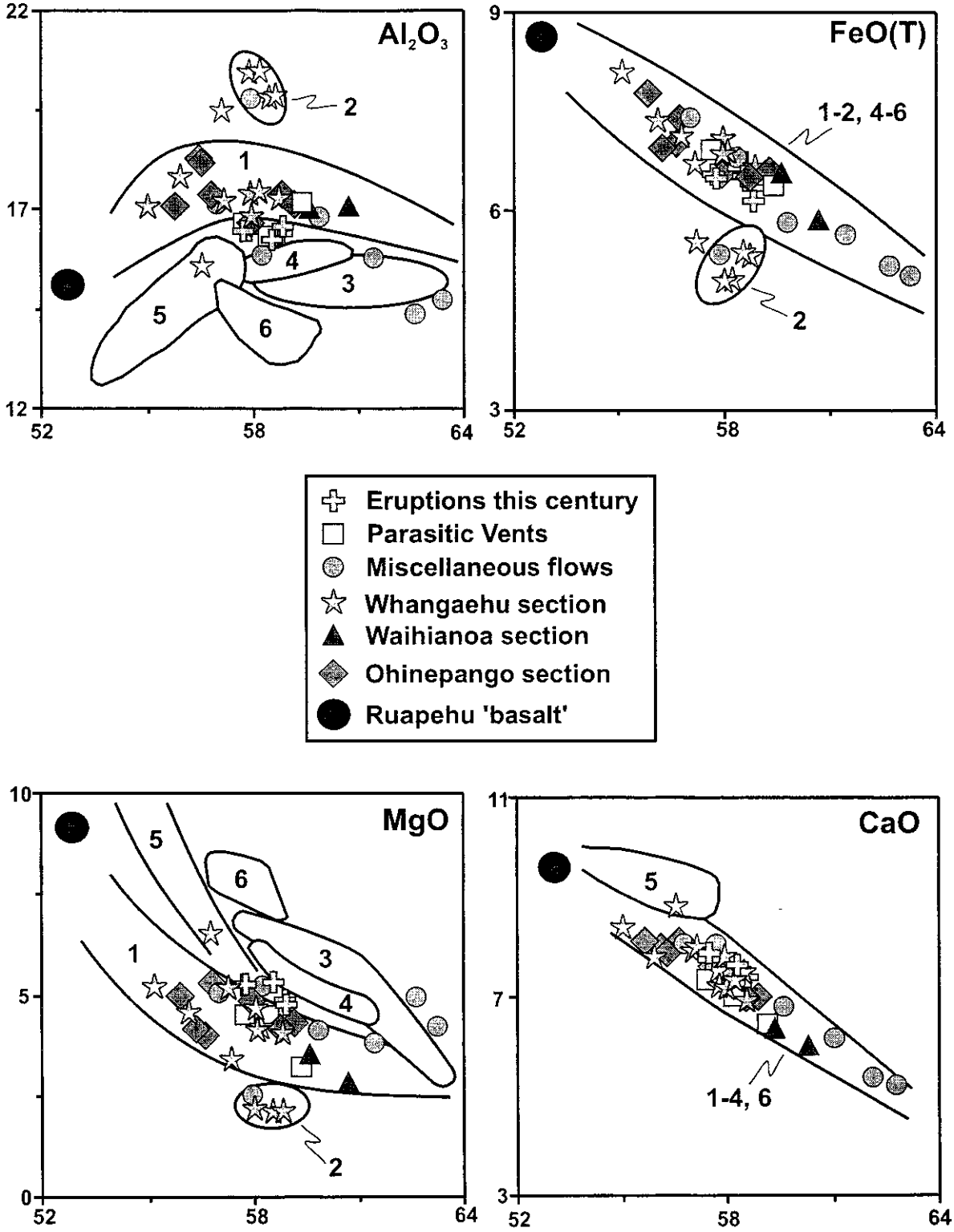

Figure 4.7: Plots showing variation of selected major elements with SiO_2 for all samples used in this study. Numbered fields discriminate between different andesite types found on Ruapehu (after Graham & Hackett, 1987). The Ruapehu 'basalt' composition is taken from Gamble et al. (1990). All axes are expressed as oxide wt%.

accumulative lavas (Graham and Hackett, 1987). The presence of an unusually high proportion of plagioclase to mafic (predominantly clino- and orthopyroxene) phases results in a reduction of the MgO and FeO(T) abundances, whereas CaO, K_2O and P_2O_5 are consistent with the SiO_2 abundances and fall within the observed trends.

There is very little correlation between TiO_2 and SiO_2. Within the scatter observed on the SiO_2 vs TiO_2 plot there is a hint that the samples erupted this century and the samples from the parasitic vents form positive arrays, although the compositional range over which these trends form is very limited. The data for the Ohinepango sequence appear to form a negative array, however it is likely that this sequence contains lavas from several different magma batches (R.C. Price, pers. comm.) which makes such simple observations unrealistic.

Positive correlations are observed for P_2O_5, K_2O and Na_2O, and it appears that as mentioned above, the presence of apatite in the crystallising assemblage of the most evolved rocks has had very little effect on the bulk chemistry. As with TiO_2, the samples for the Ohinepango sequence form an apparently negative P_2O_5-SiO_2 array, although this may well represent two separate positive arrays due to the presence of two somewhat different magma batches. The array for Na_2O shows considerably more scatter when plotted against SiO_2 rather than MgO. The reasons for this additional scatter are not totally clear for estimates of the composition of partial melts of local crust both from xenoliths (Graham and Hackett, 1987) and experimental melting studies (Conrad et al., 1988) suggest that such an assimilant should have high Na_2O in addition to high K_2O and SiO_2. Thus, such assimilation should produce a good correlation of Na_2O with SiO_2. As Na_2O forms a better trend with MgO, whereas K_2O correlates better with SiO_2, it is likely that crystallisation is exerting a greater control on Na_2O than K_2O. The manner of this crystallisation control is most likely to be increasing incorporation of plagioclase relative to mafic phases because of the negative correlation between Na_2O and MgO. This suggestion is borne out by plots of Na_2O and K_2O against Al_2O_3 (Figure 4.8). There is a distinct positive correlation between Al_2O_3 and Na_2O which implies a role for plagioclase

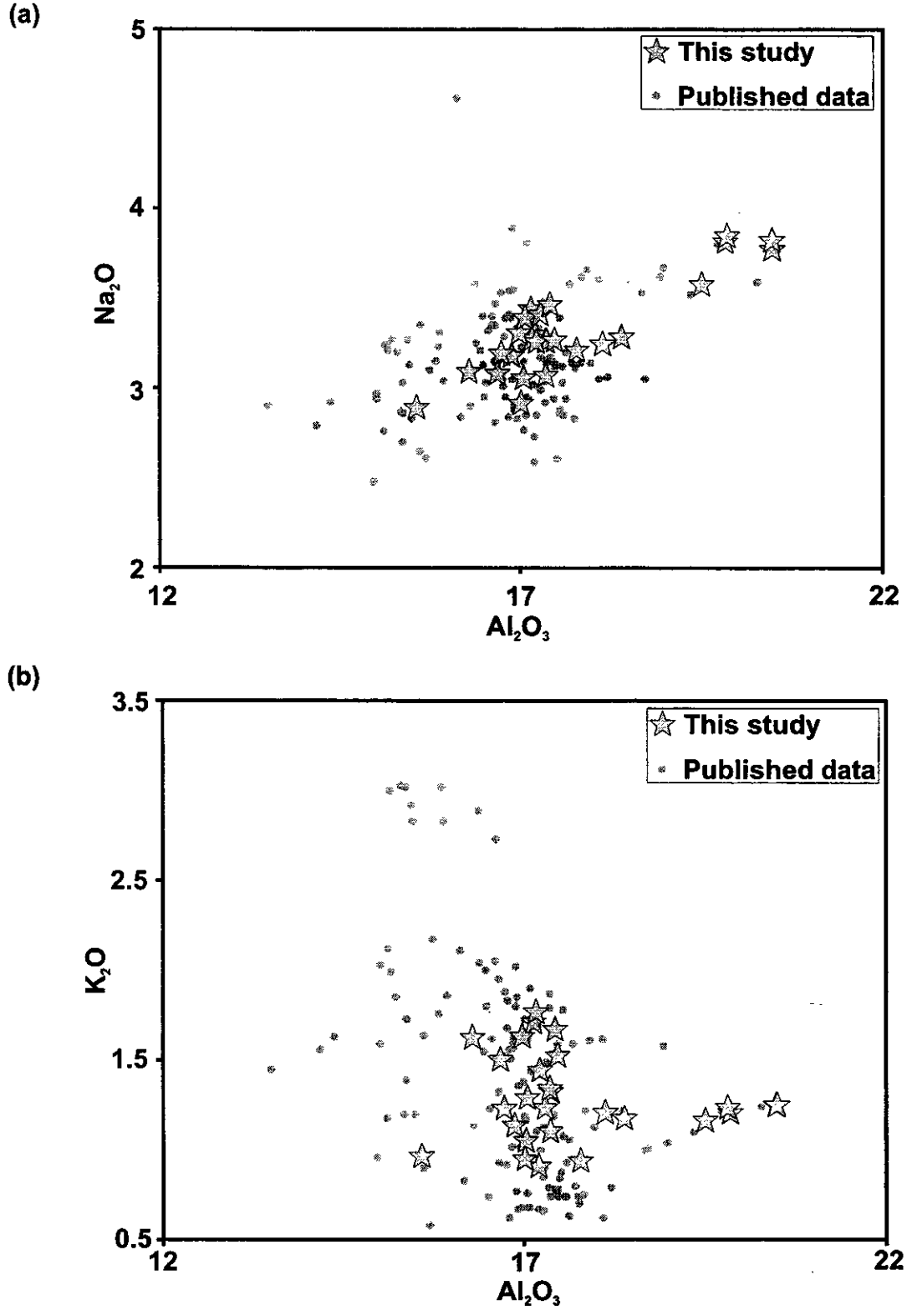

Figure 4.8:

(a) - Variation of Na_2O with Al_2O_3 for Ruapehu lavas. Data for samples not analysed in this study are from Graham (1994). Major elements are expressed as oxide wt%.

(b) - Variation of K_2O with Al_2O_3 for Ruapehu lavas. Data sources and units as for (a).

in controlling both Na_2O and Al_2O_3, whereas K_2O doesn't form an identifiable trend with Al_2O_3.

The classification system for TVZ intermediate rocks proposed by Graham and Hackett (1987) uses major element variations with SiO_2 as a powerful tool for distinguishing the groups. The data from this study are presented on these diagrams in Figure 4.7. As mentioned earlier, a number of samples clearly fall into the fields of type 2 plagioclase accumulative lavas on plots of SiO_2 vs FeO(T), MgO and Al_2O_3, and a further sample appears transitional between type 1 and type 2 andesites. In practice this probably represents limited sampling of a continuum of compositions. Determinations of the modal proportions of the various phenocryst phases by Graham and Hackett (1987) for a number of samples illustrated the effects of plagioclase accumulation rather nicely; in the majority of samples which plot outside the field for type 2 lavas, plagioclase accounts for some 35-65% of the phenocryst population and 10-25% of the total rock, whereas in the case of type 2 lavas, plagioclase can comprise up to 95% of the phenocryst population, and 30% of the total rock.

The data presented herein show a systematic progression out of the type 1 field into the fields for type 3 and 4 andesites with increasing SiO_2 on a plot of Al_2O_3 vs SiO_2. This progression is less obvious on the plot of SiO_2 vs MgO, although the samples from eruptions this century plot towards the field for type 4 lavas and two young lavas plot near the field for type 3 andesites. One sample (R95-20) consistently plots within the field for type 5 andesites on plots of SiO_2 vs Al_2O_3, MgO and CaO. These olivine-pyroxene phyric lavas have only previously been identified from the satellite vents of Hauhungatahi, Ohakune, Pukekaikiore and Waimarino, but this sample may represent a rare occurrence of such a magma on the main edifice.

4.3.3 Trace Element and Rare Earth Element Variations

This section presents new data for trace element abundances in the samples used in this study. These elements are often more sensitive indicators of magmatic processes

than major elements, and it is therefore important to consider the basic nature and trends of their concentrations so that complex processes and models can subsequently be considered.

A selection of samples characteristic of the compositional range observed in the Ruapehu eruptives are plotted on a N-MORB normalised trace element variation diagram and a chondrite normalised rare earth element (REE) variation diagram in Figure 4.9. A limited amount of data has been plotted because the entire suite of samples shows essentially the same features but with differing degrees of differentiation.

Ruapehu lavas in general show considerable enrichments of large ion lithophile elements (LILE) such as Rb, Ba and K, and other highly incompatible elements such as U and Th relative to N-MORB even in the most primitive composition identified, Ruapehu 'basalt' (Graham and Hackett, 1987; Gamble et al., 1990). In contrast, the high field strength elements (HFSE) such as Ti, Zr, Hf, Nb and Ta and most of the heavier REE show MORB-like values with only minor enrichments and depletions. This contrast leads to high LILE / HFSE ratios, characteristic of many arc lavas (e.g. summary of Pearce and Peate, 1995). Large positive K and Pb anomalies are present with concentrations in the most evolved samples up to 40 times those of N-MORB, although the accuracy of the Pb concentrations may be poor because these samples have abundances close to machine detection limits. A slight negative Ti anomaly can be seen which becomes increasingly pronounced in the more evolved lavas, because the Ti concentration remains almost constant, apparently buffered during crystallisation and assimilation processes.

The REE data for Ruapehu lavas show enrichment of the LREE relative to HREE, with a range in abundances of 20-80 times chondrite for La, whereas Yb and Lu show near constant concentrations of 10-13 times chondritic values. Negative Eu anomalies are characteristic of most samples with values of Eu / Eu^* varying between 0.93 in the least evolved samples analysed to 0.65 in the most differentiated lavas (see Appendix D for details of the calculation), indicative of increasing degrees of fractional crystallisation of plagioclase in the more evolved samples.

Variations of individual trace elements with MgO and SiO_2 concentrations are shown in Figures 4.10 and 4.11 respectively. Against MgO, most of the trace elements

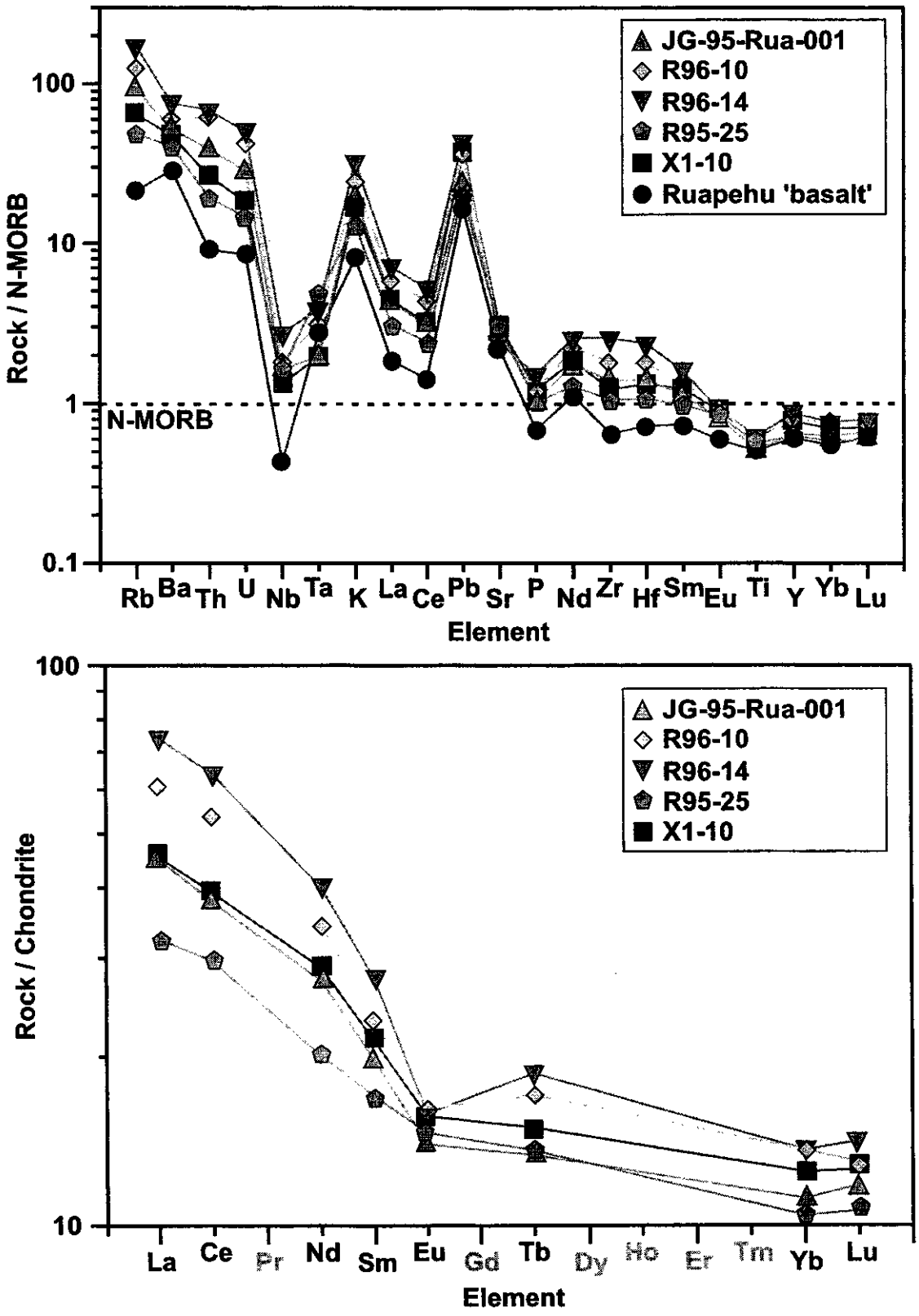

Figure 4.9: MORB normalized trace element and chondrite normalised REE variation diagrams for selected samples from Ruapehu. Normalising values from Sun & McDonough (1989). Data for Ruapehu Basalt from Graham & Hackett (1987) and Gamble et al. (1993).

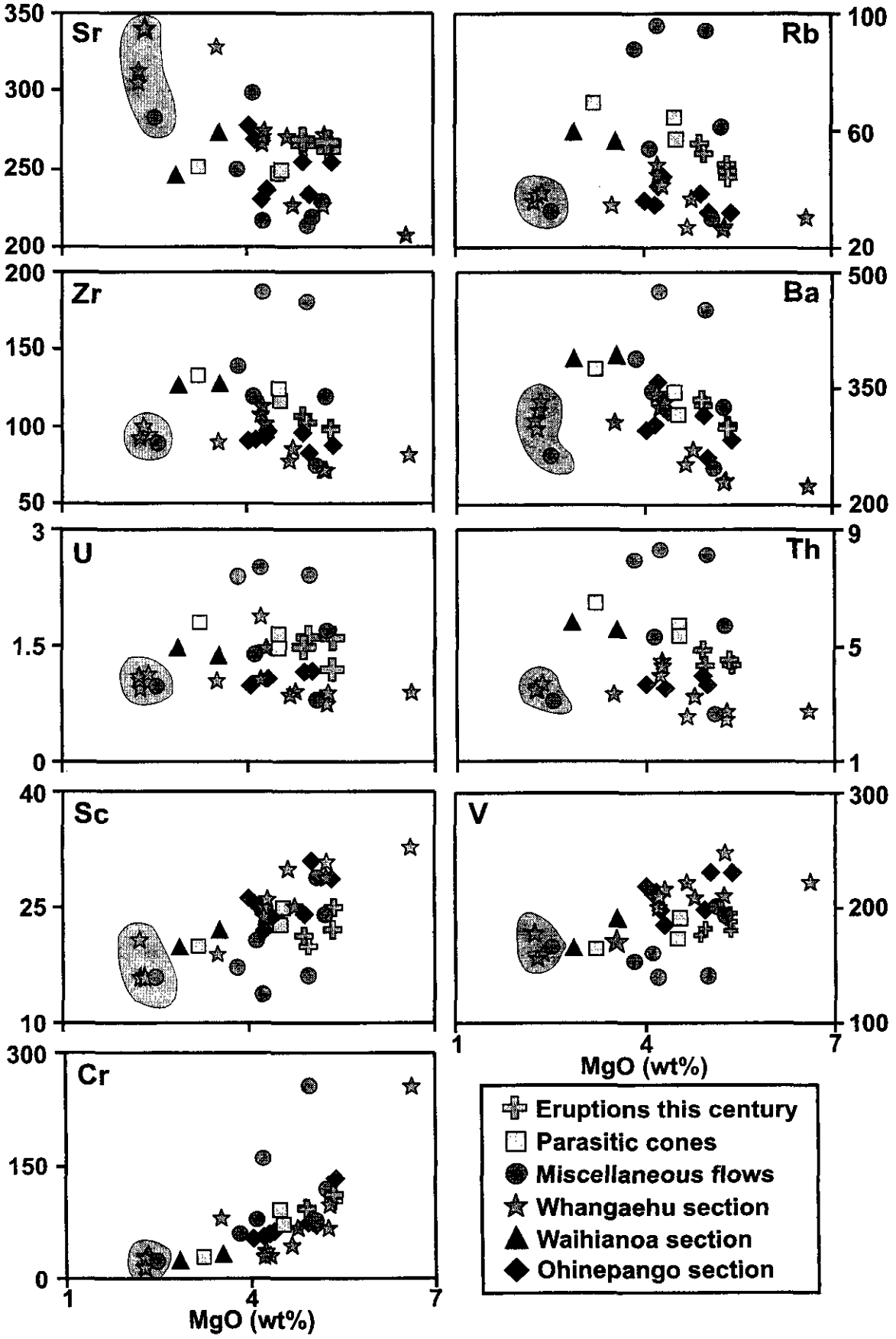

Figure 4.10: Variations of selected trace elements with MgO content for samples from this study. All trace element abundances are expressed as μg g^{-1}. All trace elements concentrations except those for U and Th were determined by XRF analysis. Th and U abundances were determined by INAA. Fields highlighted in orange are for samples which are plagioclase accumulative.

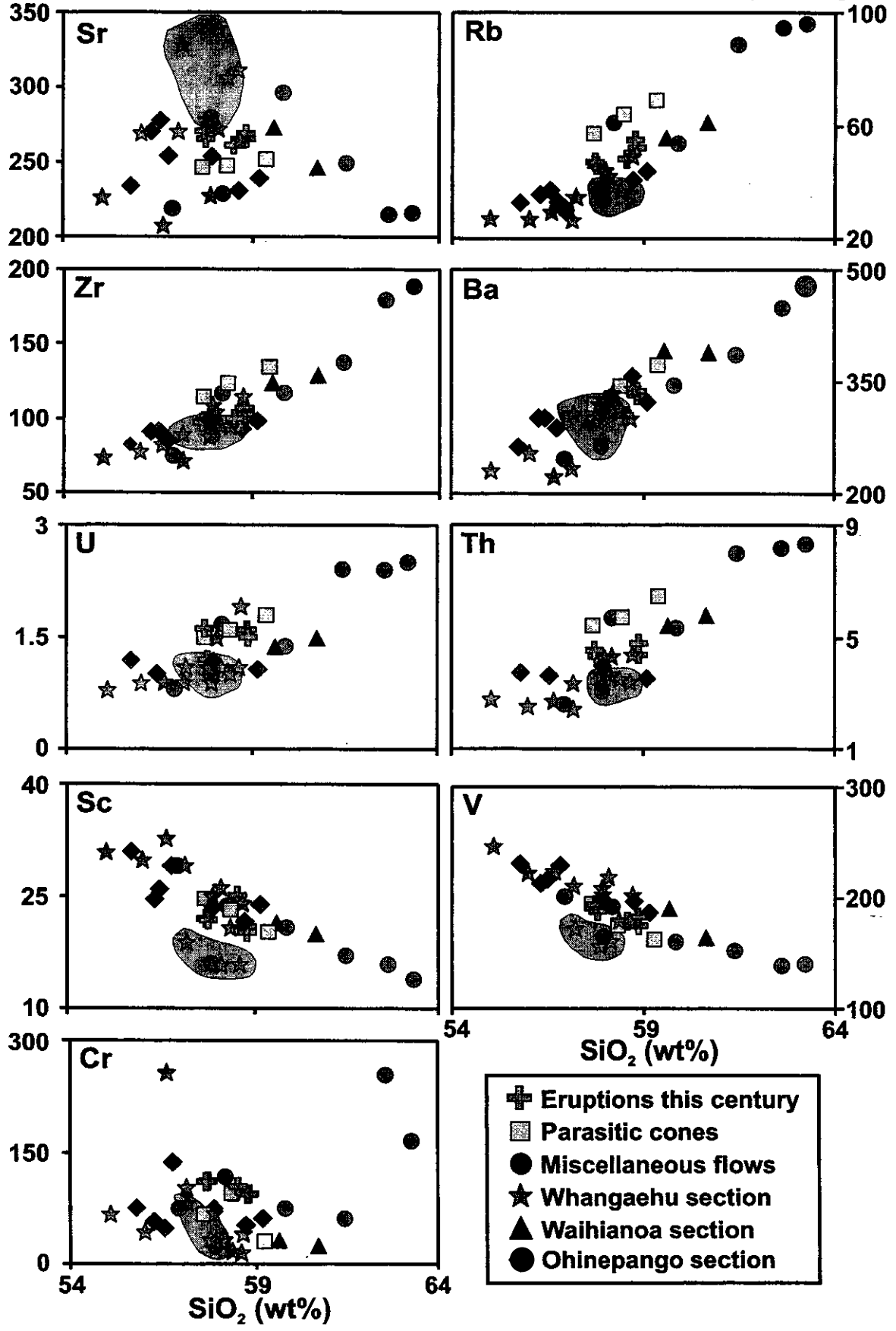

Figure 4.11: Variations of selected trace elements with SiO_2 content for samples from this study. All trace element abundances are expressed as μg g^{-1}. All trace elements concentrations except those for U and Th determined by XRF analysis. Th and U abundances were determined by INAA. Fields highlighted in orange are for samples which are plagioclase accumulative.

show very poor correlations. The incompatible elements (Rb, Ba, Zr, U, Th) show crude negative arrays, with the plagioclase accumulative type 2 andesites and olivine-pyroxene accumulative type 3 and 4 lavas tending to plot away from the trends (see Section 4.2 for a discussion of this classification). The transition metals (Sc, V, Cr) show positive correlations against MgO as expected because Cr is compatible in olivine, ortho- and clinopyroxene, and the other elements are compatible in both ortho- and clinopyroxene.

Most of the trace elements show much better correlations against SiO_2 (Figure 4.11). The incompatible elements Rb, Ba, Zr, U and Th all show well defined positive arrays and the transition metals Sc and V show well constrained negative arrays suggesting that both assimilation and crystallisation may be controlling these elements, whereas Cr shows no correlation, implying that olivine, and to a lesser extent pyroxene, crystallisation are the main controls on Cr abundance. The type 2 plagioclase accumulative andesites are clearly distinguishable on plots of SiO_2 against Sc and V, plotting below the main trend because of the lower proportions of mafic phases relative to plagioclase. These samples also show enrichments in Sr relative to other samples, because of the presence of larger quantities of plagioclase. Although V and Ti are both compatible in titanomagnetite, V is also modestly compatible in pyroxene (e.g. partition coefficient compilation of Rollinson, 1993), and better correlations of V with MgO and SiO_2 probably reflect pyroxene influences, because of its much greater modal abundance.

4.3.4 Crystallisation Models

The evolution of primary, mantle derived basalts to the basaltic andesites, andesites and dacites which have been erupted at Ruapehu and other volcanic centres in New Zealand has been the subject of a number of studies. Two different kinds of basalt predominate in arc environments, high alumina basalt (HAB) and high magnesium basalt (HMB). Both of these kinds of basalt are seen, if infrequently, in the TVZ, and several models have been put forward in recent work to explain the origins and differences between these compositions.

It has been suggested that the most primitive compositions erupted in the TVZ are HAB, which are derived from primary magmas through crystallisation of olivine and minor amounts of plagioclase (e.g. Gamble et al., 1990). Where these basalts reach the surface rapidly, and undergo only limited crystallisation, the high alumina characteristic is retained. Where the magmas are stalled in the crust, more complex crystallisation, accumulation and assimilation processes produce the low alumina, relatively high magnesium basalts and basaltic andesites observed at composite volcanoes such as Ruapehu.

In an alternative model for the differences between the HAB and HMB erupted in New Zealand it has been envisaged that the primary mantle derived melts were closer to HMB in nature (e.g. Smith et al., 1997). Their high magnesium characteristic can be maintained even at relatively high SiO_2 contents through fractional crystallisation of amphibole. More commonly however, plagioclase-olivine-clinopyroxene-titanomagnetite (POCT) crystallisation and plagioclase accumulation at shallow levels tends to drive parental HMB melts to high Al_2O_3 compositions. This model is consistent with other work on the origin of HAB (e.g. Crawford et al., 1987; Gust and Perfit, 1987) and is preferred here, because abundances of Ni and Cr, are consistent with HMB lavas erupted in the TVZ being closer to primary, mantle derived compositions than HAB.

In addition if the trace element patterns for the two possible parental compositions are examined (Figure 4.12), it can be seen that Ruapehu 'basalt' (a primitive HMB) matches the samples analysed in this study fairly closely but at lower abundances. In contrast, Kakuki basalt (a primitive HAB) generally has higher HFSE and HREE abundances and lower LILE abundances than Ruapehu 'basalt' and therefore lower LILE/HFSE ratios. It would be difficult to derive Ruapehu 'basalt' from Kakuki basalt through shallow level crystallisation processes as it would require increasing LILE but *decreasing* HFSE abundances. It is therefore argued that Ruapehu 'basalt' is not derived from HAB, but is a near-primary, mantle derived basalt.

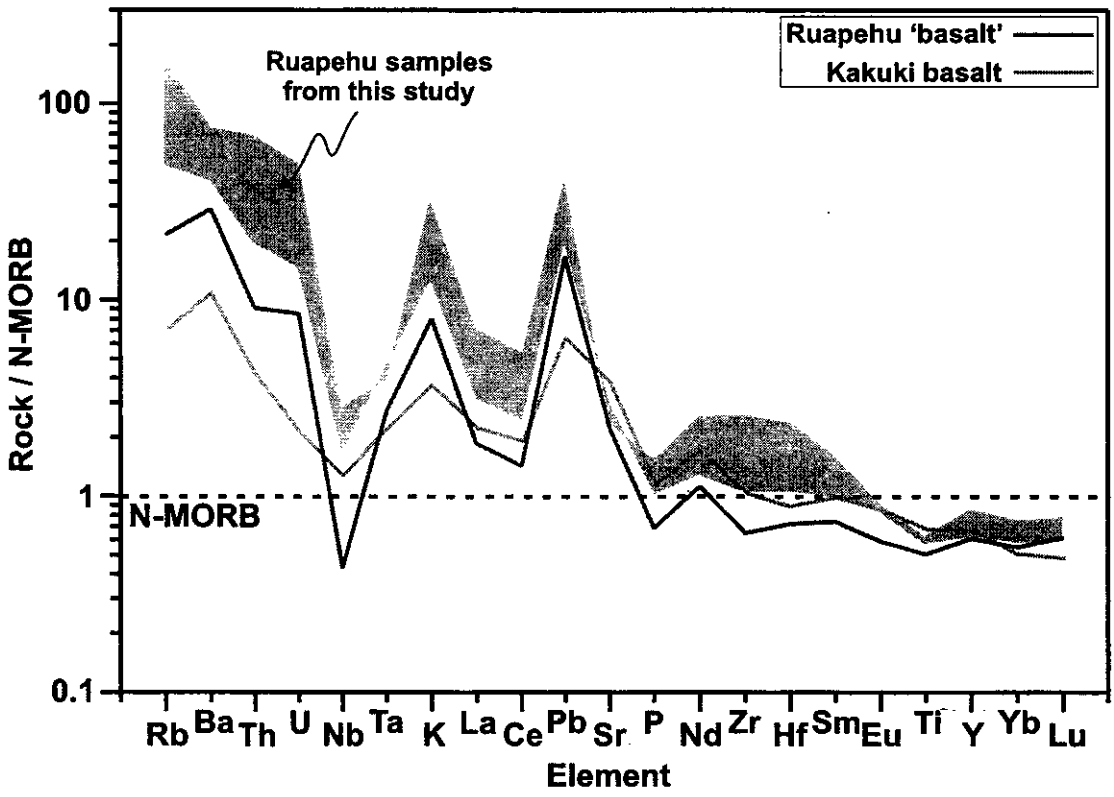

Figure 4.12: MORB normalised trace element variation diagram showing the differences between Ruapehu 'basalt' and Kakuki basalt relative to the Ruapehu samples analysed in this study. Data for Ruapehu 'basalt' and Kakuki basalt are from Gamble et al. (1993). N-MORB normalising values from Sun and McDonough (1989). Note that Ta abundances for some samples have been contaminated by crushing in tungsten carbide mills.

The crystallisation modelling undertaken here uses the most primitive HMB composition yet described from Ruapehu, the so called Ruapehu 'basalt' (Graham and Hackett, 1987) as a starting composition. This primitive lava is on the borderline between basalt and basaltic andesite with 52.3 wt% SiO_2 and 9.15 wt% MgO, it contains olivine phenocrysts with compositions between Fo_{88} and Fo_{79} and has a magnesium number of 70 (Graham and Hackett, 1987; Gamble et al., 1990). Despite this, it does not represent a primary liquid, because some mineral compositions imply some degree of mixing with more evolved magmas (Graham and Hackett, 1987) and the concentrations of Ni and Cr (Ni = 139 $\mu g\ g^{-1}$, Cr = 375 $\mu g\ g^{-1}$) are low compared with the expected abundances for a mantle derived basalt (i.e. Ni > 200 $\mu g\ g^{-1}$ and Cr > 400 $\mu g\ g^{-1}$ – Tatsumi and Eggins, 1995). However, it plots within the field of near-primary MORB on a plot of Mg-number vs CaO / Al_2O_3, and so it probably represents a liquid which has largely evolved through limited plagioclase and olivine crystallisation (Gamble et al., 1990).

Previous work by Graham & Hackett (1987) used least squares modelling as a quantitative assessment of the amount of fractionation and assimilation required to produce the observed compositions. This modelling suggested that up to 55% crystallisation was required with variable amounts of assimilation up to 30% not directly correlated with the amount of crystallisation (the proportions of each phase required are discussed in Section 4.3.4.2). This modelling is expanded on in this section and tied more directly into existing knowledge of phase equilibria and crystallisation thermodynamics using the MELTS computer program (Ghiorso and Sack, 1995), in order to try and improve the existing knowledge of crystallisation conditions.

4.3.4.1 Intensive Parameters: Pressure, Temperature and Oxygen Fugacity

Existing knowledge of the physical conditions during crustal AFC processes in magma chambers under Ruapehu is limited. Most of the published data come from extensive petrographic and electron microprobe analyses of phenocrysts (Graham and Hackett, 1987). This work suggested that crystallisation temperatures spanned a range from 1200°C to 1050°C (from basaltic andesite to dacite respectively) based on coexisting

ortho- and clinopyroxene compositions using the pyroxene thermometer of Lindsley (1983).

The available data on pressure is much more limited, but on the basis of coexisting olivine and plagioclase phenocrysts, and pyroxene chemistry, it has been suggested that crystallisation pressures are certainly no greater than 7-10 kb (Graham and Hackett, 1987). Given that seismic evidence suggests that the crust under the TVZ may be as little as 15 km thick (Stern and Davey, 1987) and physical evidence for assimilation of crustal material is widespread, it is probable that most of the compositional range observed at Ruapehu was produced at pressures no greater than 5 kb. Such pressures are consistent with arguments put forward by Gamble et al. (1990), who suggested that many of the more evolved basalts erupted in the TVZ crystallised along cotectics at pressures as low as 0.5-2 kb.

Discussion of water contents and oxygen fugacity has been extremely limited in published studies, however, it has been suggested that water contents were in the range 2-5 wt% H_2O, derived from calculated crystallisation temperatures and experimentally determined andesite liquidii (Graham and Hackett, 1987). This is again consistent with work by Gamble et al. (1990) which implies water contents of 2-3 wt% H_2O. There are no published estimates of oxygen fugacity for Ruapehu lavas, however most subduction lavas fall within ±2 log units of the nickel-nickel oxide (NNO) buffer (Gill, 1981).

4.3.4.2 MELTS Modelling

For the reasons outlined above, the primitive Ruapehu 'basalt' composition was used as the starting composition in this modelling. Two basic models were employed, one for equilibrium crystallisation and the other for fractional crystallisation. In both models, the evolution of Ruapehu 'basalt' was calculated isobarically at pressures of 1 kbar, 3.5 kbar and 5 kbar (equating approximately to depths of 3 km, 10 km and 15 km respectively) so that the entire crustal thickness beneath the TVZ was considered. At each depth, separate models were produced for three different water contents; anhydrous, 2 wt% H_2O and 5 wt% H_2O. In all cases, the FeO / Fe_2O_3 ratio was calculated at the NNO oxygen

fugacity buffer, but no constraints on oxygen fugacity were in place during crystallisation. Another model was produced with FeO / Fe_2O_3 ratios calculated at a raised level of oxygen fugacity, the quartz-fayalite-magnetite buffer (QFM) + 3 log units (equivalent to NNO + 2.25 log units) which is effectively the upper limit of the typical range noted by Gill (Gill, 1981).

The results of the modelling are shown on AFM and FeO(T) / MgO vs SiO_2 discrimination plots in Figure 4.13 and the crystallisation sequences and final assemblages are given in Tables 4.2 and 4.3. The vectors represent the liquid line of descent and are equivalent to ~50% crystallisation in each case, except for the fractional crystallisation model with 2% H_2O at 3 kbar where the MELTS algorithm failed at ~15% crystallisation. Anhydrous trends for both equilibrium and fractional crystallisation at all pressures, tend to produce enrichment in FeO(T) as a result of crystallisation mainly of forsteritic olivine and relatively sodic plagioclase (~An_{70}-An_{75}), and on AFM diagrams they do not show the downturn towards the alkalis characteristic of calc-alkaline compositions. Anhydrous trends also tend to produce very little enrichment of SiO_2 and so rapidly trend into the tholeiitic field on a plot of FeO(T) / MgO vs SiO_2. These two features make it unlikely that the magmas were anhydrous during crystallisation consistent with previous estimates of water content (e.g. Graham and Hackett, 1987).

Hydrous trends with either 2 or 5 wt% H_2O show calc-alkaline trends on AFM diagrams at all pressures, although the downturn becomes progressively later with increasing pressure. At pressures of 3.5 kbar or 5 kbar, the hydrous trends on FeO(T) / MgO vs SiO_2 diagrams all show too little SiO_2 enrichment relative to the FeO(T) enrichment, and thus they still tend to cross into the tholeiitic field. Equilibrium crystallisation of a hydrous melt at low pressures produces a trend that runs up the calc-alkaline—tholeiitic boundary, along the base of the data array for Ruapehu lavas.

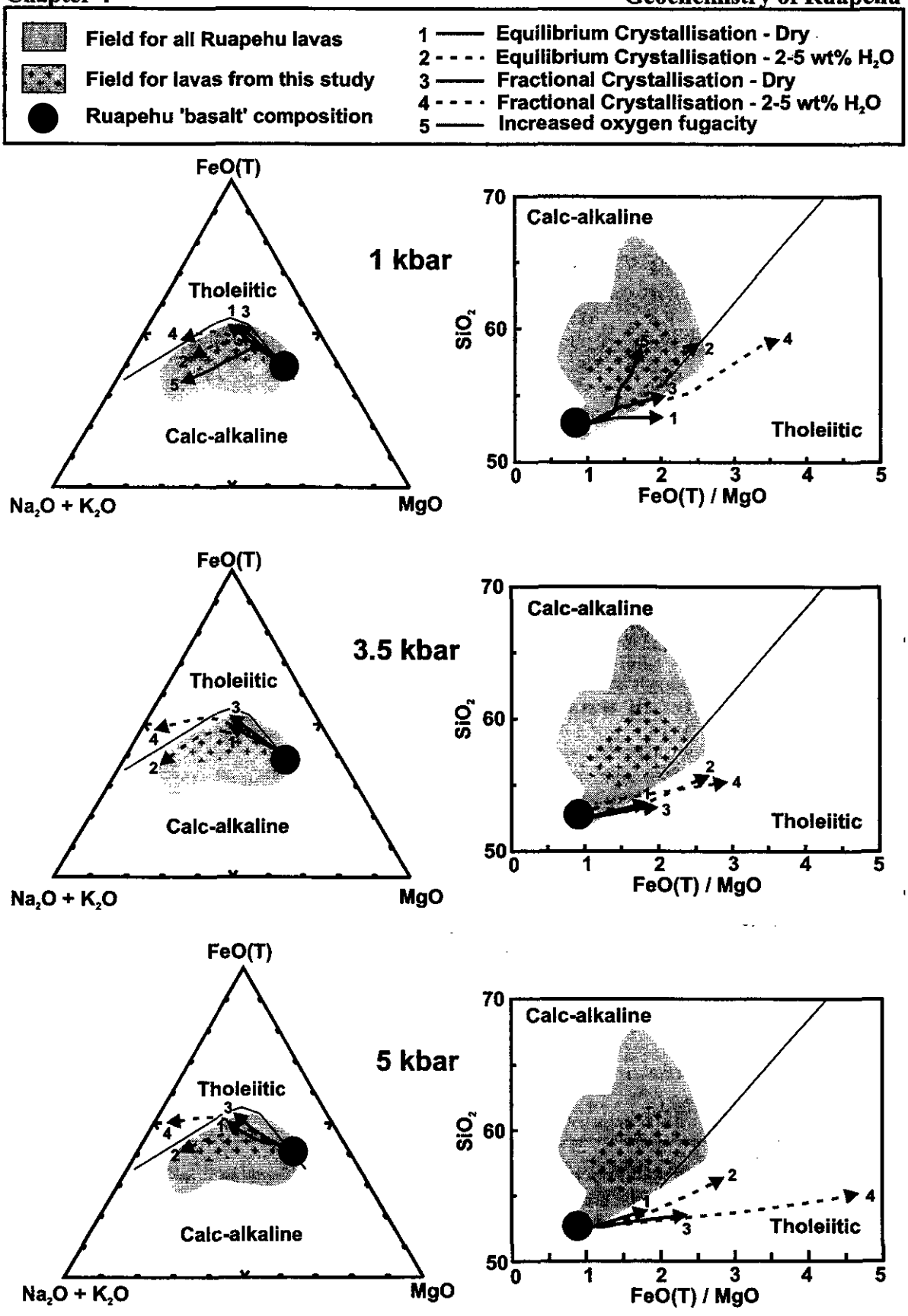

Figure 4.13: Crystallisation modelling using the MELTS program (Ghiorso & Sack, 1995) to examine the effects of pressure and water content on the liquid descent paths of Ruapehu magmas. Data for Ruapehu 'basalt' is from Gamble et al. (1990), data compilation for all Ruapehu lavas from Graham (1994). AFM discrimination diagrams after Irvine & Barager (1971) and FeO(T) / MgO vs SiO_2 diagrams after Miyashiro (1974). All oxides are expressed as wt%.

Pressure	H_2O	fO_2	Crystallisation Sequence	Final Assemblage
1 kbar	0%	NNO	ol, plag, opx (reacts with ol), cpx	53% liquid, 21.5% opx, 4% cpx, 22% plag
1 kbar	2%	NNO	ol, cpx, plag, tm, opx (reacts with ol)	50% liquid, 7.3% ol, 21% cpx, 6.5% opx, 14% plag, 1% tm
1 kbar	4%	NNO	ol, H_2O, cpx, plag, tm, opx (reacts with ol)	45% liquid, 5.81% ol, 20.5% cpx, 9% opx, 16% plag, 1% tm, 2% H_2O
3.5 kbar	0%	NNO	opx, cpx (reacts with opx), plag	48% liquid, 32% cpx, 20% plag
3.5 kbar	2%	NNO	ol, cpx, opx (reacts with ol), plag	51% liquid, 28% cpx, 15% opx, 6% plag
3.5 kbar	5%	NNO	ol, cpx, opx (reacts with ol), tm, H_2O	51% liquid, 32% cpx,16% opx, 0.5% tm, 0.01% H_2O
5 kbar	0%	NNO	opx, cpx (reacts with opx), plag	50% liquid, 32.5% cpx, 17.5% plag
5 kbar	2%	NNO	opx, cpx, plag	52% liquid, 13.5% opx, 32% cpx, 2.5% plag
5 kbar	5%	NNO	ol, cpx, opx (reacts with ol)	53% liquid, 32% cpx, 15% opx
1 kbar	2%	NNO + 2.25	ol, cpx, tm, opx (reacts with ol), plag	49% liquid, 23.5% cpx, 13% opx, 11% plag, 3.5% tm

Table 4.2: Crystallisation sequence and final phase assemblage for equilibrium crystallisation models produced using MELTS (Ghiorso and Sack, 1995). Mineral abbreviations are as follows: ol = olivine, cpx = clinopyroxene, opx = orthopyroxene, plag = plagioclase, tm = titanomagnetite. The H_2O column refers to the initial amount of water added to Ruapehu 'basalt' composition, which was then renormalised to 100%.

Pressure	H_2O	fO_2	Crystallisation Sequence	Final Assemblage
1 kbar	0%	NNO	ol in, plag in, cpx in, ol out	53% liquid, 5% ol, 14.5% cpx, 20% plag
1 kbar	2%	NNO	ol in, cpx in, ol out, plag in, ol in, tm in, opx in, ol out	53% liquid, 9.5% ol, 20% cpx, 1.5% opx, 12.5% plag, 1% tm
1 kbar	4%	NNO	ol in, H_2O in, H_2O out, cpx in, ol out, H_2O in, plag in, ol in, tm in, ol out, opx in, cpx out	50% liquid, 9.5% ol, 20.5% cpx, 1% opx, 11.5% plag, 1% tm
3.5 kbar	0%	NNO	opx in, cpx in, opx out, plag in	54% liquid, 23% cpx, 13% plag, 10% opx
3.5 kbar	2%	NNO	ol, cpx & opx in, ol out	85% liquid, 5% ol, 6% cpx, 4% opx
3.5 kbar	5%	NNO	ol, cpx in, ol out, tm in, plag in, opx in, opx out	57% liquid, 8% ol, 31% cpx, 0.01% opx, 1.5% plag, 1% tm
5 kbar	0%	NNO	opx in, cpx in, opx out, plag in	49% liquid, 24% cpx, 4% opx, 14.5% plag
5 kbar	2%	NNO	opx, cpx in, opx out, opx in, plag in, tm in, opx out	50% liquid, 37% cpx, 7% opx, 5.5% plag, 0.5% tm
5 kbar	5%	NNO	ol, cpx in, ol out, opx in, tm in	59% liquid, 7% ol, 32% cpx, 0.5% opx, 0.75% tm

Table 4.3: Crystallisation sequence and final phase assemblage for fractional crystallisation models produced using MELTS (Ghiorso and Sack, 1995). Mineral abbreviations and explanation of H_2O are as for Table 4.2.

The final model considered used a raised level of oxygen fugacity of QFM + 3 log units in a hydrous magma (2 wt% H_2O) at low pressure (1 kbar), because at higher pressures, the trend moves into the tholeiitic field on a plot SiO_2 vs FeO(T) / MgO before titanomagnetite enters the assemblage. The trend from this model runs broadly through

middle of the data array on an AFM diagram, and shows a sharp rise in SiO_2 relative to FeO(T) / MgO compared to the other models examined. The difference in this trend at raised levels of oxygen fugacity is due to the early crystallisation of a titanomagnetite phase.

Model	1	2	3	4	5	6	7	8
% ol	4	5.7	7.2	6	5.5	3.2	0	0
% opx	0	0	0	7.1	8.5	1.7	7.5	6.3
% cpx	8.5	10.3	12.6	14.9	16	4.9	5.4	6.6
% plag	3.7	2.7	11.6	22.4	20.7	10.5	19.6	14.6
% tm	0.7	0.9	2.6	3.2	3.1	2.1	2.3	0.9
% crystals	16.9	19.7	33.9	53.6	53.9	22.4	34.8	28.4
% assimilant	0.5	9.4	7.4	12.8	29	8.1	6.2	29.5
% liquid	82.6	70.9	58.7	33.6	17.1	69.5	59	42.1
% ol in crystals	23.7	28.9	21.2	11.2	10.2	14.3	0	0
% opx in crystals	0	0	0	13.2	15.8	7.6	21.6	22.2
% cpx in crystals	50.3	52.3	37.2	27.8	29.7	21.9	15.5	23.2
% plag in crystals	21.9	13.7	34.2	41.8	38.4	46.9	56.3	51.4
% tm in crystals	4.1	4.6	7.7	6.0	5.8	9.4	6.6	3.2

Table 4.4: Summary of least squares modelling for the evolution of Ruapehu andesites from a parental magma assumed to have a similar composition to Ruapehu 'basalt'. Data is from Graham and Hackett (1987), and the model numbers refer to those given by Graham and Hackett (see Table 9 in Graham and Hackett, 1987). These models were derived for various different evolved compositions. The mineral abbreviations are the same as those used for Tables 4.2 and 4.3. The top section of the table refers to abundances as a percentage of the total mass, whereas the bottom part of the table refers to the phase abundances as a percentage of the total crystals.

The amount of crystallisation of each phase predicted by MELTS (Tables 4.2 and 4.3) compares reasonably well with previous least squares modelling (Graham and Hackett, 1987), typical results of which are listed in Table 4.4. The proportions of phases and probable order of appearance in the crystallising (based on the proportions) calculated using a least squares model for the less evolved rocks tend to show the best match with MELTS predictions, with plagioclase subordinate to olivine and clinopyroxene. The least squares models for the more evolved compositions which have undergone ~50% crystallisation tend to predict more plagioclase crystallisation than MELTS. Interestingly, least squares modelling suggests that titanomagnetite is required in moderate proportions (up to 10% of the crystallising assemblage) in all of the examples given in Table 4.4. This is most compatible with the MELTS model with a raised oxygen fugacity, which is discussed further subsequently.

Selected models for liquid evolution during equilibrium crystallisation are also shown on plots of major elements against MgO in Figure 4.14. The models shown have been chosen to show the effects of varying pressure and water content. The anhydrous trends for all pressures show only limited drops in MgO due to greater amounts of plagioclase crystallisation and the absence of olivine in the final assemblage. As a result, these models do not reproduce the full range of MgO contents observed in Ruapehu lavas. The anhydrous trends also show significant FeO(T) and TiO_2 enrichments not observed in analytical data because titanomagnetite doesn't crystallise and olivine is absent in the final crystal assemblage.

The low pressure, hydrous trends generally fit the fields of the analytical data well, considering the data are not true reflections of liquid compositions and represent many different magma batches undergoing crystallisation and assimilation across a range of physical conditions. Much of the divergence of the predicted trends from the analytical data may well result from there being a range of compositions at a similar MgO content, and the choice of parental magma for this modelling is at one extreme of this range.

The predicted trends for K_2O and SiO_2 tend to run along the base of the data array. This may in part be due to the choice of parental magma composition as mentioned above, but also reflects assimilation processes. Assimilation is more likely to involve partial melts of local basement than bulk incorporation (e.g. Graham and Hackett, 1987). These authors have identified glasses in crustal xenoliths with high SiO_2 and K_2O which are inferred to represent such melts. Incorporation of such melts will result in higher SiO_2 and K_2O abundances in the data than the modelled trends, particularly in the more evolved (lower MgO) compositions which is what is seen in Figure 4.14.

The predicted trends for Na_2O from all the models are always higher than the observed data. This may reflect late stage, shallow level, fractional crystallisation of sodic plagioclase, as it was shown previously that Na_2O and Al_2O_3 correlate reasonably well. It is also possible that fractional crystallisation of a sodium-rich hornblende is responsible for the analytical data having lower Na_2O than the predicted liquid compositions. Amphibole is extremely rare in erupted lavas at Ruapehu, although it has been suggested that

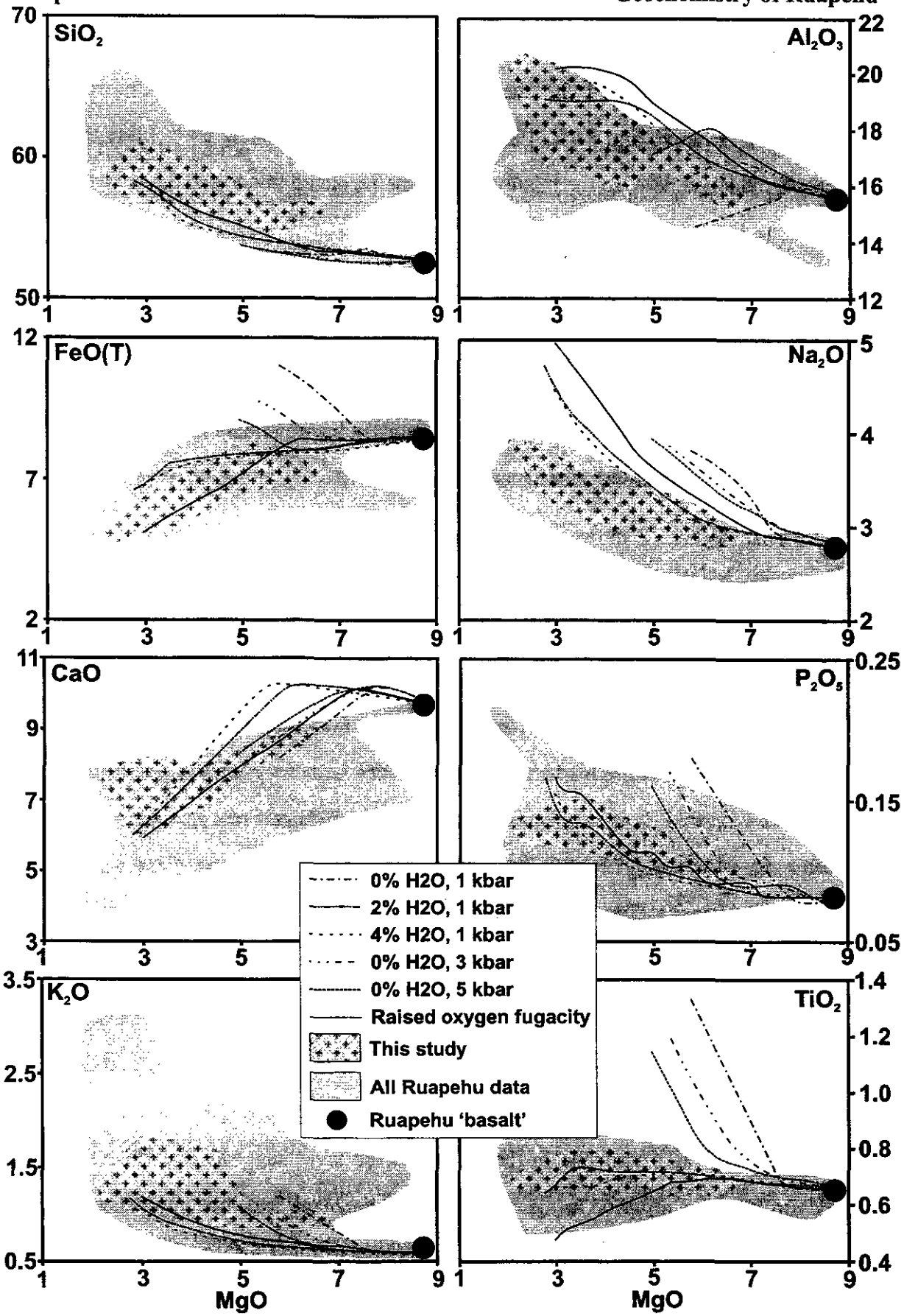

Figure 4.14: Crystallisation trends for Ruapehu lavas modelled with MELTS (Ghiorso & Sack, 1995). Data for Ruapehu 'basalt' is from Gamble et al. (1990). Data compilation for Ruapehu lavas is from Graham (1994). All oxides are expressed as wt%. All models shown here are for equilibrium crystallisation - see text for explanation.

crystallisation of amphibole may be important in deep magma chambers (Smith et al., 1997). The algorithm used in the MELTS program cannot calculate amphibole crystallisation (Ghiorso and Sack, 1995) and does not predict sodic plagioclase under the conditions modelled here, so the misfit between the predicted trends and the analytical data is difficult to resolve further.

Modelled trends for CaO show initial enrichments which are not observed in the data. The downturn in the modelled trends for CaO corresponds with plagioclase entering the crystallising assemblage. The misfit most likely arises from approximating parental liquid compositions from an actual rock, as it is clear from the data that plagioclase must be present in the crystallising assemblage throughout.

This modelling shows that with up to 50% crystallisation it appears possible to produce a considerable part of the compositional range observed on Ruapehu. In order to assess how reasonable this might be, considerations of experimental data and the petrography of the lavas must be made. It may appear strange at first that equilibrium crystallisation models seem to fit better than those for fractional crystallisation. One reason for this is that whilst many of the phenocrysts in the lavas may well in practice not be in equilibrium with their host magma and in some cases form part of cumulate clusters, they were for the most part in equilibrium with liquids of similar compositions derived from similar parental melts. Thus, the whole rock compositions in practice represent a mixture that lies somewhere along the liquid descent path.

Petrographic observations in this study and others (Graham and Hackett, 1987; Gamble et al., 1990), suggest that olivine was the earliest phase to form, followed by clinopyroxene and plagioclase and subsequently orthopyroxene. The absence of olivine and presence of orthopyroxene in the more evolved lavas suggests that olivine is either being consumed or replaced in the crystallising assemblage once orthopyroxene begins to crystallise (Grove and Kinzler, 1986; Myers and Johnston, 1996), and these features are reproduced by the MELTS model. Titanomagnetite is extremely common throughout the range of lava compositions whilst aluminous spinels are rare and only found as inclusions

in olivine (Graham and Hackett, 1987) which is consistent with the MELTS model, but only at raised oxygen fugacity levels.

The MELTS model is consistent with experimental evidence, such that increasing either H_2O contents or pressure has the effect of suppressing plagioclase crystallisation (Sisson and Grove, 1993a; Sisson and Grove, 1993b). In addition, increasing pressure reduces the olivine phase volume and leads to early crystallisation of pyroxene phases (e.g. Grove and Kinzler, 1986; Sisson and Grove, 1993a; Sisson and Grove, 1993b; Myers and Johnston, 1996). It is therefore likely that crystallisation occurred at relatively shallow levels and under only moderately hydrous conditions in order that olivine and plagioclase can be early crystallising phases. Relatively undersaturated H_2O contents are also implied by the plagioclase compositions (An_{70}-An_{75}) in the more primitive lavas (Graham and Hackett, 1987; Gamble et al., 1990), as increasing water contents tends to lead to more calcic plagioclase, typically An_{80}-An_{90} (Sisson and Grove, 1993a).

Experimental evidence suggests that the effects of H_2O are considerable on the timing of titanomagnetite crystallisation. Silicate minerals appear at much lower temperatures in a water-saturated melt than an anhydrous equivalent, but oxides (e.g. titanomagnetite) are not destabilised to the same degree and so enter the crystallising assemblage much earlier (Sisson and Grove, 1993a). Titanomagnetite crystallisation can also help to reduce the FeO(T) enrichment and produce greater increases in SiO_2 contents than any other major phase, and so it has been suggested that it is extremely important in helping to produce many calc-alkaline trends (Sisson and Grove, 1993a). The ubiquitous presence of titanomagnetite both as a free phenocryst phase and within glomerocrysts in all erupted lavas means it is important to have a model which allows the early appearance of magnetite. In order achieve this using the MELTS model, it is necessary either to increase the H_2O contents significantly, which would inhibit plagioclase formation to an unrealistic degree, or to raise the initial oxygen fugacity level. This may either represent a true feature of Ruapehu lavas, or it may be indicative of the MELTS program failing to predict titanomagnetite crystallisation as early as might be possible in modestly hydrous melts at lower oxygen fugacities. However a relatively high oxygen fugacity would be consistent

with the derivation of parental basalts from a mantle which has been modified by fluids from the subducted slab (see Chapters 5 and 6) (Wood et al., 1990).

4.4 Radiogenic Isotopes

The samples used in this study have been analysed for Sr, Nd and Pb isotopes by TIMS at the Open University (full analytical details are given in Appendix D). Radiogenic isotope signatures are potentially powerful tools for investigating both mixing and assimilation processes, and source variations. This section looks at the general systematics of Sr, Nd and Pb isotopes in Ruapehu lavas and uses these data to constrain assimilation processes.

4.4.1 Sr and Nd isotopes

The Sr and Nd isotopic data obtained in this study are shown in Figure 4.15, and these are compared with data for TVZ basalts, MORB and published results for Ruapehu andesites. The data for the basalts and andesites form a broad, coherent negative correlation which trends towards higher $^{87}Sr/^{86}Sr$ and lower $^{143}Nd/^{144}Nd$ in the more evolved samples, and extends almost to the MORB field in more primitive compositions.

The relationship between the degree of evolution of the lavas and their Sr and Nd isotope signatures is clear in plots of SiO_2 against both $^{87}Sr/^{86}Sr$ and $^{143}Nd/^{144}Nd$ (Figure 4.16). A broad positive correlation exists between SiO_2 and $^{87}Sr/^{86}Sr$, and a corresponding negative correlation can be seen between SiO_2 and $^{143}Nd/^{144}Nd$. On the basis of major element data it has been suggested that SiO_2 abundances reflect in part at least the degree of assimilation of local crust (see Section 4.3.4.2). The correlations between SiO_2 and Sr, Nd isotope signatures are consistent with this hypothesis, with a general trend towards crustal isotope ratios with increasing SiO_2 (e.g. Graham and Hackett, 1987; Gamble et al., 1993).

As discussed in Chapter 3, the nature of the local basement beneath the TVZ is equivocal, although greywackes of the Torlesse and Waipapa terranes are found immediately adjacent to the TVZ. Xenoliths incorporated into lavas erupted at Ruapehu

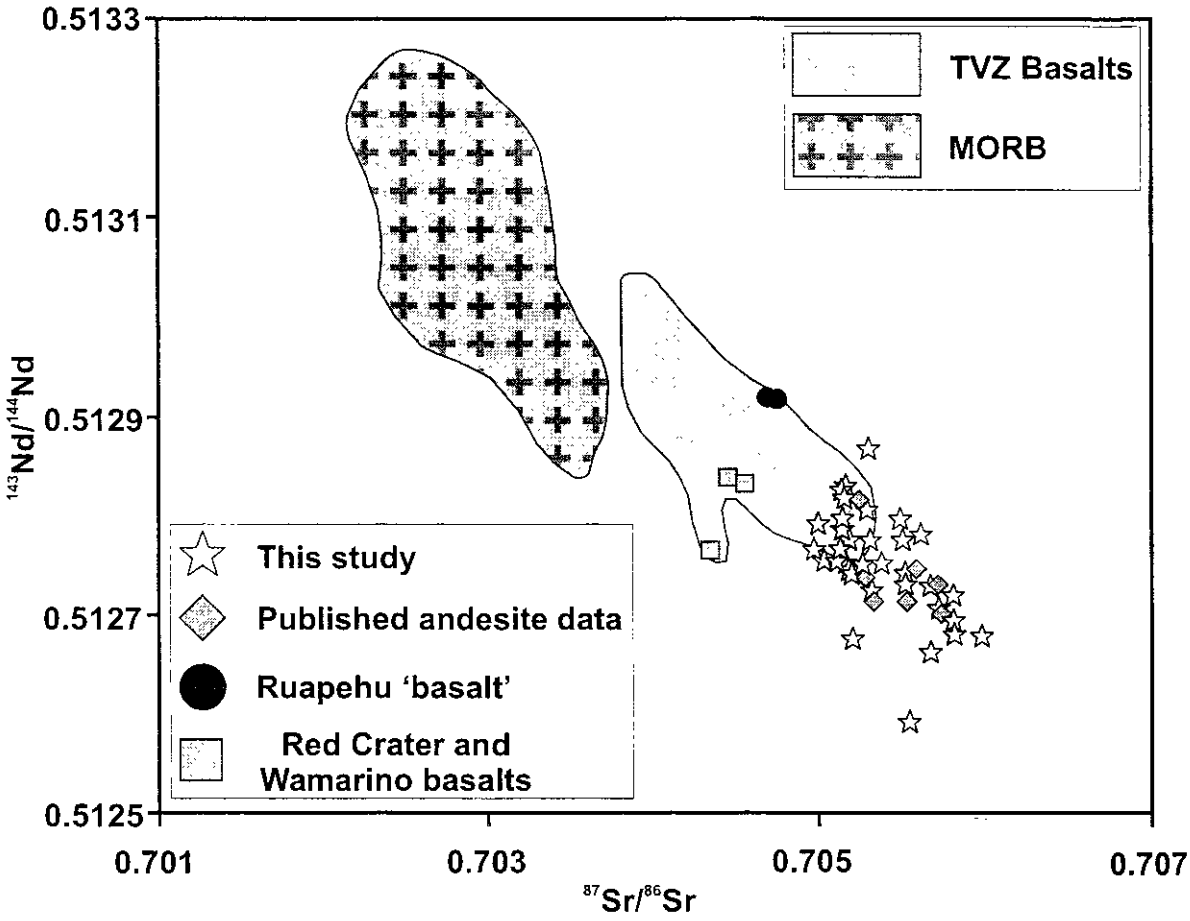

Figure 4.15: Sr isotopes against Nd isotopes for Ruapehu samples. Data for other andesites from Graham & Hackett (1987) and Graham (1994). Red Crater, Waimarino and TVZ basalt data from Gamble et al. (1993) and Gamble et al. (1996). Ruapehu basalt analyses from Graham & Hackett (1987) and Gamble et al. (1996). MORB data from Dupré & Allègre (1983), Hamelin et al. (1984), Hamelin et al. (1986), Ito et al. (1987), Shirey et al. (1987), White et al. (1987). Data precision at the 2σ level is typically less than symbol size.

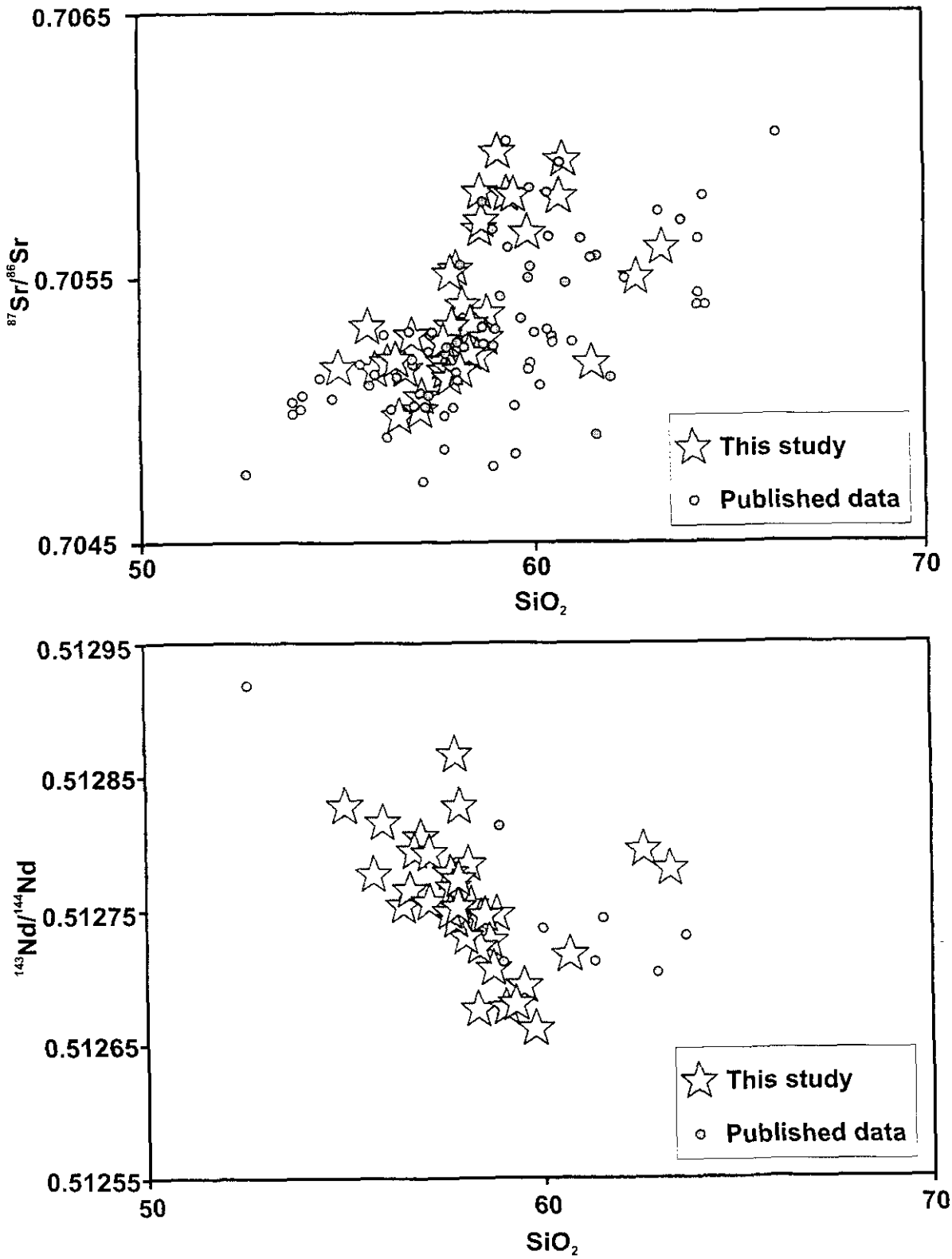

Figure 4.16: Plots of SiO_2 against $^{87}Sr/^{86}Sr$ and $^{143}Nd/^{144}Nd$. The published data for Ruapehu samples taken from Graham & Hackett (1987) and Graham (1994). Errors for both SiO_2 and the isotope ratios obtained in this study are smaller than symbol size at the 2σ level.

and other volcanic centres in the Tongariro Volcanic Centre appear to have two main sources (Graham and Hackett, 1987; Graham et al., 1988; Graham et al., 1990). The majority of the xenoliths can be linked either petrographically or chemically to rocks of Torlesse affinities, although a significant proportion of the xenoliths are meta-igneous granulites derived from some kind of underlying igneous basement.

Modelling of assimilation processes has been undertaken using the AFC equations of DePaolo (1981) in order to constrain the effects of assimilation. The results of this modelling are shown in Figure 4.17. The partition coefficients of both Sr and Nd for typical intermediate rocks have been estimated from the compilation of Rollinson (1993). The values of r (ratio of mass assimilated to mass crystallised) used for the modelling are taken from estimates of this value calculated using least squares modelling (Graham and Hackett, 1987), and AFC modelling with Pb, Sr and Nd isotopes (Graham et al., 1992). The initial magma composition for the models presented in Figure 4.17 is Ruapehu 'basalt' except in Figure 4.17d, which is explained in more detail subsequently. The end-member compositions used for the modelling are given in Table 4.5.

Bulk Sr and Nd abundances have been used for this modelling as the residual mineralogy and degree of melting of local basement during assimilation are unknown. It is likely that both elements may be relatively compatible during melting. If plagioclase is residual then Sr will be retained in the restite, and if biotite is residual Nd will be retained in the restite, as $D_{Nd}^{biotite}$ ~ 1-6 in silicic melts (Mahood and Hildreth, 1983; Nash and Crecraft, 1985). There is unlikely to be any great change in Sr/Nd although absolute abundances may change to a degree. However the use of bulk abundances does allow a first order approximation to be made.

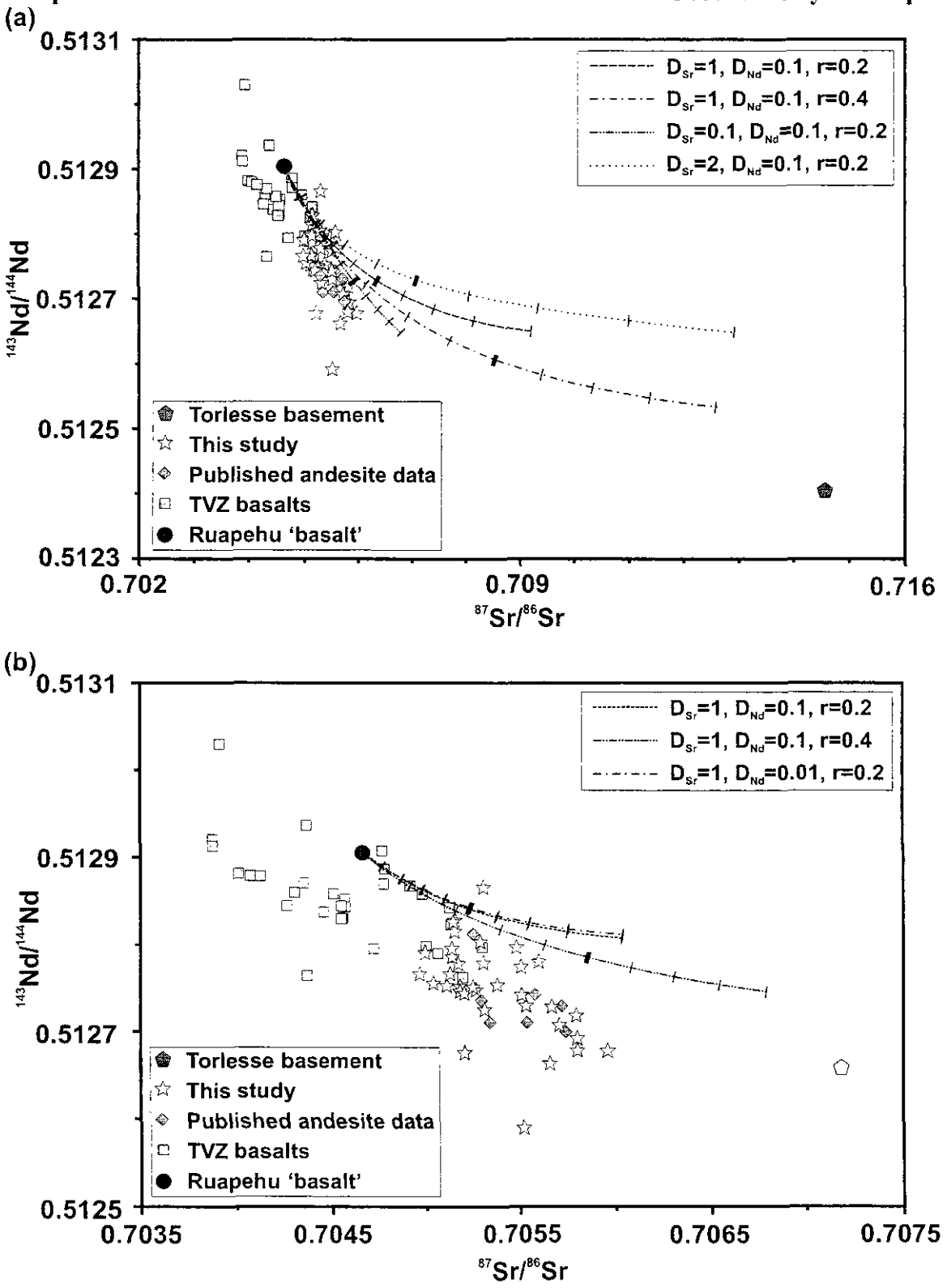

Figure 4.17:

(a) - AFC trends modelled for Ruapehu 'basalt' mixing with Torlesse basement. Curves calculated using the equations of DePaolo (1981), and the choice of parameters is discussed in the text. The tick marks on the curves are at intervals of 10% mass remaining, with the thicker tick indicating 50% mass remaining. Published andesite data from Graham & Hackett (1987) and Graham (1994). TVZ basalt compositions from Graham & Hackett (1987), Graham et al. (1992), Gamble et al. (1993) and Gamble et al. (1996). Crustal compositions are from Graham et al. (1992), except for one model as indicated in the key, which is discussed in the text.

(b) - AFC trends modelled for Ruapehu 'basalt' mixing with Waipapa basement. All sources are as for (a).

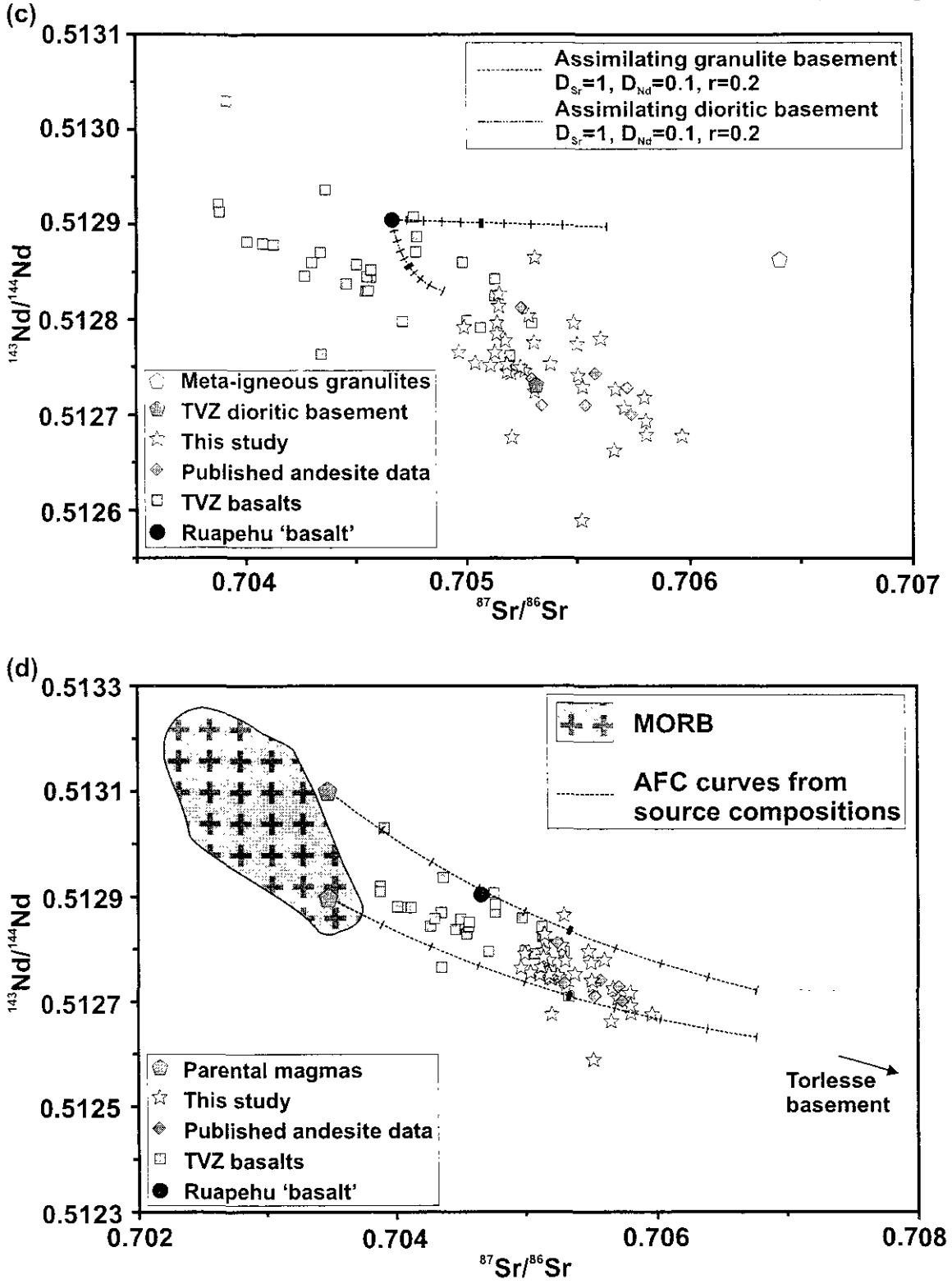

Figure 4.17 (cont.):

(c) - AFC models for Ruapehu 'basalt' mixing with TVZ igneous basement compositions. Meta-igneous granulite compositions from Graham et al. (1990) and TVZ diorite compositions from Brown et al. (1998). Other sources as for (a). Tick marks are at intervals of 10% mass remaining with a thick tick mark at 50% mass remaining.

(d) - AFC models for mixing between two hypothetical parental magmas and Torlesse basement. See text for discussion of the source compositions. MORB data is from Dupré & Allègre (1983), Hamelin et al. (1984), Hamelin et al. (1986), Ito et al. (1987), Shirey et al. (1987), White et al. (1987). Other sources are as for (a). Tick marks are as for (a). Tick marks are at intervals of 10% mass remaining with a thick tick mark at 50% mass remaining.

	Ruapehu 'basalt'	Source A	Source B	Torlesse	Waipapa	MIG	TVZ diorite
Sr μg g^{-1}	200	150	150	217	309	324	141
Nd μg g^{-1}	8.2	7.3	7.3	35	22	7.12	24.8
$^{87}Sr/^{86}Sr$	0.70466	0.7035	0.7035	0.71459	0.70718	0.70640	0.70532
$^{143}Nd/^{144}Nd$	0.51290	0.5131	0.5129	0.51240	0.51266	0.51286	0.51273

Table 4.5: End-member compositions for AFC models. Ruapehu 'basalt', Torlesse and Waipapa greywackes are from Graham et al. (1992), average meta-igneous granulite composition is taken from Graham et al. (1990), TVZ diorite xenolith compositions are from Brown et al. (1998), source A and source B are calculated from the observed data trend and typical southern Kermadec Arc lavas as explained in the text.

Assimilation of Torlesse basement has been modelled for a range of AFC parameters as shown in Figure 4.17a. Most of the curves tend to follow roughly along the top edge of the data array. If the partition coefficient of Sr is somewhat higher than 1 however, the curve tends to move away from the analytical data. This is because of the increasing dominance of the assimilant as Sr is progressively removed from the liquid through crystallisation. Decreasing the partition coefficient of Nd has a similar, but much smaller effect to increasing the partition coefficient of Sr (see Figure 4.17b), because Nd becomes progressively enriched in the liquid. Whilst the trace element data presented in Section 4.3.3 can only give a crude idea of the partition coefficients of Sr and Nd, some constraints can be suggested. The consistent increases in Nd content in conjunction with other REE demonstrate its incompatibility (see Figure 4.9), and the exact magnitude of the partition coefficient is relatively unimportant as discussed above. Correlations of Sr with MgO and SiO_2 are fairly poor, however Figures 4.10 and 4.11 suggest that with the exception of the plagioclase accumulative lavas, Sr contents are relatively constant across the range of observed MgO contents and may show a slight inflection when plotted against SiO_2. This tends to suggest that $\overline{D}_{Sr}^{cryst/liq}$ may start slightly incompatible at low SiO_2, and becomes slightly compatible with increasing differentiation, consistent with an average bulk partition coefficient of ~1. Increasing the amount of assimilation relative to crystallisation produces a greater shift in $^{143}Nd/^{144}Nd$ for a given change in $^{87}Sr/^{86}Sr$. This is because although Sr is relatively constant regardless of the amount of crystallisation, Nd

abundances in the magma will be lower for a given change in mass, and therefore the effect of assimilation is greater.

The total amount of crystallisation and assimilation required to produce the observed range of values for the Ruapehu data is quite variable between the different models described above. For the most viable models, the range of crystallisation required is 18-58%, and the range of assimilation is 11-18% (both of these percentages are expressed in terms of the original mass of the system). This is entirely consistent with estimates on the basis of least squares modelling (Graham and Hackett, 1987).

Models of assimilation of Waipapa greywackes are shown in Figure 4.17b. Whilst it is possible to produce trends which fit the top of the data array reasonably well, the lower $^{87}Sr/^{86}Sr$ of the assimilant compared with Torlesse means that a greater amount of assimilation and crystallisation (25-30% assimilation with 40-80% crystallisation) is required to produce the same shift in Sr isotopic ratio. One way of testing the viability of such AFC models based on isotope ratios is to consider the effects on the concentrations of Sr and Nd. With the partition coefficients and values of r used, crystallisation in excess of ~35-40% and assimilation in excess of ~10-15% produces Nd abundances greater than those measured in the most evolved rocks on Ruapehu. This consideration adds a further constraint which suggests that Torlesse basement is a better option as the major assimilant than Waipapa basement.

The possible assimilation of igneous basement is considered in Figure 4.17c. Two models are illustrated; first for assimilation of a melt with a composition similar to the meta-igneous granulite xenoliths erupted in Ruapehu magmas (Graham et al., 1990), and second, assimilation of igneous basement with characteristics similar to dioritic xenoliths erupted in rhyolites from the central TVZ (Brown et al., 1998). In both cases it is clear that these compositions are not responsible for the whole range of observed compositions, although small amounts of assimilation of such material cannot be ruled out. The dioritic xenoliths found in the central TVZ have a very similar composition to the average of erupted rhyolites (e.g. Sutton et al., 1995). Therefore, the model for assimilation of dioritic

basement means that mixing between an average rhyolitic and basaltic magma as a means of generating the andesitic lavas erupted on Ruapehu is unlikely.

One of the most interesting features of the data array for both basalts and andesites of the TVZ (Figure 4.15) is that there is considerable variation in $^{143}Nd/^{144}Nd$ for a given $^{87}Sr/^{86}Sr$ across the whole range of Sr isotopic ratios observed. This has the effect of producing a broad, linear trend of near constant width. It has been suggested that the range of isotope ratios in TVZ basalts may be related in part to source variations rather than crustal assimilation (Gamble et al., 1993; Gamble et al., 1996). In Figure 4.17d, assimilation of Torlesse basement is modelled using two very primitive compositions which differ only in $^{143}Nd/^{144}Nd$ and have $^{87}Sr/^{86}Sr$ ratios close to those of MORB. The Nd and Sr abundances for these parental magmas were estimated from primitive basalts erupted in the southern Kermadec Arc (e.g. Gamble et al., 1993; Turner et al., 1997a). The two curves reproduce the observed data well, and show that whilst the trend does tend to narrow in more evolved compositions, the width of the trend may well reflect source variations.

It is also possible to argue for a variation in $^{87}Sr/^{86}Sr$ ratio in primary magmas in a similar way to the argument for Nd isotopes outlined above. It is difficult to show conclusively whether there is only significant source variation in one or the other isotope system, or whether source variations had an influence on both. However, it is noted that if a similar model to that presented in Figure 4.17d is produced for two compositions with variable $^{87}Sr/^{86}Sr$ ratio (e.g. 0.7025 and 0.7035), the AFC trend for the initial magma with lower $^{87}Sr/^{86}Sr$ has a flatter trend and passes through middle of the data field and approaches the second AFC trend at the evolved end of the data array. This implies that the source variation in $^{143}Nd/^{144}Nd$ may be more significant than the variation in $^{87}Sr/^{86}Sr$. The problem of source variation, its origins and magnitude is discussed in more depth in Chapter 6.

4.4.2 Pb Isotopes

In addition to constraints from Sr and Nd isotopes, Pb isotopes offer the potential to constrain further source and assimilation processes. Determinations of Pb isotope ratios for samples used in this study and available published data are shown in Figures 4.18 and 4.19. On both plots, the trends originate in the fields for MORB, close to the NHRL (after Hart, 1984) and show a general progression to more radiogenic compositions, although only $^{207}Pb/^{204}Pb$ ratios exceed those of MORB.

There is considerable overlap between the Pb isotopic ratios of TVZ basalts and those of the more evolved compositions. Analyses of Ruapehu 'basalt' and Kakuki basalt have been made in two studies (Graham et al., 1992; Gamble et al., 1996), and there is a significant difference between the two measurements, as illustrated in Figures 4.18 and 4.19 for Ruapehu 'basalt'. This is most likely linked to differences in correcting for mass fractionation during analysis as one study used a double spiking technique (Gamble et al., 1996) and the other a single spiking method (Graham et al., 1992). The results of Gamble et al. (1996), tend to plot to higher $^{206}Pb/^{204}Pb$, $^{207}Pb/^{204}Pb$ and $^{208}Pb/^{204}Pb$ compositions than those of Graham et al. (1992). The data from this study, obtained using a single spiking technique, seem to match the results of Graham et al. (1992) better. These differences make it difficult to assess the true degree and significance of overlap between the basalts and more evolved compositions.

Modelling of assimilation processes using Pb isotope systematics was undertaken by Graham et al. (1992). Fields for measurements of Pb isotope ratios for samples of Torlesse and Waipapa greywackes by Graham et al. (1992) are shown in Figures 4.18 and 4.19. Whilst the number of samples used to delineate these fields is somewhat limited, the broad conclusions drawn by Graham et al. are confirmed and reiterated here. To generate the full range of Pb isotope ratios observed in evolved lavas from Ruapehu requires the involvement of Torlesse basement. It is difficult to discount the involvement of Waipapa basement entirely, but it is constrained to having at most a subordinate role to Torlesse greywacke in controlling the Pb isotope ratios of Ruapehu andesites. The fact that the trend for Ruapehu lavas runs into the field for Torlesse basement, and one sample has a

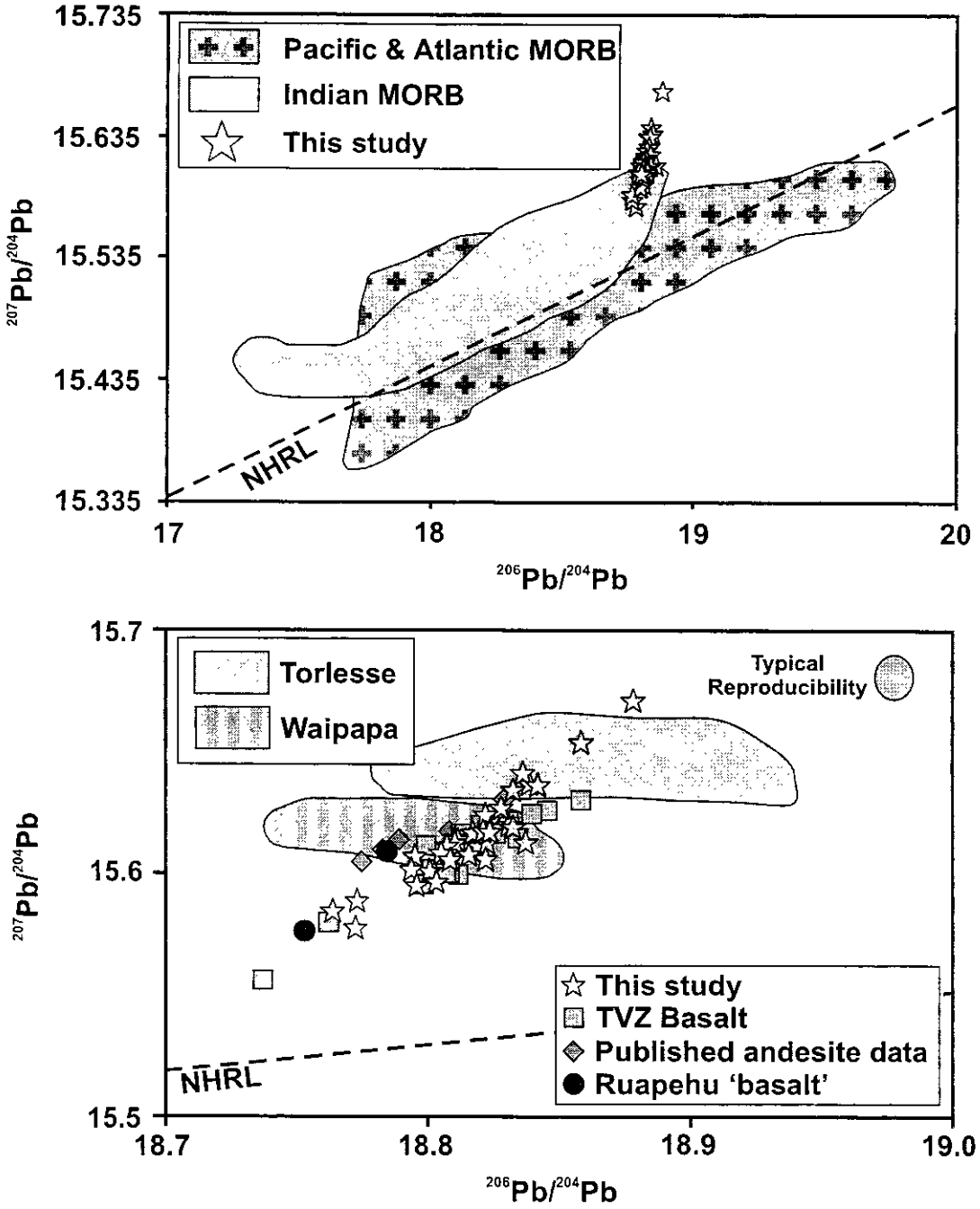

Figure 4.18: Plots of $^{206}Pb/^{204}Pb$ vs $^{208}Pb/^{204}Pb$. The NHRL is plotted after Hart (1984). The fields for MORB are plotted using data from Sun (1980), Dupré & Allègre (1983), Hamelin et al. (1984), Hamelin & Allègre (1985), Hamelin et al. (1986), Ito et al. (1987), Shirey et al. (1987) and White et al. (1987). Data for TVZ basalts and Ruapehu 'basalt' are taken from Graham et al. (1992) and Gamble et al. (1996). Data for Torlesse and Waipapa basement and Ruapehu andesites are from Graham et al. (1992). In the top diagram, errors are smaller than symbol size; in the bottom diagram, typical 2σ reproducibility is shown.

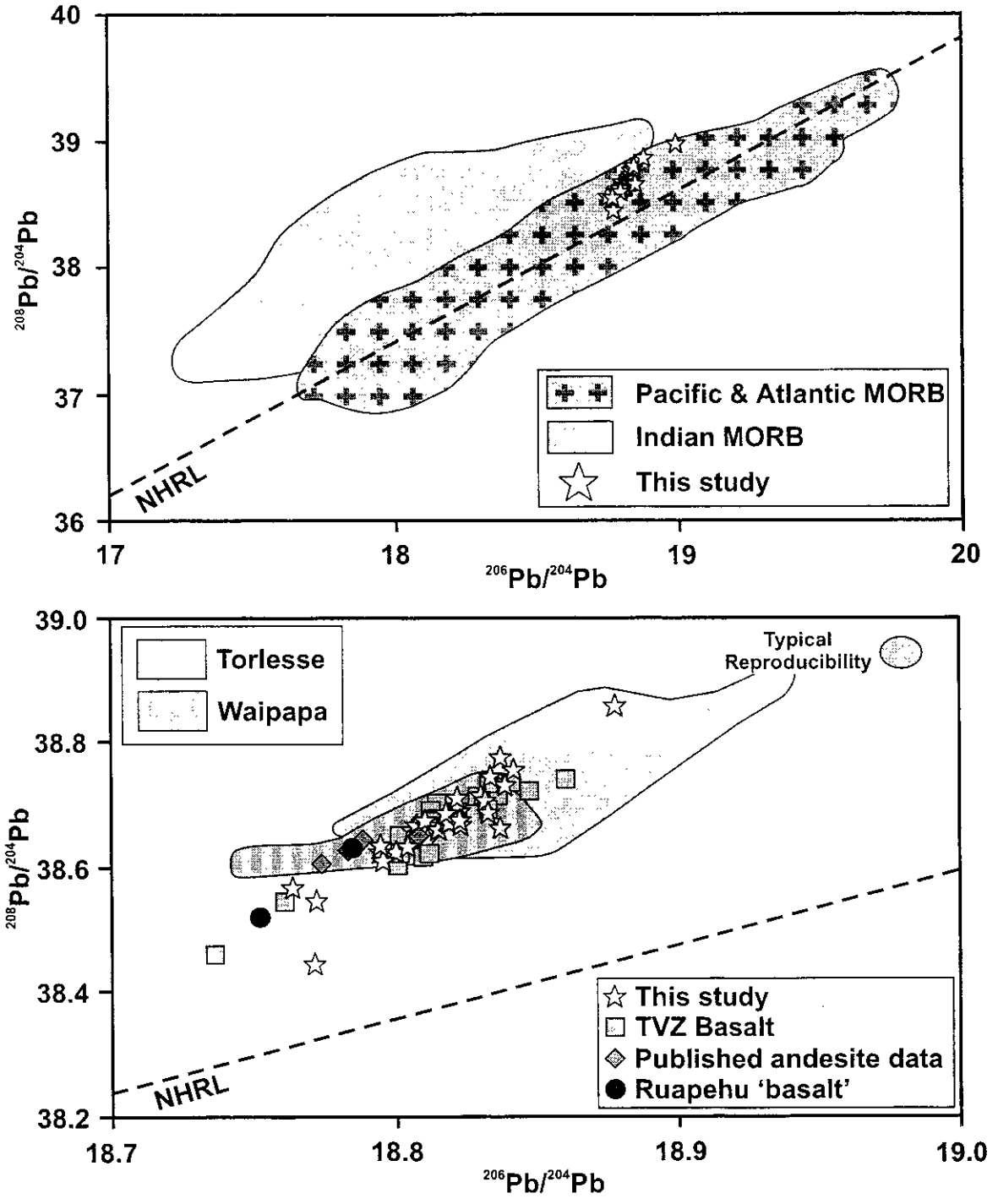

Figure 4.19: Plots of $^{206}Pb/^{204}Pb$ vs $^{208}Pb/^{204}Pb$. The NHRL is plotted after Hart (1984). The fields for MORB are plotted using data from Sun (1980), Dupré & Allègre (1983), Hamelin et al. (1984), Hamelin & Allègre (1985), Hamelin et al. (1986), Ito et al. (1987), Shirey et al. (1987) and White et al. (1987). Data for TVZ basalts and Ruapehu 'basalt' are taken from Graham et al. (1992) and Gamble et al. (1996). Data for Torlesse and Waipapa basement and Ruapehu andesites are from Graham et al. (1992). In the top diagram, typical errors are smaller than symbol size; in the bottom diagram, 2σ reproducibility is shown.

$^{207}Pb/^{206}Pb$ ratio in excess of any measured values for Torlesse, implies that the range of basement compositions in Pb isotope space may be more extensive than so far seen.

4.5 Summary

In summary, the lavas erupted at Mount Ruapehu throughout its eruptive history have had fairly constant composition and petrography. The crystallising assemblage has been dominated by plagioclase, clinopyroxene, orthopyroxene and olivine with lesser amounts of titanomagnetite. A number of samples have high Al_2O_3 and Na_2O and correspondingly low FeO(T) and MgO at particular SiO_2 contents. From this it is inferred that preferential accumulation and incorporation of plagioclase phenocrysts can be an important process in controlling the composition of erupted lavas. Poor correlation between MgO and SiO_2 compared with a good correlation between SiO_2 and K_2O demonstrates the importance of assimilation in producing the geochemical characteristics of Ruapehu lavas.

Modelling of the conditions of crystallisation indicates that much of the crystallisation took place at relatively shallow depths ($\leq$ 5-10 km), which has led to the crystallisation of olivine and subsequently clinopyroxene and plagioclase in preference to orthopyroxene, which is a late arrival in the crystallising assemblage. The ubiquitous presence of magnetite during differentiation, suggests that the either the water contents of the magmas were quite high (2-4 wt%), and/or that the oxygen fugacity was high.

Radiogenic isotope signatures show a strong crustal component, and reflect the importance of assimilation processes in the differentiation of Ruapehu magmas. Modelling of these processes suggests that the compositional range observed in analytical data can be explained by up to 35-40% crystallisation and 10-15% assimilation of Torlesse basement. Other potential assimilants in the region cannot be ruled out but are inferred to play only a minor role.

Probably suitable for the next chapter...,

Nvnc ille est magicvs

The motto of the Conjurors' Guild.

from 'The concife and possibly even accuratte Mapp' and 'Discworld Companion' – Terry Pratchett & Stephen Briggs.

Chapter 5

Timescales of Magma Generation and Differentiation at Mount Ruapehu

5.1 Introduction

This chapter presents U-Th-Ra disequilibrium data for Ruapehu lavas, and discusses what these can tell us about the timescales of melt generation, transport and differentiation processes. These timescales will be used to put together a model for the volcanism at Ruapehu over the last ~150 ka, and the possible relationship between regional tectonic processes and volcanic activity in the southern TVZ.

5.2 The Application of U-Series to Subduction Zones

The earliest use made of short-lived isotopes in igneous systems was as a dating system as detailed in Section 2.2.5. Increasingly, however, there has been interest in the interpretation of whole rock data as a means of understanding the rates of magmatic processes. If a whole rock analysis shows that a short-lived isotope system (principally U-Th and Ra-Th isotopes for the purposes of this discussion) is out of secular equilibrium, then it implies that some process has occurred within the last 300 ka (U-Th) or 8 ka (Ra-Th) which has fractionated the parent and daughter isotopes. Clearly, if the process or processes involved can be identified, there is enormous potential for constraining their timescales.

As an increasingly large number of data have been published, it has become evident that there is a clear difference in the ^{230}Th-^{238}U isotope values between lavas erupted in different volcanic environments. This is illustrated in Figure 5.1, where analyses

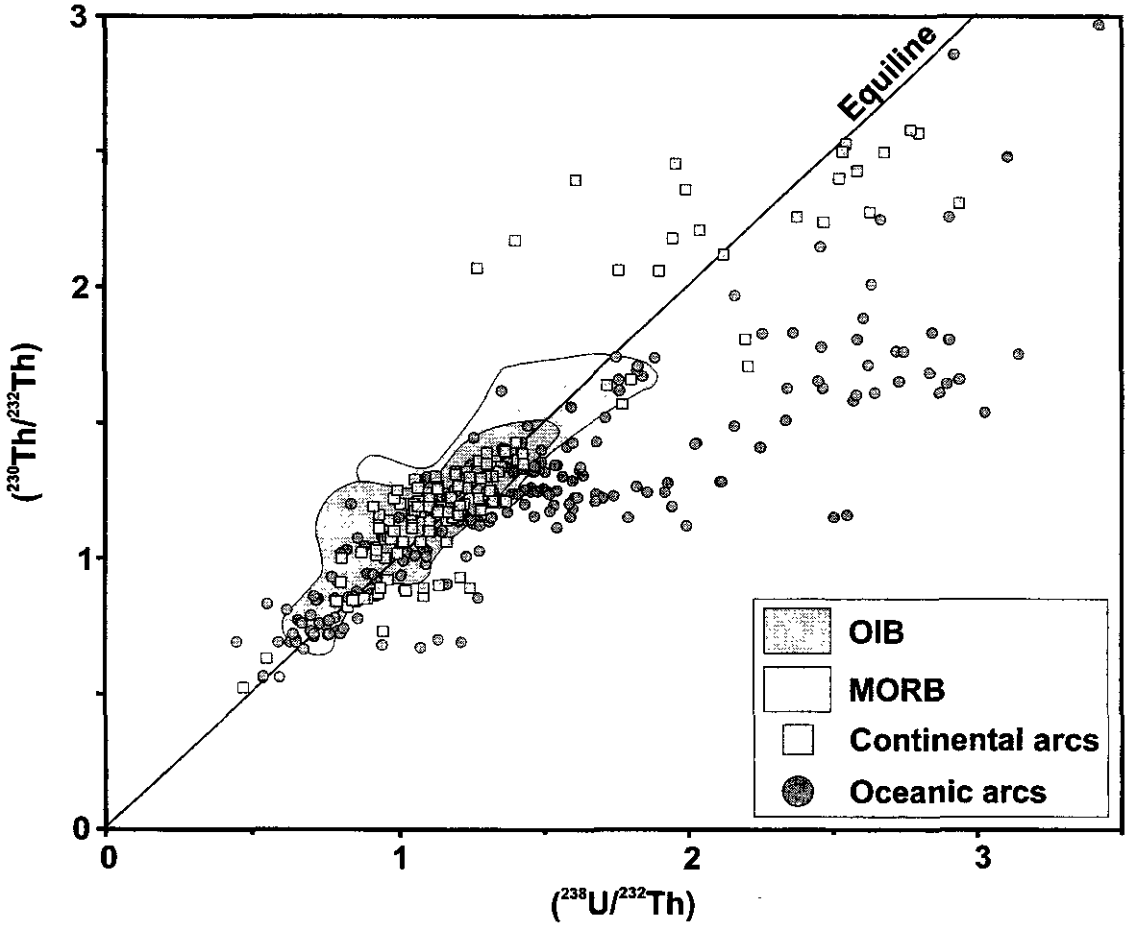

Figure 5.1: Equiline diagram showing the distribution of ^{230}Th-^{238}U disequilbrium data in different tectonic environments. The data for arcs is from Condomines and Allègre (1980), Capaldi et al. (1982), Krishnaswami et al. (1984), Newman et al. (1984), Newman et al. (1986), Rubin et al. (1989), Gill and Williams (1990), Sigmarsson et al. (1990), McDermott and Hawkesworth (1991), Volpe and Hammond (1991), Volpe (1992), Gill et al. (1993), Schaeffer et al. (1993), Reagan et al. (1994), Turner et al. (1996), Elliott et al. (1997), Hoogewerff et al. (1997), Regelous et al. (1997), Turner and Hawkesworth (1997), Turner et al. (1997a). MORB field is from Rubin and MacDougall (1988), Goldstein et al. (1989), Ben Othman and Allègre (1990), Goldstein et al. (1992), Goldstein et al. (1993), Sims et al. (1995), Bourdon et al. (1996a, 1996b), Lundstrom et al. (1998). OIB field is from Krishnaswami et al. (1984), Newman et al. (1984), Cohen and O'Nions (1993), Chabaux et al. (1994), Hémond et al. (1994), Sims et al. (1995), Turner et al. (1997b).

of lavas from subduction related settings are shown relative to fields for MORB and OIB magmas. It is clear that whilst OIB and MORB magmas have very similar characteristics and generally plot in secular equilibrium, or show modest Th excess, magmas from subduction zones show a much wider range of compositions on the U-Th equiline diagram. A large number of arc samples from both intra-oceanic and continental arcs are similar to MORB and/or OIB in that they either lie in secular equilibrium or show small to moderate U or Th excesses, and many show a similar range in U/Th ratio and Th isotopic composition to OIB and MORB. However a number of intra-oceanic arcs, in particular the Tonga-Kermadec arc system and the Marianas arc (Elliott et al., 1997; Regelous et al., 1997; Turner and Hawkesworth, 1997; Turner et al., 1997a), are very different and show large U excesses and generally have relatively high ($^{230}Th/^{232}Th$) ratios. Data from Nicaragua are unusual in that they have very high Th isotopic ratios and both large U and large Th excesses compared with other continental arcs (McDermott and Hawkesworth, 1991; Reagan et al., 1994).

In principle there are many factors which can affect U-Th isotope disequilibria such as source processes, mixing/assimilation or post-eruptive alteration. However, the last two of these can be ruled out for many samples with conventional geochemical systematics, examination of ($^{234}U/^{238}U$) ratios, or sampling of rocks at the time of eruption (Condomines et al., 1988; Gill and Williams, 1990; Gill et al., 1992). It is therefore widely believed that in most cases the observed isotope disequilibrium reflects some kind of fractionation of U from Th in the mantle source, either directly as a consequence of melting, or in response to the addition of a component which is itself out of secular equilibrium.

In the case of MORB and OIB which tend to show Th excess, it is argued that dynamic melting processes in the presence of residual garnet is responsible for the observed disequilibrium (e.g. Spiegelman and Elliott, 1993; Chabaux and Allègre, 1994). It is possible to compose models whereby both U and Th excesses can be generated during mantle melting, although this requires that the physical conditions of melting and melt extraction are different from those producing MORB and OIB (e.g. Gill and Williams,

1990; Gill and Condomines, 1992). As noted by Gill and Williams (1990), whilst it is possible there may be a difference in melting styles between mid-ocean ridge and arc environments, there is no requirement based on models of melt generation and transport for this to be so (e.g. Spiegelman and McKenzie, 1987). It might also be possible to explain the range of compositions by more variable partitioning of U and Th during magma genesis in subduction zones than in the generation of MORB and OIB. However, such a view has yet to be justified on the basis of experimental partitioning data (Gill and Williams, 1990; Condomines and Sigmarsson, 1993).

In the last decade, mass fluxes during subduction zone magma genesis have become better understood as studies have begun to resolve the so called 'subduction component' (e.g. Pearce, 1982) into separate fluid and sediment influences (e.g. summary of Arculus, 1994). It has also been pointed out that the only other tectonic setting in which large U excesses are observed is in magmas from continental rifts which are believed to be strongly associated with CO_2 rich fluids (e.g. Gill and Williams, 1990). As fluids are also believed to be important in the generation of subduction zone magmas, various authors have suggested that the U excesses can be related to these (Condomines et al., 1988; Gill and Williams, 1990; McDermott and Hawkesworth, 1991; Condomines and Sigmarsson, 1993; Hawkesworth et al., 1997a; Hawkesworth et al., 1997b). This suggestion has been backed up in recent experimental studies on the partitioning of U and Th into different fluids which suggest that U can be mobile in hydrous fluids under oxidising conditions whereas Th is not (e.g. Keppler and Wyllie, 1990; Bailey and Ragnarsdottir, 1994; Keppler, 1996).

5.3 U-Th Disequilibria in Ruapehu Lavas

Most of the Ruapehu samples used in this study have been analysed for U-Th isotope ratios by TIMS at the Open University (see Appendix C for data tables and Appendix D for details of the analytical techniques). The U-Th data are shown on an equiline diagram in Figure 5.2.

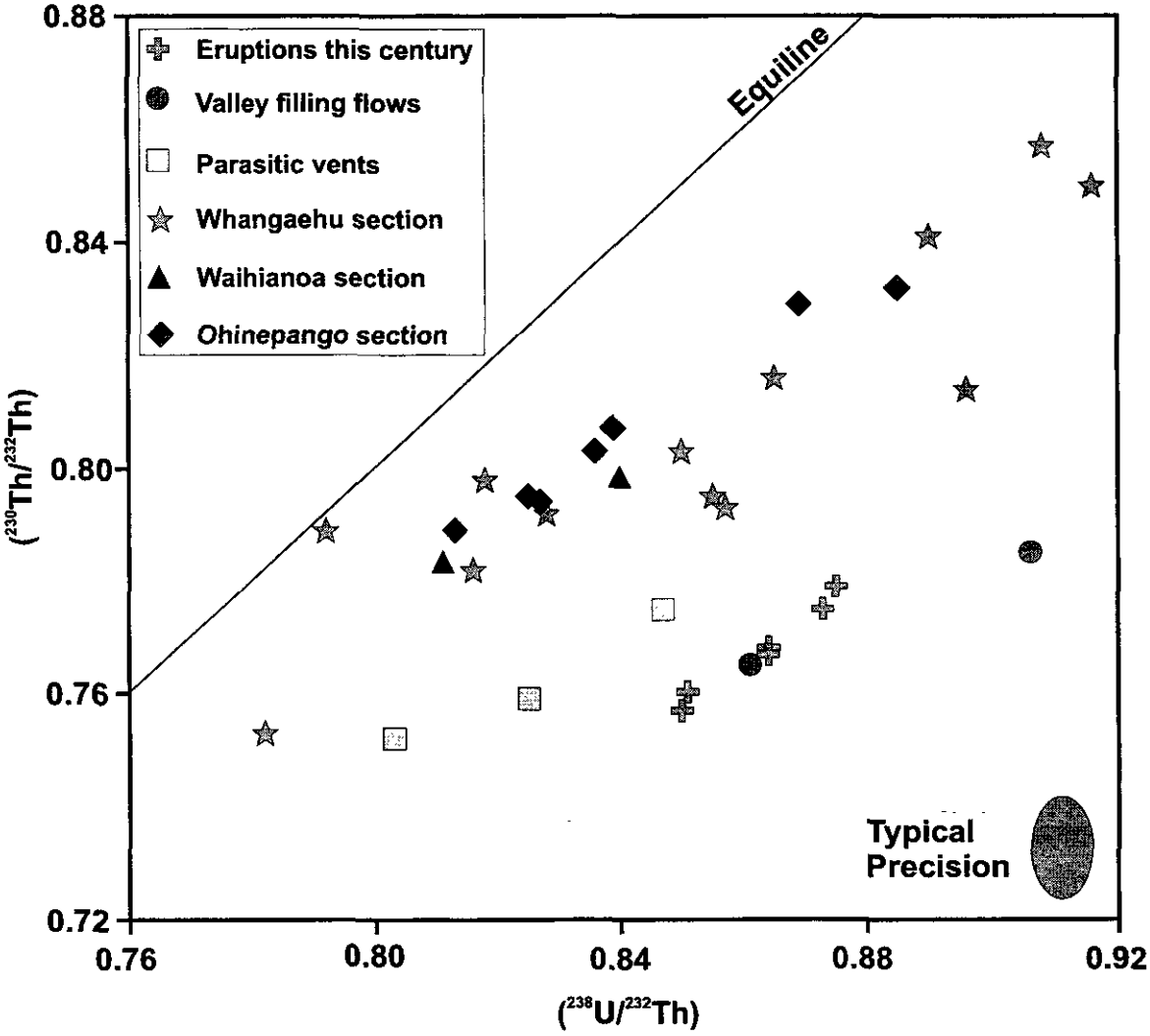

Figure 5.2: ^{230}Th-^{238}U disequilibrium data for Ruapehu samples. See text for discussion.

All of the data obtained for Ruapehu samples plot to the right of the equiline, with U excess. Although the variations are small, it is clear that within each stratigraphic group there is a coherent relationship on the U-Th equiline diagram. The samples which show the greatest degree of disequilibrium (12-14% U excess), and have some of the lowest ($^{230}Th/^{232}Th$) ratios obtained for Ruapehu lavas, are from eruptions this century and from two valley filling flows (X1-6 and W9-5) which are thought to be very young on the basis of field evidence. Samples from lavas erupted from small parasitic cones ~10-20 ka ago (R96-10, R96-25 and R96-26) show slightly less disequilibrium (6-9% U excess), and samples from the Whangaehu, Waihianoa and Ohinepango sequences show the least disequilibrium (1-8% U excess).

Whilst the eruption ages of most of the samples analysed are not well established, the relative stratigraphy is known reasonably well. The distribution of the U-Th data on an equiline diagram demonstrates that not only do the different stratigraphic groups have an internal coherency, but there is also a systematic relationship between the groups which corresponds largely with the known stratigraphy. This relationship means that for a given ($^{238}U/^{232}Th$) ratio, the ($^{230}Th/^{232}Th$) value is higher in samples which are believed to be older, and hence ($^{230}Th/^{238}U$) is closer to unity. This implies that there is some degree of consistency in the ($^{230}Th/^{232}Th$)-($^{238}U/^{232}Th$) compositions of the lavas at the time of eruption.

Simply on the basis of visual inspection of Figure 5.2, it can be suggested that the relative stratigraphy (from youngest to oldest) for the samples analysed in this study is: historic eruptions, young valley filling flows (which form part of the miscellaneous flows grouping used in Chapter 4), lavas from parasitic cones, and samples from the Whangaehu, Waihianoa and Ohinepango sequences (which are statistically indistinguishable on a U-Th equiline diagram). This can be compared with the relative stratigraphy that has been derived from field evidence: i.e. historic eruptions, valley filling flows and parasitic cone eruptions, samples from the Ohinepango sequence, and lastly lavas from the Whangaehu and Waihianoa sequences.

It is necessary at this stage to discuss the U-Th data for the Whangaehu sequence in more detail. Of all the stratigraphically coherent groups analysed in this study, the Whangaehu shows the greatest variation. The sequence is shown in Figure 5.3 with the sampling localities marked for lavas analysed in this work. Field evidence and detailed examination of major element and isotope variations observed in lavas from the Whangaehu sequence has been used to infer a number of sub-groups within the sequence (R.C. Price, pers. comm., Price et al., 1997; Price et al., 1998), and these are detailed in Table 5.1. Note that this table also includes samples from the Waihianoa sequence which is thought to form part of the same part of the same eruptive series (see Chapter 3).

Group	Samples	Groupings used in this study
Group 5	*R95-20*	*Upper Whangaehu*
Group 4	R94-6	?Upper Whangaehu
Group 3	R95-21, R95-22, R95-23, *R96-2, R96-3, R96-6, R96-7*	Upper Whangaehu
~~	~~~~~~~~~~ major break? ~~~~~~~~~~	
Group 2	R95-18, R95-19, R96-5	Upper Whangaehu
~~	~~~~~~~~~~ major break? ~~~~~~~~~~	~~~~~~~~~~~~~~~~
Group 1D	R95-17, R95-25, R95-27, R95-28	Lower Whangaehu
Group 1C	R94-8, R94-9, R95-26	Lower Whangaehu
Group 1B	*R96-4, R96-8, R96-9*, R96-17, R96-18	Lower Whangaehu
Group 1A	R96-15, R96-16, R96-19, R96-20, R96-21, R96-22	Lower Whangaehu

Table 5.1: Stratigraphy of the Whangaehu and Waihianoa sequences based on field observation and geochemical trends after R.C. Price (pers. comm.). The groups are given in stratigraphic order from top to bottom (i.e. group 5 forms the top of the sequence and group 1A the bottom). Note that sample numbers in italics are from the Waihianoa valley. Also shown are the temporal groupings made in this study on the basis of field evidence and U-Th data (see the text for further discussion of these groups).

A detailed consideration of the U-Th data and field evidence shows that there are three distinct groupings which are illustrated in Figures 5.3 and 5.4. The majority of the samples fall on a linear trend which approximately coincides with data for the Waihianoa and Ohinepango sequences (see Figure 5.2). Two samples (R96-18 and R95-22) fall to the left of this trend, and these may have been affected by post-eruption U loss, for reasons which will be explained fully in Section 5.3.1.1. When the stratigraphy shown in Figure 5.3 and given in Table 5.1 is taken into account, it is apparent that four samples from the top of the sequence fall below the main trend and form a separate correlation (R95-18, R95-19, R95-20, R95-21). Although the sample with the lowest U/Th ratio in this array

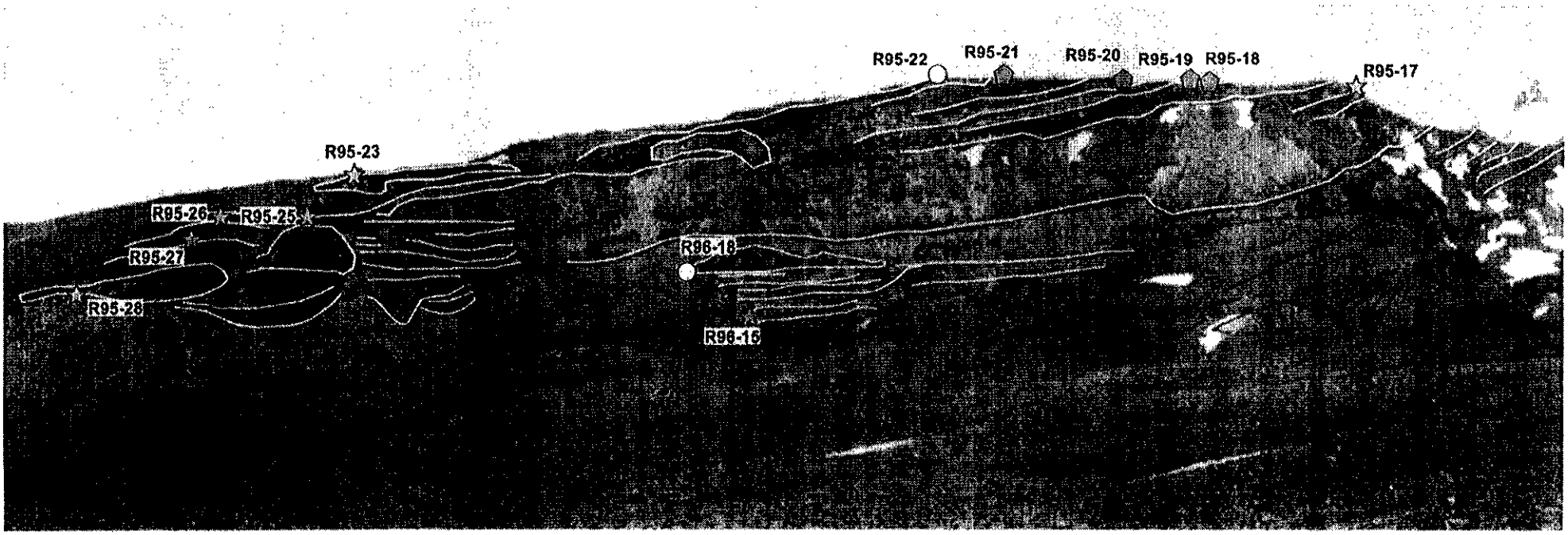

Figure 5.3: Composite photograph of the Whangaehu Section, showing the location of samples used in this study. Stars indicate samples which form part of the Lower Whangaehu group, pentagons denote samples from the Upper Whangaehu group and circles show the two samples which may have had their U-series systematics disturbed by post-eruptive alteration or have had an unusual pre-eruptive history. The definition of the Upper and Lower Whangaehu groups is based in part on the relative stratigraphy evident from this diagram and is discussed in further detail in the text. Sketch outlines of flow boundaries are taken from sketches made by R.C. Price. Photographs taken looking south from the Whangaehu Gorge.

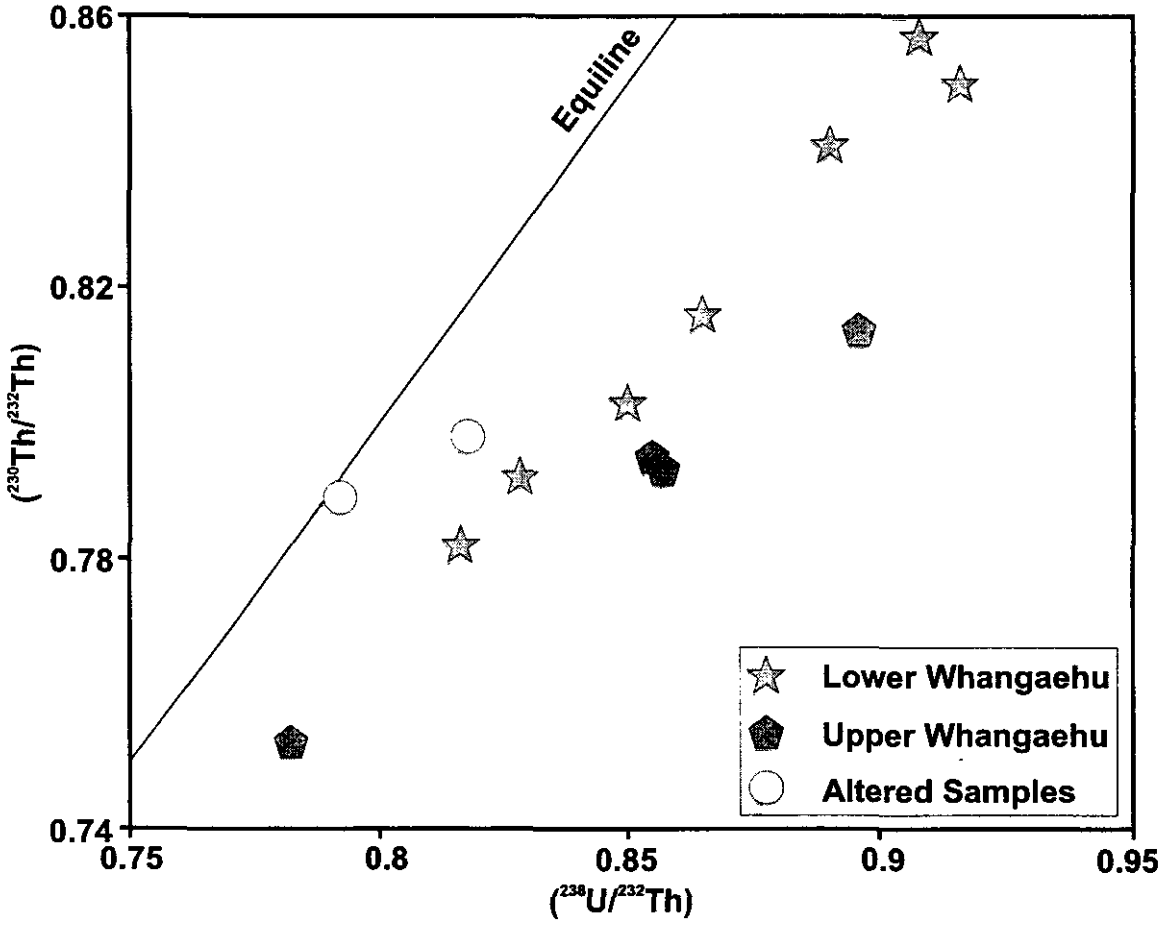

Figure 5.4: Division of the Whangaehu Gorge Section on the basis of U-series and field observations. Two samples (R95-22 and R96-18) appear to have undergone post-eruption uranium loss, which is considered further in the text. The remaining samples are divided into the Upper and Lower Whangaehu groups based on their stratigraphic position.

(R95-21) could equally form part of the main trend, its stratigraphic position at the top of the sequence implies that it should be grouped with the other three Upper Whangaehu samples. There is no evidence from the U-series data for the uppermost major break shown in Table 5.1, although this may represent a significant change in volcanic style without a major time break. Samples R96-2, R96-7 (from the Waihianoa sequences - see Figure 5.2) and R95-23 appear to be more closely related to groups 1A-1D on the basis of the U-Th data. The two main linear correlations for the Whangaehu sequence will be termed the Lower Whangaehu and Upper Whangaehu groups on the basis of their stratigraphic position.

5.3.1 Controls on U/Th Ratio in Ruapehu Lavas

It is order to make quantitative statements about the timescales of magma generation and differentiation at Ruapehu it is necessary to understand the principle controls on the U and Th abundances and hence the U/Th ratios in these rocks. In principle, a number of processes can have altered U/Th and therefore ($^{238}U/^{232}Th$), such as pre- or post-eruptive mobilisation of U in hydrous fluids, fractional crystallisation, crustal assimilation and fractionation of the two elements by magma generation processes. These processes will be considered in turn below.

5.3.1.1 Pre- or Post-Eruption Mobilisation of U by Hydrous Fluids

As mentioned in Section 5.2, uranium can exist in a number of oxidation states (+3, +4, +5 and +6), of which U(IV) and U(VI) are the principle forms of interest in hydrous fluids (Shock et al., 1997), whereas Th only exists as Th(IV). It is well established that U abundances in rocks can be affected by weathering and alteration processes (e.g. Osmond and Cowart, 1992; Osmond and Ivanovich, 1992 and references therein), and experimental evidence has shown that whilst both U(IV) and Th(IV) are essentially immobile in most fluids, U(VI) is much more readily soluble in oxidising or acidic fluids (e.g. Bailey and Ragnarsdottir, 1994; Keppler, 1996; Shock et al., 1997).

However, the fact that weathering can leach U from igneous rocks has also provided a mechanism which can help determine if such leaching or contamination by U

rich groundwater has occurred. Measurements of ($^{234}U/^{238}U$) ratios in modern groundwater and other sinks for leached U show that ^{234}U is commonly enriched relative to ^{238}U (Osmond and Cowart, 1992). As ^{234}U forms by radioactive decay of ^{238}U, it is thought that preferential leaching of ^{234}U from sites in crystal lattices which have been damaged by radiation is the principal cause of this enrichment. Two situations can therefore be envisaged; firstly, if a rock has had U leached from it recently, the ($^{234}U/^{238}U$) ratio ought to be less than unity, and secondly if in some way contamination by U rich groundwater has occurred, the ($^{234}U/^{238}U$) value ought to be greater than unity.

The ($^{234}U/^{238}U$) activity ratios obtained from Ruapehu samples were within 1% of unity, with the exception of a few samples (R95-19, R96-10, P57535, P57536) which had a value above 1.01, although all were < 1.015. Reproducibility of samples and standards suggests that the few samples which were not within 1% were probably a feature of analytical error due to low ^{234}U count rates, which will not have affected measurement of U concentration.

As mentioned previously, two samples are thought to have lost U subsequent to contemporaneous samples becoming essentially closed system with respect to both U and Th. The analyses on both samples have been reproduced, and their position to the left of the trends confirmed. One of these samples (R96-18) was collected under difficult field conditions, and the only material which could be collected had numerous penetrative red veins resulting from post-eruptive alteration. The other sample (R95-22) was collected from the top of the Whangaehu sequence, and is thought to be related to the Upper Whangaehu sequence. Although there is no direct evidence for alteration of this sample, its position to the left of the well defined trends occupied by contemporaneous samples would suggest that the systematics have been disturbed subsequent to the other flows from the Upper Whangaehu group becoming a closed system. In order to produce the current U/Th ratio in these two samples through post-eruption U loss, assuming that they would have fallen on the relevant trends prior to leaching, would require 6.7% U loss for R95-22 and 2.9% U loss for R96-18. Whilst there is no evidence for fractionation of ^{234}U from ^{238}U

during leaching, a similar observation has been reported for other systems where U leaching has clearly occurred (Sturchio et al., 1987).

An alternative explanation for these samples might be that a longer time has passed since the time of U/Th fractionation, and that it was coincidence that they were erupted at the same time as the other lavas from the Whangaehu sequence. Such a model would require isolated storage of these magmas in the crust. There is no simple way to distinguish between these hypotheses, although on balance, given that sample R96-18 showed clear evidence for post-eruption alteration in hand specimen, the former suggestion is preferred.

Another possibility which must be considered is that the observed excess of ^{238}U relative to ^{230}Th in all the Ruapehu rocks was produced by U addition as a result of some kind of fluid-magma interaction whilst the melts were resident in the crust prior to eruption. Several arguments can be made which indicate that this hasn't affected Ruapehu magmas. Firstly, as noted above, the ($^{234}U/^{238}U$) ratios show no signs of having been disturbed by groundwater. In the older samples, it might be argued that any anomaly between ($^{234}U/^{238}U$) may have been obscured as a result of radioactive decay bringing the system back towards equilibrium. However, the historic eruptions from Ruapehu also show no evidence for perturbed ^{234}U-^{238}U systematics and have U/Th ratios which fall within the observed range for all of the samples analysed, implying that there is nothing unusual about the amount of U excess observed in lavas erupted this century.

Secondly, as will be discussed in Chapter 6, there is an apparent relationship between the lavas analysed from New Zealand in this study and young lavas from the Kermadec and Tonga arcs to the north. As other studies have made a strong case for the U-series systematics of the Tongan and Kermadec lavas being related to source processes (e.g. Regelous et al., 1997; Turner and Hawkesworth, 1997; Turner et al., 1997a), any systematic behaviour between samples from these arcs and analyses of New Zealand volcanics would have to be put down to coincidence if the U excess in Ruapehu lavas is a feature of crustal fluid-magma interaction.

It is concluded from the above arguments that the observed U-Th systematics in Ruapehu lavas are not related to the mobility of U in hydrous fluids at a crustal level, either prior to eruption or during post-eruption alteration. Two samples appear to be the exceptions to this and have U/Th ratios which imply that they may either have suffered U loss during alteration and weathering processes, or the time between U/Th fractionation and eruption was longer for these magmas.

5.3.1.2 Fractionation of U from Th by Crystallisation Processes

The effects of crystallisation on U-series systematics can be understood by constraining the shift in U/Th ratio which could be produced by such a process in the Ruapehu lavas. The phase assemblage observed in Ruapehu lavas is essentially dominated by major phases in which U and Th are highly incompatible (i.e. olivine, clino- and orthopyroxene, and plagioclase). The partition coefficients of U and Th in these minerals are generally not well known (see Tables 2.1 and 2.2), although experimental studies tend to suggest that values are probably in the range 0.05-0.0001 (e.g. Hauri et al., 1994; LaTourrette and Burnett, 1992; Lundstrom et al., 1994; Dunn and Sen, 1994). In addition to such major phases, lavas from Ruapehu almost always contain a small proportion of titanomagnetite, and rare apatite inclusions in plagioclase have been described in previous studies (Graham and Hackett, 1987). Partition coefficients for titanomagnetite are typically between 0.05 and 0.5 (see Tables 2.1 and 2.2 and references given there). Partition coefficients for apatite are quite variable but both U and Th are normally compatible. This is confirmed by analyses of individual apatite crystals from granites by laser ablation ICP-MS, which shows that concentrations of U are in the range 1-800 $\mu g\ g^{-1}$, and Th abundances are typically 0.5-80 $\mu g\ g^{-1}$ (Bea, 1996).

Using the data on partitioning behaviour given above, the magnitude and direction of the shift in U/Th which might result from fractional crystallisation can be addressed. Examination of the partition coefficient data presented in Tables 2.1 and 2.2 shows that values of $K_{D\ U/Th}$ are variable for the minerals crystallising in Ruapehu magmas and can be both greater and less than unity. It is therefore difficult to suggest a general case for the direction in which fractional crystallisation is likely to drive U/Th ratios in the liquid. To

test whether producing the range of U/Th values observed in Ruapehu lavas through fractional crystallisation was feasible, some rough calculations were made based on the typical mineral proportions obtained by the crystallisation modelling described in Chapter 4. It was assumed that there was 50% fractional crystallisation, and that the crystallising assemblage comprised olivine (11%), clinopyroxene (30%), orthopyroxene (13%), plagioclase (42%), titanomagnetite (6%) and apatite (0.1%). A range of partition coefficients for U and Th in the various phases were tried. Even by setting the partition coefficients of one of the major phases (e.g. plagioclase) and of apatite so that there is a considerable preference for either Th or U in the crystals (e.g. $D_U^{plag} = 0.01, D_{Th}^{plag} = 0.1$ and $D_U^{ap} = 1, D_{Th}^{ap} = 10$), it is not possible to generate shifts of more than 3-5% in U/Th ratio of the liquid.

If crystallisation does play an important role in controlling U/Th ratios, it would be expected that correlations would be observed between this ratio and indices of crystallisation. One such index may be $(La/Yb)_N$ which forms a good positive correlation with SiO_2 (Figure 5.5). Plots of U and Th abundances and also U/Th ratio against $(La/Yb)_N$ are shown in Figure 5.6. Whilst $(La/Yb)_N$ will increase as a result of both crystallisation and assimilation (positive correlations are also observed against $^{87}Sr/^{86}Sr$ and $^{143}Nd/^{144}Nd$ – see Figure 5.7), it provides a useful index of differentiation which will be unaffected by variations in absolute abundances in different parental magmas. As would be expected from two incompatible elements, both U and Th show positive correlations with $(La/Yb)_N$. However no such correlation is observed for the plot of U/Th versus $(La/Yb)_N$, providing evidence that crystallisation did not exert a major control on this parameter.

In summary, modelling the effects of fractional crystallisation on U/Th ratios for Ruapehu magmas shows that it is very difficult to produce significant shifts even after 50% fractional crystallisation. Maximum shifts in U/Th ratio of < 5% even using favourable partition coefficients compare with an overall observed range of ~14% for the samples analysed in this study. The lack of correlation between U/Th ratios and indices of differentiation also confirms that fractional crystallisation is not responsible for the observed variations in U/Th.

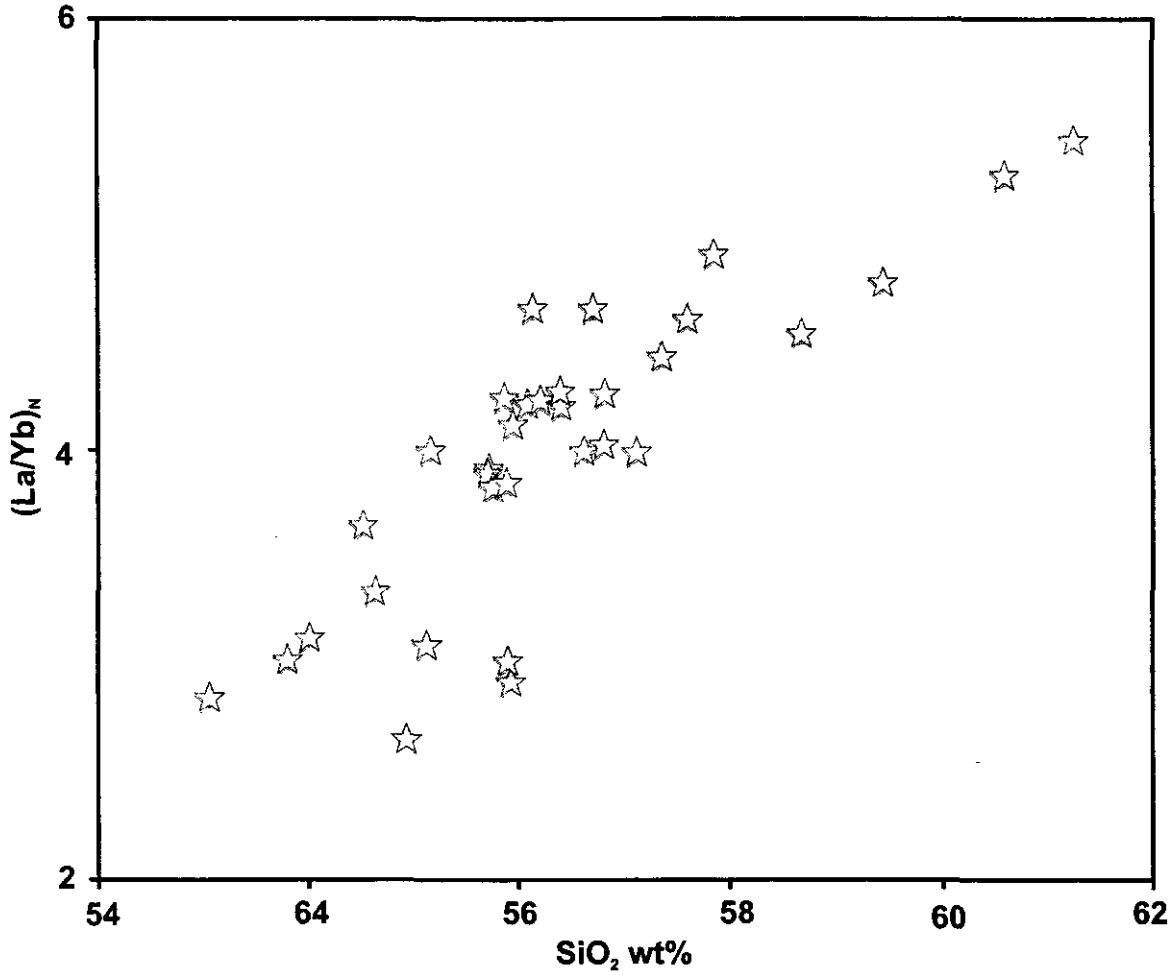

Figure 5.5: Variation of $(La/Yb)_N$ with SiO_2 for samples analysed in this study, showing a positive correlation which can be attributed to a combination of crystallisation and assimilation processes.

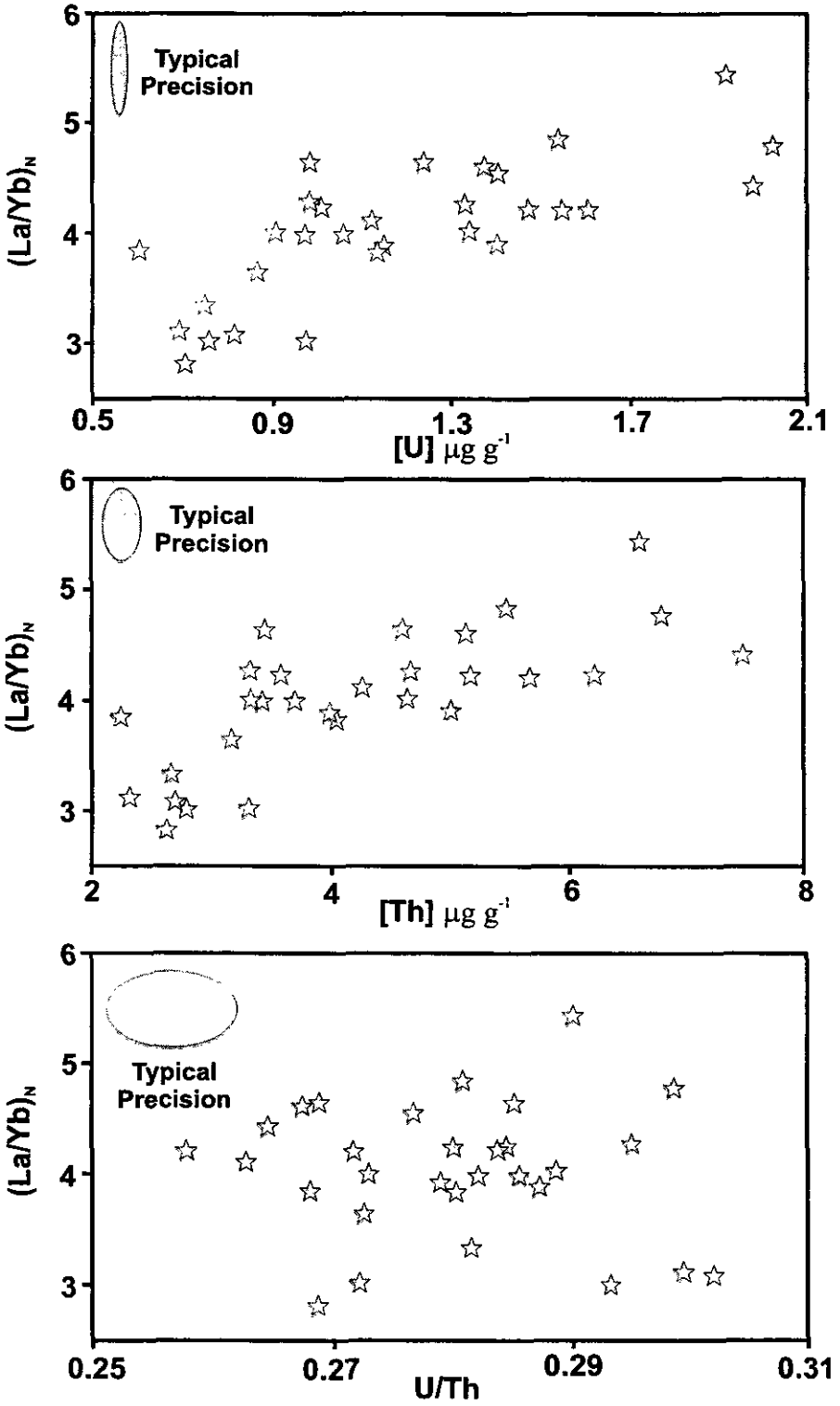

Figure 5.6: Variation of $(La/Yb)_N$ with U and Th concentrations, and U/Th ratio. All U and Th data were obtained by isotope dilution, and La and Yb concentrations were determined by INAA. La and Yb concentrations have been normalised to values for chondrites from Sun & McDonough (1989).

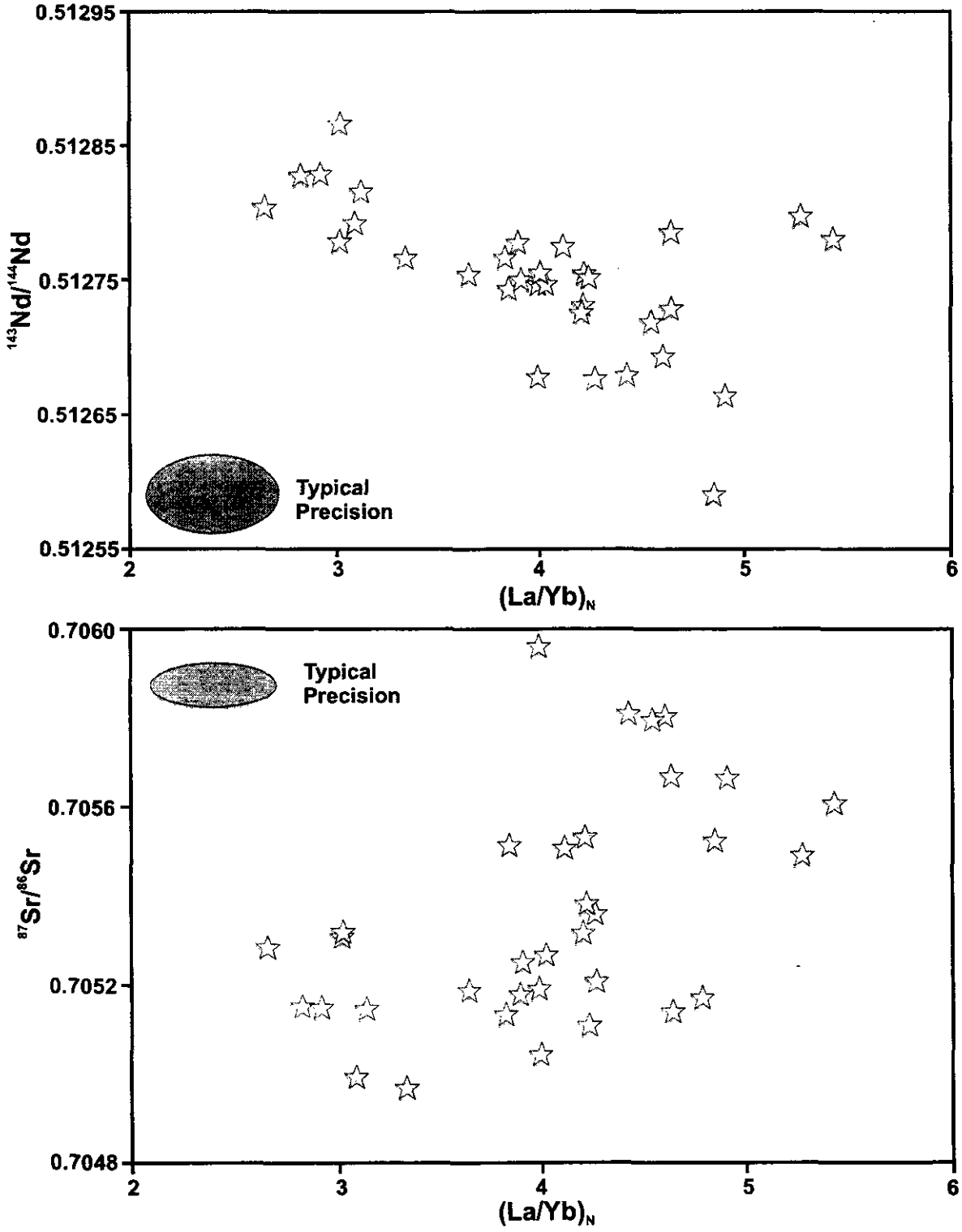

Figure 5.7: Variation of $(La/Yb)_N$ with Sr and Nd isotopes. Both isotope ratios show a correlation with $(La/Yb)_N$, implying that this ratio is at least in part controlled by assimilation.

5.3.1.3 Assimilation Controls on U/Th Ratio

It has already been demonstrated in Chapter 4 that assimilation of partial melts of Torlesse basement is an important factor in the differentiation of Ruapehu lavas. Clearly, if 10-15% assimilation of crustal material occurs, the potential for modification of U-series systematics is significant and must be considered in some detail.

Variations in $^{87}Sr/^{86}Sr$ and $^{143}Nd/^{144}Nd$ are sensitive to assimilation of crustal material and are shown plotted against U/Th ratio in Figure 5.8. The samples which are thought to have had their U/Th ratios modified by post-eruption alteration processes are identified separately (see Section 5.3.3.1). In order to reduce the number of different groups plotted, the two samples from the Waihianoa sequence have been combined with those from the Lower Whangaehu sequence, which are believed to related, a fact which will be discussed in more depth in Section 5.3.3. In both plots, there is a suggestion of some degree of correlation between U/Th ratios and Sr and Nd isotope systematics, and this has been shown on the diagrams. Within the stratigraphic groups there is generally very little evidence of any correlation, although many of these groups undoubtedly comprise multiple magma batches with somewhat different differentiation histories. The possible correlations between U/Th ratios and Sr and Nd isotopes are certainly not statistically significant and should perhaps just be regarded as a worst case scenario.

To an extent, the use of $(La/Yb)_N$ in Figure 5.6 also acts as a check for the effects of assimilation. This ratio is likely to be affected by both crystallisation and contamination by partial melts of local crust, and the correlation between SiO_2 and $(La/Yb)_N$ supports this hypothesis (see Figure 5.5). The lack of correlation in Figure 5.6, argues against a strong crustal influence on U/Th ratio, however this can be checked more thoroughly by the use of a trace element ratio which is unlikely to change significantly in response to crystallisation. In Figure 5.9, Rb/Zr ratios are plotted against both $^{87}Sr/^{86}Sr$ and U/Th ratios. As both Rb and Zr should be highly incompatible in the phases crystallising from Ruapehu magmas, Rb/Zr values should only be modified by some kind of mixing process such as assimilation. In addition, Rb/Zr ratios in North Island Torlesse basement have a range of 0.3-1.2 (Palmer et al., 1995), in contrast to the value of 0.25 in Ruapehu 'basalt'

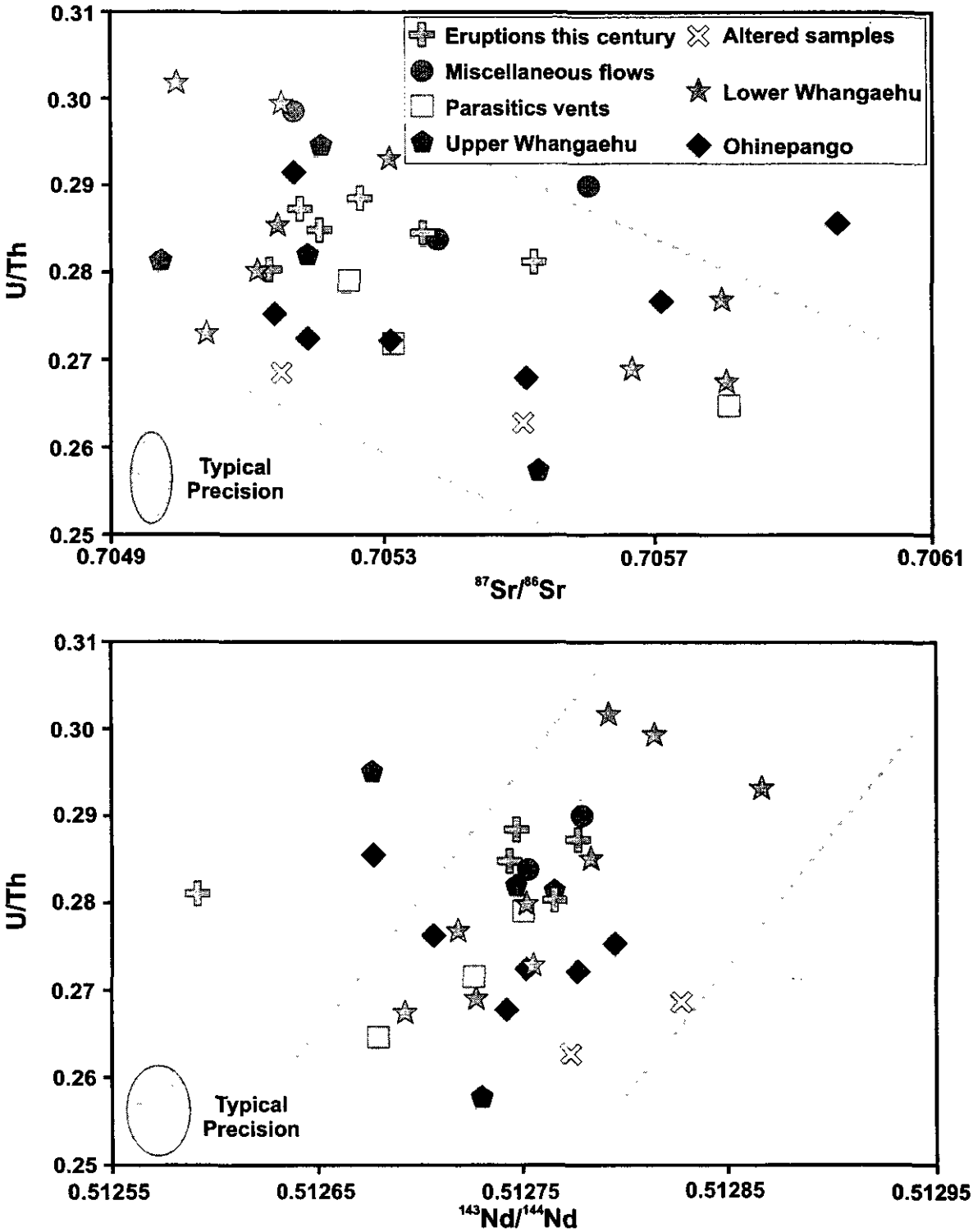

Figure 5.8: Variation of U/Th ratio with $^{87}Sr/^{86}Sr$ and $^{143}Nd/^{144}Nd$. The key is the same for both diagrams. Note that samples from the Waihianoa section have been combined with the Lower Whangaehu samples, with which they are believed to be related. The two samples which are inferred to have lost U during post-eruption alteration are identified separately here. The lines drawn on each plot show the inferred general trend for a worst case assimilation model, although there is no statistically significant correlation in the data.

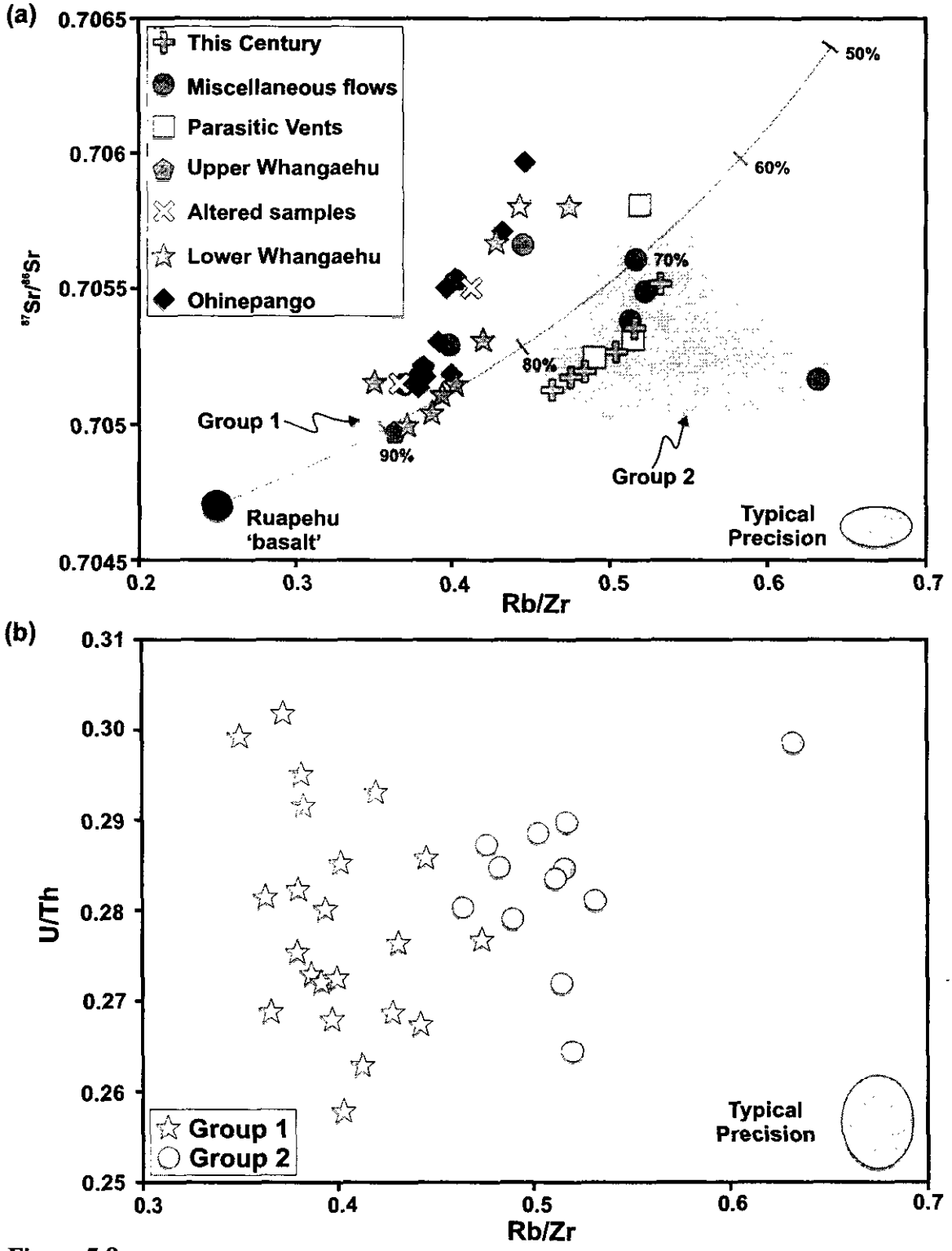

Figure 5.9:

(a) - Variation of Rb/Zr ratio with $^{87}Sr/^{86}Sr$. See the text for a discussion of the two groups identified. Waihianoa samples have been combined with data for the Lower Whangaehu sequence. The AFC curve shows the effect of contamination of Ruapehu 'basalt' with partial melts of Torlesse basement, with tick marks showing the percentage mass remaining. The AFC curve was calculated using the equations of DePaolo (1981) for r=0.2, $D_{Rb}=D_{Zr}=0.01$, $D_{Sr}=1$. The composition of partial melts of Torlesse (Rb=270 μg g^{-1}, Zr=190 μg g^{-1}) is taken from Graham & Hackett (1987) and is discussed further in the text. Data for Ruapehu 'basalt' is from Gamble et al. (1993).

(b) - Variation of U/Th with Rb/Zr. The samples are divided into the two groups identified from (a).

(Gamble et al., 1993). Thus assimilation of a partial melt of such rocks (particularly in the presence of residual zircon) is likely to increase Rb/Zr ratios in Ruapehu lavas.

When Rb/Zr is plotted against $^{87}Sr/^{86}Sr$, a distinct split in the data can be identified. Examination of the samples which form each of the groups identified in Figure 5.9a shows a clear stratigraphic distinction between them. Group 1 principally comprises older samples from the Upper and Lower Whangaehu groups, the Ohinepango group and a couple of the miscellaneous flows. The second group comprises samples from historic eruptions, from parasitic vents and some of the flows from the miscellaneous group. These two groups show reasonably tight correlations with $^{87}Sr/^{86}Sr$ with the exception of one sample (W9-5) which plots to very high Rb/Zr but has been included as part of Group 2 for the purposes of this discussion. The AFC curve illustrates that it is perfectly feasible to generate the observed data from a primitive composition such as Ruapehu 'basalt'. The Rb concentration chosen for partial melts of Torlesse basement in this model is considerably higher than those of the bulk rocks and is based on previous estimates for partial melts of Torlesse rocks (Graham and Hackett, 1987). The Zr abundance of the partial melt is much closer to that of the bulk rock analyses, because residual zircon is likely to have been present during crustal melting (e.g. Graham et al., 1988). The two different groupings seen in Figure 5.9 imply either a difference in parental composition and/or slightly different AFC parameters.

When Rb/Zr values are compared with U/Th ratios (Figure 5.9b), there is no distinct trend obvious in either of the two groups identified from Figure 5.9a. The younger samples forming Group 2 show a slightly more limited range in U/Th ratio although this may be a consequence of fewer analyses for this group. Overall it is very difficult from Figure 5.9b or La/Yb-U/Th to make a case for assimilation having had a significant influence on the observed U/Th values. It is worth noting from this diagram that there is also no evidence for a shift in U/Th value corresponding to the shift in Rb/Zr observed between the groups. Clearly, whether parental magma variations or differences in crustal level differentiation are responsible for the differences in Rb/Zr ratios between the groups, the processes involved have not affected the U/Th ratios to an identifiable degree.

Given the difficulty in demonstrating a link between U/Th variations and crustal assimilation processes, it is important to give consideration to the reasons for this. It was noted in Chapter 2 that U and Th concentrations in crustal melts are in practice often controlled by accessory minerals in which these elements are essential structural components (ESCs). The Torlesse basement of North Island is known to be dominated by two main lithologies, greywackes and argillites (Graham, 1985). Abundances of both U and Th are much higher in the argillites (Graham, 1985; Graham et al., 1992), resulting primarily from higher abundances of accessory phases such as monazite, zircon, xenotime, sphene and apatite both as detrital phases and inclusions in biotite. Both U and Th are ESCs in monazite and xenotime, and can be present in the other phases in abundances up to several wt% (e.g. Bea, 1996). The U and Th (and LREE) contents of crustal melts are determined by complex dissolution and buffering relationships between various accessory phases such as those mentioned above, and these interactions are themselves dependant upon temperature, water content and melt composition (e.g. Ayres and Harris, 1997).

There is insufficient knowledge as yet, of the behaviour of U and Th during melting of crustal rocks to discuss the consequences of assimilation on Ruapehu U/Th ratios in any depth. Comparisons can be drawn, however, with studies of crustal melting at other locations. An ideal example is that of Himalayan leucogranites, which are thought to be derived by partial melting of pelitic schists found in close proximity to the derived melts (Ayres, 1997). A summary of the U and Th abundances determined for both schists and leucogranites is given in Table 5.2. It is clear that if the schists of the High Himalayan Crystalline Series are parental to the leucogranites, then it is possible to generate extreme fractionations of U from Th during crustal melting. Whilst the metamorphic grade of the Himalayan sediments is higher than that of Torlesse basement rocks exposed at the surface, the bulk chemistry is similar, and both lithologies have similar accessory phases.

	Schists (n = 9)	Leucogranites (n = 8)
U μg g^{-1}	3.73	9.61
Th μg g^{-1}	15.69	2.15
U/Th	0.203	5.99
1σ	0.023	4.28
($^{238}U/^{232}Th$)	0.62	18.17
1σ	0.07	12.99

Table 5.2: Average U and Th abundances in Himalayan metasediments and leucogranites (Ayres, 1997).

Given that there is abundant evidence for assimilation of partial melts of basement in Ruapehu lavas, it is not totally evident why very large shifts in U/Th ratio are not observed. It may be that the time available for partial melting is short compared with the timescales of the order of 10-200 ka required to produce the leucogranites (Ayres, 1997). Whereupon there might have been very little dissolution of the principle U and Th bearing minerals such as monazite and apatite, and so the crustal melts would have had very low U and Th contents. Alternatively, it may be that the dissolution and buffering reactions controlling the behaviour of U and Th during melting may be very different as a result of different temperature conditions, and that the Ruapehu contaminants had similar U/Th ratios to the parental magma. The work of Ayres (1997) suggests that the melting event which produced the Himalayan leucogranites had a temperature of ~700°C, whereas the temperatures recorded by xenoliths in Ruapehu eruptives are in the range 800-1000°C.

A series of points can be made to summarise this section, as follows:

1. Assimilation is clearly an important crustal level petrogenetic process controlling many of the trace element and isotopic systematics observed in Ruapehu lavas.
2. Whilst many trace element ratios and abundances correlate with indices of assimilation such as Sr and Nd isotopes, no significant variation of U/Th ratios with these indices can be identified. It is therefore important to consider why this might be.
3. U-Th fractionation during partial melting of continental crust is poorly constrained, but it is likely to be dominated by the presence of very small quantities of accessory phases such as monazite and xenotime. The lack of correlation between U/Th and indices of assimilation argue against large fractionations of U/Th as a result of assimilation.

4. It might be argued that assimilation has in effect shifted the U/Th ratio of all of the samples to more or less the same degree which would account for the lack of correlation with other systematics. This is deemed unlikely, however, as the samples analysed show a considerable range of compositions using other systematics.

5. The clear effects of assimilation on trace element and isotope systematics, and lack of correlation between indices of assimilation and U/Th ratio argues for a particular set of circumstances. Since the assimilated melt is likely to contain some U and Th (50% crystallisation of Ruapehu 'basalt' would only produce ~2 $\mu g\ g^{-1}$ Th), it is necessary to suggest that it had a similar U/Th ratio to the parental magmas.

6. The final point which is worth making here is regarding the ($^{230}Th/^{232}Th$) ratio of the assimilant. Provided that partial melting of local basement and subsequent incorporation of this liquid into the parental magma are quick (i.e. < 5-10 ka), then regardless of U-Th fractionation during melting, the assimilant should have a ($^{230}Th/^{232}Th$) equal to the bulk ($^{238}U/^{232}Th$) of the basement rocks prior to melting. For analyses of basement rocks from North Island (both Waipapa and Torlesse, which have very similar bulk U/Th and so have been combined) this is ~0.72 (Palmer et al., 1995). This will be returned to when the age significance of the U-Th data is considered.

5.3.1.3 Source Processes as the Origin of U/Th Variation

In the previous three sections, the production and/or modification of U/Th ratios, and by implication ^{230}Th-^{238}U disequilibria by crustal level processes has been discussed. In general, crystallisation and mobilisation of U in hydrous fluids within the crust are not considered to have had a major effect on U-series systematics. It has been demonstrated that assimilation could have produced modest shifts in U/Th ratio, but no correlations have been observed between U/Th and an index of assimilation. For a given Sr isotopic composition there is a marked range in U/Th data and it is inferred that this represents a true variation in the parental magmas feeding crustal magma reservoirs beneath Ruapehu. It is also noted that similar although more limited ranges are observed within coherent stratigraphic groups, and this has important implications for the nature of magma storage

and transport within the crust which will discussed in more detail with reference to the time information that can be deduced from the U-series systematics in Section 5.3.3.

The source of the U/Th variations in parental magmas remains a difficult issue to address. Not only do the effects of mantle melting processes have to be considered, but it is also necessary to assess the effects of fluid and/or melt components derived from the subducted slab. In order to examine the potential effects of melting processes on ^{230}Th-^{238}U disequilibria in arc magmas, it is instructive to review some of the principal ideas regarding the effects of melting at mid-ocean ridges in terms of short-lived isotope systematics.

There has been a considerable effort in recent years in attempting to understand further the origin of ^{230}Th excesses in MORB. In general, dynamic melting models (see the review of Elliott, 1997) are thought to be physically reasonable and they have been shown to produce ^{230}Th excesses of similar magnitude to those observed in MORB (McKenzie, 1985b; Williams and Gill, 1989). More complex models have emphasised the importance of the so called chromatographic effect (Navon and Stolper, 1987), where melt extracted from the base of the melting column interacts with the matrix it passes through as it ascends (Spiegelman and Elliott, 1993). The significance of such interactions during melt migration is also important and has implications for the time available for the melt to interact with the residual matrix and therefore the magnitude of ^{230}Th-^{238}U disequilibrium (Iwamori, 1994). All of these models are dependant on knowing the partition coefficients of U and Th in mantle minerals. It is thought that the principal mineral capable of producing ^{230}Th-^{238}U disequilibria is garnet, in which D_U^{grt} is an order of magnitude higher than D_{Th}^{grt} (Beattie, 1993).

Melting processes in subduction zones are less well constrained than in MORB. Whilst it is now generally accepted that for most subduction environments, the mantle wedge melts in some fashion in response to fluid addition from the descending slab (e.g. Kushiro, 1983; Plank and Langmuir, 1988; Tatsumi, 1989), the exact mechanism by which this occurs remains unclear.

Two major debates remain unresolved in terms of the melting process beneath arcs. Firstly, does melting of the wedge occur because infiltration of slab-derived fluids lowers the solidus temperature of mantle peridotite (e.g. Tatsumi, 1989), or is it also because the fluids effectively lower the density of the wedge and thereby induce diapirism, adiabatic decompression and melting (e.g. Plank and Langmuir, 1988). Subsequent detailed numerical models have suggested that the former is probably more important, although limited buoyancy may induce a small degree of melting in response to adiabatic decompression (Davies and Stevenson, 1992). In contrast, detailed analysis of trace element systematics in primitive arc basalts suggests that decompression melting may account for a greater proportion of the observed melting (Pearce and Parkinson, 1993). Secondly, the nature of melt migration is uncertain. Two distinct models can be proposed which probably in practice represent end-member situations, porous flow and channelled flow. In principle it is possible to explain melt extraction from a source region once sufficient interconnecting pathways along grain boundaries are established (McKenzie, 1984; McKenzie, 1985a). There is also evidence from metamorphosed subduction complexes such as the Catalina Schist and from peridotite massifs, that channelled flow of hydrous fluids and/or melts may be extremely important (e.g. Nicolas, 1986; Sorenson and Grossman, 1989; Bebout and Barton, 1993).

In order for the observed U-Th disequilibria in Ruapehu lavas to be related directly to the melting processes occurring in the underlying mantle wedge would require that some phase was present in which Th was more compatible than U. In addition, it would require that the size of melt fraction invoked was sufficiently small that a significant fractionation of U from Th could be produced. Experimental data on the partitioning of U and Th into major mantle phases under subduction zone conditions are limited, and to date no evidence has been found for a phase in which Th is significantly more compatible than U. Whilst there are few constraints on the nature of melting processes in subduction zones, it has been demonstrated on the basis of trace element data that it is likely that the total degree of melting (15-30%) is generally greater than in MORB (2-15% for N-MORB) (Pearce and Parkinson, 1993). The same authors found no evidence for the predicted 'chromatographic effects' on trace element abundances during melt migration and

suggested that this might be a consequence of the higher degree of melting. Taking all these factors together makes it difficult to support the notion that the observed ^{230}Th-^{238}U disequilibria are related to directly to melting in the mantle wedge, or have even been modified significantly during melting.

As has been mentioned in Section 5.2, certain subduction zone environments show very large excesses of ^{238}U relative to ^{230}Th, and the only other locations in which similar systematics have been observed are in continental rift environments, where volatile rich fluids are inferred to have played an important role in melt generation (Williams et al., 1986; Pyle et al., 1991). This has generally been put down to the mobilisation of U in volatile rich fluids, and in the case of subduction zones, it is believed that this fluid is probably derived from the descending slab (e.g. Gill and Williams, 1990). In the Tonga-Kermadec arc system to the north of the New Zealand arc, very large U excesses are observed, which various authors have argued are related to the influence of slab derived fluids and sediments (Gill and Williams, 1990; McDermott and Hawkesworth, 1991; Regelous et al., 1997; Turner and Hawkesworth, 1997; Turner et al., 1997a).

The presence of U excesses in Ruapehu lavas, and the evidence from the Tonga-Kermadec arcs suggests the observed disequilibrium may likewise be related to slab-derived fluids fluxing the mantle wedge. However, the samples for which U-Th systematics have been determined as part of this study are by no means primary magmas. It is therefore difficult directly to quantify source processes from these data, however the link between the observed U excesses and source processes will be considered further by comparison with other centres in the New Zealand arc system and the Tonga-Kermadec arc (see Chapter 6).

5.3.2 The Effects of Time on the Crustal Evolution of U-Series Systematics in Ruapehu Lavas

In Chapter 2, a detailed model was presented for the behaviour of U-series systematics during crustal level magmatic processes when a time factor was added. For

several reasons it is quite difficult to assess the effect of adding a timescale to crustal level processes on Ruapehu lavas.

Firstly, given the discussions of Section 5.3.1, there is considerable doubt over how much crustal level processes have affected U/Th ratios in Ruapehu lavas. The range of U/Th ratios observed are, on the basis of available evidence, more likely to reflect sub-crustal fractionation processes. However, it is worth mentioning other reasons why application of the model developed in Chapter 2 is difficult to apply to with the available data.

If crystallisation and assimilation operate over a long timescale, the most obvious effect as demonstrated in Chapter 2 is to produce curved trajectories for the U-Th composition of the magma on an equiline diagram. One of the difficulties involved with interpreting short-lived isotope data is that subtle detail tends to become obscured with time (e.g. Capaldi et al., 1983). In addition, it was shown in Chapter 2 that if an evolving magma batch is sampled at intervals through its differentiation history, the resulting data will lie on a straight line in certain cases. Therefore, in order to assess the timescales of crustal level magmatic processes using U-series data, it is necessary to have good constraints on the eruption ages.

With the available data for Ruapehu samples, it is only possible to make a direct assessment of the timescales of differentiation processes using the historic samples. These samples appear to lie on a linear trend, and in order to argue that the data reflect crustal processes operating on a long timescale, it would be necessary to invoke a complex mechanism. This would require that following differentiation, each of the magma batches was extracted and then held separately without modification until being erupted almost simultaneously. In addition, the lack of stratigraphic correlation along the array, implies that the samples do not reflect progressive tapping of a single magma body. Detailed examinations of geochemical systematics in material from historic eruptions has led to the suggestion that these reflect injection of fresh magma from deep sources which then have variable differentiation histories immediately prior to eruption (Gamble et al., 1997). A similar interpretation has been placed on older sequences (Price et al., 1997; Price et al.,

1998), although the timescales of shallow level differentiation histories are not constrained in this instance.

In summary, it is difficult to demonstrate that U/Th ratios have been significantly affected by crustal level processes regardless of what timescale they operate on. In addition, the sample suite available from Ruapehu does not represent an ideal test of the modelling presented in Chapter 2 because the samples clearly have not come from a single evolving magma body. Better tests of the model may be provided by examining the Ra-Th systematics of young volcanic systems where age constraints are better, as discussed briefly in Section 7.6.

5.3.3 Temporal Inferences from U-Th Disequilibria in Ruapehu Lavas

The primary reason for determining ^{230}Th-^{238}U disequilibria is to extract useful time information about magmatic processes which are too rapid for the timescales to be readily constrained by other techniques. In previous sections it has been argued that the U-Th data obtained from Ruapehu lavas primarily represent some kind of U addition to the mantle wedge, and that they have apparently suffered little modification by crustal assimilation processes. In this section the data is examined in detail in order to try and understand what it can tell us about the rates of magmatic processes at both crustal and subcrustal levels.

5.3.3.1 Statistical Analysis and Data Reduction

One of the main observations made on examination of the Ruapehu data on an equiline diagram (Figure 5.2) was that samples from coherent stratigraphic groups appeared to plot along linear arrays. The first step in extracting time information from these data is to fit a whole rock pseudo-isochron (hereafter termed a pseudo-isochron for brevity) through the data where possible. This has been achieved using the Isoplot program (Ludwig, 1998), which makes use of the standard isochron equations of York (1967, 1969), but uses the maximum likelihood method of handling errors (Titterington and Halliday, 1979; Ludwig and Titterington, 1994). The pseudo-isochron fits are shown in Figure 5.10 and several points need to be made regarding the choice of samples for which

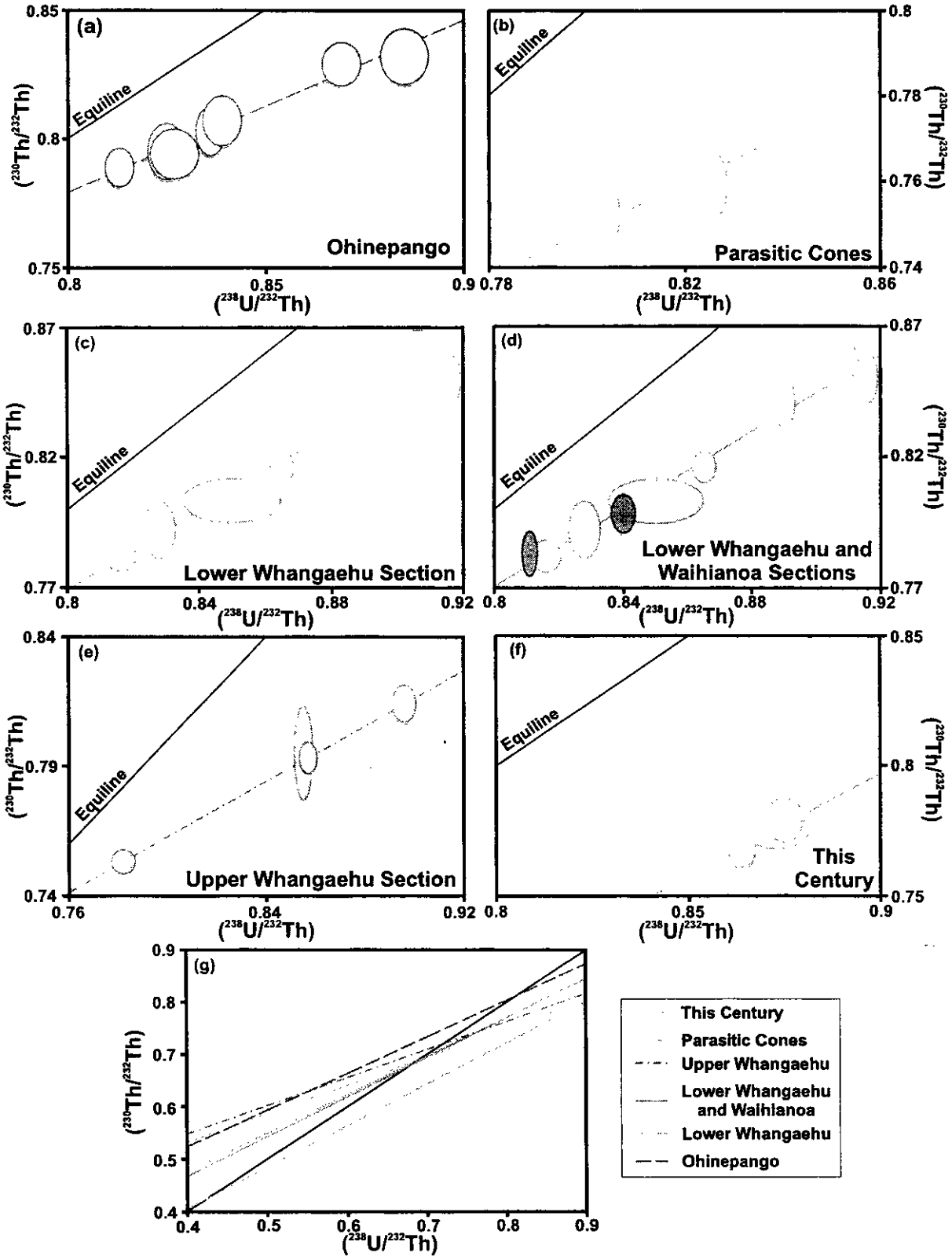

Figure 5.10:
(a)-(f): Whole rock pseudo-isochrons fitted through data for stratigraphic groups. Statistical fitting performed using Isoplot (Ludwig, 1998). See Table 5.3 for ages calculated from the pseudo-isochrons and MSWD values for the fits. All the illustrated pseudo-isochrons are for unforced models - see the text for a full discussion.
(g) - Ruapehu whole rock psuedo-isochrons on a larger scale to show the relative positions of where the trends cross the equiline.

pseudo-isochrons were fitted. Firstly, the Upper and Lower Whangaehu groups have been treated separately, and the two samples which may have undergone post-eruption U loss have been left out of the regressions. Two pseudo-isochrons have been fitted for the Lower Whangaehu group, the second of which includes the two Waihianoa samples which are thought on the basis of field evidence and geochemical data to be related. Lastly, the three samples from parasitic vent eruptions have also been treated as a coherent group. It is thought that these samples were erupted within 10 ka of one another and probably relate to the same period of cone building activity, although it is accepted that there may be no real justification in treating these samples together. Any ages obtained from these samples must therefore be treated with caution.

Before the results obtained from the pseudo-isochrons are discussed, it is instructive to consider the trends of the best-fit lines, which are shown in Figure 5.10g. One of the principle difficulties that can be encountered in fitting any isochron is where the range of data along the x-axis is very limited. In all of the whole rock pseudo-isochrons produced in this study this may be a problem, but is particularly true of historic eruptions from this century. It is clear that the pseudo-isochron fitted through this data crosses the equiline at a very much lower ($^{238}U/^{232}Th$) value and has a much lower intercept with the y-axis than the other trends, principally because of the very limited range in U/Th ratio exhibited by these samples. It is possible to see simply by visual examination (see for example Figure 5.2) that almost any line from nearly horizontal to parallel with the equiline could be fitted through these data quite reasonably.

In order to try and reduce this problem as far as possible, various models have been tried where each of the pseudo-isochrons is anchored by the same point on the equiline. There are a number of justifications for this which must be examined. If the pseudo-isochron for samples erupted this century is ignored, it is clear from Figure 5.10g that there is a reasonable consistency in where the best fit lines cross the equiline, especially considering the limited range of U/Th ratios the other stratigraphic groups themselves show. Given that it is thought that the U excesses are produced in the source by fluids carrying U preferentially to Th, and that these disequilibria are possibly then

modified by assimilation, it is necessary to invoke radical differences in the lavas erupted this century if the lower intercept of their pseudo-isochron is considered reasonable. Either these samples must have come from a mantle source with very different and extremely low ($^{238}U/^{232}Th$) and ($^{230}Th/^{232}Th$) values, or they must have been affected to a significant degree by a different assimilant with a very low ($^{238}U/^{232}Th$) ratio. None of the geochemical data discussed in Chapter 4 argued for a significant difference in the trace element systematics of primary magma compositions between the lavas erupted this century and older samples. In addition, the young samples have similar ($^{238}U/^{232}Th$) values to the other data, and so it seems therefore unlikely that either mantle or crust with extraordinarily low ($^{238}U/^{232}Th$) and ($^{230}Th/^{232}Th$) ratios was involved in the petrogenesis of the historic lavas.

If an average is taken of where the Ohinepango, Upper Whangaehu and Lower Whangaehu pseudo-isochrons cross the equiline, it turns out to be at a ($^{238}U/^{232}Th$) ratio of ~0.71. As will be demonstrated later in this chapter, this happens to correlate with where data from other TVZ localities such as Edgecumbe (this study) and Taupo (B. Charlier, unpublished data) also plot. The possible reasons for this coincidence of values is discussed in more detail later when variations within the arc are examined, but for the purpose of this discussion it is reasonable at least to examine the data obtained when pseudo-isochrons are anchored by a constant point. Four different anchoring values for ($^{238}U/^{232}Th$) and ($^{230}Th/^{232}Th$) were used, 0.72, 0.7, 0.68 and 0.65. In each case, 2% errors (double the typical 2σ precision of $\leq 1\%$ obtained for sample analyses) were assigned to the point so that errors on the pseudo-isochron fit could be calculated, but without imposing unrealistically good uncertainties on the derived ages. The assigned variation of 2% is equivalent to a ($^{238}U/^{232}Th$) range of approximately ± 0.015. The age data for both the unforced and the various forced models are presented in Table 5.3.

Examination of the age data for the various models shows that for the most part the effects of anchoring the pseudo-isochrons are limited. The range of values obtained for the Lower Whangaehu (± Waihianoa samples) and Ohinepango groups are within error of one another although a much larger variation is shown by the latter. The Upper

Whangaehu group shows little variation between derived ages with the exception of the last model. The same general pattern is observed for the lavas from the parasitic vents although a somewhat larger range of ages is obtained. As mentioned above, the main effect of anchoring the pseudo-isochrons is to change the ages obtained for historic samples from $157^{+inf}_{-87.5}$ ka (without anchoring) to 47-85 ka depending on the anchoring value, although all the anchored ages are statistically indistinguishable. The MSWDs (Mean Squares of Weighted Deviates) calculated are generally very good, with or without forcing, and give a feel for how statistically reasonable the isochron fitting is. In general, an MSWD value of 2.5 is taken as the upper limit for the range in which it is reasonable to assume that the scatter is entirely analytical, and above this it is deemed likely that some of the scatter results from geological processes (Wendt and Carl, 1991). Only one of the regressions summarised in Table 5.3 has an MSWD above 2.5, and most of the regressions have a much lower value. It is noted however that despite the good MSWDs, only three samples have been regressed in the trend for parasitic vent lavas and with so few data points there is a tendency to overestimate the goodness of fit.

		OH	LWHA	LWHA+ WAI	UWHA	PAR	TC
Unforced	**Age**	$111.5^{+50.3}_{-33.4}$ ka	$142.3^{+37.6}_{-27.3}$ ka	$134.7^{+29.1}_{-22.6}$ ka	$77.4^{+14.2}_{-12.6}$ ka	$78.5^{+57.7}_{-36.5}$ ka	$157.4^{+inf}_{-87.5}$ ka
	MSWD	0.51	1.5	1.4	0.076	1.13	0.19
Forced to 0.72±2%	**Age**	$118.1^{+37.4}_{-27.2}$ ka	$133.9^{+28.4}_{-22.1}$ ka	$130.2^{+24.4}_{-19.6}$ ka	$77.4^{+13.2}_{-11.7}$ ka	$61.6^{+25.2}_{-20.1}$ ka	$46.8^{+27.5}_{-21.6}$ ka
	MSWD	0.47	1.5	1.3	0.051	1.14	2.2
Forced to 0.7±2%	**Age**	$127.0^{+37.9}_{-27.5}$ ka	$137.0^{+27.8}_{-21.8}$ ka	$132.8^{+24.1}_{-19.4}$ ka	$80.8^{+13.2}_{-11.7}$ ka	$72.2^{+23.1}_{-18.8}$ ka	$62.0^{+18.1}_{-15.4}$ ka
	MSWD	0.59	1.3	1.2	0.38	0.63	1.6
Forced to 0.68±2%	**Age**	$136.2^{+38.4}_{-27.7}$ ka	$140.6^{+27.4}_{-21.5}$ ka	$136.2^{+23.6}_{-19.1}$ ka	$85.1^{+13.5}_{-11.9}$ ka	$83.0^{+23.7}_{-19.2}$ ka	$71.1^{+17.8}_{-15.1}$ ka
	MSWD	0.76	1.3	1.2	1.3	0.59	1.11
Forced to 0.65±2%	**Age**	$150.9^{+39.1}_{-28.1}$ ka	$147.8^{+269}_{-21.2}$ ka	$142.7^{+23.8}_{-19.2}$ ka	$106.7^{+52.1}_{-34.2}$ ka	$98.4^{+23.7}_{-19.2}$ ka	$84.4^{+17.2}_{-14.7}$ ka
	MSWD	1.05	1.3	1.3	3.7	0.96	0.71

Table 5.3: Tabulated ages and MSWDs calculated for pseudo-isochrons fitted through data from Ruapehu lavas. The abbreviations for stratigraphic groups are as follows: OH – Ohinepano, LWHA – Lower Whangaehu, WAI – Waihianoa, UWHA – Upper Whangaehu, PAR – parasitic vents, TC – historic eruptions this century. The arguments for the different models listed here are given in the text. All the errors are calculated for internal 2σ precision on individual analyses. Isochron fitting and error calculation were performed using Isoplot (Ludwig, 1998). Ages were calculated using the Bateman decay equation (Equation 2.8).

It is difficult to be certain which is the best model of those presented in Table 5.3 to use in discussing the interpretation of the calculated ages. It is suggested here that anchoring the trends through a point with ($^{238}U/^{232}Th$) and ($^{230}Th/^{232}Th$) values of 0.7 is the most reasonable approach. This value is within error of the average of where the main trends cross the equiline and appears to have a systematic importance amongst New Zealand volcanic centres, which will be discussed in Chapter 6.

5.3.3.2 Comparison of U-Th ages and Eruption Ages

There are two principle ways in which the ages obtained from the linear trends can be interpreted. Firstly, the slope of the data could be regarded as giving an age for an initial event which fractionated U from Th in the mantle source along an initially horizontal vector on an equiline diagram. Secondly, the data could be regarded as reflecting an initial fractionation event as above, but where the U-Th systematics have subsequently been disturbed by mixing as in crustal assimilation processes. In this section, the U-Th ages will be compared with data for eruption ages of the various groups in order to constrain the origin and interpretation of the observed U-Th disequilibrium.

As outlined in Chapter 3, there is very little reliable chronological data published for the main edifice of Ruapehu. However, recent Ar-Ar work on some of the older sequences studied as part of this thesis has placed some apparently reasonable constraints on eruption ages (J. Gamble pers. comm.). These ages are shown in Table 5.4.

Sample	Sequence	Age
X1-6	MISC	23±10 ka 21±6 ka
R95-20	UWHA	74±37 ka
R96-5	WAI	129±15 ka
R96-9	WAI	147±12 ka
R96-22	LWHA	119±12 ka
R95-26	LWHA	130±23 ka
R95-27	LWHA	135±14 ka
R95-28	LWHA	133±11 ka
R96-17	LWHA	134±12 ka
R96-16	LWHA	131±27 ka
R96-20	LWHA	154±12 ka 132±14 ka
X1-10	OH	138±14 ka

Table 5.4: Summary of Ar-Ar dates for sequences analysed for U-series data as part of this study. Data reproduced with permission of J. Gamble. Quoted errors are at the 2σ level.

In principle, the Ar-Ar system dates the eruption age of a lava, because of the very low closure temperature of most minerals to Ar. In contrast, ages produced from U-Th whole rock analyses essentially date some event or events which have fractionated U from Th and which could have occurred some significant period of time prior to eruption. The U-Th ages obtained for the various groups are compared with Ar-Ar ages and known eruption dates in Figure 5.11. The U-Th ages shown are those calculated by anchoring the pseudo-isochrons to a point on the equiline with a ($^{238}U/^{232}Th$) ratio of 0.7, although in practice this makes little difference except to the age shown for eruption this century as mentioned above. The U-Th age for the valley filling flows is the same as that for the eruptions this century, as the data fall on the same trend on an equiline diagram (see Figure 5.2). This diagram shows some important details which help in understanding the meaning of the U-Th ages, and these are discussed below.

The oldest three groups have U-Th ages which are within error of their Ar-Ar eruption ages. The most robust of these comparisons is between the Ar-Ar and U-Th age data for the Lower Whangaehu sequences because of the number of analyses which have been made by both techniques. Regardless of which of the forcing models for the U-Th data is used, the ages derived by the two techniques are almost identical and fall well within analytical error of one another. The Ar-Ar data also confirm the hypothesis put

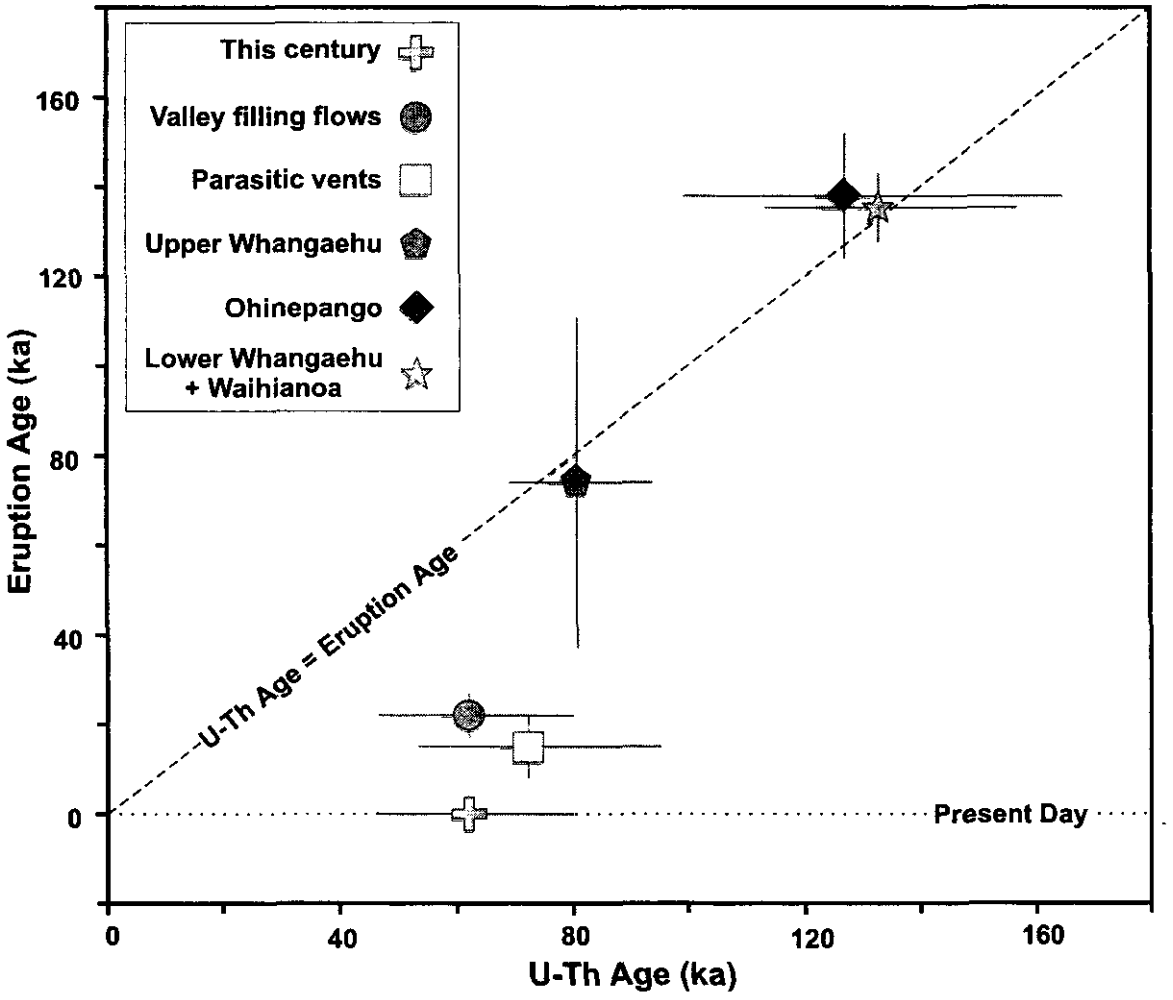

Figure 5.11: Comparison of eruption ages and dates calculated from U-Th whole rock isochrons. Eruption ages for the Lower Whangaehu, Upper Whangaehu, Ohinepango and Valley filling flows are from Ar-Ar analyses. Where multiple analyses are available, a weighted average at the 95% confidence interval has been used (calculated with Isoplot, Ludwig, 1998). The eruption age for the parasitic vents is an average of their estimated ages. The error for this eruption age has been assigned such that it is sufficient to take in the maximum and minimum ages thought possible for these samples. The U-Th ages plotted are those derived by anchoring the isochrons to a value of 0.7 (see the text for a discussion).

forward earlier that on the basis of the U-Th data the Lower Whangaehu and Waihianoa sequences were of indistinguishable age. There is limited data available to make robust comparisons of the Ohinepango ages, however the ages agree within error, and the U-Th models which forced the trends through specific points tend to improve the correspondence in ages. As with the Ohinepango data, there are insufficient Ar-Ar analyses of the Upper Whangaehu sequences to make more than a brief comparison. With the exception of the model which forced the U-Th trends through a ($^{238}U/^{232}Th$) value of 0.65 on the equiline, the agreement with the available Ar-Ar age is excellent, although it is noted that the errors on the Ar-Ar age are relatively large.

In contrast, the youngest three groups show significant differences between the eruption and U-Th ages. Although the exact magnitude of the difference is dependant on the forcing model used, the U-Th age is always considerably in excess of the eruption age (40-80 ka). It is also important to note that the U-Th ages of these three groups and of the Upper Whangaehu sequence are within error of one another, which is a point which will be returned to.

As the sequences where U-Th ages are equal to eruption ages are those where eruption ages were determined by Ar-Ar, it is important to consider whether it is possible that the correlation is a reflects problems with techniques rather than geological phenomena. The obvious potential problem is with excess Ar, however a number of arguments can be made which support the interpretations put forward in this study. Firstly the Ar-Ar were determined by step heating, which permits problems with excess Ar to be readily identified. Secondly, in general it would be expected that problems with excess Ar should increase scatter, whereas the excellent agreement between ages determined for the Lower Whangaehu sequence argues against any such problem at least in these samples. Thirdly, the fact that U-Th ages and Ar-Ar ages for three sequences are in agreement would require the remarkable coincidence that each sample had been contaminated with the right amount of excess Ar to increase the Ar-Ar age to be the same as the U-Th age.

5.3.3.3 Interpretation of U-Th Ages

It has been demonstrated in this Chapter that the ^{238}U-^{230}Th disequilibria observed in Ruapehu lavas appear largely to reflect a subcrustal fractionation process. It is likely that this fractionation event is related to U being carried in hydrous, slab-derived fluids which flux the overlying mantle wedge. The following discussion forms two parts; firstly the *agreement* between U-Th ages and eruption ages for the older sequences is discussed, and secondly the *differences* between U-Th age and eruption ages for the younger sequences are discussed. It is worth emphasising however, that the presence of U excesses in both the older and younger sequences is inferred to reflect subcrustal processes.

The agreement between U-Th ages and eruption ages for the older sequences demonstrated in Figure 5.11 is one of the most important features of the U-Th systematics of Ruapehu lavas. The following discussion largely centres on the Lower Whangaehu and Waihianoa sequences for which there is the best data, but in essence it applies to the Ohinepango and Upper Whangaehu sequences as well.

If the observed U-Th disequilibria in the Lower Whangaehu and Waihianoa sequences are related to a subcrustal fractionation event there are a number of important implications. Firstly, the combined wedge transit and residence times for these magmas must be very short. Assuming that the U-Th age must in practice be older than the Ar-Ar ages and the forcing model which gives the greatest separation in ages from Table 5.3 (i.e. anchored to 0.65), then within analytical errors, the maximum difference between U-Th age and eruption age is 40 ka (calculated using a weighted average of the Lower Whangaehu and Waihianoa Ar-Ar data which gives an age of 135.4±7.7 ka).

U-series data from the Marianas arc have been used to infer wedge transit times of ~30 ka (Elliott et al., 1997), estimates of minimum transit times on the basis of U-Th data from the Tonga-Kermadec arc system are ~30-50 ka (Turner and Hawkesworth, 1997; Turner et al., 1997a), and estimates of total transit and residence times from Chile are ~20 ka (Sigmarsson et al., 1990). In contrast, much longer combined transit and residence times from U-Th data are reported for other arcs, i.e. 90 ka from the Lesser Antilles (Turner et al., 1996), 150 ka for Santorini (Zellmer, 1998) and > 150 ka from Kamchatka

(Turner et al., 1998). The very short combined transit and residence times from the Lower Whangaehu and Waihianoa sequences (« 40 ka) requires further consideration.

Such short combined transfer and residence times imply that the mechanism of melt transport from the site of melting to the surface must be efficient. There has been little work on the nature of melt transport in subduction zone environments, although it has been suggested that there may be two distinct end-member transport mechanisms, porous and channelled flow (Iwamori, 1993; Iwamori, 1994). This is supported by evidence for veining observed in peridotite complexes (e.g. Sleep, 1988; Takahashi, 1992). It has been suggested that the latter of these mechanisms must be important in the Tonga-Kermadec arc system in order to explain the existence of Ra-Th disequilibria (Turner et al., 1997a). There are few constraints on which mechanism is likely to dominate beneath New Zealand, but it is suggested that in principle at least, rapid melt extraction from the mantle is entirely feasible.

Equally, the apparently short transfer and residence times require that there is little stalling of the magmas generating the Lower Whangaehu and Waihianoa sequences. Extraction of the melts through the crust must be efficient, with only short residence times at shallow levels. Comparisons can be made with a recent study of a series of tephras erupted ~10 ka ago from a series of vents across the Tongariro Volcanic Centre, which contain relatively abundant hornblende, in contrast to the lavas erupted from the ToVC (Nairn et al., 1998; Nakagawa et al., 1998). These studies use the presence of hornblende to infer extremely rapid transfer times from deep magma chambers to the surface. As noted in these studies, experimental studies on amphibole breakdown at shallow levels imply that it is possible to ascend > 8 km in a matter of days (Rutherford and Hill, 1993). The absence of amphibole in Ruapehu eruptives does not therefore preclude transfer times on the order of hundreds to thousands of years as might be inferred from the U-Th data.

The short combined transit and residence times inferred for the older sequences analysed in this study also have implications for the origins of the observed U excesses. Although U excesses in arcs have been widely ascribed to the fluxing of the mantle wedge by oxidising fluids as described in Section 5.2, it is unclear at what stage during the

melting process the U-Th signature is set. A model might be invoked whereby fluids amphibolitise the mantle and this zone of metasomatically altered wedge then migrates laterally into the zone of melting (e.g. Davies and Stevenson, 1992). In this instance, then it is important to understand whether the U excesses reflect the initial entry of the fluids into the mantle wedge, or whether during subsequent dehydration reactions during migration of the amphibolitised region can also generate U-Th fractionations. The difficulty in these models is that the rate of induced convection in the mantle is generally poorly constrained (Davies and Stevenson, 1992). Clearly however, induced mantle convection is likely to have a maximum value equivalent to the rate of subduction, i.e. 40-50 mm a^{-1}, which even using highly simplistic migration models would mean that it would take ~20 ka to travel 1 km. In reality, if slab subduction and induced convection are somewhat decoupled as has been established for the Tonga-Kermadec arc (e.g. Turner et al., 1997a) this rate will be considerably slower. Clearly such timescales are not supported by the short transfer and residence times inferred for the older Ruapehu sequences. In addition, as fluids migrate across the wedge, continued interaction with the low fO_2, unmodified mantle (e.g. Wood et al., 1990) is likely to mean that the fluids become progressively more reducing, thereby reducing U mobility and making it increasingly hard to fractionate U and Th.

It is also possible that hydraulic fracture mechanisms are important as a means of producing U excesses (Davies and Rowland, 1997). Whilst these authors primarily discuss such a process as a means of getting fluids from the slab into the adjacent wedge, they do suggest that large fractures might penetrate into the centre the wedge and directly induce melting. This would remove difficulties in maintaining the oxidising nature of the fluid in the melting region. In addition, the U-Th data tend to support a mechanism whereby the last (or indeed only) subcrustal fractionation of U from Th occurred relatively shortly (i.e. on a scale of hundreds to thousands of years rather than tens of thousands of years) prior to melting, melt segregation and eruption.

The above discussion has centred on subcrustal processes as the origin of the U-Th disequilibria as it has not been possible to demonstrate significant modification of U-series systematics by assimilation processes. However brief consideration is given here

to the possible effects of assimilation within the known constraints. The fact that U-Th ages and eruption ages for the Lower Whangaehu and Waihianoa sequences are similar implies that at the time of eruption, these data would have plotted on a horizontal trend on an equiline diagram. Assuming an pseudo-isochron model with no forcing, the ($^{230}Th/^{232}Th$) ratio of this line is ~0.685, and as mentioned in Section 5.3.2.1, an average of the ($^{230}Th/^{232}Th$) ratios of where all of the pseudo-isochrons cross the equiline (except for the eruptions this century) is ~0.71. Given the constraints on this value, and on the ($^{230}Th/^{232}Th$) ratio of the assimilant, i.e. ~0.72 (see Section 5.3.1.3), it is possible to speculate on the effects of assimilation. The fact that at the time of eruption these samples would have plotted on a horizontal trend on an equiline diagram implies that the parental magmas had similar ($^{230}Th/^{232}Th$) ratios. Whilst the parental magma could represent an aged melt, and therefore the horizontal arrays just represent a fortuitous mixing relationship, the lack of correlation between U/Th ratios and indices of assimilation argue against this. Furthermore, constraints on the source composition which will be discussed in Chapter 6 tend to argue for a ($^{230}Th/^{232}Th$) ratio close to 0.7. It is argued therefore that any disturbance of the U-Th systematics by contamination processes in the older sequences must be relatively limited, and within the limits of analytical uncertainty, a relatively small effect.

The correlation between eruption ages and U-Th ages in the older sequences has allowed important constraints to be placed on both crustal and subcrustal processes. However the discrepancy between eruption ages and U-Th ages in the younger sequences (Figure 5.11) is equally striking and requires further discussion (the implications of the U-Th ages in terms of the evolution of the volcano are discussed in Section 5.3.3). A number of possible interpretations can be placed on these differences. They might reflect longer combined transit and residence times, mixing between an aged parental melt and crustal melts or a different U-Th composition of the parental magma, and these possibilities are discussed below.

The first of these possibilities is conceptually the simplest to address. The basic idea is that an initial horizontal trend with a similar ($^{230}Th/^{232}Th$) ratio as for the older

sequences is allowed to age to a much greater degree prior to eruption. In this case it becomes important once again to consider the effects of assimilation on the U-Th systematics. The discussion can best be illustrated using the eruptions this century because the ($^{230}Th/^{232}Th$) ratios at the time of eruption are unambiguous and in the range 0.75-0.78. These are somewhat higher than those estimated for partial melts of local basement (i.e. 0.72), and there is clear potential for modification of the U-Th ages as a result. It has been argued that the assimilant must have had a U/Th ratio very similar to that of the parental magmas, and therefore any variations due to assimilation are going to be largely vertical on an equiline diagram. This will tend to mean that if anything assimilation will make the U-Th ages underestimates and so such ages might in practice be regarded as minimum ages.

The second possibility suggests the arrays for the younger sequences essentially represent mixing arrays between an aged parental melt and partial melts of local basement. This has largely been discounted by the lack of correlation between U/Th ratio and indices of assimilation. The model does imply that either wedge transit times are greater than for the older sequences, and/or the parental magma was stored for a relatively long period of time without significant modification of U/Th ratios through assimilation, possibly at the base of the crust.

The third possibility is that these ages are overestimates because the ($^{230}Th/^{232}Th$) ratio of the source is somewhat higher. As is discussed in Chapter 6, it is relatively easy to produce a small shift in the ($^{230}Th/^{232}Th$) ratio of the mantle wedge, and it is therefore difficult to rule this possibility out. However, from Table 5.3 it is observed that the MSWDs obtained for models which force the pseudo-isochrons through a point in secular equilibrium with a ($^{230}Th/^{232}Th$) ratio of 0.72 are higher than for models which use a lower ($^{230}Th/^{232}Th$) composition to anchor the pseudo-isochrons. If the pseudo-isochrons for the parasitic vents and eruptions this century are anchored to a point on the equiline with a ($^{230}Th/^{232}Th$) ratio of 0.75, then ages of 32^{+130}_{-55} ka and 24^{+33}_{-23} ka are obtained respectively (with MSWDs of 3.7 and 3.9). The poor fit for these models tends to argue against a

significant shift in the ($^{230}Th/^{232}Th$) ratios of the mantle wedge producing the parental magmas.

In general, the first model discussed above seems to fit the observations best. This argues for much longer transfer and residence times probably of the order of 40-80 ka. This implies that there must be a difference in either magma transport mechanisms, and/or the timescales of magma storage. It may be that channelled flow became relatively less important in the mantle wedge, and without better models for the formation of such channels this is an issue that is difficult to address quantitatively. More likely perhaps, is that magmas have stalled at some point during ascent and have pooled for a period of time on a scale of thousands to tens of thousands of years. The fact that magmas from the younger sequences show few compositional differences from the older lavas implies that during this storage period relatively little crystallisation and assimilation occurred.

It is worth noting, however, that subtle differences are seen in certain trace element ratios. It was shown in Figure 5.9 that two distinct groups could be identified on the basis of Rb/Zr ratio, and it is now clear that the two groups correspond with the older and younger sequences discussed in this section. This is shown in Figure 5.12a where Rb/Zr is plotted against SiO_2, and as with $^{87}Sr/^{86}Sr$ and U/Th it is noted that differences in Rb/Zr ratios are not reflected in SiO_2. A similar pattern is also observed with Rb/Y ratio (Figure 5.12b), but it is clear from Figure 5.12c that in terms of SiO_2 and $^{87}Sr/^{86}Sr$ there is no discernible difference between the groups. There is also no split between the groups evident on similar plots using other incompatible trace element ratios such as Zr/Nb or Zr/Y. There has clearly been some slight difference in the differentiation history of the younger lavas which is only seen in a few trace element ratios, and most importantly, is *not* reflected in U/Th ratios.

This would tend to argue for the presence of areas of magma storage, probably at the base of the crust or perhaps in largely igneous lower crustal rocks. The local basement at depth may well be more refractory (see discussion of basement litholigies in Chapter 3) and therefore less likely to melt, which would limit assimilation, and the temperature of the surrounding rocks will be sufficiently high to slow down the rate of cooling and

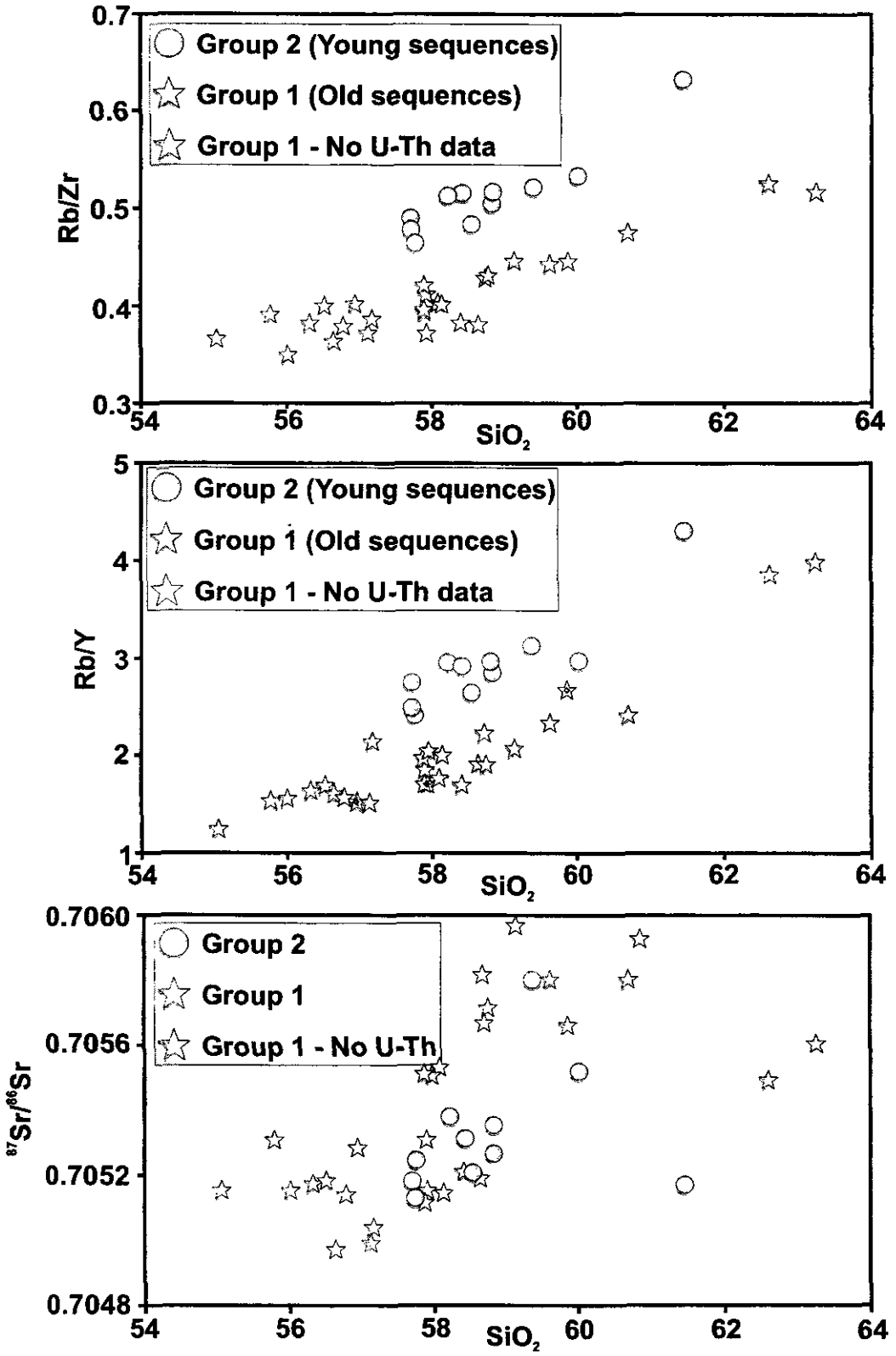

Figure 5.12:

(a) - Variation of Rb/Zr with SiO_2 showing the two distinct groups which can be identified by Rb/Zr (e.g. Figure 5.9). The samples from eruptions this century, parasitic vents and young valley filling flows plot in Group 2, whereas samples from the Upper and Lower Whangaehu, Ohinepango and Waihianoa sequences plot in Group 1.

(b) - Variation of Rb/Y with SiO_2. Samples divided into groups as in (a).

(c) - Variation of SiO_2 with $^{87}Sr/^{86}Sr$. Samples are divided into groups as in (a).

crystallisation of the magma. It may be during this period that the younger lavas picked up the distinct Rb/Zr and Rb/Y signatures, and it may also account for why Group 2 in Figure 5.12 tend to plot towards higher SiO_2. Following storage at depth, the magmas may have ascended to shallow levels where they underwent further crystallisation and assimilation of local basement, which may have reset the ($^{230}Th/^{232}Th$) ratios to an unknown degree.

5.3.4 Volcanological and Tectonic Implications of U-series Data from Ruapehu Lavas

The U-Th ages discussed in the preceding sections have a number of tectonic and volcanological implications which are discussed in this section. The data obtained from this study allow constraints to be placed on the past evolution of Ruapehu volcano.

As discussed in Chapter 3, four main stratigraphic formations have been identified on Ruapehu, although to date, the published chronology is extremely poor. The oldest Te Herenga Formation was not sampled in this study. Of the other formations, the Waihianoa Formation has been studied in the most detail, as the Waihianoa and Whangaehu sequences are thought to represent a section close to the main active vent during this cone building episode (Hackett and Houghton, 1989). The Waihianoa Formation had previously been inferred to be ~50-150 ka old (Graham and Hackett, 1987), but recent Ar-Ar determinations (J. Gamble, unpublished data) suggest that the Waihianoa Formation may represent a fairly short but intense pulse of magmatism at ~130 ka. This is also confirmed by the Ohinepango sequence from the northeastern flanks of the volcano, which gives a very similar age both by Ar-Ar and U-Th, and suggests that the cone building activity was widespread at least on the eastern side of the volcano.

It is difficult to constrain the age of the Mangawhero Formation from the data in this study, although several inferences can be made. On the basis of the U-Th evidence discussed in previous sections, a number of flows from the top of the Whangaehu sequence appear to be considerably younger, which is confirmed by a single relatively imprecise Ar-Ar date. This suggests that there is another pulse of magmatism at ~80 ka, but it isn't clear whether this is part of either the Mangawhero Formation or the Waihianoa

Formation, or whether this should be regarded as a separate stratigraphic unit. It is possible that sample X1-6 is part of the Mangawhero Formation on the basis of two Ar-Ar age determinations (see Table 5.4), but the U-Th isotopes of this sample and of another valley filling flow (W9-5) are similar to those for eruptions this century and are equivocal in terms of age.

The Whakapapa Formation has not been sampled as part of this study. Samples from two parasitic vents may be related to this event, and historic eruptions may also reflect the waning of this pulse of magmatism.

The picture which is gleaned from the U-Th and Ar-Ar ages is that much of the eastern side of the present edifice was built up in period of a few thousand years ~130 ka ago. From the U-Th ages it is inferred that the magma erupted at this time was transported rapidly from the zone of melt generation to the surface. A similar event appears to have occurred at ~80 ka, but in contrast recent lavas erupted within the past 25 ka show evidence for much longer transit and residence times. It is interesting to note that a recent K-Ar study of lavas from the Tongariro Volcanic Centre to the north of Ruapehu shows evidence for a major pulse of magmatism between 60-130 ka (Hobden et al., 1996).

It may be that the major and rapid pulse of magmatism seen on Ruapehu is linked to tectonic events, which might help to explain the rapid transfer times from the wedge to the surface. The TVZ is a region which is known to be actively extending (see Chapter 3), and this extension may have facilitated magmatism ~130 ka ago. There is some support for this from studies of the Pahoka-Mangamate tephras erupted ~10 ka ago, which occur across much of the ToVC and northern Ruapehu (Nairn et al., 1998; Nakagawa et al., 1998). These authors suggest that the tephras ascended extremely rapidly and postulated that they reflect a regional rifting event. It is argued here that a similar mechanism might help to explain the extremely short transit and residence times inferred from the U-Th data. This event may well have affected the ToVC as well given the evidence for a major pulse of magmatism beginning at around 130 ka. By contrast, the more recent eruptions appear to reflect a longer transit and residence time and therefore may indicate that regional extension in this part of the TVZ has diminished to some degree since ~80 ka ago.

5.4 Ra-Th Disequilibria

Little is known about the behaviour of ^{226}Ra-^{230}Th disequilibria in any igneous environment despite a growing body of data. Most of the available data from any tectonic setting shows variable ^{226}Ra excesses (Figure 5.13) (e.g. Capaldi et al., 1976; Bennett et al., 1982; Rubin et al., 1989; Gill and Williams, 1990; Volpe and Hammond, 1991; Cohen and O'Nions, 1993; Condomines et al., 1995; Sigmarsson, 1996; Black et al., 1998; Chabaux et al., 1999), although several studies have shown ^{230}Th excesses which have been related to fractional crystallisation of feldspar (e.g. Reagan et al., 1992; Volpe, 1992; Zellmer, 1998; Evans, 1999). In general, Figure 5.13 shows that there is considerably more variation in subduction zone magmas than in melts from other settings. There have been a number of ideas which have been put forward to explain ^{226}Ra excesses in the different tectonic settings. Numerical models have shown that ^{226}Ra excesses in MORB and OIB can be generated using dynamic melting models, although our knowledge of the physical constraints on these models is poor (Spiegelman and Elliott, 1993; Iwamori, 1994). In subduction zone settings there is more controversy over the origins of ^{226}Ra excesses. Geochemical constraints and comparisons with timescales derived from U-Th systematics suggest that the Ra-Th system must be decoupled from U-Th system, and that ^{226}Ra excesses are related to mantle melting (Elliott et al., 1997; Turner et al., 1997a). In contrast, a correlation between U excesses and ^{226}Ra excesses have been demonstrated in the Lesser Antilles arc, and it is inferred that this must result from a metasomatic event (Chabaux et al., 1999).

Most of the Ruapehu samples studied in this thesis are too old for any initial ^{226}Ra-^{230}Th disequilibria to remain (i.e. erupted > 8 ka ago). However, the historic eruptions this century have provided an opportunity to examine this decay scheme in conjunction with ^{230}Th-^{238}U disequilibria.

In Figure 5.14a, the data obtained from samples erupted this century are shown on a radium equiline diagram. Also shown are two determinations made on samples from the Ohinepango sequence to check if they plotted in secular equilibrium. Both of the older samples are very close to the equiline, and the slight apparent disequilibrium may reflect a

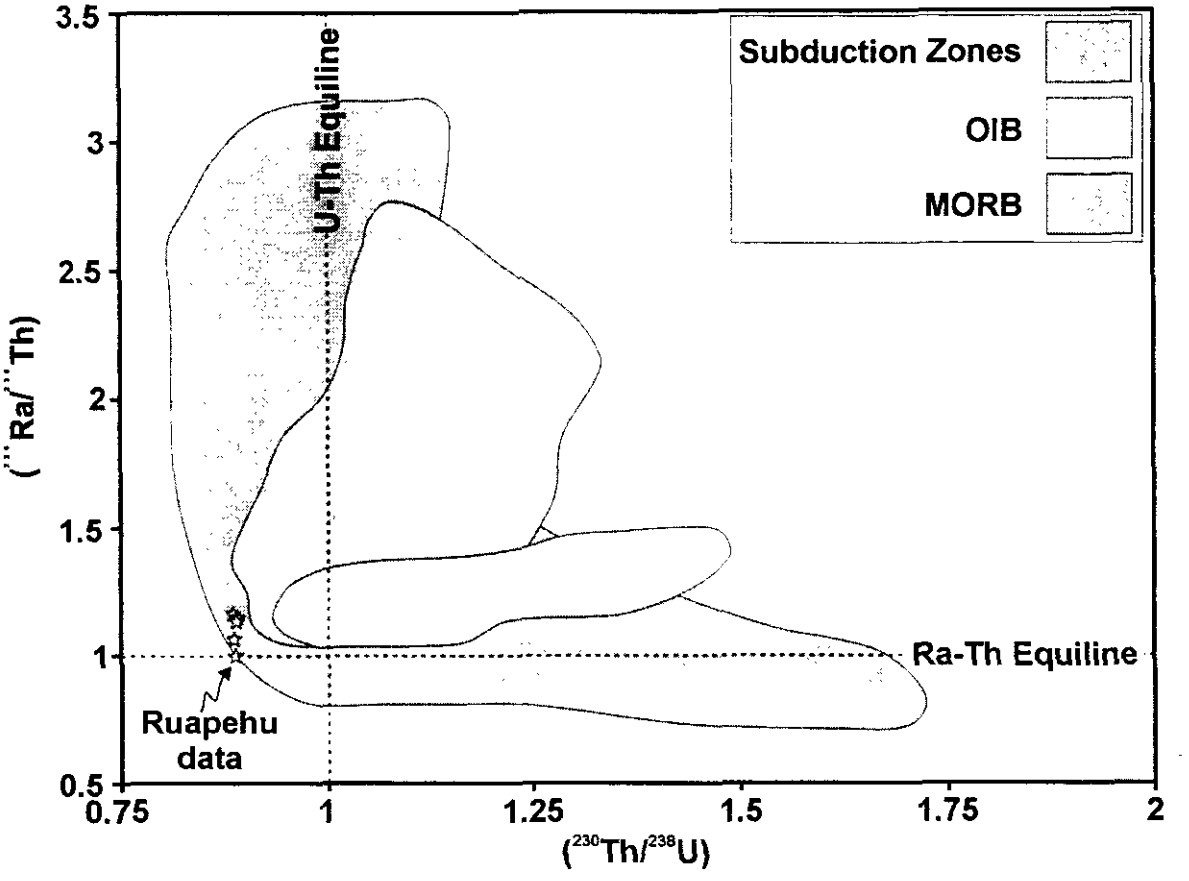

Figure 5.13: Global variation of Ra-Th and U-Th disequilibria. The data for subduction zones is taken from Rubin et al. (1989), Gill and Williams (1990), Volpe and Hammond (1991), Volpe (1992), Chabaux and Allègre (1994) and Clark et al. (1998). The data for OIB is taken from Cohen and O'Nions (1993), Chabaux and Allègre (1994) and Hemond et al. (1994). The data for MORB is taken from Rubin and Macdougall (1988). N.B. The field for subduction zones is extended to high Th excess by a single analysis from Chabaux and Allègre (1994), but for all other samples ($^{230}Th/^{238}U$) is < 1.25.

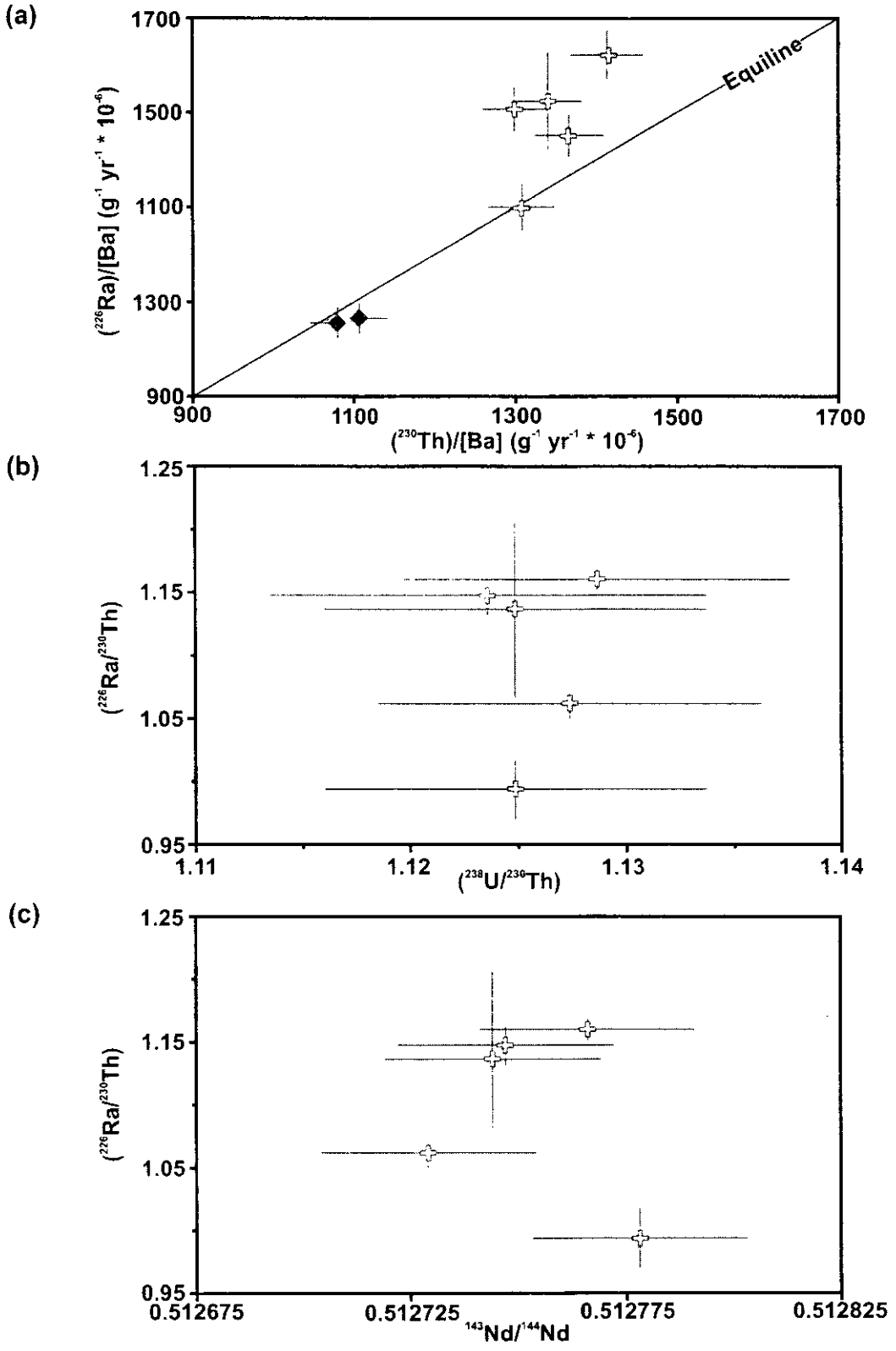

Figure 5.14:

(a) - Radium equiline diagram for samples erupted this century (crosses) and two old (> 8 ka) samples from the Ohinepango sequence (diamonds).

(b) - Variation of ^{226}Ra-^{230}Th and ^{238}U-^{230}Th disequilibria for samples erupted this century.

(c) - Variation of ^{226}Ra-^{230}Th with ^{143}Nd/^{144}Nd for samples erupted this century

problem with calibration of the Ra spike used during analysis. The discrepancy is small enough to not be a cause of great concern in terms of interpreting the data. The data for samples erupted this century show up to 15% radium excess with the exception of P57536 which is in secular equilibrium. Figure 5.14b shows that although there is a small range in ($^{226}Ra/^{230}Th$), the degree of ^{238}U-^{230}Th disequilibrium is invariant, which implies that the two systems are decoupled, which is discussed further below. It can be seen from Figure 5.14c that the $^{143}Nd/^{144}Nd$ ratios in the samples analysed is almost constant. As far as can be seen with the limited amount of data available, there is no clear relationship between Nd isotopes (or Sr isotopes) and ^{226}Ra-^{230}Th disequilibrium, so it is difficult to assess if assimilation is an important process.

One possible explanation for the ^{226}Ra excesses in young Ruapehu lavas is that Ra has been introduced by hydrous fluids at some stage in the recent past. As argued extensively in Section 5.3.1.1, there is little evidence in most samples for U mobility or alteration, and therefore it must be considered unlikely that such processes have affected Ra but not U. If the ^{226}Ra excesses reflect some kind of subcrustal process, then several possibilities must be considered.

As discussed above, a number of studies have suggested that ^{226}Ra excesses may reflect subcrustal processes. The extremely small variations of geochemical parameters in the recent eruptives from Ruapehu make it very difficult to directly assess whether ^{226}Ra excesses in these samples are produced by either melting or a metasomatic fractionation event. However, regardless of the exact model for the generation of ^{226}Ra excesses, if these are generated in the mantle in some way then it would imply that most of the 40-80 ka combined transit and residence time estimated for the eruptions this century must be taken up in processes which occurred *before* the ^{226}Ra excesses were imparted on the magma.

Alternatively, if the ^{226}Ra excesses can be generated during partial melting of local crust, the small disequilibria observed might just reflect assimilation. If Th is residual in accessory phases such as monazite during crustal melting, then generating ^{226}Ra excesses in this way is certainly conceivable. The lack of variation of other geochemical systematics makes it very difficult to chose between a crustal or subcrustal Ra-Th

fractionation. However, given that a subcrustal fractionation event would be difficult to reconcile with the U-Th age data, it seems more likely that the ^{226}Ra excesses reflect an assimilation process. Irrespective of the process producing ^{226}Ra excesses in recent Ruapehu magmas, the differences in timescales inferred from Ra-Th and U-Th systematics in historic samples contributes to the growing body of evidence that these systems are decoupled in many cases.

5.5 Summary

U-series analysis of samples from coherent rock sequences spanning ~150 ka, show systematic relationships which can be explained primarily in terms of variable transit and residence times. Despite the relatively evolved nature of the rocks and clear evidence for crustal assimilation, U/Th ratios do not correlate with indices of fractionation which is taken to indicate that the U/Th ratios of the parental basalts and partial melts of the local basement are very similar. It is therefore concluded that linear arrays observed for the coherent sequences are produced during fluid addition processes affecting the mantle wedge.

Comparisons of U-Th ages derived from whole rock pseudo-isochrons and Ar-Ar eruption ages show that samples from the Whangaehu, Waihianoa and Ohinepango sequences have very short transit and residence times, which it is argued may reflect regional tectonic processes ~130 ka ago. In contrast, younger sequences show U-Th ages significantly in excess of eruption ages. These are attributed to longer transit and residence times, and it is suggested that storage in deep magma bodies, possibly near the base of the crust may explain why the older and younger samples have very similar chemistry. A small number of ^{226}Ra-^{230}Th data for historical eruptions are equivocal, but it is argued that it is most likely that these reflect assimilation processes rather than a subcrustal fractionation event.

One reason for doing a PhD?,

Actvs id verberat

The motto of Guild of Thieves, Burglars and allied trade..

from 'The concife and possibly even accuratte Mapp' and 'Discworld Companion' – Terry Pratchett & Stephen Briggs.

Chapter 6

Regional Variations and Source Processes in the Taupo Volcanic Zone

6.1 Along- and Across-Arc Variations

Detailed studies of rock suites from individual volcanic centres are useful as a means to examine the crustal level differentiation processes. It is more difficult from such studies to investigate the composition of the mantle wedge and the variable components which might be added from the descending slab. Numerous studies have shown that examination of geochemical variations within the same arc or between arcs provides the most powerful tool for looking at subcrustal processes (e.g. Davidson, 1987; Ellam and Hawkesworth, 1988; Plank and Langmuir, 1988; Tatsumi et al., 1992; Edwards et al., 1993; Gill et al., 1993; Hawkesworth et al., 1993; Hawkesworth et al., 1994; Turner et al., 1996; Peate et al., 1997; Turner et al., 1997a; Ewart et al., 1998; Moriguti and Nakamura, 1998; Plank and Langmuir, 1998; Woodhead et al., 1998).

The location of New Zealand at the southern end of the intra-oceanic Tonga-Kermadec arc offers an excellent opportunity to look at the differences between mantle processes in intra-oceanic and continental arcs. This is further enhanced by the availability of recent detailed studies of these systems in the literature (Regelous et al., 1997; Turner and Hawkesworth, 1997; Turner et al., 1997a; Ewart et al., 1998). This section looks at variations between volcanic centres in New Zealand and compares geochemical data for New Zealand volcanoes with published data for the Tonga-Kermadec arc system. In addition to samples from Ruapehu, a number of lavas from Edgecumbe and

White Island (along-arc) and Taranaki (across-arc) have been analysed as part of this study, and these are compared with the more extensive Ruapehu database.

6.2 The Composition of the Mantle Wedge Beneath New Zealand

It has long been recognised that most arc lavas are depleted in HFSE (such as Nb, Ta, Zr, Hf) relative to LILE (e.g. Pearce, 1982). In addition, many primitive arc lavas also show depletion in HFSE and REE relative to MORB and basalts produced in associated back-arcs (BAB) (e.g. Ewart and Hawkesworth, 1987; Turner et al., 1997a; Woodhead et al., 1998). There have been a number of interpretations placed on these observations. It has been suggested that the depletion of HFSE is related to residual rutile or ilmenite at some stage during the melting process (e.g. Ryerson and Watson, 1987; Ionov and Hoffman, 1995). It has also been proposed that chromatographic effects in the upper mantle might produce HFSE depletions (Kelemen et al., 1993). Where primitive lavas are depleted in HFSE and a wide range of other trace elements relative to MORB it commonly thought that prior back-arc melt extraction may have depleted the mantle wedge (Ewart and Hawkesworth, 1987; McCulloch and Gamble, 1991; Woodhead et al., 1993).

Lavas from the Tonga-Kermadec arc system are highly depleted in the north, but become progressively less depleted relative to MORB to the south, and this correlates with a decrease in back-arc spreading rate (Turner et al., 1997a). These authors examined the degree of wedge depletion using major elements, by extrapolating data trends for individual volcanic suites to 8% MgO and comparing these values with estimates of fertile and depleted peridotite compositions. A simplified version of the diagram given by Turner et al. (1997) is shown in Figure 6.1, with extrapolations for Ruapehu and Taranaki lavas (there is insufficient available data to extrapolate trends for White Island and Edgecumbe).

The Tonga and Kermadec data from Turner et al. (1997) have been divided into three groups, in order to show clearly how the southern Kermadec lavas (Rumble seamounts) were derived from a relatively fertile mantle source, whereas the northern Kermadec (Raoul, Macauley, L'Esperance) and Tongan samples were derived from a

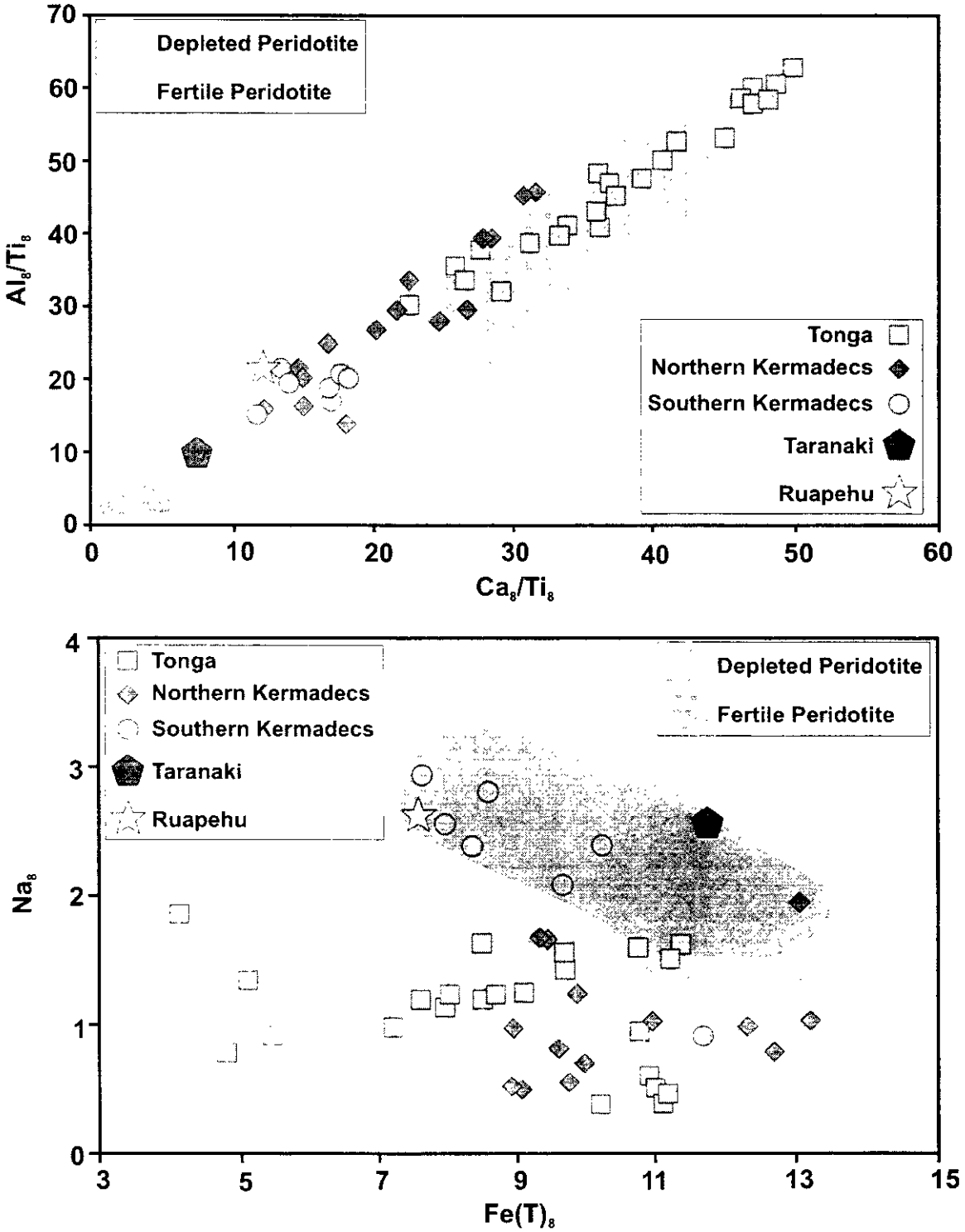

Figure 6.1: Major element diagrams with values for individual rocks suites extrapolated to 8% MgO (for rationale, see Klein & Langmuir, 1986; Plank & Langmuir, 1988), after Turner et al. (1997). All data is as given by Turner et al. (1997a) with the exception of the points for Ruapehu and Taranaki. The Ruapehu values were extrapolated from values obtained in this study and from Graham (1994). The Taranaki values were extrapolated from data given by Price et al. (1999). Only samples with MgO > 4% were used in the regressions. The fields for depleted and fertile peridotite are those given by Turner et al. (1997), which are derived from experimental melts by correction to 8% MgO (see reference for full details).

progressively more depleted source. Ruapehu plots with the southern Kermadec data in both diagrams shown in Figure 6.1, despite the southern Kermadec lavas being derived from an intra-oceanic setting, and similarly indicates that the primary magmas feeding this volcano are derived from a relatively fertile mantle wedge. Taranaki plots to even more fertile peridotite compositions than Ruapehu and the southern Kermadec samples on a plot Al_8/Ti_8 vs Ca_8/Ti_8, and it falls in the fertile peridotite field on a plot Na_8 vs $Fe(T)_8$, although to slightly higher $Fe(T)_8$ than most of the other data. The evidence that Taranaki was derived from a fertile mantle source is in contrast to previous interpretations which suggested that the source was relatively depleted on the basis of trace element data and mineral compositions (Stewart et al., 1996; Price et al., 1999). It may be that the extrapolations of major element trends to 8% MgO are erroneous for Taranaki, as the high MgO samples used in the correlations may include accumulations of ferromagnesian minerals (Stewart et al., 1996). It may also be a result of the smaller degree of melting thought to be responsible for producing the Taranaki lavas (Price et al., 1992; Stewart et al., 1996; Price et al., 1999), since this would have resulted in an increase of Ti in the melt relative to Al and Ca (e.g. Plank and Langmuir, 1988). However Na_8 should also be higher in a smaller melt fraction, although if the source was already depleted (i.e. lower Na_2O due to prior melt extraction), the effect of a smaller degree of melting might be to move Na_8 from the depleted peridotite field in Figure 6.1 into the field for fertile peridotite.

6.3 Along- and Across-Arc Sr, Nd and Pb Isotope Variations

Variations of Sr and Nd isotope ratios in New Zealand volcanics and Tonga-Kermadec samples are shown in Figure 6.2. The data for Taranaki, White Island and Edgecumbe essentially extend the observed broad trend for evolved New Zealand lavas. The White Island samples plot with the more primitive Ruapehu samples and data for the Ngatoro Ridge which forms part of the offshore TVZ (Gamble et al., 1993; Turner et al., 1997a), consistent with evidence from their MgO rich compositions that they had undergone relatively limited assimilation. The Edgcumbe samples have some of the highest $^{87}Sr/^{86}Sr$ and lowest $^{143}Nd/^{144}Nd$ ratios observed for basaltic to dacitic compositions from the TVZ, consistent with their evolved major element compositions and

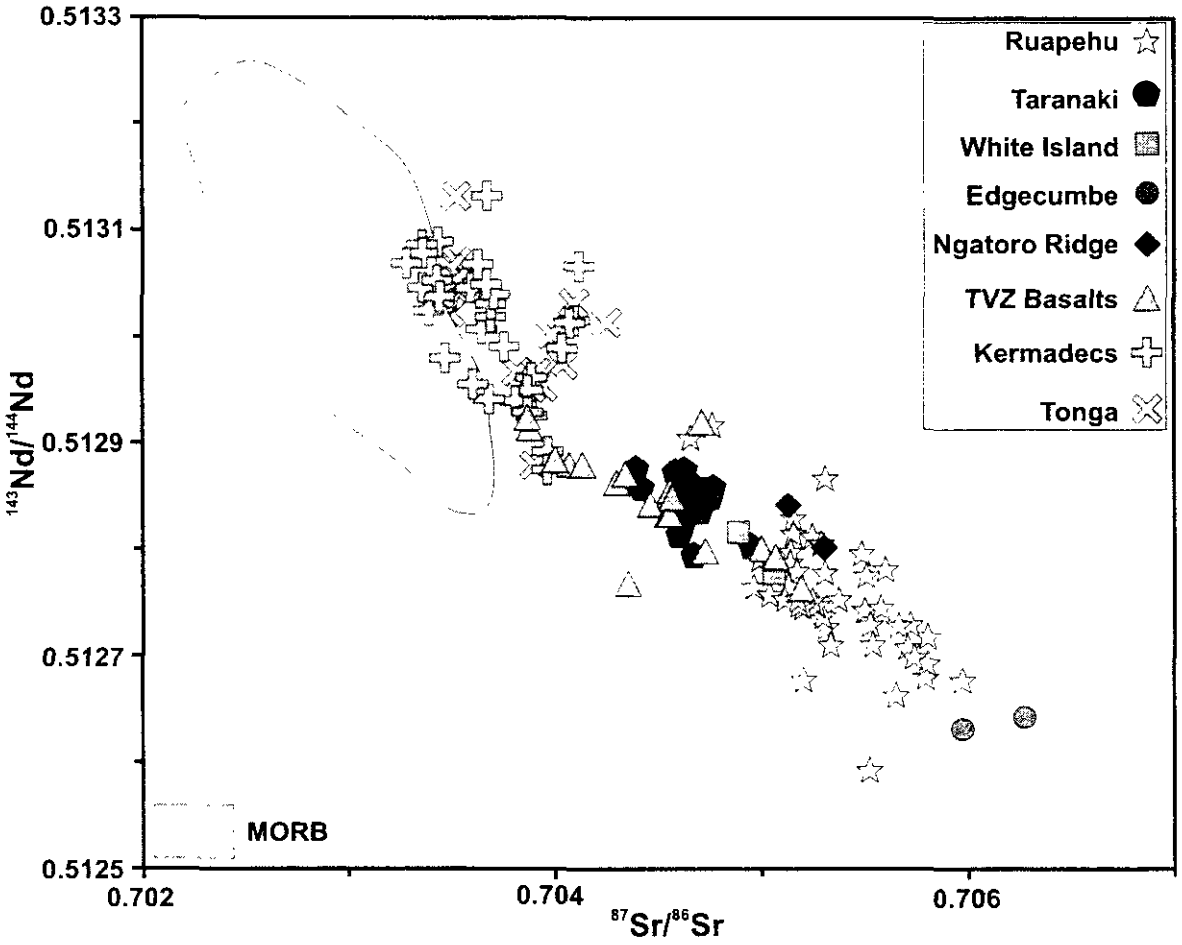

Figure 6.2: Regional variations in $^{87}Sr/^{86}Sr$ and $^{143}Nd/^{144}Nd$ for the New Zealand, Kermadec and Tonga arcs. Data for Ruapehu, White Island and Edgecumbe are from this study. Further Ruapehu data are from Graham (1994). Taranaki data from Price et al. (1992). Tonga and Kermadec data from Gamble et al. (1993, 1996), Regelous et al. (1997) and Turner et al. (1997). Ngatoro Ridge data is from Turner et al. (1997a) and other TVZ basalt data from Gamble et al. (1993, 1996). MORB data are from Dupré and Allègre (1983), Hamelin et al. (1984), Hamelin et al. (1996), Ito et al. (1987), Shirey et al. (1987), White et al. (1987).

indicative of a higher degree of assimilation compared to most of the Ruapehu lavas. Although the Taranaki samples are fairly evolved, they have relatively low $^{87}Sr/^{86}Sr$ and high $^{143}Nd/^{144}Nd$ ratios which have been interpreted in terms of relatively little assimilation of old crust (Price et al., 1999). Data for both Tonga and Kermadec lavas plot to lower $^{87}Sr/^{86}Sr$ and higher $^{143}Nd/^{144}Nd$ than almost all of the TVZ lavas. Although the samples from the Tonga and Kermadec arcs and the New Zealand volcanic centres form an essentially continuous array, the Tonga-Kermadec data show a greater range in $^{143}Nd/^{144}Nd$ at a given Sr isotopic composition. The Tonga-Kermadec data are largely thought to result from variations in sediment and fluid addition into the mantle wedge from the subducted slab (Gamble et al., 1996; Regelous et al., 1997; Turner et al., 1997a; Ewart et al., 1998).

Regional variations in Pb isotopes are shown in Figure 6.3. Data from all of the TVZ volcanic centres plot in a tight array extending from MORB compositions to higher $^{207}Pb/^{204}Pb$ and $^{208}Pb/^{204}Pb$ ratios. The single analysis made of a White Island lava plots at the unradiogenic end of the TVZ array consistent with its Sr and Nd isotopic composition. Data for the two Edgcumbe samples plot in the middle of the Ruapehu data, somewhat in contrast to their Sr and Nd isotopic compositions. Lavas from Taranaki have $^{207}Pb/^{204}Pb$ and $^{208}Pb/^{204}Pb$ ratios similar to samples from the TVZ, however, they plot at somewhat lower $^{206}Pb/^{204}Pb$ values. Pb isotopes from the Tonga and Kermadec arcs have a very much wider range of values. Tongan samples tend to have MORB-like $^{207}Pb/^{204}Pb$ and $^{208}Pb/^{204}Pb$ but some samples extend to very high $^{206}Pb/^{204}Pb$ which has been attributed to the influence of an unusual sedimentary component, possibly derived from the Louisville Ridge (Turner et al., 1997a). Data for the Kermadec samples have a much more restricted range of $^{206}Pb/^{204}Pb$, but extend to higher $^{207}Pb/^{204}Pb$ and $^{208}Pb/^{204}Pb$ similar to the values displayed by Taranaki and TVZ samples. This is thought to reflect an increasing sedimentary component in the source of the Kermadec lavas (e.g. Regelous et al., 1997; Turner et al., 1997a), and it has been shown that Pb isotope ratios increase to the south along the Kermadec arc (Gamble et al., 1996). Although the Kermadec samples reach $^{207}Pb/^{204}Pb$ and $^{208}Pb/^{204}Pb$ values which are as radiogenic as those observed in the TVZ, it is clearly very difficult to distinguish between some kind of sediment addition to the source

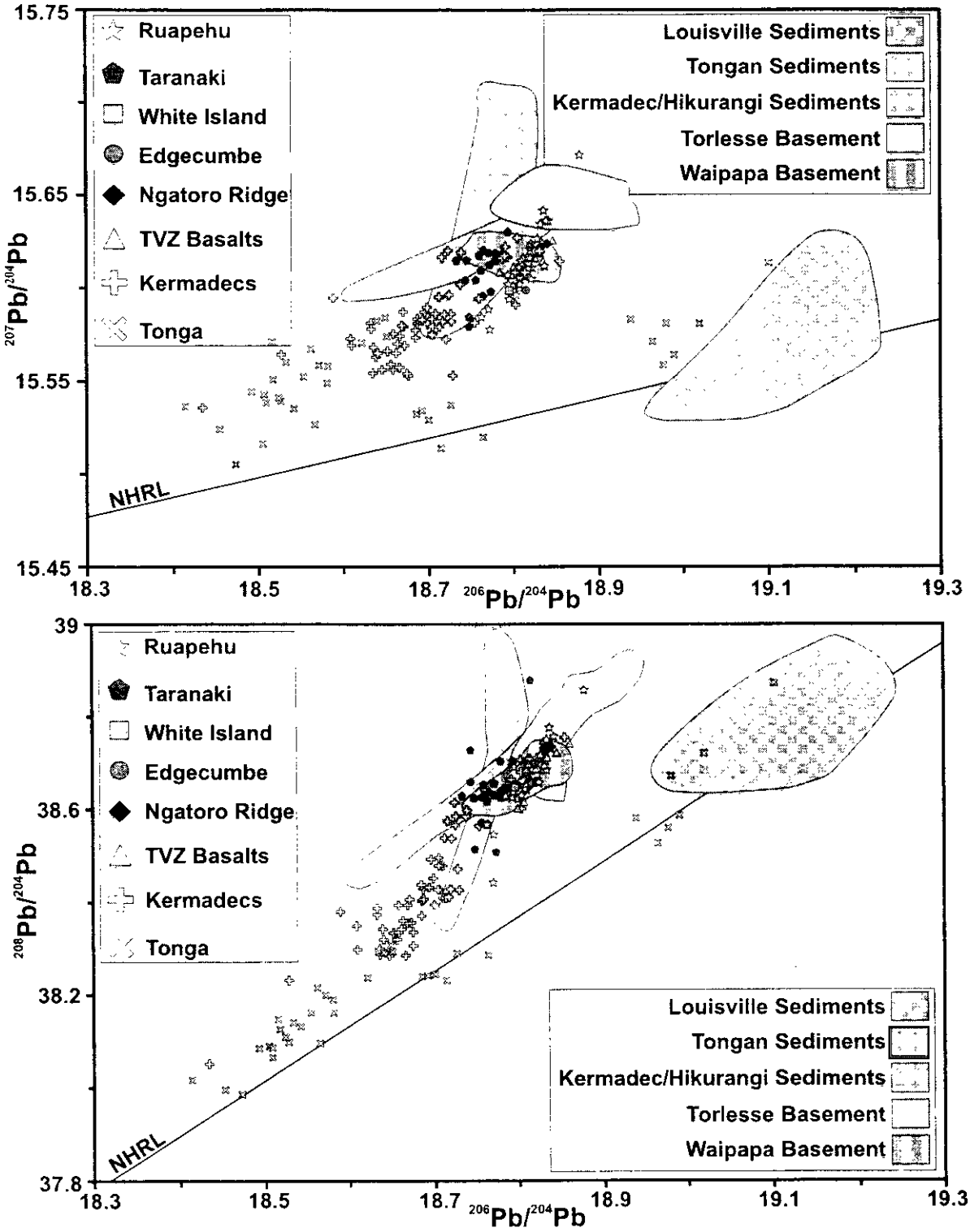

Figure 6.3: Regional variations of Pb isotope ratios along the New Zealand-Kermadec-Tonga arc system. Data for Ruapehu, Edgecumbe and White Island are from this study. Data for Taranaki is taken from Price et al. (1999). Data for TVZ basalts, some Kermadec lavas and Kermadec/Hikurangi sediments are from Gamble et al. (1993, 1996). Data for Tonga, Kermadec and Ngatoro Ridge lavas, Louisville Ridge derived and pelagic sediments are from Turner et al. (1997a). Remaining Tonga and Kermadec data are from Regelous et al. (1997). Fields for Torlesse and Waipapa basement are taken from analyses given by Graham et al. (1992). NHRL is plotted after Hart (1984).

and crustal assimilation in the New Zealand data given that sediments and continental crust have very similar Pb isotope ratios (Figure 6.3).

6.4 Trace Elements and Mass Balance

The use of trace elements in understanding the complex nature of magma generation in subduction zones is well established (e.g. Pearce, 1982; Hawkesworth et al., 1993; Pearce and Parkinson, 1993; Woodhead et al., 1993; Hawkesworth et al., 1994). However, it is difficult to apply the methods used by other studies to rocks which have been affected by crustal assimilation. The degree to which trace element systematics may have been disturbed in evolved rocks is difficult to assess and correct for in a meaningful way where crustal assimilation has occurred. In addition, the paucity of primitive, near-primary compositions makes it difficult to filter out assimilated rocks in order to examine trends which may be related to source processes such as have been identified in plots of Ce vs Yb (Hawkesworth et al., 1991a; Hawkesworth et al., 1991b).

In this section, an approach is adopted which follows a similar logic to that used by Turner et al. (1997) to model variable mantle and slab contributions in Tonga and Kermadec lavas. The principle logic of the model combines backwards and forwards modelling to try and derive a primary basalt composition, which can then be compared with models of melting in the mantle wedge. There are few samples which are primitive enough to try and apply this model to, and in this section, the discussion will centre around Ruapehu 'basalt' (Graham and Hackett, 1987; Gamble et al., 1993) and sample Wi008 from White Island analysed in this study.

6.4.1 Crystallisation Correction

In order to try and obtain primary trace element compositions for the two samples examined here, it is necessary to correct for the effects of fractional crystallisation. In both the samples it is acknowledged that trace element systematics may also have been disturbed to some degree by assimilation. To correct for assimilation in these samples would introduce increasing uncertainties to the model due to relatively poor constraints on the degree of assimilation and the composition of a partial melt of basement rock. It is

therefore more logical to ignore assimilation, but to regard the calculated subduction components as maximum values. This issue will be returned to subsequently after the subduction components have been estimated.

In order to correct for fractional crystallisation, stepwise addition of an estimated crystallising assemblage to the rock composition was performed until the Mg# reached a value of 71-73, in equilibrium with mantle olivine of Fo_{85}-Fo_{90}. The crystallising assemblage assumed was 55% olivine, 25% clinopyroxene, 10% plagioclase and 10% orthopyroxene. This was based on phase proportions given by Graham and Hackett (1987) for Ruapehu 'basalt' with the amount of plagioclase reduced to account for preferential retention of plagioclase in the liquid due to its low density. Reducing the amount of plagioclase in the assemblage has very little difference on the amount of crystallisation required to reach the desired Mg#. The mineral compositions used for the crystallisation correction were taken from typical electron microprobe analyses for Ruapehu 'basalt' phenocrysts given by Graham and Hackett (1987) and are given in Table 6.1 with the corrected and uncorrected liquid compositions.

	RB uncorrected	RB corrected	Wi008 uncorrected	Wi008 corrected	Ol	Cpx	Plag	Opx
SiO_2	52.23	51.63	56.07	55.80	40.90	51.14	50.67	53.21
TiO_2	0.66	0.59	0.593	0.570	-	0.45	-	0.81
Al_2O_3	15.57	13.79	13.18	12.65	0.06	3.67	29.87	1.82
FeO(T)	8.76	9.05	7.27	7.52	10.91	8.88	0.66	17.25
MnO	0.16	0.16	0.139	0.141	0.13	0.18	-	0.33
MgO	8.73	12.74	9.49	11.16	46.97	14.77	0.11	25.34
CaO	9.63	9.22	8.52	8.46	0.15	19.93	14.34	1.70
Na_2O	2.59	2.25	2.66	2.52	-	0.33	3.24	-
K_2O	0.58	0.49	1.17	1.10	-	-	0.09	-
P_2O_5	0.09	0.08	0.082	0.077	-	-	-	-
Mg#	64	71.5	70	72.5				

Table 6.1: Corrections to Ruapehu 'basalt' and Wi008 for fractional crystallisation. Ruapehu 'basalt' (RB) had 20% crystals added and Wi008 had 7.5% crystals added. These additions correspond to 16.7% and 7% fractional crystallisation respectively.

The amount of fractional crystallisation determined by correcting the major elements was then used to correct the trace element abundances. In order to do this relevant partition coefficients were required, and the compilation of Halliday et al. (1995) was used for olivine, clinopyroxene and orthopyroxene. Plagioclase partition coefficients were taken from Dunn and Sen (1994) (see Appendix E for a summary of the partition coefficients).

Bulk partition coefficients for the correction were derived using the phase proportions given above. The range of trace elements used is more limited than that employed by Turner et al. (1997) because of the limited data available for the two modelled samples. However the choice of trace elements includes the LILE and some of the HFSE of particular interest in terms of constraining the size and composition of slab-derived components. In addition Y and also Yb in the case of Ruapehu 'basalt' are included as these can help to constrain the degree of mantle melting as described subsequently. The effects of correcting for fractional crystallisation are shown in Table 6.2. The corrected trace element trends are shown in Figure 6.4 as the lines for primary magmas. The rest of Figure 6.4 will be explained in the subsequent text.

	$\overline{D}_{element}^{cryst/liq}$	RB uncorrected	RB corrected	Wi008 uncorrected	Wi008 corrected
Rb	0.0011	11	9	37.3	34.7
Ba	0.0401	185	155	426	397
Th	0.0155	1.09	0.91	3.127	2.912
U	0.0053	0.4	0.3	0.763	0.710
Nb	0.0034	1	1	2.8	2.6
La	0.0214	10.7	9.0	0.1	0.1
Pb	0.0222	3.5	2.9	2	2
Sr	0.1628	201	173	156	147
Nd	0.0519	8.2	6.9	0.1	0.1
Zr	0.0668	50	42	85	79
Sm	0.0704	1.95	1.65	0.1	0.1
Y	0.1245	17	14	18.8	17.6
Yb	0.1249	1.67	1.42	0.1	0.1

Table 6.2: Correction of trace element abundances for fractional crystallisation. Trace element data for Ruapehu 'basalt' (RB) is by XRF and INAA and is taken from Graham & Hackett (1987) and Gamble et al. (1993). Trace element data for Wi008 was determined by XRF in this study and is augmented by isotope dilution concentrations for U and Th.

6.4.2 Melting the Mantle Wedge

In order to constrain the subduction components, it is necessary to have a model for melting of the mantle wedge and the trace element concentrations resulting in the primary melt. In this respect, the approach taken here differs somewhat from that taken by Turner et al. (1997). Those authors preferred to constrain the amount of addition of sediment to the mantle wedge by examining Nd isotopes. In this study, the initial comparison is made by melting an amphibolitised mantle wedge with an essentially *normal*

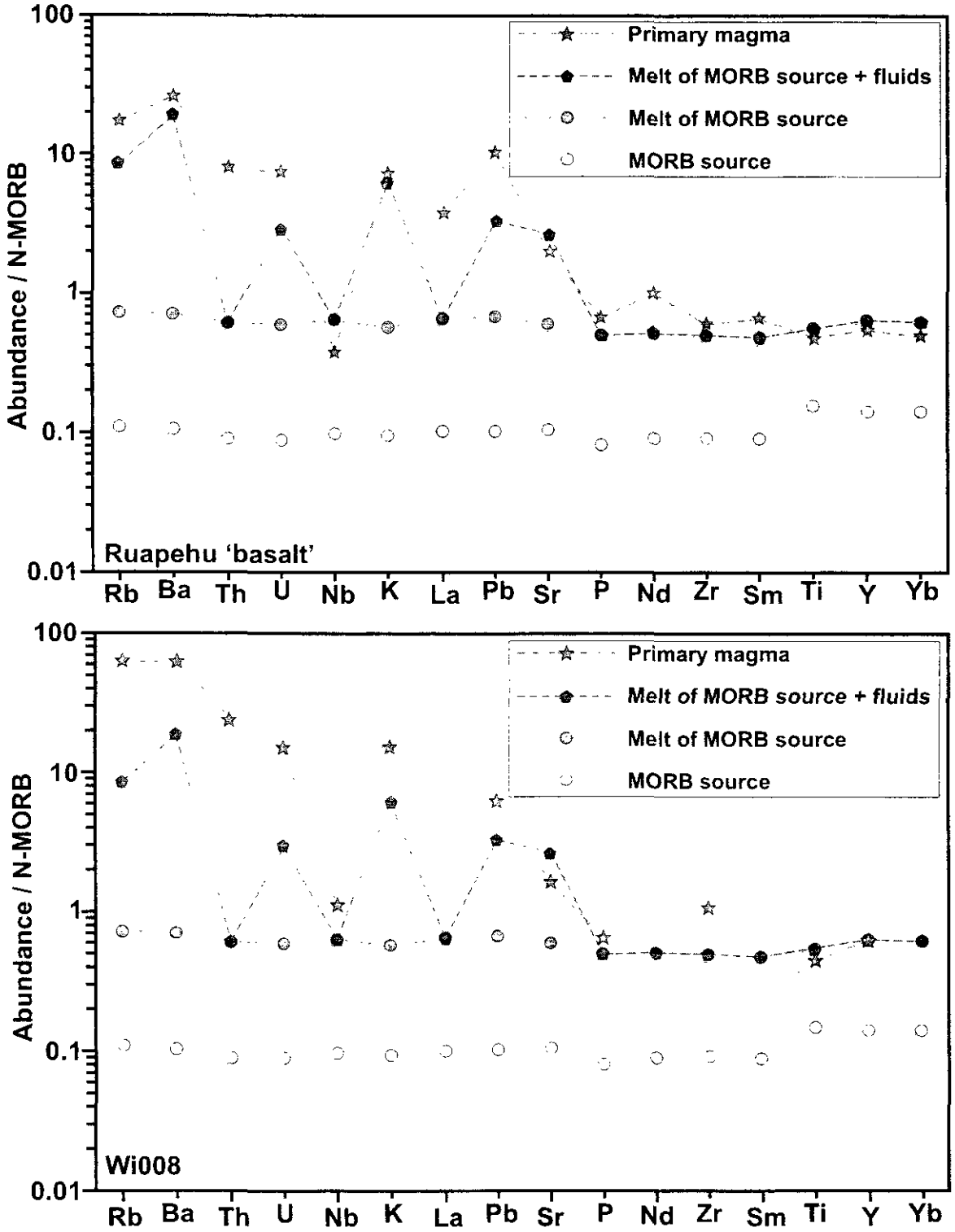

Figure 6.4: Mass balance models for the contributions of mantle wedge, slab derived fluids and sediments in primitive New Zealand basalts. The modelling largely follows the logic of Turner et al. (1997a), with certain differences which are explained in the text. The MORB source composition is taken from Stolper and Newman (1994) with extrapolations for Y and Yb from Turner et al. (1997a). The melting curves are for modal batch melting models of a mantle wedge comprising 44% olivine, 5% clinopyroxene, 41% orthopyroxene and 10% amphibole (after Turner et al. 1997a). The curves for the rock compositions have been corrected for crystal fractionation processes such that they are now in equilibrium with mantle compositions (see text for details).

trace element budget, because assimilation makes it difficult to assess sediment addition using Nd isotopes unless prior constraints are available.

It is now generally accepted that melting in the mantle wedge occurs in response to the addition of fluid provided by the breakdown of hydrous phases present in the descending slab (e.g. Tatsumi et al., 1986; Davies and Bickle, 1991). It is thought that these fluids essentially amphibolitise the mantle wedge through metasomatic reactions, and that it is this 'altered' mantle wedge which undergoes melting at some subsequent stage once the solidus for amphibole-rich mantle is crossed (e.g. Davies and Stevenson, 1992). The melting model here employs simple modal batch melting as a means of estimating the trace element abundances in the primary melts. In order to do this, a mineralogy has to be assumed and values modified from Turner et al. (1997) are used. The proportions chosen are 40% olivine, 35% orthopyroxene, 15% clinopyroxene and 10% amphibole, which reflect a somewhat more fertile source than used by Turner et al. (1997) in line with the evidence from major elements (Figure 6.1). The partition coefficients used for the melting model are those given in the compilation of Halliday et al. (1995).

The trace element composition of the mantle wedge prior to the addition of subduction components is taken to be the MORB source calculated from data for lavas from the Marianas arc (Stolper and Newman, 1994). The abundance of Yb in the pristine mantle wedge is taken from extrapolations made by Turner et al. (1997). Although an amphibolitised mantle wedge is used in the melting model, it is important to stress that the *initial trace element composition assumes no mass contribution from fluids*. The presence of amphibole simply changes the bulk partition coefficients used (It is noted, however, that if a more complex non-modal melting model were employed, then at 15% melting, both amphibole and clinopyroxene might be exhausted in the residue. This would be dependant on the chosen proportions the phases entering the melt). This means that the difference in trace element abundances between the calculated primary compositions (Section 5.4.3.1) and the estimated primitive magmas reflects the subduction component.

Although it is important to use a reasonable mantle mineralogy, the principle control on trace element abundances in wedge-derived melts is the degree of melting. For

this modelling, it is possible to constrain the degree of melting by examining Y and Yb concentrations. These elements are sensitive to the degree of melting, but in addition they are unlikely to be added to the mantle wedge in significant quantities in subduction components. Both Y and Yb are likely to be fluid immobile by comparison with Lu (e.g. Keppler, 1996) and the presence of relatively large amounts of garnet and amphibole in metamorphosed sediments (Nichols et al., 1994; Nichols et al., 1996), will mean that they are retained within the sediment during melting or dehydration. In both of the samples modelled, Y and Yb abundances are somewhat lower than MORB, implying a higher degree of melting consistent with general trace element constraints on arc magmatism (e.g. Pearce and Parkinson, 1993). It might be argued instead that the lower Y and Yb abundances reflect a depleted source, however the major element constraints of Figure 6.1 argue against this. Modelling of 15% batch melting shows that this reproduces the Y and Yb abundances in both Ruapehu 'basalt' and Wi008 reasonably well. This is illustrated in Figure 6.4 by the correspondence between Y and Yb in melts of the MORB source and the primary magma curves on MORB-normalised trace element variation diagrams. This degree of melting is the same as that determined by Turner et al. (1997) for Tonga-Kermadec lavas and implies a relative consistency in the melting process along the entire arc system despite the wedge being progressively more depleted to the north. The observation in turn can be taken to indicate that the degree of melting is driven by the fluid flux rather than lithosphere thickness, in contrast to the model of Plank and Langmuir (1988).

6.4.3 Fluid and Sediment Additions to the Mantle Wedge

It is clear from Figure 6.4 that although Ti, Y and Yb abundances in the estimated primary magma compositions are similar to those in a 15% melt of the MORB source, there are systematic differences amongst other elements. These differences have long been identified with arc magmas and it has been thought that they reflect so called 'subduction components' (e.g. Gill, 1981; Pearce, 1982; Tatsumi et al., 1986). Most of the elements apart from Ti, Y and Yb are enriched relative to the modelled melt curves with the exception of Nb and P. In this section, these enrichments are modelled in terms of addition

of a fluid component principally derived from the subducted oceanic crust, and a component derived from subducted sediments.

It is widely thought that hydrous fluids released from the descending slab promote melting in the mantle wedge. It is also likely that such fluids act as transport agents for fluid mobile elements (Tatsumi et al., 1986; Tatsumi, 1989). The principal elements which are thought to be fluid mobile are LILE, principally Cs, Rb, Ba, Sr and Pb, and this has been confirmed by experimental studies (Tatsumi et al., 1986; Brenan and Watson, 1991; Brenan et al., 1995; Keppler, 1996). With increasing interest in U-series data, the mobility of U and Th in subduction zone fluids have also been the subject of a number of investigations. These have shown that under oxidising conditions Th is essentially insoluble in slab derived fluids, whereas U can be somewhat mobile (Keppler and Wyllie, 1990; Brenan and Watson, 1991; Bailey and Ragnarsdottir, 1994; Brenan et al., 1994; Brenan et al., 1995; Keppler, 1996).

The mass balance modelling for Tonga and Kermadec samples (Turner et al., 1997a) has shown that the fluid contribution appears to be relatively constant along the arc. For an initial approximation, an average of the calculated fluid additions for the Tonga-Kermadec arc have been added to the MORB source composition to derive a fluid-modified mantle melt. The average fluid is given in Table 6.3.

	Fluid contribution ($\mu g\ g^{-1}$)
Rb	0.66
Ba	17
U	0.017
K	0.067
Pb	0.12
Sr	33.3

Table 6.3: Average fluid contribution to the mantle wedge from Turner et al. (1997).

Most of the elements which are enriched in the calculated primary magmas over melts of unmodified wedge melts, are still enriched relative to the melts produced from wedge which has undergone fluid infiltration, which implies another component is also required. The exceptions to this are Sr, which in both examples shown in Figure 6.4 is actually higher in the melt of the fluid modified wedge, and also K in the case of Ruapehu 'basalt' which is very similar to the modified wedge melt. Even if the Sr contribution from

the fluid is halved, the melts derived from the fluid modified wedge still have almost the same Sr abundance as both the calculated primary magmas.

If the assumptions regarding the composition of the fluid are reasonable, then there is still a considerable component to take account of. It has long been argued that subducted sediments can play an important role in determining the trace element and isotopic compositions of arc lavas (Armstrong, 1971; Kay, 1980; Hole et al., 1984). In recent studies, it has become clear that a single component hosted by a hydrous fluid is insufficient to explain all of the apparent subduction component observed in arc lavas (e.g. Ellam and Hawkesworth, 1988; Morris et al., 1990; Elliott et al., 1997; Kepezhinskas et al., 1997; Plank and Langmuir, 1998).

In order to derive the contribution added from subducted sediments, an amount of each element was added to the source composition until the modified wedge melt matched the calculated primary melt as far as possible. These contributions are tabulated in Table 6.4.

	Sediment addition ($\mu g\ g^{-1}$)		% of source from sediments		% of source from fluids		% of source from all components	
	RB	**Wi008**	**RB**	**Wi008**	**RB**	**Wi008**	**RB**	**Wi008**
Rb	0.7	4.5	49	86	47	13	96	99
Ba	7	40	28	69	69	29	97	99
Th	0.13	0.43	92	98	-	-	92	98
U	0.033	0.085	61	80	31	16	92	96
Nb	-	0.185	-	44	-	-	-	44
K	83	913	12	59	80	37	92	96
La	1.3	1.3	83	83	-	-	83	83
Pb	0.35	0.35	70	70	24	24	94	94
Sr	-	-	-	-	78	78	78	78
P	13	13	23	23	-	-	23	23
Nd	0.6	0.6	47	47	-	-	47	47
Zr	1	8	13	54	-	-	13	54
Sm	0.09	0.09	27	27	-	-	27	27
Ti	-	-	-	-	-	-	-	-
Y	-	-	-	-	-	-	-	-
Yb	-	-	-	-	-	-	-	-

Table 6.4: Estimated sediment contributions for Ruapehu 'basalt' (RB) and Wi008 and *percentage contributions from sediments and fluids to the total source composition.*

It is clear that even given the fact that these estimates are maximum values as crustal assimilation was not taken into account in this modelling, the budget of many elements is dominated by fluid and/or sediment components. As mentioned previously, no

attempt has been made to adjust the composition of primitive lavas to compensate for the effects of crustal assimilation. The sediment contributions must therefore be regarded as maximum, although it is important to note that a small assimilation component will be equivalent to a very much smaller change in the source component. For the models used here, a 10 $\mu g\ g^{-1}$ assimilant component for an incompatible element would be equivalent to an addition ~1.3 $\mu g\ g^{-1}$ to the source composition.

6.4.4 The Nature and Origin of Fluid and Sedimentary Components

On the basis of the data available in this study it is not possible to resolve the problem of the origin of the hydrous fluids, and whether they reflect dehydration of altered oceanic crust or subducted sediments. On the basis of other studies where samples are sufficiently primitive to retain definitive trace element and isotope ratios reflecting the source, it has been argued that the fluid component was derived from altered oceanic crust (e.g. Miller et al., 1994; Elliott et al., 1997; Hawkesworth et al., 1997a; Turner et al., 1997a).

The nature of the sediment addition is more readily addressed using data from this study. A number of points from the mass balance modelling can be used to examine whether the sediment is added as a partial melt or as some kind of bulk incorporation. Firstly, Y and Yb abundances match well with those estimated for typical degrees of melting in arc magmas, and require that there has been essentially no input of these elements from either a fluid or a sedimentary source. Bulk sediment addition would tend to increase these abundances and thereby drastically reduce the calculated degree of melting. Secondly, even if the assumptions regarding the amount of Sr in the fluid contribution were wildly wrong, bulk sediment addition would still create a large excess of Sr in the modelled melt relative to the calculated primary magmas. Finally, the fact that Nb in the calculated primary composition of Ruapehu 'basalt' falls below the modelled melt, and just above in the case of Wi008, implies that this element does not enter in the sediment contribution. Whilst the origin of HFSE depletions, particularly those seen with Nb and Ta are controversial as mentioned previously, and beyond the scope of this work to address in detail, it is clear from the mass balance modelling presented here that the sediment

contribution contains almost no Nb. This argues for residual titanite phases in the sediment during melting, but does not require complex interactions with the mantle (e.g. Kelemen et al., 1993) and is consistent with observations from the Tonga-Kermadec arc system (Turner et al., 1997a).

From the above arguments it is possible to make some considerations of the residual mineralogy during sediment melting. Very little is known about either the residual mineralogy or the partitioning behaviour of trace elements during sediment melting (Plank and Johnson, 1997). Recently, several studies have begun to make exploratory investigations into the subject, and these tend to indicate that at ~30 kbar, a variety of minerals may be present, such as clinopyroxene, garnet, amphibole, muscovite and biotite as well as a range of minor phases (Plank and Langmuir, 1992; Nichols et al., 1994; Nichols et al., 1996; Plank and Johnson, 1997).

As discussed above, the modelling presented here suggests that the abundance of Sr in a partial melt of sediment must be relatively low. Given the high Sr abundances of most sediments (e.g. Plank and Langmuir, 1998), this implies that plagioclase must be a residual phase during partial melting of the sediment. There is very limited information on the phase relationships of sediments at high pressures, but the implication from the studies of Nichols (1994, 1996) is that plagioclase disappears above ~15 kbar pressure, and that to cross the solidus at these depths requires temperatures of the order of 650°C. It is noted that the limited experiments of Nichols (1994, 1996) on red clay do not show evidence for coexisting garnet and plagioclase, whereas the arguments regarding Y and Yb abundances required these elements to be retained in the residue by garnet. This apparent contradiction may reflect the choice of sediment composition used in the experiments (Nichols et al., 1994; Nichols et al., 1996), or poor constraints on the partitioning behaviour of Y, Yb and/or Sr. Thermal models of subducting slabs suggest that for oceanic lithosphere ~50 Ma old (a reasonable proxy for the Cretaceous crust subducted along the Hikurangi margin) suggest that the temperature of the subducting plate is ~450-500°C (Peacock, 1991). It is argued here however, that the shallow angle of subduction and relatively slow convergence rates along the Hikurangi margin allow a longer time for thermal equilibration. The higher

temperatures than expected at shallow levels permit partial melting of sediment in the presence of residual plagioclase.

6.5 Sr and Nd Isotope Constraints on Sediment Addition

It is possible to use the estimated sedimentary contributions (Table 6.4) and constraints on residual mineralogy to constrain the effects of sediment addition on Sr and Nd isotope systematics. To do this, a modal batch melt of sediments was modelled assuming a relatively simplistic mineralogy of 10% biotite, 35% plagioclase, 30% garnet and 25% amphibole, and the partition coefficients listed in Table 6.5. Because Sr was compatible and Nd was only slightly incompatible in the bulk assemblage ($\overline{D}_{Sr}^{cryst/liq}=3.65$ and $\overline{D}_{Nd}^{cryst/liq}=0.55$), the degrees of melting modelled (1-10%) made very little difference to the concentrations of these elements in the melt. The model illustrated in Figure 6.5 was produced assuming 10% melting of a sediment made from a 50:50 mixture of GLOSS (Plank and Langmuir, 1998) and averages of crustal rocks from South Island (Palmer et al., 1995) which had concentrations of Sr ~300 $\mu g\ g^{-1}$, and Nd ~30 $\mu g\ g^{-1}$. The reason for this choice is that whilst GLOSS represents typical subducted sediments (including a pelagic and biogenic component), the sediments in the Hikurangi Trough are thought to comprise a large amount of continental sediment derived from South Island and carried in deep water channels and currents into the subduction zone (Lewis, 1994; Carter et al., 1996; Gamble et al., 1996).

	D_{Sr}	D_{Nd}	Ref. (Sr, Nd)
plagioclase	10	0.2	1, 2
amphibole	0.5	0.6	1, 3
garnet	0.02	0.4	4, 4
biotite	0.25	2	1, 5
$\overline{D}_{elem}^{cryst/liq}$	3.65	0.55	

Table 6.5: Parition coefficients for Sr and Nd used to model partial melting of sediments. The range of partition coefficients available in the literature, particularly for silicic compositions is considerable. To this end, partition coefficients were used which produced reasonable concentrations of Sr and Nd in the melt, although it is acknowledged that partitioning of these elements in such environments is very poorly understood. The references are: (1) Ewart and Griffin (1994), (2) Bacon and Druitt (1988), (3) Brenan (1995), (4) Sisson and Bacon (1992) and (5) Nash and Crecraft (1985).

Figure 6.5 shows a partial melt of the sediment mixing directly with a MORB source unmodified by fluids. It has been suggested that in the Tonga-Kermadec arc system, sediments must enter the wedge at a shallow level and be carried down into the region where hydrous fluids flux the wedge (Turner et al., 1997a). A similar hypothesis has been put forward to explain features of the U-series disequilibria observed in the Mariana arc (Elliott et al., 1997). These authors also acknowledge, however, that their data could be explained by a model whereby sediments do not enter the wedge until much deeper levels and migrate back into the zone of melting. On the basis that residual plagioclase appears to be required during sediment melting, it is suggested that the resulting liquids must enter the wedge at a shallow level. The sediment modified mantle is then carried down by induced convection to a region where it is fluxed by hydrous fluids.

The curve for addition of sediment melt to an unmodified MORB source shown in Figure 6.5 passes to the left and beneath the data fields for the Tonga-Kermadec data and TVZ lavas. If the sediment-enriched mantle was fluxed by hydrous fluids containing Sr, but essentially no Nd as it is fluid immobile, horizontal shifts would result. The mixing trends illustrated assume that the fluid end-member was derived solely from altered oceanic crust, and uses the $^{87}Sr/^{86}Sr$ composition for the slab-derived fluid given by Turner et al. (1997). It is demonstrated in Figure 6.5 that as discussed by Turner et al. (1997) the Sr-Nd isotope ratios in the Tonga-Kermadec arc system can be explained by mixing with < 0.5% sediment melt followed by a hydrous fluid derived primarily from altered oceanic crust. The schematic AFC curves show that it the observed data can be derived from a sediment and fluid modified mantle wedge with ~0.25-0.5% sediment addition, although it is possible to produce reasonable AFC trends with up to 1% sediment addition. Sediment additions of the order of 0.25%-1% (depending on the model parameters used for sediment melting) reproduce the Nd concentration required from Table 6.4. In general the trace element concentrations of primitive New Zealand basalts are the same as or higher than in lavas from the southern Kermadec arc (Rumble seamounts), which suggests there should be at least 0.5% sediment addition (Turner et al., 1997a).

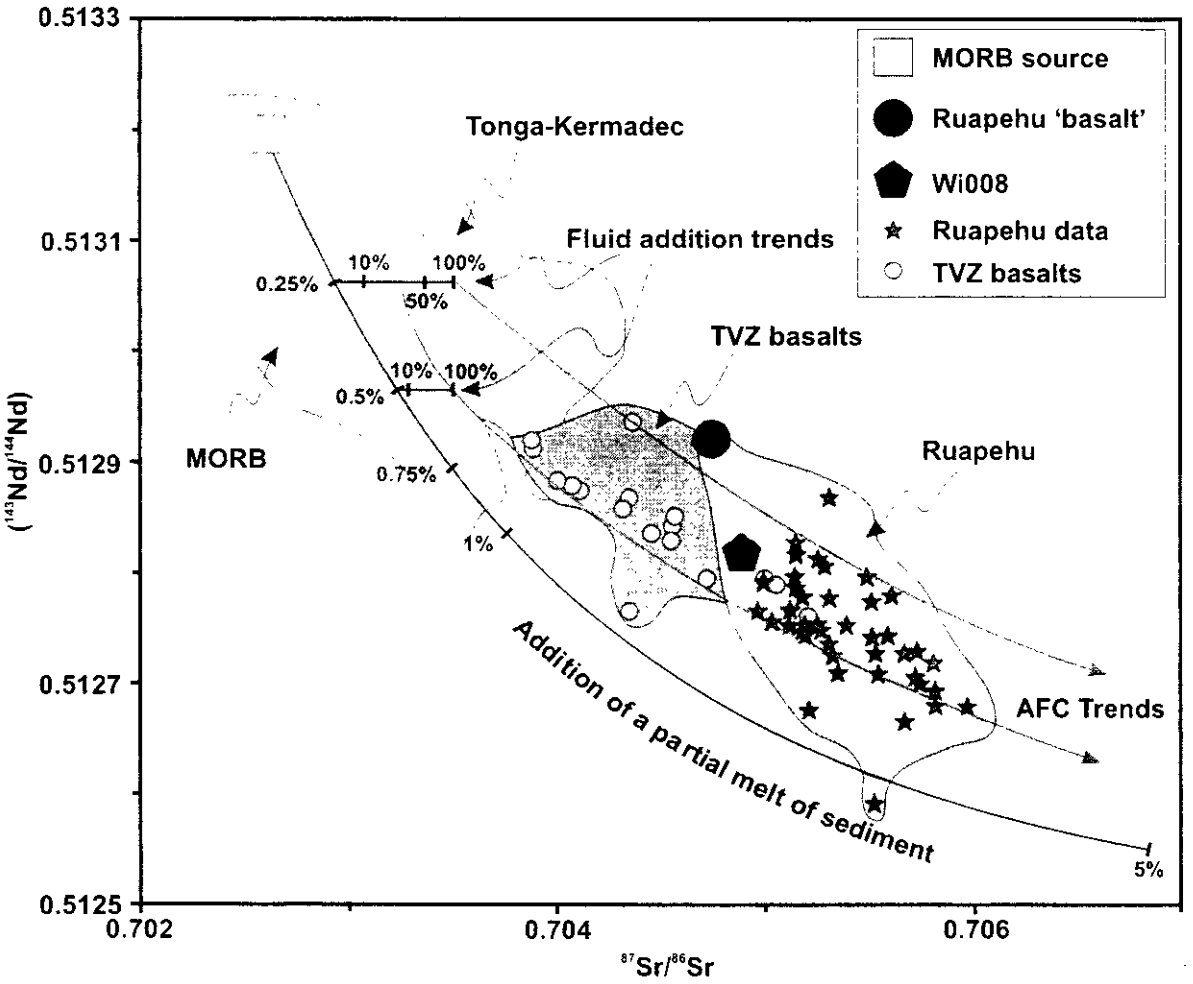

Figure 6.5: Plot of Sr isotopes vs Nd isotopes for New Zealand and Tonga-Kermadec data showing the effects of variable sediment and fluid influences on the composition of primary basalts. The two samples used in mass balance modelling (see Figure 6.4) are shown separately. The model shown here illustrates the effects of adding a partial melt of sediment to a mantle wedge with a composition similar to that of the MORB source derived by Stolper and Newman (1994). The sediment composition is based on GLOSS (Plank and Langmuir, 1998), analyses of sediments from the Hikurangi and Kermadec subduction zones (Gamble et al., 1996) and Torlesse basement (Graham et al., 1992) - see the text for full details. The sediment modified wedge composition is then mixed with a fluid derived primarily from subducted oceanic crust. See the text for a full discussion of the logic behind this model. Schematic AFC trends similar to those modelled quantitatively in Chapter 4 are shown for reference. Data for MORB is from Dupré and Allègre (1983), Hamelin et al. (1984), Hamelin et al. (1986), Ito et al. (1987), Shirey et al. (1987), White et al. (1987). Data for Tonga-Kermadec lavas is from Turner et al. (1997a) and Regelous et al. (1997). TVZ basalt compositions are taken from Gamble et al. (1993, 1996). Ruapehu 'basalt' is from Gamble et al. (1993) and the composition of Wi008 is from this study.

6.6 Regional U-Th-Ra Systematics and Source Processes

6.6.1 U-Th Systematics in New Zealand Lavas

Regional variations in U-Th systematics are shown in Figure 6.6. It can be seen from Figure 6.6a that data for New Zealand tends to form a continuation of the general trend for Tonga-Kermadec data but to lower ($^{238}U/^{232}Th$) and ($^{230}Th/^{232}Th$) compositions. These variations are not thought to be controlled by assimilation processes, as in Chapter 5 it was demonstrated that U/Th ratio did not vary with assimilation indices such as $^{143}Nd/^{144}Nd$ or SiO_2. In contrast, most of the variation of $^{143}Nd/^{143}Nd$ in the samples analysed from this study (see Figure 6.5) is thought to be due to crustal assimilation, and Nd isotopes do vary with SiO_2. Most of the samples show small degrees of U excess or are in isotope equilibrium. A number of samples from Taranaki show small degrees of Th excess, and one sample from the Ngatoro Ridge plots with greater ^{230}Th excess and to higher ($^{230}Th/^{232}Th$) (data from Turner et al., 1997a). Although fewer data are available, it appears that the samples from the Ngatoro Ridge and Taranaki have similar U/Th ratios to Ruapehu lavas, whereas the data for Edgecumbe and White Island have somewhat lower U/Th ratios.

6.6.2 Sediment, Fluid and Wedge Depletion Influences on the Regional U-Th Systematics

Using the models developed in Sections 6.4 and 6.5 it is possible to examine the effects of sediment and fluid addition to the mantle wedge on U-Th systematics. Modelling the effects of sediment melting on U and Th concentrations is even more difficult than for Sr and Nd due to the lack of constraints on partitioning behaviour and degree of melting. Given the presence of various accessory phases at high pressures, and the possibility of very small degrees of melting, it is possible, indeed it might be regarded as highly likely, that U and Th will fractionate during sediment melting (e.g. Elliott et al., 1997). For the simple model presented in Figure 6.7a, however, the sediment is assumed to be in equilibrium. Given that it is thought that the sediment-modified wedge is thought to have

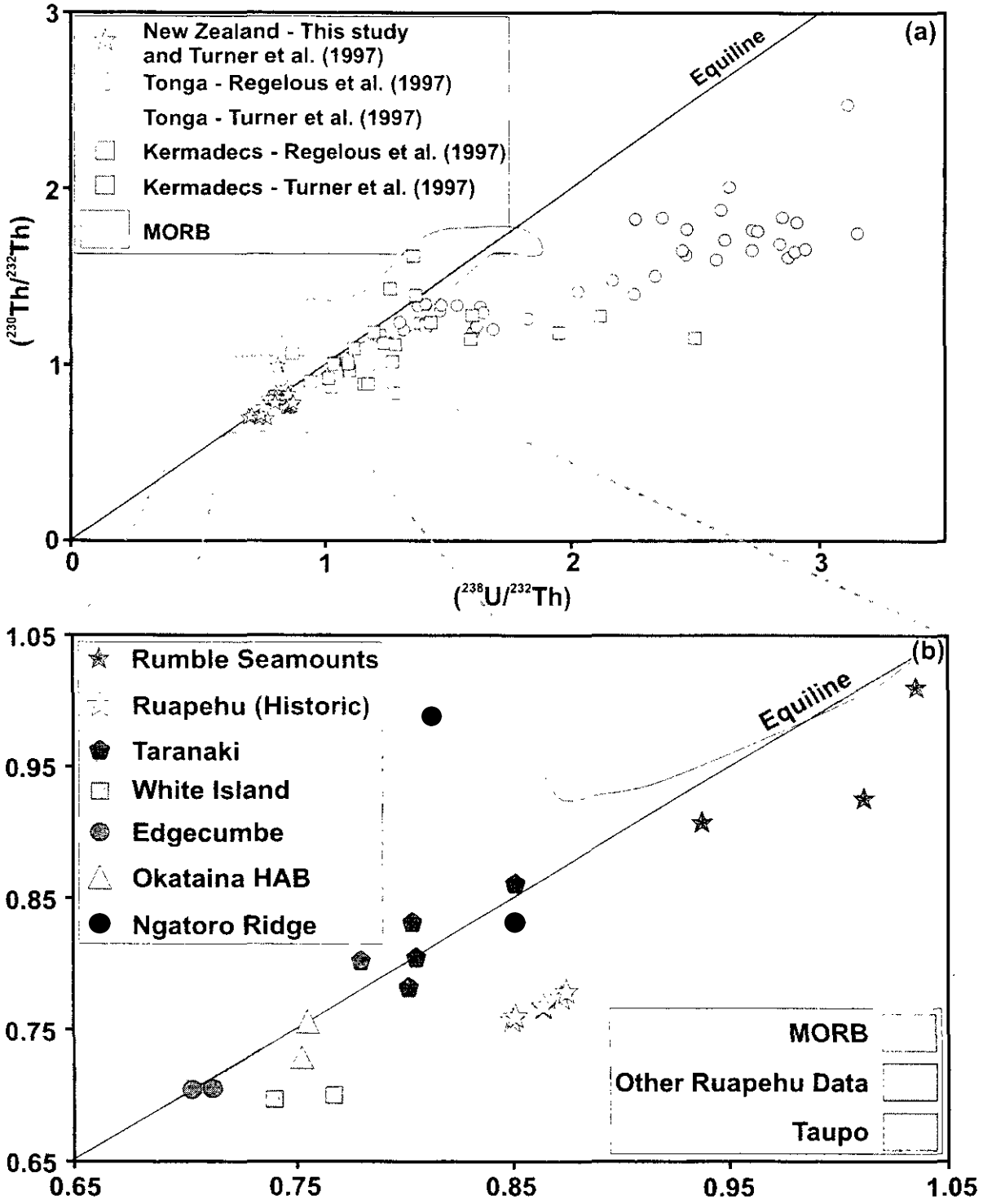

Figure 6.6: Equiline diagram showing the regional variation in U-Th systematics in New Zealand volcanics, and in lavas from the Tonga and Kermadec arcs. Data for the Tonga and Kermadec arcs are from Turner et al. (1997a) and Regelous et al. (1997). All New Zealand data are from this study with the exception of the Ngatoro Ridge samples which are from Turner et al. (1997a), and the field for Taupo data (B. Charlier, unpublished data). The Okataina HAB are repeat analyses in agreement with previous determinations made by D. Peate (unpublished data). The Rumble seamount data is shown in the bottom diagram for reference and forms part of the database of Turner et al. (1997a). The field for MORB is compiled from data given by Rubin and MacDougall (1988), Goldstein et al. (1989), Ben Othman and Allègre (1990), Goldstein et al. (1992), Goldstein et al. (1993), Sims et al. (1995), Bourdon et al. (1996a, 1996b) and Lundstrom et al. (1998).

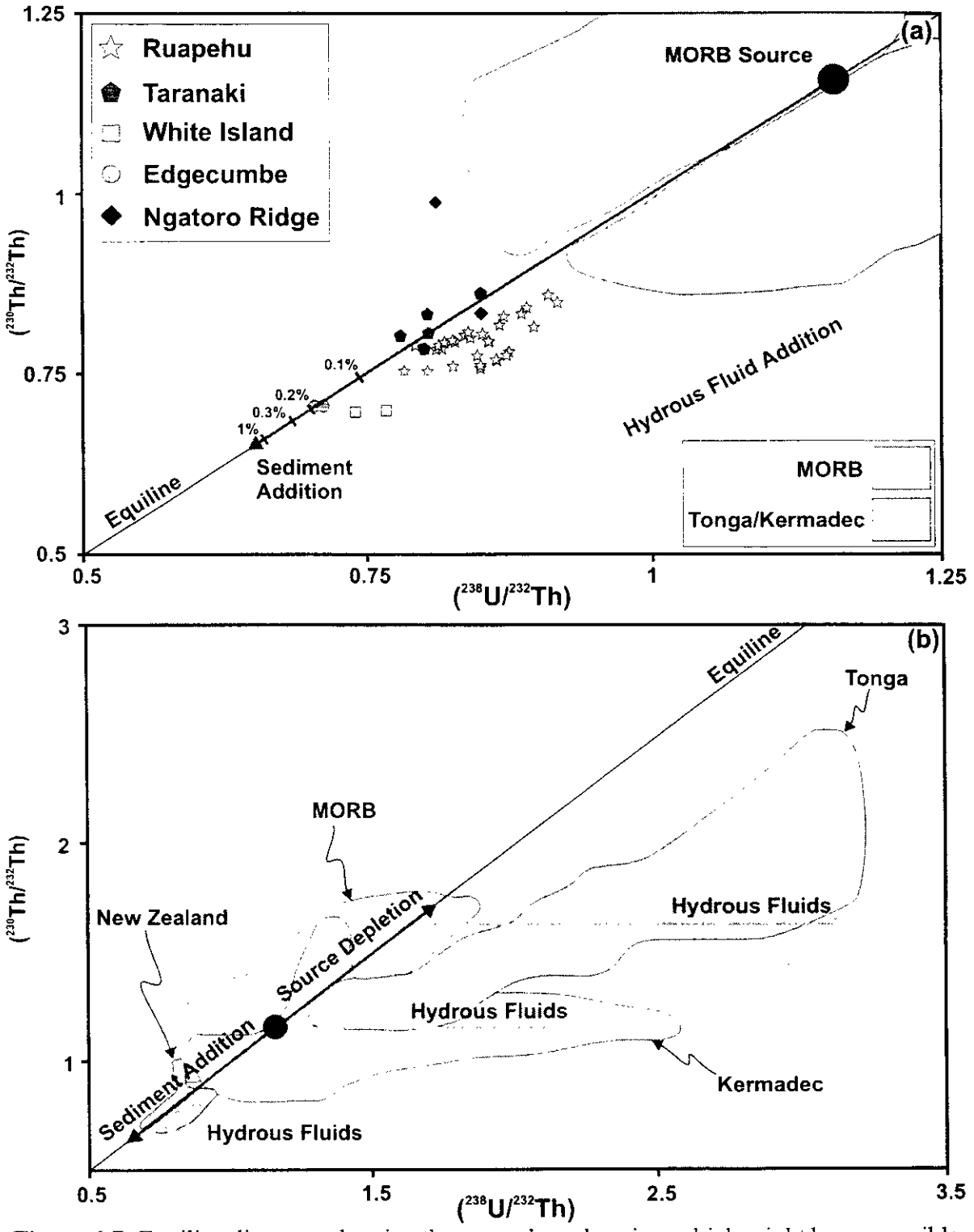

Figure 6.7: Equiline diagrams showing the general mechansims which might be responsible for generating observed U-Th disequilibrium in lavas from Ruapehu and other volcanic centres in New Zealand. (a) shows a model in which a mantle wedge composition in secular equilibrium (from Stolper and Newman, 1994) mixes with a sediment melt. The sediment is derived from a 50:50 mixture of South Island metamorphics (Palmer et al., 1991) and GLOSS (Plank and Langmuir, 1998). The logic of the sediment composition and the partition coefficients used to generate the melt are given in the text. The wedge-sediment mix is then infiltrated by hydrous fluids carrying U but not Th. The reasons for fluid infiltration following sediment addition are discussed in the text. In (b), a more general, schematic model is shown for the whole Tonga-Kermadec-New Zealand arc system (after Turner et al., 1997a). Melt extraction in a back-arc environment is likely to drive the wedge composition up the equiline, whereas sediments tend to have the opposite effect. The effects of adding a constant amount of U in fluids is variable, dependant on the composition of the mantle wedge.

time to decay back to secular equilibrium (Elliott et al., 1997; Turner et al., 1997a), and the uncertainties in U and Th abundances in the sediment melt, this assumption makes little overall difference provided that the degree of fractionation during melting is small. In general the data from this study suggests that the degree of fractionation of U from Th during melting must be small, otherwise a wedge-sediment mixture would plot to higher ($^{238}U/^{232}Th$) and ($^{230}Th/^{232}Th$).

To produce the preliminary model shown in Figure 6.7a, a mixture of GLOSS (Plank and Langmuir, 1998) and South Island metamorphic material (Palmer et al., 1995) was used as the sediment composition and added to a MORB source (Stolper and Newman, 1994) assumed to be in U-Th equilibrium. Bulk partition coefficients of 0.1 were used for both elements and the degree of melting was assumed to be 10%. Schematic vectors for fluid addition are shown, which produce horizontal vectors on the equiline diagram. Addition of hydrous fluids is again assumed to follow sediment addition as described in Section 6.5. Although the exact magnitude of the fluid addition vectors is uncertain, increasing the amount of sediment melt added prior to the fluids will result in smaller vectors if the U addition from the fluid is constant (e.g. Elliott et al., 1997; Turner et al., 1997a).On the basis of this model, in order to produce a ($^{230}Th/^{232}Th$) ratio in the parental basalts of around 0.7 (see Chapter 5 for a discussion of this value) requires ~0.3% sediment melt to be added to the mantle wedge. The difference in the amount of sediment required between this model and the Sr-Nd isotope model probably simply reflects the poor constraints available on the behaviour of trace elements during sediment melting.

Figure 6.7b shows a general model for the Tonga-Kermadec-New Zealand arc system based on ideas presented here, and in Turner et al. (1997). As shown in Figure 6.7a and discussed by Turner et al. (1997), the effect of increasing sediment addition is lower the ($^{230}Th/^{232}Th$) and ($^{238}U/^{232}Th$) ratios of the mantle wedge. Wedge depletion is an additional factor which may help to explain the range of values for Tonga-Kermadec-New Zealand lavas which lie on the equiline in Figure 6.6a. Dynamic melting models for the production of Th excesses in MORB require that the residue moves up the equiline to higher ($^{230}Th/^{232}Th$) in repeated steps of small U excesses and subsequent radioactive

decay (e.g. review of Elliott, 1997). Prior depletion of the mantle wedge, particularly in the Tonga arc due to back-arc spreading (which has produced Th excesses in the back-arc island of Niuafo'ou, Turner et al., 1997a) has been discussed elsewhere (e.g. Falloon and Green, 1986; Ewart and Hawkesworth, 1987; Turner et al., 1997a; Ewart et al., 1998), and it is interesting to note that the Tongan samples tend to intersect the equiline with higher ($^{230}Th/^{232}Th$) than the other data, and they have ($^{230}Th/^{232}Th$) ratios above those of the MORB source of Stolper and Newman (1994). It is argued here that the systematics throughout the arc system can be explained in terms of source processes. Wedge depletion and sediment addition have opposing effects on an equiline diagram and help to produce a variable wedge composition which is then infiltrated by hydrous fluids. The amount of U excess produced by a given amount of U added in a hydrous fluid depends on the U abundance of the mantle wedge. The U concentration of the wedge will increase with sediment addition and decrease with prior melt extraction, producing larger U excesses in depleted, sediment poor wedges than in fertile, sediment enriched ones. The New Zealand data require either a more fertile wedge than seen in the Kermadec arc, and/or a slightly larger sediment addition to produce the generally higher trace element abundances observed compared with Kermadec lavas.

6.6.3 Spatial Inferences from New Zealand Lavas

Given the limited number of samples analysed from other volcanic centres in New Zealand, it is difficult to make more than broad comments on the possible significance of differences in U-series systematics shown in Figure 6.6. The data for samples from Edgecumbe, White Island and Taranaki are given in Appendix C.

In the case of Taranaki, it is interesting to note that not only do the lavas plot close to the equiline, but that several have small but distinct ^{230}Th excesses. Several reasons can be put forward to explain the observed U-Th systematics in young (<10 ka) lavas from this volcano. Firstly, it may be that these lavas had U excesses similar to those observed in Ruapehu lavas, but that total transit and residence times are much longer. This argument, however, has difficulty explaining the observed ^{230}Th excesses. Secondly, it might be that there is a much smaller fluid contribution to these lavas, and therefore little U excess,

although this also has difficulty explaining the ^{230}Th excesses. The third possibility is that the smaller degree of melting inferred to have produced the Taranaki lavas (e.g. Price et al., 1999) has resulted in ^{230}Th excesses being produced during melting in a similar way to those observed in OIB and MORB. The effects of melting and fluid addition may have counterbalanced one another to an extent given the presence of small U and ^{230}Th excesses. The fact that the observed U-Th disequilibria are invariably small ($\leq$ 3.5%) implies, regardless of whether the sample is in U or ^{230}Th excess, that either transit and residence times are long, or that the excesses were never large. The greater distance to the slab beneath Taranaki (~200 km) is consistent with longer transit and residence times. In contrast, it might also be argued that Taranaki is likely to receive a smaller sediment and fluid component as it is behind the arc. In this case, the observed (^{230}Th/^{232}Th) and (^{238}U/^{232}Th) ranges might largely those of the mantle wedge under Taranaki. Until more detailed models are developed for the origin of Taranaki magmas it will be difficult to resolve this issue further.

It is difficult to make any great comment on the Edgecumbe data. The cone itself is < 10 ka old, so post-eruption decay cannot account for the observed secular equilibrium. If these samples did have U excesses, then transit and residence times must be long. The two White Island samples show distinct U excesses (6-10%) and have the same (^{230}Th/^{232}Th) ratio of ~0.7. These samples confirm that it is difficult to interpret the U excesses observed in lavas from both White Island and Ruapehu in terms of assimilation. The White Island samples are more primitive in terms of their major element and isotope systematics than any of the Ruapehu lavas analysed, and are therefore thought to have been influenced less by assimilation. If the (^{230}Th/^{232}Th) ratio of recent lavas is related primarily to AFC, it would be expected that the White Island samples had been affected to a greater degree by assimilation than the Ruapehu magmas. However the small U excesses are consistent with the higher sediment contribution suggested for sample Wi008 compared with Ruapehu 'basalt' in Section 6.4.3. There is insufficient data available to determine if White Island samples truly lie on a linear trend, and whether if they do the trend is horizontal or inclined. On the present evidence it might be suggested that there has been a

relatively short time since fractionation of U from Th which could reflect short transit and residence times.

6.6.4 Regional ^{226}Ra-^{230}Th Variations

In addition to the Ra-Th data for Ruapehu presented in Chapter 5, determinations of Ra isotopes were also determined on samples from White Island. Although attempts were also made to obtain data for Edgecumbe and Taranaki samples, analytical difficulties have prevented inclusion of a full data set for the young New Zealand lavas examined in this study (although it is intended to repeat these analyses before publishing this work). The available data is shown on a Ra equiline diagram in Figure 6.8. The White Island samples have near identical ^{226}Ra-^{230}Th compositions with 6-7% ^{226}Ra excess. This is similar to the values obtained for young Ruapehu lavas. It is difficult to place further constraints on the discussion given in Chapter 5, but it is noted that the process which is responsible for producing the ^{226}Ra excesses seems to be fairly constant along the arc on the basis of the available evidence.

Much larger ^{226}Ra excesses (50-300%) have been reported from the Tonga arc (Gill and Williams, 1990; Chabaux and Allègre, 1994; and discussion of Turner et al., 1997a). These excesses have been attributed to melting processes by Turner et al. (1997). The apparent consistency of the degree of melting and fluid flux along the Tonga-Kermadec-New Zealand arc has been discussed in this chapter, and it would therefore be likely that similar Ra excesses should be produced during melting in the mantle wedge beneath New Zealand. The absence of significant ^{226}Ra excesses would therefore require longer ascent and residence times in New Zealand. As transit and residence times on the order of 40-60 ka have been inferred for the historic samples from Ruapehu no ^{226}Ra excesses would be expected if > 8 ka of this time was spent in the crust. It is likely that any initial ^{226}Ra excess will have returned to secular equilibrium which would therefore imply that the observed ^{226}Ra-^{230}Th disequilibria are related to assimilation processes.

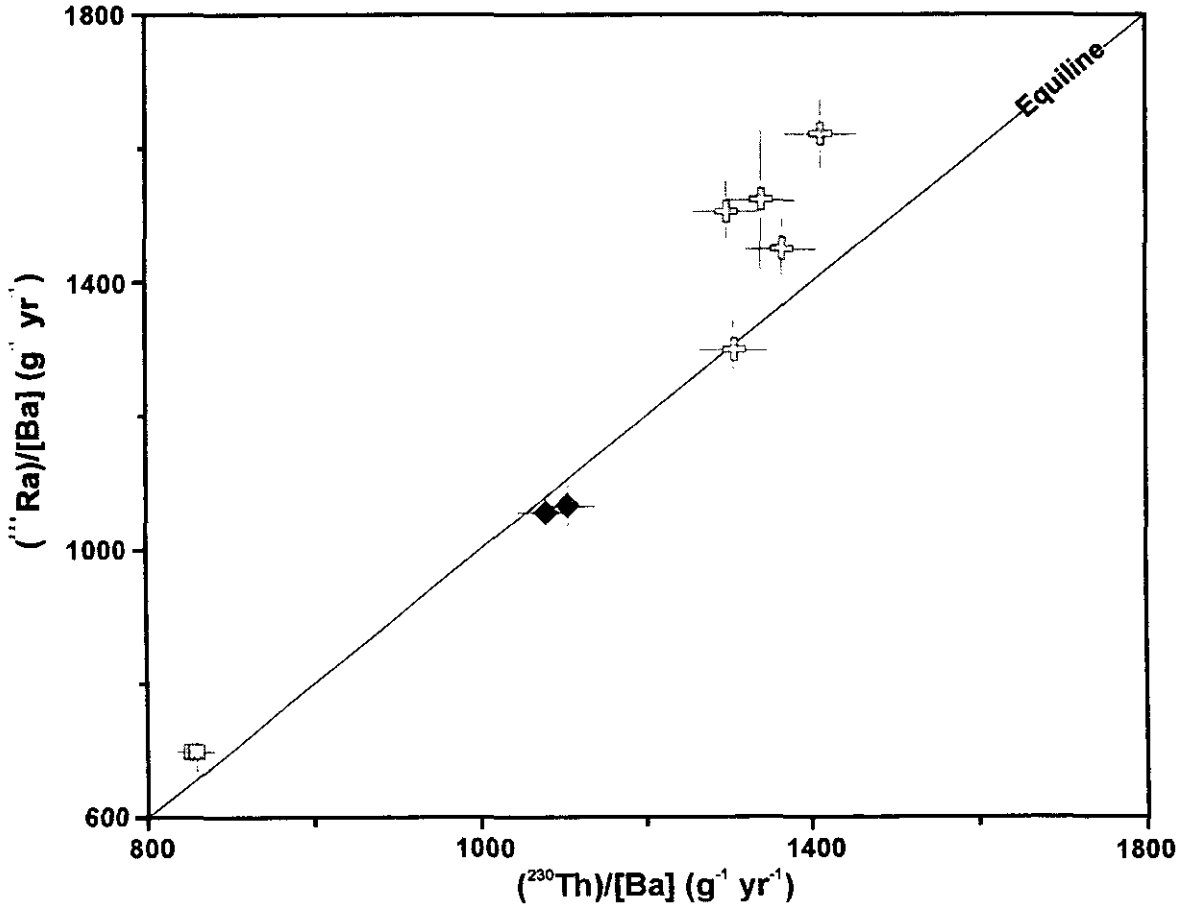

Figure 6.8: Along-arc variations in ^{226}Ra-^{230}Th disequilibrium. In addition to the Ruapehu samples (see also Figure 5.14), both samples from White Island examined in this study have had Ra isotope systematics determined.

6.7 Summary

Whilst the evolved nature of New Zealand arc volcanics makes it difficult to address issues regarding subcrustal processes, it has been demonstrated that by comparisons with the Tonga and Kermadec arcs it is possible to constrain factors such as sediment addition. Mass balance models of primitive lavas indicates that the addition of fluid and sediment components to a relatively fertile wedge which was then melted by around 15% can explain the observed trace element signatures. Modelling of the sediment contribution indicates that it probably enters the wedge as a partial melt at shallow levels, due to relatively high temperatures resulting from a long, shallow trajectory of the subducting slab. Within the poor constraints of trace element partitioning and residual mineralogy, it appears likely that only ~0.3-1% of sediment melt needs to have been added to the mantle wedge to explain the observed isotope signatures. In contrast, the hydrous fluid is largely supplied by dehydration reactions in the subducted oceanic crust and it is likely to enter the wedge at a deeper level where it promotes melting.

U-series data for New Zealand appear to be consistent with the model put forward by Turner et al. (1997) for the Tonga and Kermadec arcs. The ($^{230}Th/^{232}Th$) and ($^{238}U/^{232}Th$) composition of the wedge is controlled primarily by the degree of sediment addition, and the degree of U enrichment has an inverse correlation with the amount of sediment added. The behind-arc volcanic centre of Taranaki shows small U and Th excesses, and the most reasonable explanation with the available data suggests either very limited fluid additions and/or long transit times combined with small degrees of melting allowing small Th excesses to be produced.

More or less what fills the mind when finally writing conclusions,

Obliviscor

The motto of the Klatchian Foreign Legion.

from 'The concife and possibly even accuratte Mapp' and 'Discworld Companion' – Terry Pratchett & Stephen Briggs.

Chapter 7

Conclusions

7.1 Evolution and Differentiation of Ruapehu Lavas

Various differentiation processes occurring during the evolution of Ruapehu magmas have been quantified in previous studies and further constrained in this work. The primary basaltic magmas feeding into the crust beneath Ruapehu were derived from the underlying mantle wedge and had high MgO and low Al_2O_3 contents. These magmas may have resided at the base of the crust for some period of time, although the majority of the major element variations can be explained in terms of shallow level crystallisation processes combined with assimilation of partial melts of local basement. To generate the most evolved rocks requires of the order of 50% crystallisation and 10-15% assimilation. Trace element patterns are typical of those expected for arc magmas with high LILE abundances even in primitive magmas, and low HFSE abundances. The patterns for REE abundances show no evidence of a significant role for garnet and show a progressive fractionation of LREE relative to HREE during differentiation.

7.2 Timescales of Magmatic Processes at Ruapehu

The principal thrust of this study has been to obtain a detailed series of U-Th analyses for lavas from Ruapehu. These data lie on a series of linear correlations on a U-Th equiline diagram consistent with their stratigraphic relationships. There is no evidence that the U-Th systematics can be related to alteration or crystallisation processes, and the lack of correlation between indices of assimilation and U/Th ratios implies that the assimilated melts had very similar U/Th ratios. These observations lead to the conclusion that the U excesses observed in Ruapehu lavas are related to subcrustal fractionation events. Studies

of primitive lavas from intra-oceanic arcs show evidence for the U excesses being imparted on the mantle wedge by hydrous slab-derived fluids. It is suggested that similar fluid driven fractionations of U from Th were responsible for the observed U excesses in Ruapehu lavas.

Comparisons of eruption ages derived by Ar-Ar techniques, tephra chronology and historical observations with ages derived by treating the U-Th data as pseudo-isochrons enable combined transit and residence times to be estimated. For the older Whangaehu, Waihianoa and Ohinepango sequences these appear to be very short, probably considerably less than a maximum of 40 ka. In contrast, the younger sequences have longer transit and residence times on the order of 40-80 ka.

There are few geochemical differences between the older and younger sequences, although they can be split into to distinct groups by a small but distinct shift to higher Rb/Zr and Rb/Y ratios in the younger sequences. As there is no distinct differences in other geochemical systematics such as SiO_2 (although there are no low SiO_2 samples in the younger samples) or $^{87}Sr/^{86}Sr$, the differences cannot be linked to a higher degree of high level assimilation of melts of Torlesse basement. It is argued instead that the differences in Rb/Zr might result from increased contamination of the magmas during storage at the base of the crust, where the basement may be mainly of igneous origin and similar in composition to the erupted andesites.

It is suggested that there may have been a major pulse of magmatism at around 130 ka which was characterised by very short transit and residence times, and that most of the differentiation of these magmas occurred at shallow levels shortly prior to eruption. Another similar event may have occurred at around 80 ka to produce the Upper Whangaehu sequence although this interpretation is currently limited by a shortage of Ar-Ar data. The data for the younger sequences implies longer transit and residence times, and the geochemical systematics argue for much of this time to be taken up by storage at the base of the crust where only very limited chemical modification of the magmas occurred. It is possible that the short transit and residence times observed in the older sequences are related to higher rates of regional extension at around 60-130 ka, when a

major phase of magmatism is also recorded at Tongariro volcano to the north of Ruapehu. These models are summarised in Figure 7.1.

Limited Ra-Th data for eruptions this century shows small ^{226}Ra excesses. These do not correlate with ($^{238}U/^{230}Th$) ratios or with $^{143}Nd/^{144}Nd$, although it is suggested that on the basis of long (> 8 ka) transit and residence times inferred for these samples that the Ra-Th disequilibria are most likely to reflect assimilation processes involving a contaminant in with ^{226}Ra excess.

7.3 Subcrustal Processes in New Zealand Arc Volcanics

Major element abundances at 8% MgO indicate that the mantle wedge beneath the TVZ is fertile, consistent with the apparent increase in wedge fertility from north to south along the Tonga-Kermadec arc system which has been correlated with a decrease in back-arc spreading. A similar approach implies that the mantle source from which magmas erupted at Taranaki were derived is similarly fertile, although this not in agreement with other studies. This difference may be caused by smaller degrees of melting enriching the melts in certain major elements (Na, Ti) even though the source itself is depleted.

It has been shown from the trace element systematics of two relatively primitive, high MgO samples from Ruapehu and White Island that it is necessary to invoke a three component model for magma generation. It is suggested that the data can best be modelled by a addition of a partial melt of subducted sediment to the mantle wedge at a relatively shallow level. The modified mantle wedge is then fluxed by hydrous fluids derived primarily from the subducted oceanic crust, which promote melting in the wedge. The concentrations of Y and Yb in the primitive magmas can be modelled by ~15% mantle melting provided that sediments and fluids contribute only very small quantities of these element to the mantle wedge. Although distinguishing between exact fluid and sediment contributions is limited by relatively poor knowledge of the behaviour of trace elements during such processes, it is suggested that plagioclase is residual during sediment melting. This implies that the sediments must get relatively hot at a shallow level, which can be explained by the long, shallow trajectory of the subducted crust beneath New Zealand.

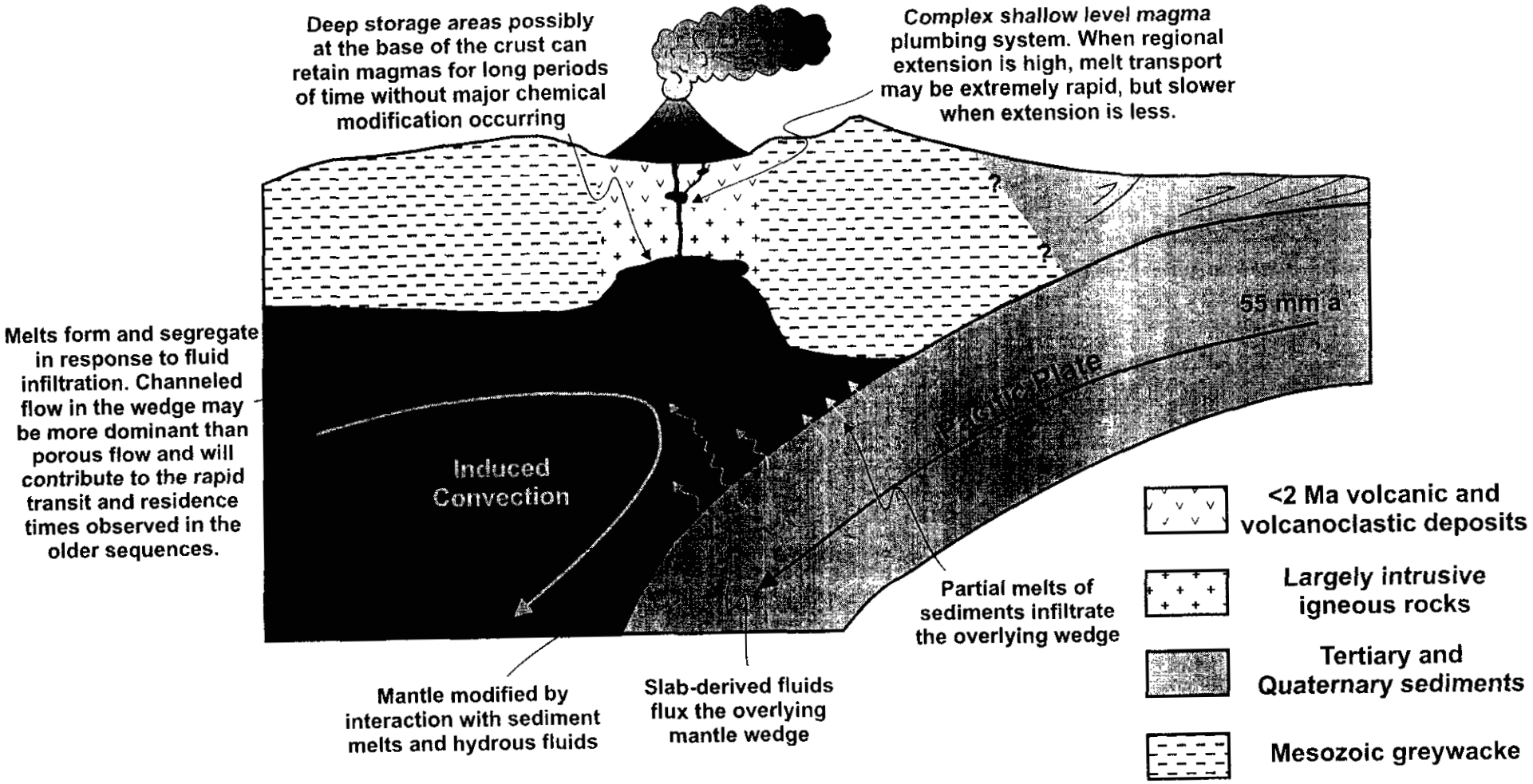

Figure 7.1: Schematic cross-section summarising some of the main ideas and conclusions of this thesis. Based on a cross-section in Stern and Davey (1987).

U-Th systematics show a limited range between various volcanic centres in New Zealand. Samples from Taranaki show small excesses of both U and ^{230}Th but a similar range in U/Th ratio to Ruapehu magmas. It is suggested that these systematics may be the combined effects of some or all of the following; smaller melt fractions producing melting conditions similar to those observed in MORB and OIB, less slab-derived fluid imparting smaller U excesses, and longer combined transit and residence times. White Island shows small U excesses, and the two samples analysed lie on a horizontal trend, although more data is needed to confirm this. Both Edgecumbe samples plot in isotope equilibrium and so it is not possible to extract much useful information.

7.4 U-Th-Ra Systematics and Crustal Level Magmatic Processes

Numerical simulations undertaken in Chapter 2 have expanded on previous models, and put a framework in place for understanding the potentially complex behaviour of U-Th-Ra disequilibria during crustal level magmatic processes. The rates of such processes are uncertain and different techniques have suggested that timescales could range from a few years to tens of thousands of years. U-Th-Ra systematics have the potential to resolve such differences in a volcanic system with good age constraints so that U-Th-Ra isotopic compositions can be constrained at the time of eruption.

Due to the lack of correlation between assimilation indices and relatively poor age constraints for many of the studied lavas, Ruapehu has not proved a good test of the model as was at first hoped. As techniques such as Ar-Ar are refined for looking at very young volcanic rocks, it should become easier to examine the model in real systems.

7.5 Concluding Remarks

This work has demonstrated the potential power of U-Th disequilibria studies in constraining the timescales of magmatic processes at complex volcanic centres despite the potential problems caused by assimilation processes.

From this study and a separate Ar-Ar study, a picture has emerged of a persistently active volcano which underwent a major pulse magmatism ~130 ka ago and second pulse of magmatism appears to have occurred ~80 ka ago. Rapid ascent and limited magma storage time is inferred for these eruptive sequences from whole rock U-Th data. In contrast, younger lavas erupted over the last 20-30 ka and during historic eruptions this century appear to indicate longer transit and residence times. The similarity in composition and degree of assimilation between the old and young sequences imply that the younger sequences must have been stored for a considerable period of time whilst undergoing little chemical modification. It is suggested that the base of the crust is the most likely place for this to have occurred. By inference therefore, it seems that much of the evolved character of these lavas is determined over relatively short timescales in shallow level magma plumbing and storage systems. Preliminary analyses of samples from Taranaki, a behind-arc volcano imply that a combination of smaller fluid additions, long transit and residence times and small degrees of melting have resulted in small U-Th disequilibria showing both U and Th excesses.

7.6 Implications for Future Work

The work undertaken in this thesis has shown how U-Th systematics can be a powerful tool for understanding the complex magmatic histories of composite, persistently active volcanoes. The potential for future studies to combine detailed fieldwork with precise U-Th-Ra analyses and dating techniques such as Ar-Ar has been demonstrated in this study.

The exploratory work presented in this study also shows the potential for further U-Th studies of other parts of the Ruapehu edifice, which would enable a more complete picture of the magmatic history and the timescales of magmatic processes to be discerned. A particular area of interest would be a detailed study of the Whakapapa Formation to establish if this major pulse of recent (< 10 ka) activity shows long transit and residence times like the young samples analysed in this study. It would also be important to try analysing material from the Te Herenga Formation to try and constrain its age better.

Analysis of mineral separates from young lavas from the Whakapapa Formation (< 10 ka) would be a useful test of whether younger lavas have had longer crustal residence times. Such work might also prove interesting on older samples where the eruption ages are now constrained. Mineral isochron ages giving the same age of the U-Th whole rock ages and Ar-Ar eruption ages would help to confirm whether these magmas had very short transit and residence times.

Although the analyses of five Taranaki samples in this study have shown very little U-Th disequilibrium, the cone is < 10 ka old, and a relatively well known chronology would make this an ideal site for reconnaissance work with the ^{226}Ra-^{230}Th system to see if constraints can be placed on the timescales of crustal level processes.

At this stage of the thesis, this is probably about right,

Farcimini!

The motto of the Embalmers' Guild.

from 'The concife and possibly even accuratte Mapp' and 'Discworld Companion' – Terry Pratchett & Stephen Briggs.

References

Adam, J., Green, T. H. and Sie, S. H., 1993. Proton microprobe determined partitioning of Rb, Sr, Ba, Y, Zr, Nb and Ta between experimentally produced amphiboles and silicate melts with variable F content. Chemical Geology, 109, 29-49.

Adams, R. D. and Ware, D. E., 1977. Subcrustal earthquakes beneath New Zealand; locations determined with a laterally inhomogeneous velocity model . New Zealand Journal of Geology and Geophysics, 20 (1), 59-83.

Albarède, F., 1985. Regime and trace-element evolution of open magma chambers. Nature, 318, 356-358.

Allègre, C. J., 1968. ^{230}Th dating of volcanic rocks: a comment. Earth and Planetary Science Letters, 5, 209-210.

Allègre, C. J. and Condomines, M., 1982. Basalt genesis and mantle structure studied through Th-isotopic geochemistry. Nature, 299, 21-24.

Allègre, C. J. and Condomines, M., 1976. Fine chronology of volcanic processes using ^{238}U-^{230}Th systematics. Earth and Planetary Science Letters, 28, 395-406.

Allègre, C. J. and Minster, J. F., 1978. Quantitative models of trace element behaviour in magmatic processes. Earth and Planetary Science Letters, 38, 1-25.

Alloway, B. V., Stewart, R. B., Neall, V. E. and Vucetich, C. G., 1992. Climate of the last glaciation in New Zealand, based on aerosolic quartz influx in an andesitic terrain. Quaternary Research, 38, 170-179.

Andrews, D. J. and Sleep, N. H., 1974. Numerical modelling of tectonic flow behind island arcs. Geophysical Journal of the Royal Astronomical Society, 38, 237-251.

Arculus, R. J., 1994. Aspects of magma genesis in arcs. Lithos, 33, 189-208.

Arculus, R. J., 1981. Island arc magmatism in relation to the evolution of the crust and mantle. Tectonophysics, 75, 113-133.

Arculus, R. J. and Johnson, R. W., 1978. Criticism of generalised models for the magmatic evolution of arc-trench systems. Earth and Planetary Science Letters, 13, 118-126.

Arculus, R. J. and Johnson, R. W., 1981. Island-arc magma sources: a geochemical assessment of the roles of slab-derived components and crustal contamination. Geochemical Journal, 15, 109-133.

Armstrong, R. L., 1971. Isotopic and chemical constraints on models of magma genesis in volcanic arcs. Earth and Planetary Science Letters, 12, 137-142.

Armstrong, R. L., 1968. A model for the evolution of strontium and lead isotopes in a dynamic earth. Reviews of Geophysics, 6, 175-199.

Ayres, M. W., 1997. Trace-element behaviour during high-grade metamorphism and anatexis of the Himalayas. Unpublished PhD thesis, The Open University.

Ayres, M. and Harris, N., 1997. REE fractionation and Nd-isotope disequilibrium during crustal anatexis: constraints from Himalayan leucogranites. Chemical Geology, 139, 249-269.

Bailey, E. H. and Ragnarsdottir, K. V., 1994. Uranium and thorium solubilities in subduction zone fluids. Earth and Planetary Science Letters, 124, 119-129.

Baker, D. R. and Eggler, D. H., 1987. Compositions of anhydrous and hydrous melts co-existing with plagioclase, augite, and olivine or low-Ca pyroxene from 1 atm to 8 kbar: application to the Aleutian volcanic center of Atka . American Mineralogist, 72, 12-28.

Ballance, P. F., 1976. Evolution of the Upper Cenozoic Magmatic Arc and plate boundary in northern New Zealand. Earth and Planetary Science Letters, 28, 356-370.

Bea, F., 1996. Residence of REE, Y, Th and U in granites and crustal protoliths; Implications for the

chemistry of crustal melts. Journal of Petrology, 37 (3), 521-552.

Bea, F., Pereira, M. D., Stroh, A., Foley, S. F. and van der Laan, S. R., 1994. Mineral/leucosome trace-element partitioning in a peraluminous migmatite (a laser ablation-ICP-MS study); trace-element partitioning with application to magmatic processes. Chemical Geology, 117, 291-312.

Beattie, P., 1994. Systematics and energetics of trace-element partitioning between olivine and silicate melts - implications for the nature of mineral melt partitioning. Chemical Geology, 117, 57-71.

Beattie, P., 1993. Uranium-thorium disequilibria and partitioning on melting of garnet peridotite. Nature, 363, 63-65.

Bebout, G. E. and Barton, M. D., 1993. Metasomatism during subduction: products and possible paths in the Catalina Schist, California. Chemical Geology, 108, 61-92.

Bennett, J. T., Krishnaswami, S., Turekian, K. K., Melson, W. G. and Hopson, C. A., 1982. The uranium and thorium decay series nuclides in Mt. St. Helens effusives. Earth and Planetary Science Letters, 60, 61-69.

Best, M. G., 1975. Amphibole-bearing cumulate inclusions, Grand Canyon, Arizona and their bearing on silica undersaturated hydrous magmas in the upper mantle. Journal of Petrology, 16 (1), 212-236.

Bibby, H. M., Caldwell, T. G. and Risk, G. F., 1998. Electrical resistivity image of the upper crust within the Taupo Volcanic Zone, New Zealand. Journal of Geophysical Research, 103 (B5), 9665-9680.

Black, S., 1997. Steady-state magma chamber residence times during vulcanian eruptions at Sakurajima volcano. Abstract, Rates and Timescales of Magmatic Processes, Meeting of the Geological Society of London.

Black, S., Macdonald, R., DeVivo, B., Kilburn, C. R. J. and Rolandi, G., 1998. U-series disequilibria in young (A.D. 1944) Vesuvius rocks: Preliminary implications for magma residence times and volatile addition. Journal of Volcanology and Geothermal Research, 82, 97-111.

Boettcher, A. L., 1977. The role of amphiboles and water in circum-Pacific volcanism. In: Manghnani, M. N. and Akimoto, S.-I. (Eds), High pressure research: applications in geophysics, Academic Press, New York, 107-125.

Bourdon, B., Zindler, A. and Wörner, G., 1994. Evolution of the Laacher See magma chamber: Evidence from SIMS and TIMS measurements of U-Th disequilibria in minerals and glasses. Earth and Planetary Science Letters, 126, 75-90.

Bowen, N. L., 1928. The evolution of the igneous rocks. Princeton University Press, Princeton, 332 pp.

Brenan, J. M., Shaw, H. F., Phinney, D. L. and Ryerson, F. J., 1994. Rutile-aqueous fluid partitioning of Nb, Ta, Hf, Zr, U and Th: implications for high field strength element depletion in island-arc basalts. Earth and Planetary Science Letters, 128, 327-339.

Brenan, J. M., Shaw, H. F., Ryerson, F. J. and Phinney, D. L., 1995. Experimental determination of trace-element partitioning between pargasite and a synthetic hydrous andesitic melt. Earth and Planetary Science Letters, 135, 1-11.

Brenan, J. M., Shaw, H. F., Ryerson, F. J. and Phinney, D. L., 1995. Mineral-aqueous fluid partitioning of trace elements at 900°C and 2.0 GPa: Constraints on the trace element chemistry of mantle and deep crustal fluids. Geochimica et Cosmochimica Acta, 59 (16), 3331-3350.

Brenan, J. M. and Watson, E. B., 1991. Partitioning of trace elements between olivine and aqueous fluids at high P-T conditions: implications for the effect of fluid composition on trace-element transport. Earth and Planetary Science Letters, 107, 672-688.

Brophy, J. G. and Marsh, B. D., 1986. On the origins of high-alumina arc basalt and the mechanics of melt extraction. Journal of Petrology, 27 (4), 763-789.

Brown, L., Klein, J., Middleton, R., Sacks, I. S. and Tera, F., 1982. ^{10}Be in island-arc volcanoes and implications for subduction. Nature, 299, 718-720.

Brown, S. J. A., Burt, R. M., Cole, J. W., Krippner, S. J. P., Price, R. C. and Cartwright, I., 1998. Plutonic lithics in ignimbrites of Taupo Volcanic Zone, New Zealand; sources and conditions of crystallisation. Chemical Geology, 148, 21-41.

Browne, P. R. L., Graham, I. J., Parker, R. J. and Wood, C. P., 1992. Subsurface andesite lavas and plutonic rocks in the Rotokawa and Ngatamariki geothermal systems, Taupo Volcanic Zone. Journal of Volcanology and Geothermal Research, 51, 199-215.

Capaldi, G., Cortini, M. and Pece, R., 1982. Th isotopes at Vesuvius: evidence for open-system behaviour of

magma-forming processes. Journal of Volcanology and Geothermal Research, 14, 247-260.

Capaldi, G., Cortini, M. and Pece, R., 1983. U and Th decay-series disequilibria in historical lavas from the Eolian Islands, Tyrrhenian Sea. Isotope Geoscience, 1, 39-55.

Capaldi, M., Cortini, M., Gasparini, P. and Pece, R., 1976. Short-lived radioactive disequilibria in freshly erupted volcanic rocks and their implications for the preeruption history of a magma. Journal of Geophysical Research, 81 (2), 350-358.

Carroll, L. D., Gamble, J. A., Houghton, B. F., Thordarson, T. and Higham, T. F. G., 1997. A radiocarbon age determination for Mount Edgecumbe (Putauaki) volcano, Bay of Plenty, New Zealand. New Zealand Journal of Geology and Geophysics, 40, 559-562.

Carter, L., 1980. NZ regional bathymetry 1:6 000 000 (2nd ed). NZ Oceanographic Institute Chart, Miscellaneous Series 15, Department of Scientific and Industrial Research, Wellington, New Zealand.

Carter, L., Carter, R. M., McCave, I. N. and Gamble, J., 1996. Regional sediment recycling in the abyssal Southwest Pacific Ocean. Geology, 24 (8), 735-738.

Cerrai, E., Dugnani Lonati, R., Gassarrini, F. and Tongiorgi, E., 1965. Il metodo ionio/uranio per la determinazione dell'eta di minerali vulcanici recenti. Rendiconti della Societa Mineralogica Italiana, 21, 47-62.

Chabaux, F. and Allègre, C. J., 1994. ^{238}U-^{230}Th-^{226}Ra disequilibria in volcanics: A new insight into melting conditions. Earth and Planetary Science Letters, 126, 61-74.

Chabaux, F., Hémond, C. and Allègre, C. J., 1999. ^{238}U-^{230}Th-^{226}Ra disequilibria in the Lesser Antilles arc: implications for mantle metasomatism. Chemical Geology, 153, 171-185.

Chase, C. G., 1978. Plate kinematics: the Americas, East Africa and the rest of the World. Earth and Planetary Science Letters, 37, 353-368.

Chen, J. H., Edwards, R. L. and Wasserburg, G. J., 1986. ^{238}U, ^{234}U and ^{232}Th in seawater. Earth and Planetary Science Letters, 80, 241-251.

Christensen, J. N. and DePaolo, D. J., 1993. Time scales of large volume silicic magma systems: Sr isotopic systematics of phenocrysts and glass from the Bishop Tuff, Long Valley, California. Contributions to Mineralogy and Petrology, 113, 100-114.

Christenson, B. W. and Wood, C. P., 1993. Evolution of a vent hosted hydrothermal system beneath Ruapehu Crater Lake, New Zealand. Bulletin of Volcanology, 53, 547-565.

Christoffel, D. A., 1971. Motion of the New Zealand Alpine Fault deduced from the pattern of seafloor spreading. In: Collins, B. W. and Fraser, R. (Eds), Recent Crustal Movements, Royal Society of New Zealand, Bulletin, 25-30.

Clark, R. H., 1960a. Petrology of the volcanic rocks of Tongariro subdivision. Appendix 2. In: Gregg, D. R. The geology of Tongariro subdivision, New Zealand Geological Survey Bulletin, 40, 107-123 pp.

Clark, R. H., 1960b. Andesitic lavas of the North Island, New Zealand. Proceedings 21st International Geolgical Congress, Norden, 23, 121-131.

Clark, S. K., Reagan, M. K. and Plank, T., 1998. Trace element and U-series systematics for 1963-1965 tephras from Irazú Volcano, Costa Rica: Implications for magma generation processes and transit times. Geochimica et Cosmochimica Acta, 62 (15), 2689-2699.

Cohen, A. S., Belshaw, N. S. and O'Nions, R. K., 1992. High precision uranium, thorium and radium isotope ratio measurement by high-dynamic range thermal ionisation mass spectrometry. International Journal of Mass Spectrometry and Ion Processes, 116, 71-81.

Cohen, A. S. and O'Nions, R. K., 1993. Melting rates beneath Hawaii: evidence from uranium series isotopes in recent lavas. Earth and Planetary Science Letters, 120, 169-175.

Cohen, A. S. and O'Nions, R. K., 1991. Precise determinations of femtogram quantities of radium by thermal ionization mass spectrometry. Analytical Chemistry, 63, 2705-2708.

Cole, J. W., 1978. Andesites of the Tongariro Volcanic Centre, North Island, New Zealand. Journal of Volcanology and Geothermal Research, 3, 121-153.

Cole, J. W., 1986. Distribution and tectonic setting of late Cenozoic volcanism in New Zealand. Royal Society of New Zealand Bulletin, 23, 7-20.

Cole, J. W., 1981. Genesis of lavas of the Taupo Volcanic Zone, North Island, New Zealand. Journal of Volcanology and Geothermal Research, 10, 317-337.

Cole, J. W., 1990. Structural control and origin of volcanism in the Taupo volcanic zone, New Zealand. Bulletin of Volcanology, 52, 445-459.

Cole, J. W., 1979. Structure, petrology and genesis of Cenozoic volcanism, Taupo Volcanic Zone, New Zealand – a review. New Zealand Journal of Geology and Geophysics, 22, 631-657.

Cole, J. W., Cashman, K. V. and Rankin, P. C., 1983. Rare-earth element geochemistry and the origin of andesites and basalts of the Taupo Volcanic Zone, New Zealand. Chemical Geology, 38, 255-274.

Cole, J. W. and Graham, I. J., 1989. Petrology of strombolian and phreato-magmatic ejecta from the 1976-82 White Island eruption sequence. New Zealand Geological Survey Bulletin, 103, 61-68.

Cole, J. W. and Lewis, K. B., 1981. Evolution of the Taupo-Hikurangi subduction system. Tectonophysics, 72, 1-21.

Condomines, M., 1994. Comment on: "The volume and residence time of magma beneath active volcanoes determined by decay series disequilibria methods". Earth and Planetary Science Letters, 122, 251-255.

Condomines, M., 1997. Dating recent volcanic rocks through ^{230}Th-^{238}U disequilibrium in accesory minerals: Example of the Puy de Dôme (French Massif Central). Geology, 25 (4), 375-378.

Condomines, M. and Allègre, C. J., 1980. Age and magmatic evolution of Stromboli volcano from ^{230}Th-^{238}U disequilibrium data. Nature, 288, 354-357.

Condomines, M., Hémond, Ch. and Allègre, C. J., 1988. U-Th-Ra disequilibria and magmatic processes. Earth and Planetary Science Letters, 90, 243-262.

Condomines, M., Morand, P., Camus, G. and Duthou, L., 1982. Chronological and geochemical study of lavas from the Chaîne des Puys, Massif Central, France: Evidence for crustal contamination. Contributions to Mineralogy and Petrology, 81, 296-303.

Condomines, M. and Sigmarsson, O., 1993. Why are so many arc magmas close to ^{238}U-^{230}Th radioactive equilibrium? Geochimica et Cosmochimica Acta, 57, 4491-4497.

Condomines, M., Tanguy, J. C., Kieffer, G. and Allègre, C. J., 1982. Magmatic evolution of a volcano studied by ^{230}Th-^{238}U disequilibrium and trace elements systematics: the Etna case. Geochimica et Cosmochimica Acta, 46, 1397-1416.

Condomines, M., Tanguy, J-C. and Michaud, V., 1995. Magma dynamics at Mt. Etna: Constraints from U-Th-Ra-Pb radioactive disequilibria and Sr isotopes in historical lavas. Earth and Planetary Science Letters, 132, 25-41.

Conrad, W. K., Nicholls, I. A. and Wall, V. J., 1988. Water-saturated and -undersaturated melting of metaluminous and peraluminous crustal compositions at 10 kb: Evidence for the origin of silicic magmas in the Taupo Volcanic Zone, New Zealand, and other occurrences. Journal of Petrology, 29 (4), 765-803.

Cox, K. G., Bell, J. D., and Pankhurst, R. J., 1979. The interpretation of igneous rocks. Chapman & Hall, London, 450 pp.

Crawford, A. J., Falloon, T. J. and Eggins, S., 1987. The origin of island arc high-alumina basalts. Contributions to Mineralogy and Petrology, 97, 417-430.

Cronin, S. J. and Neall, V. E., 1997. A late Quaternary stratigraphic framework for the northeastern Ruapehu and eastern Tongariro ring plains, New Zealand. New Zealand Journal of Geology and Geophysics, 40, 185-197.

Cronin, S. J., Neall, V. E. and Palmer, A. S., 1996. Geological history of the north-eastern ring plain of Ruapehu volcano, New Zealand. Quaternary International, 34-36, 21-28.

Cronin, S. J., Neall, V. E., Palmer, A. S. and Stewart, R. B., 1997. Methods of identifying late Quaternary rhyolitic tephras on the ring plains of Ruapehu and Tongariro volcanoes, New Zealand. New Zealand Journal of Geology and Geophysics, 40, 175-184.

Cronin, S. J., Neall, V. E., Stewart, R. B. and Palmer, A. S., 1996. A multiple-parameter approach to andesitic tephra correlation, Ruapehu volcano, New Zealand. Journal of Volcanology and Geothermal Research, 72, 199-215.

Davey, F. J., Hampton, M., Childs, J., Fisher, M. A., Lewis, K. and Pettinga, J. R., 1986. Structure of a growing accretionary prism, Hikurangi margin, New Zealand. Geology, 14, 663-666.

Davidson, J. P., 1987. Crustal contamination versus subduction zone enrichment: examples from the Lesser Antilles and implications for mantle source compositions of island arc volcanic rocks. Geochimica et Cosmochimica Acta, 51, 2185-2198.

Davies, J. H. and Bickle, M. J., 1991. A physical model for the volume and composition of melt produced by hydrous fluxing above subduction zones. Philosophical Transactions of the Royal Society of London Series A, 335, 355-364.

Davies, J. H. and Rowland, A., 1997. Importance of temperature dependant viscosity and hydraulic fracture on physical models of subduction zone magmatism. Abstract, State of the Arc '97, University of Adelaide.

Davies, J. H. and Stevenson, D. J., 1992. Physical models of source region of subduction zone volcanism. Journal of Geophysical Research, 97 (B2), 2037-2070.

Defant, M. J. and Drummond, M. S., 1990. Derivation of some modern arc magmas by melting of young subducted lithosphere. Nature, 347, 662-665.

DePaolo, D. J., 1981. Trace element and isotopic effects of combined wallrock assimilation and fractional crystallisation. Earth and Planetary Science Letters, 53, 189-202.

Dickin, A. P., 1997. Radiogenic isotope geology. Cambridge University Press, Cambridge, 490 pp.

Donoghue, S. L., Neall, V. E., Palmer, A. S. and Stewart, R. B., 1997. The volcanic history of Ruapehu during the past 2 millennia based on the record of Tufa Trig tephras. Bulletin of Volcanology, 59, 136-146.

Dostal, J., Dupuy, C., Carron, J. P., Le Guen de Kerneizon, M. and Maury, R. C., 1983. Partition coefficients of trace elements; application to volcanic rocks of St. Vincent, West Indies. Geochimica et Cosmochimica Acta, 47 (3), 525-533.

Downey, W. S., Kellett, R. J., Smith, I. E. M., Price, R. C. and Stewart, R. B., 1994. New palaeomagnetic evidence for the recent eruptive activity of Mt. Taranaki, New Zealand. Journal of Volcanology and Geothermal Research, 60, 15-27.

Dunn, T. and Sen, C., 1994. Mineral/matrix partition coefficients for orthopyroxene, plagioclase, and olivine in basaltic to andesitic systems; a combined analytical and experimental study. Geochimica et Cosmochimica Acta, 58 (2), 717-733.

Edwards, B. R. and Russell, J. K., 1998. Time scales of magmatic processes: New insights from dynamic models for magmatic assimilation. Geology, 26 (12), 1103-1106.

Edwards, C. M. H., Morris, J. D. and Thirlwall, M. F., 1993. Separating mantle from slab signatures in arc lavas using B/Be and radiogenic isotope systematics. Nature, 362, 530-533.

Edwards, R. L., Chen, J. H. and Wasserburg, G. J., 1987. ^{238}U-^{234}U-^{230}Th-^{232}Th systematics and the precise measurement of time over the past 500,000 years. Earth and Planetary Science Letters, 81, 175-192.

Ellam, R. M. and Hawkesworth, C. J., 1988. Elemental and isotopic variations in subduction related basalts: evidence for a three component model. Contributions to Mineralogy and Petrology, 98, 72-80.

Elliott, T., 1997. Fractionation of U and Th during mantle melting: a reprise. Chemical Geology, 139, 165-183.

Elliott, T., Plank, T., Zindler, A., White, W. and Bourdon, B., 1997. Element transport from slab to volcanic front at the Marianas arc. Journal of Geophysical Research, 102 (B7), 14991-15019.

Evans, P. J., 1999. A U-series disequilibrium study of Longonot Volcano. Unpublished PhD thesis, The Open University.

Ewart, A. E. and Hawkesworth, C. J., 1987. The Pleistocene-Recent Tonga-Kermadec arc lavas: interpretation of new isotopic and rare-earth data in terms of a depleted mantle source model. Journal of Petrology, 28, 495-530.

Ewart, A., Brothers, R. N. and Mateen, A., 1977. An outline of the geology and geochemistry, and the possible petrogenetic evolution of the volcanic rocks of the Tonga-Kermadec-New Zealand island arc. Journal of Volcanology and Geothermal Research, 2, 205-250.

Ewart, A., Collerson, K. D., Regelous, M., Wendt, J. I. and Niu, Y., 1998. Geochemical evolution within the Tonga–Kermadec–Lau arc–back-arc systems: the role of varying mantle wedge composition in space and time . Journal of Petrology, 39 (3), 331-368.

Ewart, A. and Griffin, W. L., 1994. Application of proton-microprobe data to trace-element partitioning in volcanic rocks. Chemical Geology, 117, 251-284.

Ewart, A. and Stipp, J. J., 1968. Petrogenesis of the volcanic rocks of the Central North Island, New Zealand, as indicated by a study of Sr^{87}/Sr^{86} ratios, and Sr, Rb, K, U and Th abundances. Geochimica et

Cosmochimica Acta, 32 (7), 699-735.

Falloon, T. J. and Green, D. H., 1986. Glass inclusions in magnesian olivine phenocrysts from Tonga : evidence for highly refractory parental magmas in the Tongan arc. Earth and Planetary Science Letters, 81, 95-103.

Faure, G., 1986. Principles of isotope geology. Wiley, New York, 589 pp.

Foden, J., 1997. Arc magmatic chemistry: the source versus process debate. Abstract, State of the Arc '97, University of Adelaide.

Froggatt, P. C. and Lowe, D. J., 1990. A review of late Quaternary silicic and some other tephra formations from New Zealand: their stratigraphy, nomenclature, distribution, volume, and age. New Zealand Journal of Geology and Geophysics, 33, 89-109.

Frost, C. D. and Coombs, D. S., 1989. Nd isotope character of New Zealand sediments: Implications for terrane concepts and crustal evolution. American Journal of Science, 289, 744-770.

Gamble, J. A., Smith, I. E. M., Graham, I. J., Kokelaar, B. P., Cole, J. W., Houghton, B. F. and Wilson, C. J. N., 1990. The petrology, phase relations and tectonic setting of basalts from the Taupo Volcanic Zone, New Zealand and the Kermadec Island Arc-Havre Trough, S.W. Pacific. Journal of Volcanology and Geothermal Research, 43, 253-270.

Gamble, J. A., Smith, I. E. M., McCulloch, M. T., Graham, I. J. and Kokelaar, B. P., 1993. The geochemistry and petrogenesis of basalts from the Taupo Volcanic Zone and Kermadec Island Arc, S.W. Pacific. Journal of Volcanology and Geothermal Research, 54, 265-290.

Gamble, J., Wood, P., Price, R., Waight, T., Smith, I., and Nakagawa, M., 1997. Major, trace element and isotope geochemistry of historic (1945-1996) eruptions from Ruapehu volcano, New Zealand with implications for open system magmatic processes in arc volcanoes. Abstract, State of the Arc '97, University of Adelaide.

Gamble, J., Woodhead, J., Wright, I. and Smith, I., 1996. Basalt and sediment geochemistry and magma petrogenesis in a transect from oceanic island arc to rifted continental margin arc: the Kermadec-Hikurangi margin, SW Pacific. Journal of Petrology, 37 (6), 1523-1546.

George, R. M. M., 1997. Thermal and tectonic controls on magmatism in the Ethiopian Province. Unpublished PhD thesis, The Open University.

Ghiorso, M. S. and Sack, R. O., 1995. Chemical mass transfer in magmatic processes IV. A revised and internally consistent thermodynamic model for the interpolation and extrapolation of liquid-solid equilibria in magmatic systems at elevated temperatures and pressures. Contributions to Mineralogy and Petrology, 119, 197-212.

Giggenbach, W. F., 1987. Redox processes governing the chemistry of fumarolic gas discharges from White Island, New Zealand. Applied Geochemistry, 2, 143-161.

Gill, J. B., 1981. Orogenic andesites and plate tectonics. Springer-Verlag, New York, 390 pp.

Gill, J. B., Morris, J. D. and Johnson, R. W., 1993. Timescale for producing the geochemical signature of island arc magmas: U-Th-Po and Be-B systematics in recent Papua New Guinea lavas. Geochimica et Cosmochimica Acta, 57, 4269-4283.

Gill, J. B., Pyle, D. M., and Williams, R. W., 1992. Igneous rocks. In: Ivanovich, M. and Harmon, R. S. (eds), Uranium series disequilibrium, applications to environmental problems, Oxford University Press, Oxford, 207-258.

Gill, J. B. and Williams, R. W., 1990. Th isotope and U-series studies of subduction-related volcanic rocks. Geochimica et Cosmochimica Acta, 34, 1427-1442.

Gill, J. and Condomines, M., 1992. Short-lived radioactivity and magma genesis. Science, 257, 1368-1376.

Goldstein, S. J., Murrell, M. T. and Janecky, D. R., 1989. Th and U systematics of basalts from the Juan de Fuca and Gorda Ridges by mass spectrometry. Earth and Planetary Science Letters, 96, 134-146.

Graham, I. J., 1985. Rb-Sr geochronology and geochemistry of Torlesse metasediments from the central North Island, New Zealand. Chemical Geology, 52, 317-331.

Graham, I. J., 1994. Petrological descriptions of TVZ mafic-intermediate volcanic rocks: Compilation of published and unpublished petrographic, geochemical and isotopic data, Institute of Geological and Nuclear Sciences Science Report 94/6, Institute of Geological and Nuclear Sciences Limited, Lower Hutt, New Zealand, 113 pp.

Graham, I. J., Blattner, P. and McCulloch, M. T., 1990. Meta-igneous granulite xenoliths from Mount Ruapehu, New Zealand: fragments of altered oceanic crust? Contributions to Mineralogy and Petrology, 105, 650-661.

Graham, I. J., Cole, J. W., Briggs, R. M., Gamble, J. A. and Smith, I. E. M., 1995. Petrology and petrogenesis of volcanic rocks from the Taupo Volcanic Zone: a review. Journal of Volcanology and Geothermal Research, 68, 59-87.

Graham, I. J., Grapes, R. H. and Kifle, K., 1988. Buchitic metagreywacke xenoliths from Mount Ngauruhoe, Taupo Volcanic Zone, New Zealand. Journal of Volcanology and Geothermal Research, 35, 217-225.

Graham, I. J., Gulson, B. L., Hedenquist, J. W. and Mizon, K., 1992. Petrogenesis of Late Cenozoic volcanic rocks from the Taupo Volcanic Zone, New Zealand, in the light of new lead isotope data. Geochimica et Cosmochimica Acta, 56, 2797-2819.

Graham, I. J. and Hackett, W. R., 1987. Petrology of calc-alkaline lavas from Ruapehu volcano and related vents, Taupo Volcanic Zone, New Zealand. Journal of Petrology, 28 (3), 531-567.

Graham, I. J. and Worthington, T. I., 1988. Petrogenesis of Tauhara Dacite, (Taupo Volcanic Zone, New Zealand) — evidence for mixing between high-alumina andesite and rhyolite. Journal of Volcanology and Geothermal Research, 35, 279-294.

Green, T. H., Adam, J. and Site, S. H., 1993. Proton microprobe determined trace element partition coefficients between pargasite, augite and silicate or carbonatitic melts. EOS, Transactions of the American Geophysical Union, 74 (16), 340.

Green, T. H. and Ringwood, A. E., 1968. Genesis of the calc-alkaline igneous rock suite. Contributions to Mineralogy and Petrology, 18, 105-162.

Grove, T. L. and Kinzler, R. J., 1986. Petrogenesis of andesites. Annual Review of Earth and Planetary Science, 14, 417-454.

Grove, T. L., Kinzler, R. J., and Bryan, W. B., 1992. Fractionation of mid-ocean ridge basalt (MORB). In: Phipps Morgan, J., Blackman, D. K., and Sinton, J. M. (Eds), Mantle flow and melt generation at mid-ocean ridges, Geophysical Monograph, 71, American Geophysical Union, 281-310 pp.

Gust, D. A. and Perfit, M. R., 1987. Phase relations of a high-Mg basalt from the Aleutian Island Arc: implications for primary island arc basalts and high-Al basalts. Contributions to Mineralogy and Petrology, 97, 7-18.

Hackett, W. R. and Houghton, B. F., 1989. A facies model for a Quaternary andesitic composite volcano: Ruapehu, New Zealand. Bulletin of Volcanology, 51 (51-68).

Haines, A. J., 1979. Seismic wave velocities in the uppermost mantle beneath New Zealand. New Zealand Journal of Geology and Geophysics, 22, 245-257.

Halliday, A. N., Mahood, G. A., Holden, P., Metz, J. M., Dempster, T. J. and Davidson, J. P., 1989. Evidence for long residence times of rhyolitic magma in the Long Valley magmatic system: the isotopic record in precaldera lavas of Glass Mountain. Earth and Planetary Science Letters, 94, 274-290.

Hart, S. R., 1984. A large-scale isotope anomaly in the Southern Hemisphere mantle. Nature, 309, 753-757.

Hart, S. R. and Dunn, T., 1993. Experimental cpx melt partitioning of 24 trace-elements. Contributions to Mineralogy and Petrology, 113 (1), 1-8.

Hatherton, T. and Syms, M., 1975. Junction of Kermadec and Hikurangi negative gravity anomalies (note). New Zealand Journal of Geology and Geophysics, 18, 753-756.

Hauri, E. H., Wagner, T. P., Grove, T. L., Foley, S. F. and van der Laan, S. R., 1994. Experimental and natural partitioning of U, Th, Pb and other trace elements between garnet, clinopyroxene and basaltic melts; Trace-element partitioning with application to magmatic processes. Chemical Geology, 117, 149-166.

Hawkesworth, C. J., Gallagher, K., Hergt, J. M. and McDermott, F., 1993. Mantle and slab contributions in arc magmas. Annual Review of Earth and Planetary Science, 21, 175-204.

Hawkesworth, C. J., Gallagher, K., Hergt, J. M. and McDermott, F., 1994. Destructive plate margin magmatism: Geochemistry and melt generation. Lithos, 33, 169-188.

Hawkesworth, C. J., Hergt, J. M., Ellam, R. M. and McDermott, F., 1991a. Element fluxes associated with subduction related magmatism. Philosophical Transactions of the Royal Society of London Series A, 335, 393-405.

Hawkesworth, C. J., Hergt, J. M., McDermott, F. and Ellam, R. M., 1991b. Destructive margin magmatism and the contributions from the mantle wedge and subducted crust. Australian Journal of Earth Sciences, 38, 577-594.

Hawkesworth, C. J., Norry, M. J., Roddick, J. C., Baker, P. E., Francis, P. W. and Thorpe, R. S., 1979. $^{143}Nd/^{144}Nd$, $^{87}Sr/^{86}Sr$, and incompatible element variations in calc-alkaline andesites and plateau lavas from South America. Earth and Planetary Science Letters, 42, 45-47.

Hawkesworth, C. J., Turner, S. P., McDermott, F., Peate, D. W. and van Calsteren, P., 1997a. U-Th isotopes in arc magmas: implications for element transfer from the subducted crust. Science, 276, 551-55.

Hawkesworth, C., Turner, S., Peate, D., McDermott, F. and van Calsteren, P., 1997b. Elemental U and Th variations in island arc rocks: implications for U-series isotopes. Chemical Geology, 139, 207-221.

Healy, J., 1962. Structure and volcanism in the Taupo Volcanic Zone, New Zealand. In: Macdonald, G. A. and Kuno, H. (Eds), The crust of the Pacific basin, American Geophysical Union Geophysical Monographs, 6, 151-157 pp.

Heath, E., Macdonald, R., Belkin, H., Hawkesworth, C. and Sigurdsson, H., 1998a. Magmagenesis at Soufriere volcano, St Vincent, Lesser Antilles Arc. Journal of Petrology, 39 (10), 1721-1764.

Heath, E., Turner, S. P., Macdonald, R., Hawkesworth, C. J. and van Calsteren, P., 1998b. Long magma chamber residence times at an island arc volcano (Soufriere, St. Vincent) in the Lesser Antilles: evidence from ^{238}U-^{230}Th isochron dating. Earth and Planetary Science Letters, 160, 49-63.

Hémond, Ch., Hofmann, A. W., Heusser, G., Condomines, M., Raczek, I. and Rhodes, M., 1994. U-Th-Ra systematics in Kilauea and Mauna Loa basalts, Hawaii. Chemical Geology, 116, 163-180.

Higgins, M. D., 1996. Crystal size distributions and other quantitative textural measurements in lavas and tuff from Egmont volcano (Mt. Taranaki), New Zealand. Bulletin of Volcanology, 58, 194-204.

Hobden, B. J., Houghton, B. F., Lanphere, M. A. and Nairn, I. A., 1996. Growth of the Tongariro volcanic complex: new evidence from K-Ar age determinations. New Zealand Journal of Geology and Geophysics, 39, 151-154.

Hochstein, M. P., 1995. Crustal heat transfer in the Taupo Volcanic Zone (New Zealand): comparison with other volcanic arcs and explanatory heat source models. Journal of Volcanology and Geothermal Research, 68, 117-151.

Hochstetter, F. von, 1864. Geologie von Neu Seeland. Beiträge zur geologie der provinzen Auckland and Nelson. K. Gerold's Sohn, Vienna, 274 pp.

Hole, M. J., Saunders, A. D., Marriner, G. F. and Tarney, J., 1984. Subduction of pelagic sediments: implications for the origin of Ce-anomalous basalts from the Mariana Islands. Journal of the Geological Society of London, 141, 453-472.

Houghton, B. F., Latter, J. H. and Hackett, W. R., 1987. Volcanic hazard assessment for Ruapehu composite volcano, Taupo Volcanic Zone, New Zealand. Bulletin of Volcanology, 49, 737-751.

Hsui, A. T. and Toksöz, M. N., 1981. Back-arc spreading: trench migration, continental pull or induced convection. Tectonophysics, 74, 89-98.

Icenhower, J. and London, D., 1996. Experimental partitioning of Rb, Cs, Sr, and Ba between alkali feldspar and peraluminous melt. American Mineralogist, 81, 719-734.

Ionov, D. A. and Hoffman, A. W., 1995. Nb–Ta-rich mantle amphiboles and micas: implications for subduction-related metasomatic trace element fractionations. Earth and Planetary Science Letters, 131, 341-356.

Irvine, T. N. and Baragar, W. R. A, 1971. A guide to the chemical classification of the common volcanic rocks. Canadian Journal of Earth Sciences, 8, 523-548.

Iwamori, H., 1994. ^{238}U-^{230}Th-^{226}Ra and ^{235}U-^{231}Pa disequilibria produced by mantle melting with porous and channel flows. Earth and Planetary Science Letters, 125, 1-16.

Iwamori, H., 1993. A model for disequilibrium mantle melting incorporating melt transport by porous and channel flows. Nature, 366, 734-737.

Jakeš, P. and Gill, J., 1970. Rare earth elements and the island arc tholeiitic series. Earth and Planetary Science Letters, 9, 17-28.

Jakeš, P. and White, A. J. R., 1972. Major and trace element abundances in volcanic rocks of orogenic areas. Geological Society of America Bulletin, 83, 29-40.

Jarrard, R. D., 1986. Relations among subduction parameters. Reviews of Geophysics, 24 (2), 217-284.

Kay, R. W., 1978. Aleutian magnesian andesites: melts from subducted oceanic Pacific ocean crust. Journal of Volcanology and Geothermal Research, 4, 117-132.

Kay, R. W., 1980. Volcanic arc magmas: implication of a melting-mixing model for element recycling in the crust- upper mantle system. Journal of Geology, 88, 497-522.

Kay, R. W., Sun, S.-S. and Hu, C.-N., 1978. Pb and Sr isotopes in volcanic rocks from the Aleutian islands and Pribilof islands, Alaska. Geochimica et Cosmochimica Acta, (42), 263-273.

Kelemen, P. B., Shimizu, N. and Dunn, T., 1993. Relative depletion of niobium in some arc magmas and the continental crust: partitioning of K, Nb, La and Ce during melt/rock reaction in the upper mantle. Earth and Planetary Science Letters, 120, 111-134.

Kennedy, A. K., Lofgren, G. E. and Wasserburg, G. J., 1993. An experimental study of trace element partitioning between olivine, orthopyroxene and melt in chondrules; equilibrium values and kinetic effects. Earth and Planetary Science Letters, 115, 177-195.

Kepezhinskas, P., McDermott, F., Defant, M. J., Hochstaedter, A., Drummond, M. S., Hawkesworth, C. J., Koloskov, A., Maury, R. C. and Hellon, H., 1997. Trace element and Sr-Nd-Pb isotopic constraints on a three-component model of Kamchatka Arc petrogenesis. Geochimica et Cosmochimica Acta, 61 (3), 577-600.

Keppler, H., 1996. Constraints from partitioning experiments on the composition of subduction-zone fluids. Nature, 380, 237-240.

Keppler, H. and Wyllie, P., 1990. Role of fluids in transport and fractionation of uranium and thorium in magmatic processes. Nature, 348, 531-533.

Kigoshi, K., 1967. Ionium dating of igneous rocks. Science, 156, 932-934.

Korsch, R. J. and Wellman, H. W., 1988. The geological evolution of New Zealand and the New Zealand region. In: Nairn, A. E. M. The Pacific Ocean, The Ocean Basins and Margins, 7, Plenum, 411-482 pp.

Kushiro, I., 1983. On the lateral variation in chemical composition and volume of Quaternary volcanic rocks across Japanese arcs. Journal of Volcanology and Geothermal Research, 18, 435-447.

Kushiro, I. and Yoder, H. S., 1969. Melting of forsterite and enstatite at high pressure under hydrous conditions. Carnegie Institute of Washington Yearbook, 67, 153-158.

LaTourrette, T. Z. and Burnett, D. S., 1992. Experimental determination of U and Th partitioning between clinopyroxene and natural and synthetic basaltic liquid. Earth and Planetary Science Letters, 110, 227-244.

LaTourrette, T. Z., Kennedy, A. K. and Wasserburg, G. J., 1993. Thorium-uranium fractionation by garnet; evidence for a deep source and rapid rise of oceanic basalts. Science, 261, 739-742.

LaTourrette, T., Hervig, R. L. and Holloway, J. R., 1995. Trace-element partitioning between amphibole, phlogopite, and basanite melt. Earth and Planetary Science Letters, 135, 13-30.

Le Cloarec, M. F., Allard, P., Ardouin, B., Giggenbach, W. F. and Sheppard, D. S., 1992. Radioactive isotopes and trace elements in gaseous emissions from White Island, New Zealand. Earth and Planetary Science Letters, 108, 19-28.

Le Maitre, R. W., 1989. A classification of igneous rocks and a glossary of terms. Blackwell, Oxford,

Leeman, W. P. and Phelps, D. W., 1981. Partitioning of rare-earths and other trace-elements between sanidine and coexisting volcanic glass. Journal of Geophysical Research, 86 (B11), 193-199.

Lemarchand, F., Villemant, B. and Calas, G., 1987. Trace element distribution coefficients in alkaline series. Geochimica et Cosmochimica Acta, 51 (5), 1071-1081.

Lewis, K. B., 1994. The 1500-km-long Hikurangi Channel: trench-axis channel that escapes its trench, crosses a plateau, and feeds a fan drift. Geomarine Letters, 14, 19-28.

Liu, J., Bohlen, S. R. and Ernst, W. G., 1996. Stability of hydrous phases in subducting oceanic crust. Earth and Planetary Science Letters, 143, 161-171.

Ludwig, K. R., 1998. Using Isoplot/Ex version 1.0 - a geochronological toolkit for Microsoft Excel, Berkeley Geochronological Center Special Publication No. 1. Berkeley Geochronological Center, Berkeley, 45 pp.

Ludwig, K. R. and Titterington, D. M., 1994. Calculation of ^{230}Th/U isochrons, ages, and errors. Geochimica et Cosmochimica Acta, 58 (22), 5031-5042.

Luhr, J. F., Carmichael, I. S. E. and Varekamp, J. C., 1984. The 1982 eruptions of El Chichon volcano, Chiapas, Mexico; mineralogy and petrology of the anhydrite-bearing pummices. Journal of Volcanology and Geothermal Research, 23, 69-108.

Lundstrom, C. C., Shaw, H. F., Ryerson, F. J., Phinney, D. L., Gill, J. B. and Williams, Q., 1994. Compositional controls on the partitioning of U, Th, Ba, Pb, Sr and Zr between clinopyroxene and haplobasaltic melts: implications for uranium series disequilibria in basalts. Earth and Planetary Science Letters, 128, 407-423.

MacKinnon, T. C., 1983. Origin of the Torlesse terrane and coeval rocks, South Island, New Zealand. Geological Society of America Bulletin, 94, 967-985.

Mahood, G. A. and Stimac, J. A., 1990. Trace-element partitioning in pantellerites and trachytes. Geochimica et Cosmochimica Acta, 54 (8), 2257-2276.

Mahood, G. and Hildreth, W., 1983. Large partition coefficients for trace elements in high-silica rhyolites. Geochimica et Cosmochimica Acta, 47, 11-30.

Malhoff, A., Feden, R. H. and Fleming, H. S., 1982. Magnetic anomalies and tectonic fabric of marginal basins north of New Zealand. Journal of Geophysical Research, 87, 4109-4125.

Marsh, B. D., 1988. Crystal size distribution (CSD) in rocks and the kinetics and dynamics of crystallisation. Contributions to Mineralogy and Petrology, 99, 277-291.

Marsh, B. D., 1998. On the interpretation of crystal size distributions in magmatic systems. Journal of Petrology, 39 (4), 353-399.

McBirney, A. R., 1978. Volcanic evolution of the Cascade Range. Annual Review of Earth and Planetary Science, 6, 437-456.

McCulloch, M. T. and Gamble, J. A., 1991. Geochemical and Geodynamical constraints on subduction zone magmatism. Earth and Planetary Science Letters, 102, 358-374.

McDermott, F., Elliott, T. R., van Calsteren, P. and Hawkesworth, C. J., 1993. Measurement of $^{230}Th/^{232}Th$ ratios in young volcanic rocks by single-sector thermal ionisation mass spectrometry. Chemical Geology, 103, 283-292.

McDermott, F. and Hawkesworth, C. J., 1991. Th, Pb, and Sr isotope variations in young island arc volcanics and oceanic sediments. Earth and Planetary Science Letters, 104, 1-15.

McKenzie, D., 1984. The generation and compaction of partially molten rock. Journal of Petrology, 25, 713-765.

McKenzie, D., 1985a. The extraction of magma from the crust and mantle. Earth and Planetary Science Letters, 74, 81-91.

McKenzie, D. P., 1985b. ^{230}Th-^{238}U disequilibrium and the melting processes beneath ridge axes. Earth and Planetary Science Letters, 72, 149-157.

McKenzie, D. P., 1969. Speculations on the consequences and causes of plate motions. Geophysical Journal, 18, 1-32.

Miller, D. M., Goldstein, S. L. and Langmuir, C. H., 1994. Cerium/lead and lead isotope ratios in arc magmas and the enrichment of lead in the continents. Nature, 368, 514-520.

Minster, J. B. and Jordan, T. H., 1978. Present-day plate motions. Journal of Geophysical Research, 83, 5331-5354.

Miyashiro, A., 1974. Volcanic rock series in island arcs and active continental margins. American Journal of Science, 274, 321-355.

Moriguti, T. and Nakamura, E., 1998. Across-arc variation of Li isotopes in lavas and implications for crust/mantle recycling at subduction zones. Earth and Planetary Science Letters, 163, 167-174.

Morris, J. D., Leeman, W. P. and Tera, F., 1990. The subducted component in island arc lavas: constraints from Be isotopes and B-Be systematics. Nature, 344, 31-36.

Myers, J. D. and Johnston, A. D., 1996. Phase equilibria constraints on models of subduction zone magmatism. In: Bebout, G. E., Scholl, D. W., Kirby, S. H., and Platt, J. P. (Eds), Subduction: top to bottom, Geophysical Monograph, 96, American Geophysical Union, 229-249 pp.

Nairn, I. A., Kobayashi, T. and Nakagawa, M., 1998. The ~ 10 ka multiple vent pyroclastic eruption sequence at Tongariro Volcanic Centre, Taupo Volcanic Zone, New Zealand: Part 1. Eruptive processes during regional extension. Journal of Volcanology and Geothermal Research, 86, 19-44.

Nakagawa, M., Nairn, I. A. and Kobayashi, T., 1998. The ~ 10 ka multiple vent pyroclastic eruption sequence at Tongariro Volcanic Centre, Taupo Volcanic Zone, New Zealand: Part 2. Petrological insights into magma storage and transport during regional extension. Journal of Volcanology and Geothermal Research, 86, 45-65.

Nash, W. P. and Crecraft, H. R., 1985. Partition coefficients for trace elements in silicic magmas. Geochimica et Cosmochimica Acta, 49, 2309-2322.

Navon, O. and Stolper, E., 1987. Geochemical consequences of melt percolation: the upper mantle as a chromatographic column. Journal of Geology, 95 (3), 285-306.

Neall, V. E., Stewart, R. B. and Smith, I. E. M., 1986. History and petrology of the Taranaki volcanoes. Royal Society of New Zealand Bulletin, 23, 251-263.

Newman, S., Macdougall, J. D. and Finkel, R. C., 1986. Petrogenesis and ^{230}Th-^{238}U disequilibrium at Mt. Shasta, California, and in the Cascades. Contributions to Mineralogy and Petrology, 93, 195-206.

Nicholls, I. A., 1974. Liquids in equilibrium with peridotitic mineral assemblages at high water pressures. Contributions to Mineralogy and Petrology, 45, 289-316.

Nichols, G. T., Wyllie, P. J., and Stern, C. R., 1996. Experimental melting of pelagic sediment, constraints relevant to subduction. In: Bebout, G. E., Scholl, D. W., Kirby, S. H., and Platt, J. P. (Eds), Subduction: Top to bottom, Geophysical Monograph, 96, American Geophysical Union, 293-298 pp.

Nichols, G. T., Wyllie, P. J. and Stern, C. R., 1994. Subduction zone melting of pelagic sediments constrained by melting experiments. Nature, 371, 785-788.

Nicolas, A., 1986. A melt extraction model based on structural studies in mantle peridotites. Journal of Petrology, 27 (4), 999-1022.

O'Hara, M. J., 1977. Geochemical evolution during fractional crystallisation of a periodically refilled magma chamber. Nature, 266, 503-507.

O'Hara, M. J. and Mathews, R. E., 1981. Geochemical evolution in an advancing, periodically replenished, periodically tapped, continuously fractionated magma chamber. Journal of the Geological Society of London, 138, 237-277.

Osmond, J. K. and Cowart, J. B., 1992. Groundwater. In: Ivanovich, M. and Harmon, R. S. (Eds), Uranium-series disequilibrium—application to Earth, Marine and Environmental Science, Oxford Science, Oxford, 290-333.

Osmond, J. K. and Ivanovich, M., 1992. Uranium-series mobilization and surface hydrology. In: Ivanovich, M. and Harmon, R. S. (Eds), Uranium-series disequilibrium—applications to Earth, Marine, and Environmental Sciences. Oxford Science, Oxford, 259-289.

Oxburgh, E. R. and Turcotte, D. L., 1970. The thermal structure of island arcs. Geological Society of America Bulletin, 81, 1665-1688.

Palmer, K., Mortimer, N., Nathan, S., Isaac, M. J., Field, B. D., Sircombe, K. N., Black, P. M., Bush, S., and Orr, N. W., 1995. Chemical and petrographic analyses of some New Zealand Paleozoic-Mesozoic metasedimentary and igneous rocks, Institute of Geological and Nuclear Sciences Science Report 95/16, Institute of Geological and Nuclear Sciences Limited, Lower Hutt, New Zealand, 37 pp.

Panjasawatwong, Y., Danyushevsky, L. V., Crawford, A. J. and Harris, K. L., 1995. An experimental study of the effects of melt composition on plagioclase - melt equilibria at 5 and 10 kbar: implications for the origins of magmatic high-An plagioclase. Contributions to Mineralogy and Petrology, 118, 420-432.

Patterson, D. B. and Graham, I. J., 1988. Petrogenesis of andesitic lavas from Mangatepopo Valley and Upper Tama Lake, Tongariro Volcanic Centre, New Zealand . Journal of Volcanology and Geothermal Research, 35, 17-29.

Peacock, S. M., 1990. Fluid processes in subduction zones. Science, 248, 329-337.

Peacock, S. M., 1993. Large-scale hydration of the lithosphere above subducting slabs. Chemical Geology, 108, 49-59.

Peacock, S. M., 1991. Numerical simulation of subduction zone pressure-temperature-time paths: constraints on fluid production and arc magmatism. Philosophical Transactions of the Royal Society of London Series A, 335, 341-353.

Pearce, J. A., 1982. Trace element characteristics of lavas from destructive plate boundaries. In: Thorpe, R. S. (Ed), Andesites, John Wiley & Sons, Chichester, 525-548.

Pearce, J. A. and Parkinson, I. J., 1993. Trace element models for mantle melting: application to volcanic arc petrogenesis. In: Prichard, H. M., Alabaster, T., Harris, N. B. W., and Neary, C. R. (Eds), Magmatic processes and plate tectonics, Geological Society of London Special Publication, No. 76, Geological Society of London, London, 373-403.

Pearce, J. A. and Peate, D. W., 1995. Tectonic implications of the composition of volcanic arc magmas. Annual Review of Earth and Planetary Science, 23, 251-285.

Peate, D. W., Chen, J. H., Wasserburg, G. J., Papanastassiou, D. A. and Geissman, J. W., 1996. ^{238}U-^{230}Th dating of a geomagnetic excursion in Quaternary basalts of the Albuquerque Volcanoes Field, New Mexico (USA). Geophysical Research Letters, 23 (17), 2271-2274.

Peate, D. W., Pearce, J. A., Hawkesworth, C. J., Colley, H., Edwards, C. M. H. and Hirose, K., 1997. Geochemical variations in Vanuatu Arc lavas: the role of subducted material and a variable mantle wedge composition. Journal of Petrology, 38 (10), 1331-1358.

Perfit, M. R., Gust, D. A., Bence, A. E., Arculus, R. J. and Taylor, S. R., 1980. Chemical characteristics of island arc basalts. Implications for mantle sources. Chemical Geology, 30, 227-256.

Plank, T. and Johnson, M., 1997. Do subducted sediments melt beneath arc volcanoes? Some experimental answers. Abstract, State of the Arc '97, University of Adelaide.

Plank, T. and Langmuir, C. H., 1988. An evaluation of the global variations in the major element chemistry of arc basalts. Earth and Planetary Science Letters, 90, 349-370.

Plank, T. and Langmuir, C. H., 1992. Sediments melt and basaltic crust dehydrates at subduction zones. EOS, Transactions of the American Geophysical Union, 72, 637.

Plank, T. and Langmuir, C. H., 1998. The chemical composition of subducting sediment and its consequences for the crust and mantle. Chemical Geology, 145, 325-394.

Poli, S. and Schmidt, M. W., 1995. H_2O transport and release in subduction zones: Experimental constraints on basaltic and andesitic systems. Journal of Geophysical Research, 100 (B11), 22299-22314.

Potts, P. J., Thorpe, O. W., Issacs, M. C. and Wright, D. W., 1985. High precision neutron activation analysis of geological samples employing simultaneous counting with both planar and coaxial detectors. Chemical Geology, 48, 145-155.

Potts, P. J., Thorpe, O. W. and Watson, J. S., 1981. Determination of rare earth element abundances in 29 international rock standards by instrumental neutron activation analysis: a critical appraisal of calibration errors. Chemical Geology, 34, 331-352.

Preston, R. J., Bell, B. R. and Rogers, G., 1998. The Loch Scridain xenolithic sill complex, Isle of Mull, Scotland: Fractional crystallisation, assimilation, magma-mixing and crustal anatexis in subvolcanic conduits. Journal of Petrology, 39 (3), 519-550.

Price, R. C., McCulloch, M. T., Smith, I. E. M. and Stewart, R. B., 1992. Pb-Nd-Sr isotopic compositions and trace element characteristics of young volcanic rocks from Egmont Volcano and comparisons with basalts and andesites from the Taupo Volcanic Zone, New Zealand. Geochimica et Cosmochimica Acta, 56, 941-953.

Price, R. C., Smith, I. E. M., Waight, T. E., and Stewart, R. B., 1998. Processes controlling magma chemistry at Ruapehu Volcano, New Zealand. Abstract, IAVCEI meeting, Cape Town.

Price, R. C., Stewart, R. B., Woodhead, J. D. and Smith, I. E. M., 1999. Petrogenesis of high-K arc magmas: evidence from Egmont Volcano, North Island, New Zealand. Journal of Petrology, 40 (1), 167-197.

Price, R. C., Waight, T. E., Chapman, J. R., Bayer, E. E., Smith, I. E. M., and Stewart, R. B., 1997. The geochemical evolution of arc magmas in a continental setting: evidence from detailed chemo-stratigraphy at Ruapehu, New Zealand. Abstract, State of the Arc '97, University of Adelaide.

Pyle, D. M., 1992. The volume and residence time of magma beneath active volcanoes determined by decay-series disequilibria methods. Earth and Planetary Science Letters, 112, 61-73.

Pyle, D. M., 1994. Reply to comment by M. Condomines on "The volume and residence time of magma beneath active volcanoes determined by decay-series disequilibria methods". Earth and Planetary Science Letters, 122, 257-258.

Pyle, D. M., Dawson, J. B. and Ivanovich, M., 1991. Short lived decay series disequilibria in the natrocarbonatites lavas of Oldoinyo Lengai, Tanzania: constraints on the timing of magma genesis. Earth and Planetary Science Letters, 105, 378-396.

Pyle, D. M., Ivanovich, M. and Sparks, R. S. J., 1988. Magma-cumulate mixing identified by U-Th

disequilibrium dating. Nature, 331, 157-159.

Rapp, R. P. and Watson, E. B., 1986. Monazite solubility and dissolution kinetics: implications for the thorium and light rare earth chemisty of felsic magmas. Contributions to Mineralogy and Petrology, 94, 304-316.

Reagan, M. K., Morris, J. D., Herrstrom, E. A. and Murrel, M. T., 1994. Uranium series and beryllium isotope evidence for an extended history of subduction modification of the mantle below Nicaragua. Geochimica et Cosmochimica Acta, 59 (19), 4199-4212.

Reagan, M. K., Volpe, A. M. and Cashman, K. V., 1992. ^{238}U- and ^{232}Th-series chronology of phonolite fractionation at Mount Erebus, Antarctica. Geochimica et Cosmochimica Acta, 56, 1401-1407.

Regelous, M., Collerson, K. D., Ewart, A. and Wendt, J. I., 1997. Trace element transport rates in subduction zones: evidence from Th, Sr and Pb isotope data for Tonga-Kermadec arc lavas. Earth and Planetary Science Letters, 150, 291-302.

Reid, F. W., 1983. The origin of the rhyolitic rocks of the Taupo Volcanic Zone. Journal of Volcanology and Geothermal Research, 15, 315-338.

Reyners, M., 1980. A microearthquake study of the plate boundary, North Island, New Zealand. Geophysical Journal of the Royal Astronomical Society, 63, 1-22.

Rollinson, H., 1993. Using geochemical data. Longman Scientific & Technical, Harlow, 352 pp.

Rubin, K. H., Wheller, G. E., Tanzer, M. O., Macdougall, J. D., Varne, R. and Finkel, R., 1989. ^{238}U decay series systematics of young lavas from Batur volcano, Sunda Arc. Journal of Volcanology and Geothermal Research, 38, 215-226.

Rudnick, R., 1995. Making continental crust. Nature, 378, 571-578.

Rutherford, M. J. and Hill, P. M., 1993. Magma ascent rates from amphibole breakdown: an experimental study applied to the 1980-1986 Mount St. Helens eruptions. Journal of Geophysical Research, 98 (B11), 19667-19685.

Ryerson, F. J. and Watson, E. B., 1987. Rutile saturation in magmas: implications for Ti-Nb-Ta depletion in island-arc basalts. Earth and Planetary Science Letters, 86, 225-239.

Saunders, A. D. and Tarney, J., 1979. The geochemistry of basalts from a back-arc spreading centre in the East Scotia Sea. Geochimica et Cosmochimica Acta, 43, 555-572.

Schaeffer, S. J., Sturchio, N. C., Murrel, M. T. and Williams, S. N., 1993. Internal ^{238}U-series systematics of pumice from the November 13, 1985, eruption of Nevado del Ruiz, Columbia. Geochimica et Cosmochimica Acta, 57, 1215-1219.

Schmidt, M. W. and Poli, S., 1998. Experimentally based water budgets for dehydrating slabs and consequences for arc magma generation. Earth and Planetary Science Letters, 163, 361-379.

Shock, E. L., Sassani, D. C. and Betz, H., 1997. Uranium in geologic fluids: Estimates of standard partial molal properties, oxidation potentials, and hydrolysis constants at high temperatures and pressures. Geochimica et Cosmochimica Acta, 61 (20), 4245-4266.

Sigmarsson, O., 1996. Short magma chamber residence time at an Icelandic volcano inferred from U-series disequilibria. Nature, 382, 440-442.

Sigmarsson, O., Condomines, M., Morris, J. D. and Harmon, R. S., 1990. Uranium and ^{10}Be enrichments by fluids in Andean arc magmas. Nature, 346, 163-165.

Sigmarsson, O., Martin, H. and Knowles, J., 1998. Melting of a subducting oceanic crust from U-Th disequlibria in austral Andean lavas. Nature, 394, 566-569.

Simkin, T. and Siebert, L., 1994. Volcanoes of the World. Geoscience Press, Tucson, Arizona,

Sisson, T. W. and Grove, T. L., 1993a. Experimental investigations of the role of H_2O in calc-alkaline differentiation and subduction zone magmatism. Contributions to Mineralogy and Petrology, 113, 143-166.

Sisson, T. W. and Grove, T. L., 1993b. Temperatures and H_2O contents of low-MgO high-alumina basalts. Contributions to Mineralogy and Petrology, 113, 167-184.

Sleep, N. H., 1988. Tapping of melts by veins and dikes. Journal of Geophysical Research, 93 (B9), 10255-10272.

Smith, I. E. M., Worthington, T. J., Price, R. C. and Gamble, J. A., 1997. Primitive magmas in arc-type

volcanic associations: examples from the southwest Pacific. The Canadian Mineralogist, 35, 257-273.

Snyder, D. and Tait, S., 1998. The imprint of basalt on the geochemistry of silicic magmas. Earth and Planetary Science Letters, 160, 433-445.

Soengkono, S., 1995. A magnetic model for deep plutonic bodies beneath the central Taupo Volcanic Zone, North Island, New Zealand. Journal of Volcanology and Geothermal Research, 68, 193-207.

Sorenson, S. S. and Grossman, J. N., 1989. Enrichment of trace elements in garnet amphibolites from a paleo-subduction zone: Catalina Schist, southern California. Geochimica et Cosmochimica Acta, 53, 3155-3177.

Sparks, R. S. J. and Marshall, L. A., 1986. Thermal and mechanical constraints on mixing between mafic and silicic magmas. Journal of Volcanology and Geothermal Research, 29, 99-124.

Spiegelman, M. and Elliott, T., 1993. Consequences of melt transport for uranium series disequilibrium in young lavas. Earth and Planetary Science Letters, 118, 1-20.

Spiegelman, M. and McKenzie, D., 1987. Simple 2-D models for melt extraction at mid-ocean ridges and island arcs. Earth and Planetary Science Letters, 83, 137-152.

Stern, T. A., 1985. A back-arc basin formed within continental lithosphere: the central volcanic region of New Zealand. Tectonophysics, 112, 385-409.

Stern, T. A., 1987. Asymmetric back-arc spreading, heat flux and structure associated with the Central Volcanic Region of New Zealand. Earth and Planetary Science Letters, 85, 265-276.

Stern, T. A. and Davey, F. J., 1985. Crustal structure studies within the central North Island: the Central Volcanic Region, Geophysics Division Report 207, Department of Scientific and Industrial Research, Wellington, New Zealand, 47 pp.

Stern, T. A. and Davey, F. J., 1987. A seismic investigation of the crustal and upper mantle structure within the Central Volcanic Region of New Zealand. New Zealand Journal of Geology and Geophysics, 30, 217-231.

Stewart, R. B., Price, R. C. and Smith, I. E. M., 1996. Evolution of high-K arc magma, Egmont volcano, Taranaki, New Zealand: evidence from mineral chemistry. Journal of Volcanology and Geothermal Research, 74, 275-295.

Stipp, J. J., 1968. The geochronology and petrogenesis of the Cenozoic volcanics of the North Island, New Zealand. Unpublished PhD thesis, Australian National University.

Stix, J. and Gorton, M. P., 1990. Variations in trace-element partition-coefficients in sanidine in the Cerro Toledo rhyolite, Jenez Mountains, New Mexico - effects of composition, temperature, and volatiles. Geochimica et Cosmochimica Acta, 54 (10), 2697-2708.

Stock, J. and Molnar, P., 1982. Uncertainties in the relative positions of the Australia, Antarctica, Lord Howe and Pacific Plates since the late Cretaceous. Journal of Geophysical Research, 87, 4679-4714.

Stolper, E. and Newman, S., 1994. The role of water in the petrogenesis of Mariana trough magmas. Earth and Planetary Science Letters, 121, 293-325.

Sturchio, N. C., Binz, C. M. and Lewis, C. H., 1987. Thorium-uranium disequilibrium in a geothermal discharge zone at Yellowstone. Geochimica et Cosmochimica Acta, 51, 2025-2034.

Sun, S.-S., 1980. Lead isotopic study of young volcanic rocks from mid-ocean ridges, ocean islands, and island arcs. Philosophical Transactions of the Royal Society of London Series A, 297, 409-445.

Sutton, A. N., Blake, S. and Wilson, C. J. N., 1995. An outline geochemistry of rhyolite eruptives from Taupo volcanic centre, New Zealand. Journal of Volcanology and Geothermal Research, 68, 153-175.

Taddeucci, A., Broecker, W. S. and Thurber, D. L., 1967. ^{230}Th dating of volcanic rocks. Earth and Planetary Science Letters, 3, 338-342.

Takahashi, N., 1992. Evidence for melt segregation towards fractures in the Horoman mantle peridotite complex. Nature, 359, 52-55.

Tatsumi, Y., 1989. Migration of fluid phases and genesis of basalt magmas in subduction zones. Journal of Geophysical Research, 94, 4697-4707.

Tatsumi, Y. and Eggins, S., 1995. Subduction zone magmatism. Blackwell Scientific, Oxford, 211 pp.

Tatsumi, Y., Hamilton, D. L. and Nesbitt, R. W., 1986. Chemical characteristics of fluid phase released from a subducted lithosphere and origin of arc magmas: evidence from high-pressure experiments and natural

rocks. Journal of Volcanology and Geothermal Research, 29, 293-309.

Tatsumi, Y., Murasaki, M. and Nohda, S., 1992. Across-arc variation of lava chemistry in the Izu-Bonin arc: identification of subduction components. Journal of Volcanology and Geothermal Research, 49, 179-190.

Taylor, B. and Karner, G. D., 1983. On the evolution of marginal basins. Review of Geophysics and Space Physics, 21, 1727-1741.

Taylor, S. R. and McLennan, S. M., 1981. The composition and evolution of the continental crust: rare earth element evidence from sedimentary rocks. Philosophical Transactions of the Royal Society of London Series A, 301, 381-399.

Taylor, S. R. and McLennan, S. M., 1995. The geochemical evolution of the continental crust. Reviews of Geophysics, 33 (2), 241-265.

Tera, F., Brown, L., Morris, J., Sacks, I. S., Klein, J. and Middleton, R., 1986. Sediment incorporation in island-arc magmas: inferences from ^{10}Be. Geochimica et Cosmochimica Acta, 50, 535-550.

Thomas, L. E., 1998. Uranium series major and trace element geochemistry of lavas from Tenerife and Lanzarote, Canary Islands. Unpublished PhD thesis, The Open University.

Titterington, D. M. and Halliday, A. N., 1979. On the fitting of parallel isochrons and the method of maximum likelihood. Chemical Geology, 26, 183-195.

Toksöz, M. N. and Hsui, A. T., 1978. Numerical studies of back-arc convection and the formation of marginal basins. Tectonophysics, 50, 177-196.

Topping, W. W., 1973. Tephrostratigraphy and chronology of late Quaternary eruptives from the Tongariro Volcanic Centre, New Zealand. New Zealand Journal of Geology and Geophysics, 16, 397-423.

Topping, W. W. and Kohn, B. P., 1973. Rhyolitic tephra marker beds in the Tongariro area, North Island, New Zealand. New Zealand Journal of Geology and Geophysics, 16, 375-395.

Turner, S. and Hawkesworth, C., 1997. Constraints on flux rates and mantle dynamics beneath island arcs from Tonga-Kermadec lava geochemistry. Nature, 389, 568-573.

Turner, S., Hawkesworth, C., Rogers, N., Bartlett, J., Worthington, T., Hergt, J., Pearce, J. and Smith, I., 1997a. ^{238}U-^{230}Th disequilibria, magma petrogenesis, and flux rates beneath the depleted Tonga-Kermadec island arc. Geochimica et Cosmochimica Acta, 61 (22), 4855-4884.

Turner, S., Hawkesworth, C., Rogers, N. and King, P., 1997b. U-Th isotope disequilibria and ocean island basalt generation in the Azores. Chemical Geology, 139, 145-164.

Turner, S., Hawkesworth, C., van Calsteren, P., Heath, E., Macdonald, R. and Black, S., 1996. U-series isotopes and destructive plate margin magma genesis in the Lesser Antilles. Earth and Planetary Science Letters, 142, 191-207.

Turner, S., McDermott, F., Hawkesworth, C. and Kepezhinskas, P., 1998. A U-series study of lavas from Kamchatka and the Aleutians: constraints on source compositions and melting processes. Contributions to Mineralogy and Petrology, 133, 217-234.

van Calsteren, P. and Schwieters, J. B., 1995. Performance of a thermal ionization mass spectrometer with a deceleration lens system and post-deceleration detector selection. International Journal of Mass Spectrometry and Ion Processes, 146, 119-129.

Villemant, B. and Fléhoc, C., 1989. U-Th fractionation by fluids in K-rich magma genesis: the Vico volcano, Central Italy. Earth and Planetary Science Letters, 91, 312-326.

Villemant, B., Michaud, V. and Metrich, N., 1993. Wall rock-magma interactions in Etna, Italy, studied by U-Th disequilibrium and rare earth element systematics. Geochimica et Cosmochimica Acta, 57, 1169-1180.

Vine, F. J., 1966. Spreading of the ocean floor: new evidence. Science, 154, 1405-1415.

Vine, F. J. and Matthews, D. H., 1963. Magnetc anomalies over oceanic ridges. Nature, 199, 947-949.

Volpe, A. M., 1992. ^{238}U-^{230}Th-^{226}Ra disequilibrium in young Mt. Shasta andesites and dacites. Journal of Volcanology and Geothermal Research, 53, 227-238.

Volpe, A. M. and Hammond, P. E., 1991. ^{238}U-^{230}Th-^{226}Ra disequilibria in young Mount St. Helens rocks: time constraint for magma formation and crystallisation. Earth and Planetary Science Letters, 107, 475-486.

Volpe, A. M., Olivares, J. A. and Murrell, M. T., 1991. Determination of radium isotope ratios and

abundances in geologic samples by thermal ionization mass spectrometry. Analytical Chemistry, 63, 913-916.

Wadge, G., 1980. Output rate of magma from active central volcanoes. Nature, 288, 253-255.

Wadge, G., 1982. Steady state volcanism: evidence from eruption histories of polygenetic volcanoes. Journal of Geophysical Research, 87 (B5), 4035-4049.

Walcott, R. I., 1987. Geodetic strain and the deformational history of the North Island of New Zealand during the late Cainozoic. Philosophical Transactions of the Royal Society of London Series A, A321, 163-181.

Walcott, R. I., 1998. Modes of oblique compression: late Cenozoic tectonics of the South Island of New Zealand. Reviews of Geophysics, 36, 1-26.

Watson, B. E. and Brenan, J. M., 1987. Fluids in the lithosphere. Part I: Experimentally-determined wetting characteristics of CO_2-H_2O fluids and their implications for fluid transport, host-rock physical properties and fluid inclusion formation. Earth and Planetary Science Letters, 85, 497-515.

Watson, J., 1996. Fast and simple method of powder pellet preparation for x-ray fluorescence analysis. X-ray Spectrometry, 25, 173-174.

Wendt, I. and Carl, C., 1991. The statistical distribution of the mean squared weighted deviation. Chemical Geology, 86, 275-285.

Williams, R. W. and Gill, J. B., 1989. Effects of partial melting on the uranium decay series. Geochimica et Cosmochimica Acta, 55, 1607-1619.

Williams, R. W., Gill, J. B. and Bruland, K. W., 1986. Ra-Th disequilibria systematics: Timescale of carbonatite magma formation at Oldoinyo Lengai volcano, Tanzania. Geochimica et Cosmochimica Acta, 50, 1249-1259.

Wilson, C. J. N., 1993. Stratigraphy, chronology, styles and dynamics of late Quaternary eruptions from Taupo Volcano, New Zealand. Philosophical Transactions of the Royal Society of London Series A, 343. 205-306.

Wilson, C. J. N., Ambraseys, N. N., Bradley, J. and Walker, G. P. L, 1980. A new date for the Taupo eruption, New Zealand. Nature, 288, 252-253.

Wilson, C. J. N., Houghton, B. F., McWilliams, M. O., Lanphere, M. A., Weaver, S. D. and Briggs, R. M., 1995. Volcanic and structural evolution of Taupo Volcanic Zone, New Zealand: a review. Journal of Volcanology and Geothermal Research, 68, 1-28.

Wilson, J. T., 1965. A new class of faults and their bearing on continental drift. Nature, 207, 343-347.

Wilson, J. T., 1966. Did the Atlantic close and then re-open? Nature, 211, 676-681.

Wilson, M., 1989. Igneous petrogenesis, a global tectonic approach. Chapman and Hall, London, 466 pp.

Wood, B. J., Blundy, J. D. and Robinson, J. A. C., 1998. Crystal chemical constraints on the partitioning of U-series elements during mantle melting. Mineralogical Magazine, 62A, 1664.

Wood, B. J., Bryndzia, L. T. and Johnson, K. E., 1990. Mantle oxidation state and its relationship to tectonic environment and fluid speciation. Science, 248, 337-345.

Wood, C. P. and Browne, P. R. L., 1996. Chlorine-rich pyrometamorphic magma at White Island volcano, New Zealand. Journal of Volcanology and Geothermal Research, 72, 21-35.

Woodhead, J. D., Eggins, S. M. and Johnson, R. W., 1998. Magma genesis in the New Britain island arc: Further insights into melting and mass transfer processes. Journal of Petrology, 39 (9), 1641-1668.

Woodhead, J., Eggins, S. and Gamble, J., 1993. High field strength and transition element systematics in island arc and back-arc basin basalts: evidence for multi-phase melt extraction and a depleted mantle wedge. Earth and Planetary Science Letters, 114, 491-504.

Wright, I. C, 1992. Shallow structure and active tectonism of an offshore continental spreading system: the Taupo Volcanic Zone, New Zealand. Marine Geology, 103, 287-309.

Wright, I. C., 1993. Pre-spread rifting and heterogeneous volcanism in the southern Havre Trough back-arc basin. Marine Geology, 113, 179-200.

Wright, I. C. and Walcott, R. I., 1986. Large tectonic rotation of part of New Zealand in the last 5 Ma. Earth and Planetary Science Letters, 80, 348-352.

Zellmer, G. F., 1998. Petrogenetic processes and their timescales beneath Santorini, Aegean Volcanic Arc, Greece. Unpublished PhD thesis, The Open University.

Appropriate for the appendices? Possibly some chapters as well...,

Nvnc id vides, nvnc ne vides

The motto of the Unseen University.

from 'The concife and possibly even accuratte Mapp' and 'Discworld Companion' – Terry Pratchett & Stephen Briggs.

Appendix A

Conventions and Abbreviations

This appendix lists the abbreviations and conventions used in this thesis. Where the abbreviations and conventions are first used in the text, they are explained. This appendix provides a subsequent reference for the reader.

A-1 Abbreviations

The majority of abbreviations used in this thesis are terms used throughout the literature, but are listed here for completeness.

AFC – Assimilation-Fractional Crystallisation
BAB – Back-Arc Basalt
CVR – Central Volcanic Region
ESC – Essential Structural Component
GLOSS – GLObal Subducting Sediment
HAB – High Alumina Basalt
HMB – High Magnesium Basalt
HFSE – High Field Strength Element
HREE – Heavy Rare Earth Elements
ICP-MS – Inductively Coupled Plasma Mass Spectrometry
INAA – Instrumental Neutron Activation Analysis
LILE – Large Ion Lithophile Elements
LREE – Light Rare Earth Elements
MORB – Mid Ocean Ridge Basalt
MSWD – Mean Squares Weighted Deviates
N-MORB – Normal MORB
NNO – Nickel-Nickel Oxide
OIB – Ocean Island Basalt
POCT – Plagioclase-Olivine-Clinopyroxene-Titanomagnetite
QFM – Quartz-Fayalite-Magnetite

REE – Rare Earth Elements
RTF – Replenished Tapped Fractionated
TIMS – Thermal Ionisation Mass Spectrometry
TVZ – Taupo Volcanic Zone
ToVC – Tongariro Volcanic Centre
XRF – X-Ray Fluorescence

A-2 Conventions for Short-Lived Isotopes

In order to remove the possibility for confusion between activity and absolute abundance of short-lived isotopes, activities are conventionally denoted by parentheses, and abundances by square brackets. Thus (^{230}Th) refers to the activity of ^{230}Th, whereas [^{230}Th] refers to the absolute abundance.

A-3 Conventions for Units

Throughout the thesis, the main units used for quoting concentrations are wt% for major element oxide abundances and μg g^{-1} for trace element concentrations. Whilst μg g^{-1} and ppm are interchangeable, the use of μg g^{-1} is preferred as it follows SI conventions. Where certain low abundance short-lived isotopes are discussed, SI conventions are followed and nanogram, picogram and femtogram quantities are denoted by ng g^{-1}, pg g^{-1} and fg g^{-1} respectively.

A-4 Conventions for Partition Coefficients

The convention used for partition coefficients in this thesis adopts the practice recommended by Beattie et al. (1993). Accordingly, the partition coefficient for a given element (X) between a mineral phase (min) and the parental magma (liq) is defined as,

$$D_X^{min} = \frac{C_X^{min}}{C_X^{liq}}$$

where C_X^{min} is the concentration of element X in the mineral phase, and C_X^{liq} is the concentration of element X in the parental magma. The bulk partition coefficient for a system is defined in terms of the whole crystallising assemblage (cryst) rather than a single mineral phase, and is denoted as follows,

$$\overline{D}_X^{cryst/liq} = \frac{C_X^{cryst}}{C_X^{liq}}$$

where C_X^{cryst} is the concentration of element X in the crystallising assemblage, and the bulk partition coefficient is denoted by an overbar.

Where partition coefficients are expressed relative to a coefficient for a different element, the term exchange partition coefficient is used, which is given by,

$$K_{DX/Y}^{min/liq} = \frac{D_X^{min}}{D_Y^{min}}$$

where X and Y are the elements of interest and K_D represents the exchange partition coefficient. As with normal partition coefficients, a bulk exchange partition coefficient is denoted by an overbar.

A-5 Conventions for Quoted Errors

The errors quoted in this thesis are based on reproducibility of samples and standards unless otherwise noted, and are given/shown at the 2σ level. Internal precision on isotope measurements are generally lower than the quoted reproducibility. Isochron fitting is done using 2σ errors for individual samples. Full details of the quality assurance procedures undertaken are given in Appendix D.

Appendix B

Sample Details

This appendix lists the location and description of the samples used in this study. Samples R95-17, R95-18, R95-19, R95-20, R95-21, R95-22, R95-23, R95-25, R95-26, R95-27 and R95-28 from the Whangaehu section were collected in 1995 by R.C. Price and I.E.M. Smith, and were only available as powders and so are not described in detail. These were collected from a ridge on the south side of the Whangaehu Gorge, between grid references T20-27360 62095 and T20-37336 62095. Samples from Edgecumbe, White Island and historic eruptions from Ruapehu were obtained from J.A. Gamble as rock fragments. Samples from Taranaki (Egmont) were obtained from R.C. Price as powders and are not described in detail – petrographic descriptions of typical Taranaki lavas are available in the literature (Price et al., 1992; Stewart et al., 1996; Price et al., 1999).

B-1 Ruapehu Sample Descriptions

X1-9
Grid Reference: T20-27357 62137
Latitude/Longitude: 39°15.20′ S / 175°36.42′ E
Rock type: Basaltic andesite
Age: Unknown, field locality suggest the flow is part of the Mangawhero Formation (15-60 ka).
Field description: ~7m thick flow at base of thick, ~200m high section in the Ohinepango Stream valley.
Petrographic description: Plag and cpx phenocrysts dominate with minor opx. Rare titanomagnetite microphenocrysts are present. Groundmass is crystalline, formed of plag microlites and abundant opaques. Occasional gabbroic glomerocrysts are present

X1-10
Grid Reference: T20-27357 62137
Latitude/Longitude: 39°15.20′ S / 175°36.26′ E
Rock type: Basaltic andesite
Age: Unknown, field locality suggest the flow is part of the Mangawhero Formation (15-60 ka).
Field description: ~10m thick flow immediately overlying X1-9 in the Ohinepango Stream valley.
Petrographic description: Plag, cpx and opx abundant with minor titanomagnetite microphenocrysts. Groundmass is crystalline, formed of plag microlites and abundant opaques.

X1-11
Grid Reference: T20-27357 62137

Latitude/Longitude: 39°15.20′ S / 175°36.26′ E
Rock type: Basaltic andesite
Age: Unknown, field locality suggest the flow is part of the Mangawhero Formation (15-60 ka).
Field description: ~6m thick flow overlying X1-10 in the Ohinepango Stream valley.
Petrographic description: Available as powder only.

X1-12
Grid Reference: T20-27357 62137
Latitude/Longitude: 39°15.20′ S / 175°36.26′ E
Rock type: Basaltic andesite
Age: Unknown, field locality suggest the flow is part of the Mangawhero Formation (15-60 ka).
Field description: ~8m thick flow overlying X1-11 in the Ohinepango Stream valley.
Petrographic description: Available as powder only.

X1-13
Grid Reference: T20-27357 62137
Latitude/Longitude: 39°15.20′ S / 175°36.26′ E
Rock type: Andesite
Age: Unknown, field locality suggest the flow is part of the Mangawhero Formation (15-60 ka).
Field description: ~2-3m thick flow overlying X1-12 in the Ohinepango Stream valley.
Petrographic description: Plag, cpx and opx are abundant. Moderately crystalline groundmass comprising plag microlites and opaques. Occasional small meta-greywacke xenoliths.

X1-14
Grid Reference: T20-27357 62137
Latitude/Longitude: 39°15.20′ S / 175°36.26′ E
Rock type: Andesite
Age: Unknown, field locality suggest the flow is part of the Mangawhero Formation (15-60 ka).
Field description: Flow overlying X1-13 in the Ohinepango Stream valley.
Petrographic description: Available as powder only.

X1-15
Grid Reference: T20-27357 62137
Latitude/Longitude: 39°15.20′ S / 175°36.26′ E
Rock type: Basaltic andesite
Age: Unknown, field locality suggest the flow is part of the Mangawhero Formation (15-60 ka).
Field description: Thin, ~2m thick flow at the top of the Ohinepango Stream section.
Petrographic description: Plag and cpx phenocrysts dominate with minor opx. Rare titanomagnetite micro-phenocrysts are present. Groundmass is crystalline, formed of plag microlites and abundant opaques. Occasional gabbroic glomerocrysts are present

R96-2
Grid Reference: T20-27350 62068
Latitude/Longitude: Indeterminate by GPS.
Rock type: Andesite
Age: Unknown, field locality suggest the flow is part of the Waihianoa Formation (60-150 ka).
Field description: Lava flow ~200m above the north bank of the Waihianoa River overlooking footbridge for the Round the Mountain Track, ~50m below ridge crest.
Petrographic description: Abundant plag, cpx and opx with minor titanomagnetite and ilmenite. Groundmass is relatively glassy with plag microlites and opaques. Glomerocrysts of pyroxenite and anorthite are present.

R96-7
Grid Reference: T20-27349 62069
Latitude/Longitude: Indeterminate by GPS.
Rock type: Andesite
Age: Unknown, field locality suggest the flow is part of the Waihianoa Formation (60-150 ka).
Field description: Lava flow ~200m above the north bank of the Waihianoa River overlooking footbridge for the Round the Mountain Track, ~50m below ridge crest.
Petrographic description: Plag more abundant than cpx and opx. Groundmass is crystalline with abundant plag microlites and opaques. Occasional meta-greywacke xenoliths are present.

R96-15

Grid Reference: T20-27359 62095
Latitude/Longitude: 39°17.46′ S / 175°36.59′ E
Rock type: Andesite
Age: Unknown, field locality suggest the flow is part of the Waihianoa Formation (60-150 ka).
Field description: Flow at base of thick section on the south side of the old Whangaehu valley.
Petrographic description: Plag, cpx and opx abundant with rare titanomagnetite phenocrysts. Groundmass is relatively glassy but contains abundant plag microlites and opaques. Rare granulite xenoliths are present.

R96-18

Grid Reference: T20-27359 62095
Latitude/Longitude: 39°17.46′ S / 175°36.59′ E
Rock type: Basaltic andesite
Age: Unknown, field locality suggest the flow is part of the Waihianoa Formation (60-150 ka).
Field description: Lava, two flows above R96-15 on the south south of the old Whangaehu valley.
Petrographic description: Plag, cpx and opx with minor titanomagnetite microphenocrysts. Groundmass is relatively glassy with plag microlites and opaques. Small veins of hydrothermal alteration are ubiquitous.

R96-25

Grid Reference: T20-27351 62181
Latitude/Longitude: 39°12.80′ S / 175°36.38′ E
Rock type: Andesite
Age: 5-10 ka (Hackett & Houghton, 1989), ~10-12 ka based on field evidence (degree of erosion and amount of overlying tephra suggests probably older than most of the Whakapapa Formation).
Field description: Lava flow forming a break-out from R96-26, erupted from Saddle Cone parasitic vent. Locality ~1 km south of Lower Tama Lake and 500m south of the Waihohonu Track.
Petrographic description: Cpx and opx are more dominant than plag, and abundant titanomagnetite phenocrysts. Groundmass is relatively glassy with large quantities of opaque minerals.

R96-26

Grid Reference: T20-27349 62181
Latitude/Longitude: 39°12.84′ S / 175°36.18′ E
Rock type: Andesite
Age: 5-10 ka (Hackett & Houghton, 1989), ~10-12 ka based on field evidence (degree of erosion and amount of overlying tephra suggests probably older than most of the Whakapapa Formation).
Field description: Main lava flow from Saddle Cone parasitic vent. Locality ~1 km south of Lower Tama Lake and 500m south of the Waihohonu Track.
Petrographic description: Cpx and opx are more dominant than plag, and abundant titanomagnetite phenocrysts. Groundmass is relatively glassy with large quantities of opaque minerals.

R96-10

Grid Reference: S20-27298 62038
Latitude/Longitude: 39°20.69′ S / 175°32.97′ E
Rock type: Andesite
Age: >17 ka and possibly >22 ka based on local tephra chronology (R.B. Stewart, pers. comm.).
Field description: One of a sequence of voluminous flows from the Rangataua vent on the southern flank of Ruapehu. Sample taken from locality near the Mangaehuehu Hut on the Round the Mountain Track.
Petrographic description: Plag, cpx and opx with minor titanomagnetite phenocrysts. Groundmass is relatively glassy with abundant opaques. Gabbroic glomerocrysts are present.

R96-24

Grid Reference: T20-27360 62099
Latitude/Longitude: 39°17.35′ / 175°17.35′
Rock type: Andesite
Age: Unknown, probably associated with Mangawhero Formation (15-60 ka).
Field description: Forms part of a large knoll between the old and recent Whangaehu valleys, north of R96-15 and R96-18.
Petrographic description: Abundant plag with minor cpx and opx. Groundmass is glassy, comprising glass, plag microlites and opaques. Meta-greywacke xenoliths and gabbroic glomerocrysts are present.

R96-14

Grid Reference: T20-27424 62107
Latitude/Longitude: 39°16.69′ S / 175°41.36′ E
Rock type: Dacite
Age: Thought to be a young flow (~10-15 ka) associated with the Whakapapa Formation on the basis of field evidence.
Field description: Small outcrop of a thin lava flow at the edge of the Tukino Mountain Road, Rangipo Desert.
Petrographic description: Very abundant, large phenocrysts of plag, cpx and opx with rare titanomagnetite microphenocrysts. Groundmass is relatively glassy with plag microlites. Some anorthite and gabbroic glomerocrysts are present.

W9-3
Grid Reference: T20-27356 62104
Latitude/Longitude: 39°17.05′ S / 175°35.00′ E
Rock type: Andesite
Age: Unknown, thought to be associated with the Mangawhero Formation (15-60 ka).
Field description: Thick, foliated lava flow near top of north side of Whangaehu Gorge.
Petrographic description: Abundant plag, cpx and opx phenocrysts with rare magnetite microphenocrysts. Groundmass is relatively crystalline with abundant opaques and plag microlites.

W9-5
Grid Reference: T20-27337 62101
Latitude/Longitude: 39°17.07′ S / 175°37.07′ E
Rock type: Andesite
Age: Unknown, probably associated with the Mangawhero Formation (15-60 ka).
Field description: ~5m thick flow from the south side of the Whangaehu Gorge, near a major waterfall at the west end of a deep cut gorge.
Petrographic description: Plag, cpx and opx are abundant, Groundmass is relatively glassy with plag microlites and opaques. Slighty vesicular.

X1-6
Grid Reference: T20-27387 62134
Latitude/Longitude: 39°14.35′ S / 175°38.57′ E
Rock type: Andesite
Age: Unknown, probably associated with the Mangawhero Formation (15-60 ka).
Field description: Crags of a 5m thick flow NNW of the Mangatoetoenui River.
Petrographic description: Plag, cpx and opx abundant with rare titanomagnetite phenocrysts. Groundmass relatively crystalline with abundant plag microlites and opaques.

RU-1971A
Grid Reference:
Latitude/Longitude:
Rock type: Andesite
Age: Erupted in 1971.
Field description: A fragment of scoriaceous bomb, erupted in the summit region.
Petrographic description: Small plagioclase phenocrysts are common with occasional pyroxene phenocrysts. The matrix is glassy and highly vesicular.

JG-95-RUA-001
Grid Reference:
Latitude/Longitude:
Rock type: Andesite
Age: Erupted in 1995.
Field description: Small tephra fragments erupted in the summit region.
Petrographic description: Glassy, vesicular matrix. Contains abundant small ?pyroxene phenocrysts. Plagioclase is not evident as a phenocryst phase.

P5731A
Grid Reference:
Latitude/Longitude:
Rock type: Andesite

Age: Erupted in 1995.
Field description: Tephra fragments erupted in the summit region.
Petrographic description: Highly vesicular, dark glassy matrix. Abundant plagioclase phenocrysts and occasional pyroxene phenocrysts.

P57535
Grid Reference:
Latitude/Longitude:
Rock type: Andesite
Age: Erupted in 1996.
Field description: Small fragments of tephra erupted in the summit region.
Petrographic description: Matrix is glassy and vesicular. The fragments have a somewhat brown, oxidised appearance. Small plagioclase and pyroxene phenocrysts are present.

P57536
Grid Reference:
Latitude/Longitude:
Rock type: Andesite
Age: Erupted in 1996.
Field description: Fragments of juvenile material erupted from the summit region.
Petrographic description: Matrix is somewhat red-brown in colour and only slightly vesicular. Abundant plagioclase and subordinate pyroxene phenocrysts are present.

B-2 Edgecumbe Sample Descriptions

Ac
Grid Reference:
Latitude/Longitude:
Rock type: Andesite
Age: 3-6 ka.
Field description: Sample of a lava flow from Edgecumbe volcano.
Petrographic description: Grey-brown matrix with occasional vesicles. Abundant large plagioclase phenocrysts (up to 3-4 mm) with small amounts of pyroxene (< 0.5 mm).

Bb
Grid Reference:
Latitude/Longitude:
Rock type: Andesite
Age: 3-6 ka.
Field description: Sample of a lava flow from Edgecumbe volcano.
Petrographic description: Grey-green granular groundmass. Abundant small plagioclase phenocrysts (< 1 mm) with subordinate pyroxene (< 0.5 mm).

B-3 White Island Sample Descriptions

WI008
Grid Reference:
Latitude/Longitude:
Rock type: Andesite
Age: Erupted this century.
Field description: Sample of lava from White Island volcano.
Petrographic description: Dark, glassy matrix with occasional vesicles. Abundant plagioclase and pyroxene phenocrysts with occasional small, ?titanomagnetite crystals present.

WIO12
Grid Reference:
Latitude/Longitude:
Rock type: Andesite

Age: Erupted this century.
Field description: Sample of scoriaceous ejecta from White Island volcano.
Petrographic description: Dark, glassy, highly vesicular matrix. Small plagioclase phenocrysts are common.

Appendix C

Geochemical Data

This appendix presents all the XRF, INAA and isotopic analyses performed during this study. Where multiple analyses of a sample were made, the data listed in the main tables are averages of all the analyses, and the individual analyses are listed in the tables of repeat analyses. Where insufficient sample prevented analysis for some data, values obtained by other workers have been included in the tables. Major elements are given as oxide wt%, and trace element and REE data are given in $\mu g\ g^{-1}$.

Although data for Mo and As was obtained for each of the samples as these elements are analysed for as standard by XRF at the Open University, the data has been omitted from the tables here as the abundances in these samples were below detection limits. Data for S has been left in the tables for reference, although concentrations are typically around machine detection limits. Data for loss on ignition is not shown as the values were insignificant (typically $-0.1 \leq LOI \leq 0.1$). Similarly, raw data is given as the effects of anhydrous normalisation are insignificant.

List of Tables

List of Abbreviations Used in Tables

OH	Ohinepango Stream Sequence
WHA	Whangaehu Gorge Sequence
WAI	Waihianoa Gorge Sequence
PAR	Parasitic cones
TC	This century
MISC	Miscellaneous young valley filling flows
EDG	Edgcumbe volcano
WI	White Island volcano
TAR	Taranaki volcano

List of Notes to Tables

a XRF major and trace element data are averages of multiple analyses

b XRF major and trace element data courtesy of John Gamble

c Isotopic data are a weighted average of multiple analyses

d XRF data, ICP-MS and Sr, Nd, Pb isotope analyses courtesy of Richard Price

Table C-1

Group	OH	OH	OH	OH	OH	OH	OH	PAR
Sample	X1-9	X1-10	X1-11	X1-12	X1-13[a]	X1-14	X1-15	R96-25
SiO_2	55.78	56.53	56.33	56.79	59.14	58.75	57.90	57.72
TiO_2	0.760	0.774	0.758	0.750	0.682	0.667	0.677	0.715
Al_2O_3	17.05	18.13	18.40	17.37	17.06	17.30	16.74	16.69
Fe_2O_3	8.63	7.85	7.73	8.21	7.34	7.23	7.35	7.71
MnO	0.140	0.124	0.123	0.130	0.110	0.110	0.123	0.126
MgO	5.02	4.05	4.16	5.37	4.33	4.25	4.92	4.56
CaO	8.15	7.89	7.98	8.13	7.03	7.07	7.65	7.31
Na_2O	3.04	3.24	3.27	3.06	3.38	3.40	3.19	3.07
K_2O	1.05	1.20	1.17	1.11	1.29	1.23	1.23	1.50
P_2O_5	0.123	0.141	0.137	0.130	0.116	0.114	0.116	0.127
Total	99.74	99.93	100.06	101.05	100.48	100.12	99.90	99.53
Rb	32.9	36.4	34.8	33.0	44.2	40.6	38.1	56.9
Sr	234	277	270	255	238	232	253	248
Y	21.5	21.6	21.3	21.2	21.4	21.3	20.6	20.6
Zr	84	91	91	87	99	94	96	116
Nb	3.4	3.1	3.5	4.5	4.5	3.6	4.0	4.5
Ba	261	300	303	288	321	357	315	318
Pb	7	11	8	4	11	4	8	9
Th	4	3	3	5	4	3	3	6
U	2	1	1	1	1	0	1	1
Sc	31	26	25	29	24	22	24	25
V	232	218	213	231	187	199	198	193
Cr	74	51	57	133	63	55	78	70
Co	30	21	47	55	23	88	25	24
Ni	26	21	24	46	27	29	30	26
Cu	63	67	46	46	53	46	50	30
Zn	79	76	70	73	70	70	74	74
Ga	19	18	18	18	20	18	18	16
S	28	35	35	35	26	29	32	44
La	9.2	10.9	n.d.	n.d.	12.0	n.d.	10.7	12.1
Ce	24.0	24.0	n.d.	n.d.	23.7	n.d.	22.9	26.3
Nd	11.2	13.5	n.d.	n.d.	13.5	n.d.	13.4	14.0
Sm	2.95	3.26	n.d.	n.d.	3.15	n.d.	3.07	3.17
Eu	0.88	0.91	n.d.	n.d.	0.94	n.d.	0.84	0.87
Tb	0.56	0.56	n.d.	n.d.	0.60	n.d.	0.51	0.57
Yb	2.16	2.12	n.d.	n.d.	2.13	n.d.	1.97	2.19
Lu	0.33	0.32	n.d.	n.d.	0.32	n.d.	0.32	0.34
Th	3.64	3.66	n.d.	n.d.	3.50	n.d.	4.03	5.37
U	1.2	1.0	n.d.	n.d.	1.1	n.d.	1.2	1.5
Ta	0.29	0.26	n.d.	n.d.	0.23	n.d.	0.25	0.34
Hf	2.86	2.71	n.d.	n.d.	2.69	n.d.	2.75	3.21
Cs	1.35	2.31	n.d.	n.d.	1.38	n.d.	2.77	3.30
Zn	81	79	n.d.	n.d.	81	n.d.	76	78
Co	24.5	23.1	n.d.	n.d.	22.6	n.d.	24.7	23.5
Cr	69	87	n.d.	n.d.	64	n.d.	113	74
Sc	25.2	26.1	n.d.	n.d.	25.2	n.d.	25.9	25.8

Table C-1 cont.

Group	PAR	PAR	WAI	WAI	WHA	WHA	WHA
Sample	R96-26	R96-10[a]	R96-2[a]	R96-7	R95-17	R95-18	R95-19
SiO_2	58.42	59.38	59.62	60.68	57.18	58.64	58.41
TiO_2	0.719	0.745	0.763	0.704	0.665	0.701	0.691
Al_2O_3	16.30	17.18	16.98	17.15	19.51	19.86	19.82
Fe_2O_3	7.52	7.06	7.30	6.52	6.20	6.00	6.06
MnO	0.122	0.117	0.115	0.104	0.095	0.090	0.093
MgO	4.50	3.22	3.56	2.87	3.52	2.26	2.25
CaO	7.18	6.50	6.43	6.14	8.07	7.57	7.38
Na_2O	3.09	3.26	3.29	3.43	3.57	3.85	3.81
K_2O	1.62	1.76	1.63	1.71	1.16	1.21	1.23
P_2O_5	0.132	0.139	0.142	0.130	0.125	0.126	0.127
Total	99.60	99.36	99.83	99.44	100.10	100.31	99.87
Rb	63.9	69.7	55.8	60.7	34.8	36.1	36.3
Sr	247	251	273	246	329	312	306
Y	21.9	22.2	23.9	25.2	16.2	19.0	21.5
Zr	124	134	126	128	90	95	95
Nb	3.5	4.2	5.2	4.8	3.9	4.1	3.9
Ba	344	375	393	389	307	303	310
Pb	8	11	9	9	6	7	7
Th	6	8	7	7	4	2	1
U	3	1	1	1	1	0	1
Sc	23	20	22	20	19	16	21
V	175	165	190	166	171	179	179
Cr	94	30	32	26	83	16	14
Co	21	17	22	18	45	50	42
Ni	26	8	14	13	37	16	16
Cu	32	23	48	34	42	57	68
Zn	68	71	72	75	59	66	67
Ga	16	19	19	18	19	19	18
S	41	32	47	32	77	24	31
La	13.0	14.5	14.7	15.6	9.5	10.6	12.8
Ce	28.0	32.7	31.8	32.6	20.2	21.9	26.1
Nd	14.9	16.1	16.9	17.6	10.5	12.6	14.4
Sm	3.27	3.52	3.68	3.88	2.62	2.91	3.49
Eu	0.87	0.94	0.98	1.00	0.81	0.86	0.92
Tb	0.60	0.64	0.64	0.69	0.43	0.52	0.60
Yb	2.19	2.32	2.26	2.43	1.68	1.88	2.12
Lu	0.32	0.33	0.37	0.39	0.26	0.29	0.32
Th	5.69	6.48	5.48	5.76	3.32	3.43	3.49
U	1.6	1.8	1.4	1.5	1.1	1.1	1.0
Ta	0.35	0.41	0.36	0.39	0.51	0.57	0.42
Hf	3.40	3.62	3.44	3.49	2.39	2.56	2.65
Cs	3.74	3.93	2.40	1.90	1.38	1.95	1.40
Zn	78	76	78	79	66	62	71
Co	22.9	16.9	19.3	16.6	39.2	43.0	36.6
Cr	94	33	35	25	82	12	13
Sc	25.6	21.7	22.7	19.8	17.9	16.4	16.6

Table C-1 cont.

Group	WHA	WHA	WHA	WHA	WHA	WHA	WHA	WHA	WHA
Sample	R95-20	R95-21	R95-22	R95-23	R95-25	R95-26	R95-27	R95-28	R96-15
SiO_2	56.65	58.09	57.95	58.72	56.02	57.13	58.14	57.88	57.90
TiO_2	0.688	0.752	0.753	0.745	0.714	0.644	0.671	0.672	0.664
Al_2O_3	15.59	17.38	17.37	17.23	17.79	17.21	20.47	20.46	16.88
Fe_2O_3	7.97	7.70	7.67	7.48	8.21	7.49	5.61	5.58	7.96
MnO	0.128	0.122	0.120	0.118	0.129	0.124	0.083	0.085	0.129
MgO	6.61	4.30	4.24	4.24	4.67	5.28	2.36	2.30	4.77
CaO	8.93	7.29	7.28	7.03	7.86	8.01	7.89	7.86	7.65
Na_2O	2.88	3.26	3.25	3.25	3.21	3.29	3.80	3.77	3.17
K_2O	0.96	1.32	1.34	1.44	0.94	0.90	1.25	1.25	1.13
P_2O_5	0.099	0.132	0.133	0.133	0.119	0.106	0.136	0.134	0.109
Total	100.51	100.35	100.11	100.39	99.66	100.18	100.41	99.99	100.36
Rb	29.8	41.9	44.5	48.8	27.3	26.8	38.2	38.6	37.0
Sr	207	272	275	266	270	272	341	342	228
Y	18.7	23.8	21.8	21.9	17.5	17.8	19.1	19.5	21.9
Zr	82	104	108	114	78	72	95	98	88
Nb	3.8	4.4	5.1	4.6	3.8	3.9	3.9	3.7	2.8
Ba	223	331	326	342	256	233	334	323	270
Pb	6	8	7	7	6	6	6	6	6
Th	5	3	6	4	3	3	5	4	7
U	0	2	0	1	2	1	2	1	2
Sc	33	26	25	24	30	29	16	16	25
V	224	218	206	202	223	212	160	157	209
Cr	259	31	30	39	45	101	31	31	68
Co	47	48	50	48	69	57	28	34	28
Ni	56	16	17	19	32	50	22	20	35
Cu	72	37	47	39	66	65	31	44	56
Zn	67	75	74	74	77	73	59	56	72
Ga	17	18	18	18	19	18	19	20	19
S	22	29	24	41	94	31	21	24	28
La	9.0	13.5	12.5	13.7	7.8	7.8	11.8	11.6	9.0
Ce	16.9	28.8	26.7	26.4	18.1	16.8	22.9	25.8	19.7
Nd	10.4	15.8	14.7	16.4	9.4	9.7	12.8	14.7	12.2
Sm	2.66	3.73	3.44	3.66	2.6	2.45	2.92	3.15	2.76
Eu	0.75	0.95	0.91	0.84	0.85	0.76	0.89	0.93	0.84
Tb	0.51	0.61	0.57	0.55	0.51	0.49	0.52	0.56	0.52
Yb	1.91	2.27	2.15	2.09	1.77	1.79	1.80	1.94	2.11
Lu	0.28	0.33	0.34	0.34	0.27	0.30	0.30	0.31	0.34
Th	2.72	4.29	4.22	4.39	2.57	2.45	3.65	3.70	3.24
U	0.9	1.5	1.1	1.9	0.9	0.9	1.1	1.1	0.9
Ta	0.44	0.54	0.52	0.51	0.63	0.46	0.40	0.51	0.22
Hf	2.21	2.83	2.84	3.02	2.19	2.13	2.58	2.72	2.47
Cs	1.71	1.20	1.80	2.70	1.70	0.80	1.00	1.10	1.30
Zn	82	79	77	76	80	78	67	54	78
Co	42.4	42.1	42.4	40.7	61.4	49.4	26.6	31.4	25.3
Cr	279	32	33	36	50	115	35	35	74
Sc	32.3	26.4	26.0	25.2	28.1	27.2	15.1	15.0	27.0

Table C-1 cont.

Group	WHA	TC	TC	TC	TC	TC	TC
Sample	R96-18	JG-95-RUA-001	1971A	P4927[b]	P5731A	P57536	P57535
SiO_2	55.05	58.83	58.83	60.02	58.55	57.72	57.77
TiO_2	0.748	0.644	0.635	0.690	0.634	0.628	0.621
Al_2O_3	17.03	16.37	16.57	16.71	16.25	16.45	16.50
Fe_2O_3	9.04	7.09	6.84	6.43	7.30	7.27	7.26
MnO	0.144	0.112	0.108	0.100	0.117	0.118	0.117
MgO	5.26	4.96	4.90	3.92	5.35	5.34	5.36
CaO	8.52	7.48	7.38	6.65	7.69	7.83	7.91
Na_2O	2.91	3.15	3.29	3.38	3.17	3.15	3.25
K_2O	0.94	1.41	1.49	1.79	1.34	1.30	1.30
P_2O_5	0.110	0.121	0.125	0.130	0.114	0.114	0.111
Total	99.75	100.17	100.17	99.82	100.52	99.92	100.20
Rb	27.1	51.9	55.2	66	47.9	46.7	45.5
Sr	227	265	268	269	262	270	265
Y	22.0	18.2	18.6	22	18.2	18.8	18.9
Zr	74	103	107	124	99	98	98
Nb	2.9	3.8	4.3	4	4.1	3.1	4.1
Ba	231	329	335	407	306	303	301
Pb	5	7	10	11	7	8	7
Th	3	5	6	7	6	6	5
U	0	0	1	n.d.	1	3	1
Sc	31	20	21	18	25	22	22
V	248	183	176	154	180	195	188
Cr	68	93	93	67	105	111	112
Co	30	27	25	n.d.	27	27	30
Ni	24	46	46	32	55	58	59
Cu	50	63	57	54	63	64	64
Zn	83	67	65	64	65	69	69
Ga	18	17	17	18	17	17	17
S	33	142	86	n.d.	45	105	171
La	8.1	10.8	11.2	13.9	n.d.	10.5	10.1
Ce	18.0	23.1	24.2	28.5	n.d.	23.4	22.9
Nd	11.0	12.8	12.5	14.8	n.d.	12.0	12.4
Sm	2.7	3.01	3.01	3.35	n.d.	2.96	2.9
Eu	0.85	0.81	0.81	0.85	n.d.	0.84	0.80
Tb	0.55	0.50	0.50	0.55	n.d.	0.52	0.50
Yb	2.03	1.90	1.86	2.03	n.d.	1.91	1.87
Lu	0.32	0.30	0.28	0.29	n.d.	0.30	0.30
Th	2.81	4.38	4.80	5.80	n.d.	4.49	4.32
U	0.8	1.6	1.5	1.6	n.d.	1.6	1.2
Ta	0.18	0.26	0.29	0.92	n.d.	0.28	0.27
Hf	2.12	2.88	2.97	3.36	n.d.	2.83	2.74
Cs	1.60	2.65	3.28	3.91	n.d.	2.96	2.77
Zn	90	74	73	68	n.d.	71	70
Co	27.5	25.0	23.3	59.9	n.d.	25.1	25.5
Cr	75	118	105	74	n.d.	102	114
Sc	34.2	24.8	23.6	20.4	n.d.	25.2	25.5

Table C-1 cont.

Group Sample	MISC R96-24	MISC X1-6	MISC W9-3	MISC W9-5	MISC W9-41[a]	MISC W9-43[a]	MISC R96-14
SiO_2	59.86	58.22	57.93	61.45	56.95	62.62	63.25
TiO_2	0.644	0.715	0.683	0.654	0.649	0.768	0.791
Al_2O_3	16.84	15.83	19.81	15.77	17.19	14.47	14.81
Fe_2O_3	6.52	7.60	5.96	6.30	8.25	5.84	5.66
MnO	0.105	0.124	0.093	0.103	0.136	0.093	0.088
MgO	4.12	5.25	2.51	3.85	5.11	4.99	4.24
CaO	6.82	7.40	8.02	6.21	8.04	5.42	5.27
Na_2O	3.65	2.96	3.58	3.27	3.02	3.29	3.38
K_2O	1.53	1.55	1.10	2.10	0.94	2.31	2.34
P_2O_5	0.123	0.130	0.122	0.130	0.097	0.174	0.177
Total	100.21	99.78	99.81	99.84	100.38	99.98	100.01
Rb	53.0	61.0	33.0	87.9	30.0	94.3	97.1
Sr	298	229	282	250	218	215	217
Y	19.8	20.6	19.4	20.4	19.7	24.5	24.3
Zr	119	119	89	139	75	180	188
Nb	4.3	5.1	2.6	4.9	2.4	7.3	6.4
Ba	346	326	263	387	248	450	476
Pb	10	7	8	11	5	12	13
Th	6	7	2	9	5	9	9
U	1	4	1	2	1	2	2
Sc	21	24	16	17	29	16	14
V	161	193	166	153	202	141	140
Cr	77	118	24	60	77	256	162
Co	22	27	16	20	27	22	19
Ni	29	37	12	29	20	91	68
Cu	22	44	39	32	33	70	60
Zn	66	68	64	64	72	61	61
Ga	18	18	20	19	17	17	16
S	51	38	29	40	24	22	29
La	13.3	12.7	8.5	14.5	7.6	17.5	17.8
Ce	28.5	27.4	18.7	32.0	17.1	38.8	39.1
Nd	14.0	14.5	11.0	15.9	11.0	20.2	18.8
Sm	3.18	3.37	2.66	3.45	2.54	4.19	4.21
Eu	0.89	0.87	0.87	0.86	0.80	0.93	0.92
Tb	0.53	0.59	0.52	0.57	0.52	0.69	0.70
Yb	1.92	2.13	2.06	2.15	2.03	2.35	2.32
Lu	0.30	0.33	0.32	0.30	0.32	0.35	0.36
Th	5.34	5.70	3.08	7.95	2.65	8.16	8.35
U	1.4	1.7	1.0	2.4	0.8	2.4	2.5
Ta	0.33	0.34	0.24	0.46	0.20	0.49	0.51
Hf	3.24	3.32	2.57	3.90	2.19	4.72	4.84
Cs	2.13	2.29	0.80	5.49	1.10	5.50	5.71
Zn	70	77	68	67	91	61	62
Co	19.2	25.1	14.6	19.0	25.5	20.1	18.5
Cr	88	139	29	66	81	268	185
Sc	21.1	27.6	17.5	20.4	28.7	18.0	17.3

Table C-2

Sample	$^{87}Sr/^{86}Sr$	$^{143}Nd/^{144}Nd$	$^{206}Pb/^{204}Pb$	$^{207}Pb/^{204}Pb$	$^{208}Pb/^{204}Pb$
X1-9	0.705307	0.512777	18.839	15.636	38.732
X1-10	0.705186	0.512753	18.819	15.611	38.672
X1-11	0.705171	n.d.	n.d.	n.d.	n.d.
X1-12	0.705142	0.512796	18.796	15.594	38.611
X1-13	0.705989[c]	0.512677	18.821[c]	15.616[c]	38.696[c]
X1-14	0.705711	0.512707	18.837	15.612	38.664
X1-15	0.705509	0.512742	18.809	15.602	38.645
R96-25	0.705248[c]	0.512764[c]	18.804	15.596	38.631
R96-26	0.705314	0.512725	18.772	15.578	38.445
R96-10	0.705807	0.512679	18.832	15.619	38.705
R96-2	0.705804	0.512693	18.823	15.611	38.676
R96-7	0.705796[c]	0.512718	18.815	15.606	38.660
R95-17	0.705041	0.512755	18.809	15.605	38.653
R95-18	0.705189	0.512746	18.810	15.615	38.676
R95-19	0.705209	0.512676	18.818	15.616	38.685
R95-20	0.704969	0.512766	18.772	15.589	38.547
R95-21	0.705520[c]	0.512729[c]	18.833	15.619	38.686
R95-22	0.705504	0.512774	18.878	15.671	38.857
R95-23	0.705669	0.512727	18.820	15.612	38.674
R95-25	0.705151	0.512813[c]	18.795	15.607	38.636
R95-26	0.704993	0.512792	18.763	15.584	38.567
R95-27	0.705144	0.512785	18.818	15.614	38.674
R95-28	0.705112	0.512752	18.829	15.626	38.714
R96-15	0.705309	0.512866	18.811	15.613	38.667
R96-18	0.705145[c]	0.512833[c]	18.822	15.623	38.711
JG-95-RUA-001	0.705266	0.512747	18.806	15.608	38.661
1971A	0.705358	n.d.	18.808	15.611	38.666
P4927	0.705522	0.512590	18.794	15.602	38.626
P5731A	0.705204	0.512744	18.810	15.612	38.643
P57536	0.705178	0.512778	18.833	15.634	38.747
P57535	0.705132	0.512766	18.801	15.601	38.625
R96-24	0.705660[c]	0.512663	18.822	15.605	38.667
X1-6	0.705380	0.512753	18.842	15.636	38.755
W9-3	0.705154[c]	0.512829[c]	n.d.	n.d.	n.d.
W9-5	0.705162[c]	n.d.	n.d.	n.d.	n.d.
W9-41	0.705286	0.512804	n.d.	n.d.	n.d.
W9-43	0.705489	0.512796	18.823	15.616	38.688
R96-14	0.705603	0.512780	18.837	15.641	38.776

Table C-3

Sample	$(^{238}U/^{232}Th)$	2σ	$(^{230}Th/^{232}Th)$	2σ	$(^{238}U/^{230}Th)$	2σ	[U]	[Th]	$(^{234}U/^{238}U)$	2σ
X1-9	0.825	±4	0.795	±9	1.038	±13	0.758	2.785	1.008	±11
X1-10	0.827	±5	0.794	±8	1.042	±11	0.864	3.170	1.000	±9
X1-11	0.885	±5	0.832	±9	1.063	±11	0.915	3.139	1.010	±7
X1-12	0.836	±3	0.803	±8	1.042	±11	0.852	3.092	1.006	±6
X1-13	0.869	±4	0.829	±7	1.049	±10	1.056	3.697	1.002	±4
X1-14	0.839	±4	0.807	±8	1.017	±11	1.007	3.643	1.001	±7
X1-15	0.813	±3	0.789	±6	1.031	±9	0.604	2.254	1.006	±5
R96-25	0.847	±3	0.775	±5	1.093	±7	1.401	5.019	1.004	±5
R96-26	0.825	±3	0.759	±7	1.086	±11	1.543	5.678	1.007	±4
R96-10	0.803	±3	0.752	±7	1.067	±10	1.977	7.471	1.011	±5
R96-2	0.811	±2	0.783	±7	1.026	±9	1.372	5.129	1.003	±4
R96-7	0.840	±3	0.798	±6	1.052	±9	1.405	5.076	1.005	±5
R95-17	0.828	±4	0.792	±9	1.045	±12	0.906	3.320	1.003	±5
R95-18	0.857	±3	0.793	±5	1.081	±7	0.968	3.429	1.007	±5
R95-19	0.896	±4	0.814	±6	1.100	±8	0.980	3.321	1.014	±5
R95-20	0.855	±3	0.795	±15	1.075	±21	0.749	2.660	1.006	±5
R95-21	0.782	±4	0.753	±4	1.040	±6	1.601	6.209	1.008	±5
R95-22	0.792	±2	0.789	±4	1.009	±5	1.120	4.263	1.010	±5
R95-23	0.816	±4	0.782	±5	1.044	±8	1.237	4.600	1.010	±5
R95-25	0.908	±4	0.857	±7	1.059	±9	0.693	2.315	1.003	±4
R95-26	0.916	±3	0.850	±8	1.078	±10	0.816	2.704	1.005	±7
R95-27	0.865	±3	0.816	±5	1.059	±9	0.981	3.439	0.995	±5
R95-28	0.850	±12	0.803	±7	1.058	±15	1.002	3.577	1.005	±3
R96-15	0.890	±3	0.841	±8	1.057	±11	0.972	3.316	0.998	±4
R96-18	0.818	±3	0.798	±6	1.024	±7	0.706	2.627	1.008	±5
JG-95-RUA-001	0.875	±4	0.779	±7	1.124	±10	1.341	4.648	0.998	±5
1971A	0.864	±3	0.767	±6	1.127	±9	1.330	4.674	1.004	±4
P4927	0.851	±4	0.760	±6	1.117	±10	1.538	5.471	1.002	±4
P57531A	0.864	±3	0.768	±6	1.125	±9	1.184	4.158	1.008	±5
P57536	0.889	±7	0.775	±6	1.125	±9	1.146	3.976	1.012	±5
P57535	0.850	±4	0.757	±5	1.129	±9	1.133	4.041	1.014	±5
R96-24	n.d.	n.d.	n.d.	n.d.	n.d.	n.d.	n.d.	n.d.	n.d.	n.d.
X1-6	0.861	±4	0.765	±11	1.126	±16	1.470	5.178	1.002	±4
W9-3	n.d.	n.d.	n.d.	n.d.	n.d.	n.d.	n.d.	n.d.	n.d.	n.d.
W9-5	0.906	±5	0.785	±9	1.155	±13	2.025	6.780	1.008	±5
W9-41	n.d.	n.d.	n.d.	n.d.	n.d.	n.d.	n.d.	n.d.	n.d.	n.d.
W9-43	n.d.	n.d.	n.d.	n.d.	n.d.	n.d.	n.d.	n.d.	n.d.	n.d.
R96-14	0.875	±4	0.830	±5	1.055	±7	1.914	6.597	1.007	±6

Table C-4

Group	OH	OH	OH	OH	PAR	PAR
Sample	X1-13 #1	X1-13 #2	X1-13 #3	X1-13 #4	R96-10 #1	R96-10 #2
SiO_2	59.14	58.87	59.01	59.00	59.38	59.95
TiO_2	0.682	0.675	0.677	0.668	0.745	0.738
Al_2O_3	17.06	17.17	17.24	17.19	17.18	17.49
Fe_2O_3	7.34	7.20	7.24	7.21	7.06	6.97
MnO	0.110	0.108	0.109	0.109	0.117	0.112
MgO	4.33	4.30	4.32	4.33	3.22	3.23
CaO	7.03	7.01	7.04	7.01	6.50	6.55
Na_2O	3.38	3.35	3.40	3.43	3.26	3.30
K_2O	1.29	1.28	1.27	1.28	1.76	1.76
P_2O_5	0.116	0.116	0.115	0.114	0.139	0.139
Total	100.42	100.12	100.53	100.46	99.45	100.11
Rb	44.2	n.d.	n.d.	43.5	69.7	69.0
Sr	238	n.d.	n.d.	237	251	248
Y	21.4	n.d.	n.d.	20.7	22.2	22.0
Zr	99	n.d.	n.d.	99	134	132
Nb	4.5	n.d.	n.d.	4.7	4.2	6.1
Ba	321	n.d.	n.d.	317	375	366
Pb	11	n.d.	n.d.	10	11	9
Th	4	n.d.	n.d.	5	8	6
U	1	n.d.	n.d.	3	1	3
Sc	24	n.d.	n.d.	23	20	18
V	187	n.d.	n.d.	193	165	164
Cr	63	n.d.	n.d.	73	30	37
Co	23	n.d.	n.d.	25	17	18
Ni	27	n.d.	n.d.	28	8	11
Cu	53	n.d.	n.d.	54	23	22
Zn	70	n.d.	n.d.	68	71	70
Ga	20	n.d.	n.d.	18	19	19
S	26	n.d.	n.d.	24	32	24

Table C-4 cont.

Group Sample	WAI R96-2 #1	WAI R96-2 #2	MISC W9-41 #1	MISC W9-41 #2	MISC W9-43 #1	MISC W9-43 #2
SiO_2	59.62	59.73	56.95	56.93	62.62	62.85
TiO_2	0.763	0.757	0.649	0.635	0.768	0.766
Al_2O_3	16.98	17.22	17.19	17.38	14.47	14.63
Fe_2O_3	7.30	7.16	8.25	8.10	5.84	5.74
MnO	0.115	0.113	0.136	0.133	0.093	0.09
MgO	3.56	3.57	5.11	5.06	4.99	4.99
CaO	6.43	6.46	8.04	7.99	5.42	5.43
Na_2O	3.29	3.31	3.02	3.04	3.29	3.3
K_2O	1.63	1.61	0.94	0.92	2.31	2.3
P_2O_5	0.142	0.140	0.097	0.093	0.174	0.176
Total	99.73	100.19	100.32	100.31	100.09	100.18
Rb	55.8	56.4	30.0	29.0	94.3	90.1
Sr	273	269	218	216	215	209
Y	23.9	23.0	19.7	19.8	24.5	23.8
Zr	126	125	75	76	180	170
Nb	5.2	5.9	2.4	3.5	7.3	6
Ba	393	385	248	244	450	439
Pb	9	9	5	4	12	12
Th	7	6	5	5	9	10
U	1	2	1	1	2	4
Sc	22	22	29	29	16	17
V	190	183	202	198	141	143
Cr	32	42	77	78	256	249
Co	22	23	27	29	22	21
Ni	14	18	20	23	91	93
Cu	48	48	33	32	70	67
Zn	72	71	72	72	61	58
Ga	19	17	17	17	17	16
S	47	44	24	21	22	34

Table C-4 cont.

Sample	$^{87}Sr/^{86}Sr$	$^{143}Nd/^{144}Nd$	$^{206}Pb/^{204}Pb$	$^{207}Pb/^{204}Pb$	$^{208}Pb/^{204}Pb$
X1-13 #1	0.705994	n.d.	18.793	15.585	38.573
X1-13 #2	0.705922	n.d.	18.788	15.572	38.522
X1-13 #3	n.d.	n.d.	18.800	15.582	38.559
R96-25 #1	0.705246	0.512687	n.d.	n.d.	n.d.
R96-25 #2	0.705233	0.512641	n.d.	n.d.	n.d.
R96-7 #1	0.705797	n.d.	n.d.	n.d.	n.d.
R96-7 #2	0.705782	n.d.	n.d.	n.d.	n.d.
R95-21 #1	0.705488	0.512641	n.d.	n.d.	n.d.
R95-21 #2	0.705536	0.512646	n.d.	n.d.	n.d.
R95-25 #1	n.d.	0.512731	n.d.	n.d.	n.d.
R95-25 #2	n.d.	0.512726	n.d.	n.d.	n.d.
R96-18 #1	0.705106	0.512753	n.d.	n.d.	n.d.
R96-18 #2	0.705130	0.512730	n.d.	n.d.	n.d.
R96-24 #1	0.705662	n.d.	n.d.	n.d.	n.d.
R96-24 #2	0.705643	n.d.	n.d.	n.d.	n.d.
W9-3 #1	0.705126	0.512739	n.d.	n.d.	n.d.
W9-3 #2	0.705160	0.512746	n.d.	n.d.	n.d.
W9-5 #1	0.705164	n.d.	n.d.	n.d.	n.d.
W9-5 #2	0.705142	n.d.	n.d.	n.d.	n.d.

Table C-4 cont.

Sample	$(^{238}U/^{232}Th)$	2σ	$(^{230}Th/^{232}Th)$	2σ	$(^{238}U/^{230}Th)$	2σ	[U]	[Th]	$(^{234}U/^{238}U)$	2σ
X1-10 #1	0.829	±8	n.d.	n.d.	n.d.	n.d.	0.882	3.228	1.001	±4
X1-10 #2	0.827	±5	0.794	±8	1.042	±11	0.864	3.170	1	±9
X1-12 #1	0.834	±4	0.804	±5	1.037	±9	0.848	3.086	1.006	±6
X1-12 #2	0.837	±4	0.802	±10	1.044	±13	0.854	3.096	1.006	±5
R96-18 #1	n.d.	n.d.	n.d.	n.d.	n.d.	n.d.	0.696	n.d.	1.006	±6
R96-18 #2	0.801	±9	0.801	±9	1.225	±8	0.718	2.667	1.008	±5
R96-18 #3	0.836	±11	n.d.	n.d.	n.d.	n.d.	0.705	2.558	1.012	±6
R96-18 #4	0.817	±4	0.796	±7	1.026	±9	0.702	2.608	1.003	±6
R96-2 #1	0.825	±3	n.d.	n.d.	n.d.	n.d.	1.364	5.015	0.995	±5
R96-2 #2	0.804	±2	0.783	±7	1.026	±9	1.378	5.203	1.003	±4
P4927 #1	0.853	±6	n.d.	n.d.	n.d.	n.d.	1.534	5.459	1.006	±5
P4927 #2	0.850	±5	0.760	±6	1.117	±10	1.543	5.479	1.002	±4
1971a #1	0.866	±4	0.765	±7	1.133	±10	1.330	4.657	1.004	±4
1971a #2	0.860	±6	0.771	±10	1.115	±15	1.333	4.703	1.006	±6
P57536 #1	0.872	±3	0.775	±8	1.125	±9	1.145	3.985	1.012	±5
P57536 #2	0.859	±5	n.d.	n.d.	n.d.	n.d.	1.166	4.120	1.002	±10
P57536 #3	0.889	±7	0.790	±10	1.126	±15	1.147	3.913	1.01	±7
R95-17 #1	0.828	±4	0.789	±9	1.048	±12	0.906	3.321	1.003	±5
R95-17 #2	0.826	±7	0.821	±29	1.007	±37	0.904	3.320	1.005	±7
R95-22 #1	0.783	±3	0.788	±7	0.994	±9	1.121	4.341	1.01	±5
R95-22 #2	0.798	±4	0.790	±6	1.010	±8	1.120	4.259	1.009	±7
R95-22 #3	0.804	±6	n.d.	n.d.	n.d.	n.d.	1.117	4.214	1.016	±8

Table C-5

Sample	EDG Ac	Bb	WI Wi008	Wi012	TAR T89-15[d]	T89-24[d]	T90-4A[d]	T90-10[d]	BR6[d]
SiO_2	60.71	61.09	56.07	58.25	54.57	54.7	54.22	53.45	56.00
TiO_2	0.685	0.745	0.593	0.628	0.98	0.94	0.96	0.97	0.84
Al_2O_3	16.58	16.6	13.18	13.78	17.78	17.48	17.63	18.28	18.00
Fe_2O_3	7.05	6.99	8.08	7.68	8.19	8.50	8.49	8.70	7.54
MnO	0.128	0.121	0.139	0.13	0.17	0.17	0.15	0.15	0.16
MgO	3.48	2.96	9.49	7.87	3.55	3.87	4.81	3.76	3.15
CaO	7	6.48	8.52	8.29	8.19	8.49	8.91	9.08	8.33
Na_2O	2.74	2.89	2.66	2.34	3.69	3.9	3.35	3.25	3.58
K_2O	1.57	1.65	1.17	1.38	2.5	2.22	1.77	2.07	2.21
P_2O_5	0.119	0.138	0.082	0.089	0.39	0.29	0.29	0.34	0.31
Total	100.06	99.66	99.98	100.44	100.01	100.56	100.58	100.05	100.12
Rb	55.1	58.7	37.3	44.8	60	54	43	48	58
Sr	244	260	156	166	719	635	648	664	635
Y	18.7	21.1	18.8	19.8	n.d.	22	20	n.d.	n.d.
Zr	95	112	85	99	114	103	92	97	121
Nb	4.4	4.7	2.8	3.9	n.d.	1	7	n.d.	n.d.
Ba	451	456	426	511	981	958	705	889	803
Pb	8	8	2	5	n.d.	16	11	n.d.	n.d.
Th	6	6	5	6	n.d.	n.d.	n.d.	n.d.	n.d.
U	0	1	0	1	n.d.	n.d.	n.d.	n.d.	n.d.
Sc	24	22	31	28	17	18	15	15	14
V	166	149	214	203	210	207	190	237	173
Cr	40	24	480	340	11	9	100	13	16
Co	19	13	42	31	4	6	41	6	8
Ni	5	6	160	105	118	161	98	91	85
Cu	14	14	79	80	80	73	69	70	74
Zn	61	59	64	61	23	22	21	21	21
Ga	17	18	12	13	n.d.	n.d.	n.d.	n.d.	n.d.
S	82	54	84	59	n.d.	n.d.	n.d.	n.d.	n.d.
Pb	n.d.	n.d.	n.d.	n.d.	12.1	n.d.	n.d.	12	24.3
La	n.d.	n.d.	n.d.	n.d.	20.4	15.6	13	15.3	16.8
Ce	n.d.	n.d.	n.d.	n.d.	43.4	34	29	31.7	35.4
Pr	n.d.	n.d.	n.d.	n.d.	5.2	n.d.	n.d.	4.2	4.8
Nd	n.d.	n.d.	n.d.	n.d.	23.5	19	16.8	17.9	19.7
Sm	n.d.	n.d.	n.d.	n.d.	5.2	4.1	3.8	4.4	4.5
Eu	n.d.	n.d.	n.d.	n.d.	1.36	1.26	1.21	1.48	1.41
Gd	n.d.	n.d.	n.d.	n.d.	4.46	n.d.	n.d.	4.39	4.43
Tb	n.d.	n.d.	n.d.	n.d.	0.75	0.72	0.66	0.66	0.64
Dy	n.d.	n.d.	n.d.	n.d.	4.19	n.d.	n.d.	3.67	3.83
Ho	n.d.	n.d.	n.d.	n.d.	0.84	0.7	0.7	0.8	0.81
Er	n.d.	n.d.	n.d.	n.d.	2.48	n.d.	n.d.	2	2.18
Tm	n.d.	n.d.	n.d.	n.d.	n.d.	n.d.	n.d.	0.34	0.32
Yb	n.d.	n.d.	n.d.	n.d.	2.34	2.1	1.9	2.04	2.26
Lu	n.d.	n.d.	n.d.	n.d.	n.d.	0.31	0.28	0.31	0.35
Hf	n.d.	n.d.	n.d.	n.d.	4.2	2.6	2.3	3.1	3.5
Ta	n.d.	n.d.	n.d.	n.d.	n.d.	n.d.	n.d.	0.35	0.56
U	n.d.	n.d.	n.d.	n.d.	5	1.4	1.1	1.4	1.4
Th	n.d.	n.d.	n.d.	n.d.	7.6	5	3.8	4.5	5

Table C-6

	Ac	Bb	Wi008	Wi012	T89-15	T89-24	T90-4a	T90-10	BR6
$^{87}Sr/^{86}Sr$	0.705984	0.706255	0.704892	0.705058	0.704630	0.704362	0.704395	0.704363	0.704617
$^{143}Nd/^{144}Nd$	0.512632	0.512647	0.512778	0.512815	0.512852	0.512865	0.512858	0.512873	0.512826
$^{206}Pb/^{204}Pb$	18.821	18.815	n.d.	18.796	18.773	18.765	18.757	18.749	18.779
$^{207}Pb/^{204}Pb$	15.621	15.599	n.d.	15.599	15.614	15.595	15.610	15.584	15.642
$^{208}Pb/^{204}Pb$	38.698	38.654	n.d.	38.647	38.628	36.567	38.594	38.547	38.706
$(^{238}U/^{232}Th)$	0.712	0.703	0.767	0.740	0.780	0.802	0.851	0.805	0.804
2σ	±3	±2	±3	±3	±4	±5	±5	±3	±5
$(^{230}Th/^{232}Th)$	0.705	0.705	0.700	0.697	0.802	0.782	0.861	0.805	0.832
2σ	±9	±16	±9	±8	±11	±11	±21	±11	±8
$(^{238}U/^{230}Th)$	1.007	0.997	1.096	1.062	0.973	1.025	0.988	1.000	0.967
2σ	±13	±22	±12	±12	±14	±15	±24	±14	±11
[U] μg g^{-1}	1.176	1.245	0.938	0.763	1.504	1.399	1.085	1.348	1.431
[Th] μg g^{-1}	5.014	5.373	3.708	3.127	5.848	5.293	3.871	5.077	5.399
$(^{234}U/^{238}U)$	1.006	1.009	1.006	1.010	1.009	1.009	1.006	1.008	1.012
2σ	±6	±5	±6	±5	±6	±5	±4	±5	±12

Table C-7

Sample	^{226}Ra fg g^{-1}	2σ	(^{226}Ra) atoms g^{-1} yr^{-1}	2σ	^{230}Th pg g^{-1}	2σ	(^{230}Th) atoms g^{-1} yr^{-1}	2σ
P5731A	409.4	±24.9	466.1	±28.3	410.1	±3.0	6.81	±0.05
JG-95-Rua-001	468.9	±4.7	533.5	±5.4	464.9	±4.2	7.72	±0.07
P57536	346.2	±8.1	393.8	±9.0	396.2	±3.0	6.58	±0.05
P57535	399.2	±1.5	453.5	±1.8	390.8	±2.4	6.49	±0.04
1971a	427.2	±2.6	486.0	±3.0	457.7	±4.2	7.60	±0.07
X1-14	331.3	±2.2	377.0	±2.4	385.4	±4.2	6.40	±0.07
X1-11	283.6	±1.4	322.8	±1.8	335.4	±3.6	5.57	±0.06
WI008	261.5	±7.9	297.5	±9.0	280.0	±3.0	4.65	±0.05
WI012	312.9	±1.4	356.5	±1.8	333.0	±3.6	5.53	±0.06

Appendix D

Analytical Techniques

D-1 Sample Crushing

Each sample was split into two parts using a hydraulic splitter; a small piece of hand-specimen size for reference and thin section preparation, and a larger piece for powdering. Any weathered edges which were not removed in the field were split away from the samples. The sample was then split into smaller centimetre sized fragments, of which a small proportion was retained (~100-200 g). Several small pieces were passed through a stainless steel jaw crusher and discarded, to precontaminate the apparatus before crushing the main portion of the sample into millimetre sized fragments. An aliquot (~150-300 g) of the crushate was retained for future use if required, and the remainder (~100-200 g) was ground to a fine powder in an agate ball mill for ~20 minutes. Powders were immediately transferred to glass jars for storage.

D-2 X-Ray Fluorescence Analysis (XRF)

D-2.1 Glass Disc Preparation

Aliquots of powder for analysis were placed in an oven overnight at 100°C in clean porcelain crucibles to ensure the samples were dry before glass disc preparation. The powders were allowed to cool and ~3.5 g (exact mass required dependant on the batch of flux) of lithium metaborate/tetraborate flux (Johnson Matthey Spectroflux 100B). Onto the flux, 0.7 g of sample powder was weighed, and stirred using a polythene rod to ensure a homogenous mixture was obtained. Each sample was fused for ~15 minutes at 1100°C in a muffle furnace, and the mixture was swirled at five minute intervals during fusion in order

to homogenise the mix and allow any gas bubbles to escape. The melt was poured into a preheated brass mould and compressed to form a glass disc, which was allowed to cool before analysis.

Using the same aliquots of powder as used for glass disc preparation, 1-2 g of powder was accurately weighed into alumina crucibles which had been pre-ignited at 1000°C for ~15 minutes. The samples were then ignited at 1000°C for ~30-45 minutes before being reweighed to determine loss on ignition for each sample.

D-2.2 Pressed Pellet Preparation

Approximately 9-10 g of sample powder was weighed out into a small plastic bag and 0.7-0.9 ml of polyvinylpyrollidone (PVP) binder was added and mixed with the powder (Watson, 1996). The mixture was emptied into a hardened steel mould, and placed into a hydraulic press. The mixture was subjected to pressures of 1.5 MPa to form a pressed pellet. The completed pellet was dried overnight at ~100°C prior to analysis to improve durability.

D-2.3 Technical Specification and Quality Assurance

Analysis of the glass discs and pressed powder pellets was undertaken on an ARL 8420+ dual goniometer wavelength dispersive XRF spectrometer. The spectrometer is equipped with a 3 kW Rh anode end-window X-ray tube, and uses fully collimated flow proportional and scintillation counters. The machine is equipped with 5 diffraction crystals; a multilayer AX06 crystal, a PET crystal, a Ge111 crystal, a LiF200 crystal and a LiF220 crystal.

Within each run, elemental intensities are corrected for background and peak overlap interferences. Medium-term instrumental drift is corrected for using a drift normalisation monitor built into the software. Matrix corrections for major elements use the Traill-Lachance procedure, and trace element matrix corrections were achieved by ratioing with the Compton scattered tube lines, or in the case of trace elements of atomic number < 27 (and Ba), a Lucas-Tooth correction using iron and Compton scatter peak

intensities was employed. Typical detection limits, and approximate 2σ errors for average trace element concentrations obtained in this study are listed in Table D-1. The 2σ error estimates are based on curves put through the least precise data for monitor samples (compositions known from national databases of inter-laboratory analyses) across a wide range of concentrations of a given element.

Element	Detection Limit (μg g^{-1})	Approximate 2σ (μg g^{-1})
Rb	2	1.25 - 1.5
Sr	2	1.75 - 2
Y	2	1.5
Zr	2	1.5 - 2.5
Nb	1.5	1
Ba	12	10 – 15
Pb	5	2.5 – 3
Th	4	2 – 2.5
U	3	1.5
Sc	5	4.5 - 5.5
V	5	7 – 9
Cr	4	2.5 - 4.5
Co	2	-
Ni	3	2 – 3
Cu	3	2 - 2.25
Zn	3	2.5
Ga	3	2
Mo	2	-
As	5	-
S	50	-

Table D-1: Approximate detection limits for XRF trace element analyses and typical 2σ precisions for typical concentrations determined in samples from this study.

XRF analysis was carried out over a period of ~2 years, with a number of sample analyses repeated for both major and trace element abundances at the end of the period to assess data quality (see Appendix C). For each batch of glass discs which was prepared, discs of two Open University monitor samples (containing high and low abundances of each element analysed) were prepared to ensure that there were no problems with the preparation or with the analysis. In addition, glass discs of sample X1-13 were prepared at several times throughout the period to act as an internal standard for the data set.

D-3 Instrumental Neutron Activation Analysis (INAA)

This technique was used to determine concentrations of the REE elements La, Ce, Nd, Sm, Eu, Tb, Yb and Lu as well as other trace elements, Th, U, Ta, Hf, Cs, Zn, Co, Cr and Sc. Exactly 0.3000g of sample powder was weighed out into plastic vials which were

sealed using a soldering iron. Discs of lacquered iron foil of known mass were placed between each sample in a sealed plastic tube in order to monitor the neutron flux during irradiation. Sample tubes were sent to the Imperial College Reactor Centre where they were subjected to a thermal neutron flux of 10^{12} ncm^{-2} s^{-1} for ~24-30 hours.

The neutron flux causes the formation of short-lived radioactive isotopes of the elements of interest, which emit characteristic gamma radiation proportional to the abundance of the isotope and therefore the element of interest. The samples were analysed by simultaneously counting emitted gamma rays using a planar low energy photon spectrometer (LEPS) and a coaxial Ge(Li) crystal detector, and were counted twice during the month following radiation. The initial count time of 8000 seconds within a week of irradiation, produced precise data for shorter-lived isotopes and was followed by a 6-10 hour counting period to ensure good precision for longer-lived isotopes. Full details of the technique and data interpretation used are given by Potts et al. (Potts et al., 1981; Potts et al., 1985). Typical detection limits and standard deviations as determined by Potts et al. (Potts et al., 1985) are given in Table D-3.1.

Reproducibility was monitored by inclusion of two standards, one of Ailsa Craig microgranite, and one of Whin Sill dolerite with each tube of samples. Repeat samples also show the internal reproducibility of the data set (see Appendix C). Detection levels are shown in Table D-2. Comparison of samples recently analysed using INAA and ICP-MS is given by George (George, 1997), and shows that whilst the correlation between most elements is excellent, there is a systematic offset in HREE (principally Lu, Yb and Tb, but to a slight extent Sm) to higher concentrations by INAA analysis. The offset appears to be constant regardless of concentration, which may be due to calibration problems with the INAA system (George, 1997). This implies that whilst absolute HREE concentrations may deviate slightly from actual values, the range of variation should still be accurate.

Element	Detection limits Short counts	Detection limits Long counts	Relative Precision (2 σ %)
La	0.3 - 2.9		5.2
Ce	2.2 - 2.9	0.9 - 1.2	6.2
Nd	2.7	2.9	7.0
Sm	0.06 - 0.2		4.2
Eu	0.1 - 0.9	0.03 - 0.1	7.8
Gd		2.3 - 2.7	22.0
Tb	0.14 - 0.9	0.1 - 0.4	7.8
Tm	0.6	0.2	11.8
Yb	0.2 - 1.0	0.08 - 0.5	6.2
Lu	0.04 - 0.08	0.08 - 0.2	3.4
Co	0.6 - 0.8	0.08 - 0.2	6.2
Rb	11	6	22.0
Cs	0.4 - 0.5	0.1 - 0.14	19.0
Hf	0.5 - 2.9	0.1 - 1.2	6.0
Ta	0.16 - 2.4	0.04 - 0.8	9.4
Th	0.3 - 1.0	0.13 - 0.5	8.6
U	0.3 - 1.7		53.0

Table D-2: Typical detection limits for elemental abundances determined by INAA. The range for each element represents an amalgamation of data for different energy peaks for each given element, which are accounted for during data processing using a weighting procedure based on counting precision. Relative precisions are calculated as (s.d. / mean) x 100. Data is from Potts et al. (Potts et al., 1985).

D-4 Isotope Analysis

D-4.1 General Procedures

Acids used for cleaning and sample dissolution were of two grades. Analytical grade reagent was purified initially by distillation in a quartz boiling still (QD acid). Increased purity was obtained by using teflon sub-boiling stills (TD acid). Water used in the chemistry was either cleaned through reverse osmosis (RO H_2O) or had a second cleaning stage in the teflon sub-boiling stills. Acids for use in Pb dissolutions were put through a second set of teflon sub-boiling stills (2 x TD acid). Sample evaporations took place under infra-red lamps, in covered hoods which had supplies of clean, filtered compressed air. The HCl used for radium chemistry was prepared directly from analytical grade reagents, to reduce the possibility of contamination by small quantities of HNO_3 which could wash radium off the ion exchange resin earlier than expected. The saturated boric acid solution (H_3BO_3) used in U-Th-Ra chemistry was prepared by dissolving ~7 g of

H_3BO_3 crystals per 100 ml of RO H_2O on a hotplate. The solution was then allowed to cool to become super-saturated.

All dissolutions for isotopic analysis were carried out in sealable Savillex® beakers. These beakers were cleaned by a cycle of acid addition and rinses. Firstly, the beakers were filled with QD 6M HCl and allowed to warm overnight before rinsing with RO H_2O. The beakers were then totally immersed in 14M HNO_3 and warmed for 24 hours before being rinsed with RO H_2O which was followed by immersion in hot RO H_2O for 24 hours. During this period, beakers were boiled several times in fresh RO H_2O. Following rinsing with RO H_2O, the beakers had a small quantity (~1-2 ml) of TD 6M HCl added and were sealed and placed under evaporating lamps for a short period. The beakers were rinsed thoroughly with TD H_2O to remove all traces of acid residues and allowed to dry before use.

D-4.2 Sr and Nd Isotope Analysis

D-4.2.1 Sample Preparation

Strontium and neodynium separations were prepared from single dissolutions where possible. Aliquots of approximately 100-150 mg of sample powder were weighed out into clean Savillex® beakers. The powders were wetted with a few drops of TD 14M HNO_3 to suppress any vigorous reaction upon addition of ~2-3 ml of HF. The beakers were sealed and placed on a warm hotplate for 24 hours to ensure dissolution. The resulting solutions were evaporated, and once the samples were just dry, ~3 ml of TD 14M HNO_3 was added. The resulting solutions were evaporated to dryness again and ~3-4 ml TD 6M HCl added. The beakers were then allowed to stand for 24 hours on a hotplate. If any fluoride residue was still present, the beakers were tightly sealed and placed under evaporating lamps for a short time to increase the temperature and pressure of dissolution to remove the fluorides. The solutions were evaporated to dryness and the residue was taken up in ~2 ml QD 2.5M HCl.

A 1 ml aliquot of the 2.5M HCl solution was loaded onto an ion exchange column (made up with Bio-Rad AG® 50W-X8 200-400 mesh H^+ form cation exchange resin), and

the second half of the solution retained for future analysis if required. The Sr fraction was eluted and collected with QD 2.5M HCl, and a further elution and collection with QD 3M HNO_3 produced a REE fraction for subsequent Nd separation. The Sr fraction was evaporated to dryness and loaded onto single Ta filaments in 2 µl of TD H_2O. The filaments were pre-loaded with a small (~1 µl) spot of H_3PO_4 to prevent the sample from spreading along the filament. The Nd fraction was evaporated to dryness and taken up in ~0.5 ml QD 0.25M HCl. The solution was loaded onto reverse chromatography ion exchange columns (made up with 1 g of Voltalef 300 LD PL micro teflon powder and 100 g of DEP (2-diethylhexyl phosphate)) and a clean Nd fraction eluted and collected with QD 0.25M HCl. The fraction was evaporated to dryness and loaded onto Ta double filaments in 2 µl of H_2O. A second Re double filament was used for ionisation during analysis.

D-4.2.2 Machine Specification and Quality Assurance

Analyses of Sr were undertaken on a Finnigan MAT 261 multicollector mass spectrometer operating in static collection mode. Samples were normally collected for 100-120 ratios with a ^{87}Sr beam ≥ 1 pA, which gave typical internal precision for each run of ±10-20 2σ in the sixth decimal place to be obtained. Each sample was corrected for mass fractionation during the run to $^{86}Sr/^{88}Sr = 0.1194$. Analysis of NBS987 standards allowed long-term reliability and reproducibility to be monitored. All sample data presented in Appendix C are normalised to an NBS987 value of 0.710250. For most of the analyses undertaken in this study, the weighted average value of NBS987 was 0.710233±54 2σ (n=106), however, ~10 samples were undertaken in an earlier period when NBS987 had a weighted average value of 0.710241±72 2σ (n=108). Repeat analyses of samples in both periods of analysis yield good reproducibility as listed in Appendix C. Total procedural blanks were monitored regularly and were typically ≤ 1 ng Sr.

Analyses of Nd were made using a Finnigan MAT 262 multicollector mass spectrometer operating in static collection mode. Samples were collected for 150-200 ratios with ^{143}Nd and ^{144}Nd beams ≥ 2 pA. Samples were corrected for mass fractionation during the run to $^{144}Nd/^{146}Nd = 0.7219$. Internal precision for each run was typically

±6-12 2σ in the sixth decimal place. Reproducibility was monitored using a 1:10 dilution of Johnson Matthey Nd standard with a long term reproducibility of 0.511764±28 2σ (n=58). This solution is made up to have the same $^{143}Nd/^{144}Nd$ ratio as the La Jolla standard, and samples were normalised to a value of $^{143}Nd/^{144}Nd = 0.511850$ for this standard. Contamination was monitored through periodic total procedural blanks, which were typically ≤ 200 pg. Repeat sample analyses over the analysis period showing the internal reproducibility of the data set are given in Appendix C.

D-4.3 Pb Isotope Analysis

D-4.3.1 Sample Preparation

Aliquots of ~100 mg of powder were weighed out into clean Savillex® beakers. Samples were wetted with < 1 ml 2 x TD 14M HNO_3, and 2-3 ml 2 x TD HF added. The samples were allowed to dissolve on a warm hotplate overnight and evaporated to dryness, after which ~2 ml 2 x TD 14M HNO_3 was added and the residue allowed to dissolve again on a hotplate. The solution was dried down and the residue taken up in ~2 ml 2 x TD 6M HCl. If fluorides still remained, additions of HNO_3 and HCl were repeated until the solutions were completely clear. Once perfect solutions were obtained, they were dried down (ensuring no remanent of HCl remained) and ~1 ml 2 x TD 1M HBr was added. The samples were left to redissolve at room temperature prior to loading onto columns for separation.

In order to reduce the amount of reagent used during Pb chemistry (and thus reduce contamination), very small volume columns are used. These are made from 1 ml pipette tips, which have a polypropylene frit added to the tip. The columns are stored in HCl once made, and rinsed with RO H_2O and QD 6M HCl several times prior to addition of 5 drops (~100 µl) of Bio-Rad AG® 1-X8 (200-400 mesh Cl^- form) anion exchange resin. The resin was washed with two rinses of 2 x TD H_2O and 2 x TD 6M HCl, and then preconditioned with 0.5 column volumes (CV) of 2 x TD 1M HBr. Samples were loaded onto the preconditioned columns and washed on with 0.5 CV 2 x TD 1M HBr. A further elution of 1 CV 2 x TD 1M HBr was followed by collection of the Pb fraction in 2 CV

2 x TD 6M HCl. To the collected fraction, ~50-100 µl 2 x TD 14M HNO_3 was added to remove any bromine present. The fractions were dried, and the column process repeated, after which the fractions were again dried, ready for loading onto filaments. Analyses of Pb isotopes were performed on Re single filaments, and were loaded in 2 µl of silica gel which had a small amount of phosphoric acid added in order to prevent migration of the sample along the filament during loading.

D-4.3.2 Machine Specification and Quality Assurance

Analysis for Pb isotopes was undertaken on a Finnigan MAT 261 multicollector mass spectrometer at the Open University. The machine was run in static mode, and data was typically collected for 100 ratios (continued collection of data tended to lead to increased problems with mass fractionation). In order to reduce mass fractionation effects as far as possible, all runs were undertaken at temperature controlled conditions of 1100-1125°C, and all samples were normalised to standards run in the same magazine. The normalising values used were those of Todt et al (1993). All runs were started with ^{208}Pb beams of at least 10-20 pA because maintaining constant temperature meant that beams had to be left to fall back over the course of the run. Any runs where the ^{208}Pb beam fell below 5 pA were rejected. Typical internal precisions for each run were $^{206}Pb/^{204}Pb$: ±1-4, $^{207}Pb/^{204}Pb$: ±1-4 and $^{208}Pb/^{204}Pb$: ±2-10 in the third decimal place.

Long term reproducibility was monitored by repeated analysis of NBS981 standard solution. During the study, multiple analyses (n = 19) of the standard gave $^{206}Pb/^{204}Pb = 16.901 \pm 15$, $^{207}Pb/^{204}Pb = 15.445 \pm 19$ and $^{208}Pb/^{204}Pb = 36.544 \pm 51$, at the 2σ level. Sample X1-13 was also analysed a number of times and the details are given in Appendix C. Contamination was monitored by frequent total procedural blanks, which were typically ≤ 500 pg compared with typical sample sizes of ~500-1000 ng loaded onto a filament for analysis.

D-4.4 U-Th Isotope Analysis

D-4.4.1 Sample Preparation

An aliquot of sample powder was weighed out into a clean Savillex® beaker. For whole rock analyses, the ideal amount of sample is sufficient to yield ~500 ng of Th, a tradeoff between having enough Th to produce a stable beam for a long enough time period during analysis and having so much Th loaded onto the filament that ionisation efficiency is badly impaired. The aliquot of powder then had ~0.5-0.6 g of a ^{229}Th-^{236}U mixed spike added. The amount of spike was calculated to produce a ^{232}Th/^{229}Th ratio of ~2500, a sufficiently small amount of spike to have negligible ^{232}Th and ^{230}Th blanks relative to the concentrations in the sample, but enough to make mass spectrometric analysis as precise as possible.

The spiked samples had ~3 ml of TD HF added to which ~1 ml TD 6M HCl was mixed in order to reduce fluoride formation. The samples were placed on a hotplate for 24 hours and then dried down under evaporating hoods as for Sr and Nd analysis. The residue was taken up in ~3-4 ml TD 6M HCl and then the beakers were sealed and placed on a hotplate overnight. The samples were dried down and the addition of HCl repeated. After drying the samples down again, ~4 ml of TD 6M HCl was added with ~1 ml of boric acid (H_3BO_3) to remove any remaining fluoride. Boric acid has proved useful both in removing fluoride, and in stabilising Th beams during mass spectrometric analysis. This mixture was placed on a hotplate overnight and then evaporated to dryness. If the H_3BO_3-HCl solutions were not totally clear, HCl addition was repeated until all fluoride residue was removed. The samples were taken up in ~5 ml TD 14M HNO_3 and then left on a hotplate for a short time before being evaporated to dryness and taken up in ~5 ml TD 7M HNO_3 ready for separation on ion exchange columns.

The sample solutions were centrifuged to check for any residue, before being loaded on preconditioned ion exchange columns. The columns were made up prior to analysis by addition of 4 ml of cleaned (repeated RO H_2O-QD 6M HCl rinses) Bio-Rad AG® 1-X8 (200-400 mesh Cl^- form) anion exchange resin to clean quartz columns

(rinsed with RO H_2O and stored in QD 6M HCl between uses). The resin was allowed to settle and washed twice with alternate rinses of QD 6M HCl and RO H_2O. The resin was then preconditioned with ~12 ml TD 7M HNO_3 ready for sample loading. The sample solutions were loaded onto the top of the resin bed, and washed on with 2 rinses of 1 ml TD 7M HNO_3 which was followed by eluting 15-18 ml TD 7M HNO_3 and then 4 ml TD 6M HCl. Clean Savillex® beakers were placed under each column, and a Th fraction was collected in 4 ml TD 6M HCl. A further 2 ml of TD 1M HBr was eluted and a U fraction collected in 6 ml TD 1M HBr in a second set of clean beakers. Each fraction was then dried down ready for loading onto filaments.

Prior to loading onto filaments, each of the fractions had a few drops of TD 14M HNO_3 added and were dried down again to ensure the samples were in nitrate form. The U fractions were redissolved in 2 µl TD 0.1M HNO_3 and loaded onto Re single filaments which had a small spot of ~1-2 µl graphite solution loaded in the centre. The Th fractions were dissolved in ~2 µl of loading solution (a mixture of H_3PO_4 and 0.1M HNO_3) and loaded onto the centre of a Re double filament. A second Re double ionisation filament was used during analysis of the the Th fraction.

D-4.4.2 Machine Specification and Quality Assurance

Samples for U and Th isotopic analysis were run on a Finnigan MAT 262 multicollector mass spectrometer. The system was equipped with a RPQ-II (retardation potential quadrupole) deceleration lens system. The function of the RPQ is to filter out ions with divergent flight directions and/or lower energies resulting from collisions with other ions, which contribute to tails at lower masses on large ion peaks, and raised baseline levels. The performance of the RPQ is discussed in further detail by van Calsteren and Schwieters (van Calsteren and Schwieters, 1995). The effect of the RPQ system is to reduce the error imparted by poor abundance sensitivity (relative count rate at 1 mass unit below the main peak) whilst retaining ~95% of accelerated ions.

Analysis of U isotopes was performed dynamically, measuring the beams of ^{236}U, ^{234}U and ^{235}U consecutively on an SEM (secondary electron multiplier). Measurement of

^{235}U was preferred over ^{238}U in order to obtain $^{234}U/^{238}U$ ratios, because of the much larger size of the ^{238}U beam relative to the ^{234}U beam would make the analysis more difficult (Edwards et al., 1987). Ratios were converted assuming a natural $^{238}U/^{235}U$ ratio of 137.88. Typically 100-120 ratios were collected with a ^{234}U beam ≥ 100 counts s^{-1}, such the internal precison of the run was ~0.5% 2σ on the $^{234}U/^{236}U$ ratio, consistent with standard reproducibility.

Analyses of Th isotopes were run in two parts. Firstly, ^{229}Th and ^{232}Th were measured to determine Th concentrations. This was run on a static collection routine, measuring ^{232}Th on a faraday cup and ^{229}Th on an SEM collector. Normal ^{232}Th beams were ~0.2-0.4 pA producing corresponding ^{229}Th beams ≥ 1000 counts s^{-1}, collected over 50-60 ratios. The second part of the analysis was to collect ^{230}Th and ^{232}Th on a static collection routine with ^{230}Th on an SEM collector. In order to ensure good ionisation, ^{187}Re beams above 1 pA were required and in ideal circumstances ^{187}Re beams of 3-5 pA were sought, and data was only collected if ^{232}Th beams could be maintained above 1 pA throughout the analysis. Under these conditions, the ^{230}Th beam was typically 25-50 counts s^{-1}. In order to obtain good precision, 150-200 ratios were collected, yielding internal precisions of 0.5-1% 2σ, consistent with standard reproducibility.

Long term reproducibility was monitored with two internal standards. For U measurements, analyses of the U456 standard yielded $^{234}U/^{236}U$ of 0.09758±25 and $^{235}U/^{236}U$ of 13.2680±0.0286. For Th measurements, analyses of the Th 'U' standard yielded $^{230}Th/^{232}Th$ of 6.149±0.111 (n=182). During the period of analysis no runs of ATHO rock standard were achieved due to lack of powder although the value of the internal Th'U' standard did not vary from periods when ATHO were run. During the analysis period, work was undertaken by the author and P. Evans to set up an internal rock standard, but this has not yet been fully characterised. Repeat analyses for samples from this study indicate the general reproducibility of concentrations (see Appendix C). Reproducibilities were: [U] ~0.5-1%, [Th] ~1-2%, ($^{238}U/^{232}Th$) ~1% and ($^{230}Th/^{232}Th$) ~1-2%.

D-4.5 Ra Isotope Analysis

The procedure described briefly here has been developed at the Open University based on techniques described by Cohen & O'Nions (Cohen and O'Nions, 1991). The full procedure and details of various specialised variations not used in this study are described by Thomas (Thomas, 1998).

D-4.5.1 Sample Preparation

An aliquot of the sample to be analysed was weighed out into a clean Savillex® beaker. The amount of sample weighed out was calculated to produce ~50-100 fg ^{226}Ra assuming equilibrium between ^{230}Th and ^{226}Ra. The sample aliquot then had ~0.9 g of a ^{228}Ra spike added. The amount of spike was calculated to yield a $^{228}Ra/^{226}Ra$ ratio > 1, in order to assist determining if interferences by organic compounds were significant during mass spectrometric analysis.

The sample was dissolved using the same procedure as for U-Th analysis, and an initial clean up was performed using the U-Th column procedure and collecting the initial elutions of TD 7M HNO_3 which contained the Ra. The solution was dried down and taken up in TD 6M HCl to convert the residue to chlorides. This solution was then dried down and redissolved in ~2 ml 3M HCl. The resulting solution was then passed through a polypropylene column with a 2 ml bed of Bio-Rad AG® 50W-X12 (200-400 mesh H^+ form) resin. The resin was allowed to settle in the column and washed with QD 6M HCl and RO H_2O. The column was then preconditioned with 6 ml 3M HCl, and the sample loaded onto the resin bed. The sample was washed onto the resin with 2 ml 3M HCl, and a further 8 ml of 3M HCl was eluted. A second elution of 2 ml RO H_2O was then passed through the column and the fraction containing Ra was collected in 12 ml 3.75M HNO_3. The collected fraction was dried down and converted to chlorides using 2-3 ml TD 6M HCl. This solution was then dried down and taken up in 0.2 ml TD 6M HCl. The solution was then passed through a second column containing 0.6 ml of Bio-Rad AG® 50W-X12 (200-400 mesh H^+ form) resin, using a procedure scaled down

from the larger cationic column. The collected solution was dried down and then redissolved in 50 µl 3M HNO_3.

The final separation of Ra from Ba was carried out on a polypropylene column containing 150 µl of ElChroM Sr Resin SPS (50-100 µm). The resin was first washed with 300 µl 0.5M HNO_3, and then preconditioned with 600 µl 3M HNO_3. The sample was loaded onto the resin bed, and 150 µl 3M HNO_3 eluted through the resin. The Ra fraction was collected with 300 µl 3M HNO_3. The sample was dried down and then redissolved in 2 µl of a solution of TD 0.1M HNO_3 containing a small amount of H_3PO_4, HF and $TaCl_5$ activator, and loaded into the centre of a Re single filament.

D-4.5.2 Machine Specification and Quality Assurance

Samples were analysed for Ra on a Finnigan MAT 262 thermal ionisation mass spectrometer at the Open University. The mass spectrometer was run in dynamic mode, with all measurements made on an SEM collector, with the RPQ in use as described in Section D-4.4.2.

The very low count rates typically observed make it extremely hard to focus the ion beam well, and standard procedure is to use Ba as a proxy in order to maximise the beam size (e.g. Cohen and O'Nions, 1991). The ionisation temperature of Ra is extremely low, and as a result, there are commonly organic interferences present at running temperatures. These interferences tend to occur at a constant level across all the masses between 225 and 229, and therefore mass 225, 227 and 229 are monitored to check the level of interference. The organic material usually burns off leaving a Ra which can be measured precisely. Data was normally collected for a minimum of 50 ratios with ≥ 20 counts s^{-1}. Below this count rate, systematic variations have been observed.

Data quality and reproducibility has been assessed by periodic analysis of a Mount Lassen rock standard, yielding results of 1041±11 fg g^{-1} 2σ ($n = 11$), which compares with published values of 1065±7 ($n = 2$) (Volpe et al., 1991). Although no specific standard solution is used, spike calibrations are run periodically, allowing any variations due to machine problems to be detected. In this study, samples older than 8 ka

have been analysed to check that they are in secular equilibrium, and repeat analyses have been performed. Total procedural blanks were monitored, although no detectable contamination was observed.

Appendix E

Miscellaneous Calculations and Notes

E-1 Calculation of Eu / Eu* and Ce / Ce*

The ratio of Eu / Eu* has been calculated by taking a geometric mean between Sm_N and Tb_N because Gd concentrations were not determined in this study. The formula used is,

$$\frac{Eu}{Eu^*} = \frac{Eu_N}{\sqrt[3]{Sm_N^2 * Tb_N}} \tag{E-1}$$

similarly, the ratio of Ce / Ce* can be calculated as,

$$\frac{Ce}{Ce^*} = \frac{Ce_N}{\sqrt[3]{La_N^2 * Tb_N}} \tag{E-2}$$

E-2 AFC Equations

The AFC equations used in this thesis are those given by DePaolo (DePaolo, 1981). They are given here for reference. The equation for elemental concentrations during AFC is as follows,

$$C_m = C_m^o \left\{ F^{-z} + \left(\frac{r}{r-1} \right) \frac{C_a}{zC_m^o} \left(1 - F^{-z} \right) \right\} \tag{E-3}$$

where C_m^o is the initial concentration of the element of interest in the magma, C_a is the concentration of the element in the assimilant, r is the ratio of the mass of crust assimilated to the mass of magma crystallised, F is mass of magma remaining, and z is defined as follows,

$$z = \frac{r + \bar{D} - 1}{r - 1} \tag{E-4}$$

where $\overline{D}$ is the bulk partition coefficient for the element of interest between the crystallising assemblage and the magma. The equation for the evolution of isotope ratios during AFC is,

$$\varepsilon_m = \frac{\frac{r}{r-1}\frac{C_a}{z}\left(1-F^{-z}\right)\varepsilon_a + C_m^o F^{-z}\varepsilon_m^o}{\frac{r}{r-1}\frac{C_a}{z}\left(1-F^{-z}\right)+C_m^o F^{-z}} \quad \text{(E-5)}$$

where ε_m is the isotope ratio of the magma, ε_m^o is the initial isotope ratio of the magma, ε_a is the isotope ratio of the assimilant, and all other symbols are as previously defined.

E-3 Equations for Fractional Crystallisation

Fractional crystallisation calculations made in this thesis uses the standard equation derived from the Rayleigh law (Cox et al., 1979), where C_L is the concentration in the liquid after crystallisation, C_0 is the initial concentration in the liquid, F is the proportion of the original liquid remaining, and D is the partition coefficient for the element of interest.

$$\frac{C_L}{C_0} = F^{(D-1)} \quad \text{(E-6)}$$

E-4 Equations for Mixing

Binary mixing calculations between different elemental and isotopic abundances are made using the equations given by Faure (Faure, 1986). Element abundances are mixed using equation E-7, where X_{mix} is the concentration of the element X in the mixture, X_A and X_B are the concentrations of X in components A and B respectively and f is the mass fraction of component A in the total mass of A and B (i.e. $f = \frac{A}{(A+B)}$ where A and B are the masses of the two components).

$$X_{mix} = X_A f + X_B(1-f) \quad \text{(E-7)}$$

Two components with differing isotopic ratios of the same element (e.g. $^{87}Sr/^{86}Sr$) can be mixed according to Equation E-8, where R^X_{mix} is the isotope ratio of element X in the mixture, R^X_A and R^X_B are the isotope ratios of element X in components A and B respectively and all other symbols are the same as for Equation E-7.

$$R^{x}_{mix} = \frac{R^{x}_{A}X_{A}f + R^{x}_{B}X_{B}(1-f)}{X_{A}f + X_{B}(1-f)} \quad \text{(E-8)}$$

E-5 Partial Melting Equations

The simple models of partial melting used in this thesis use the modal batch partial melting equation as given by Wilson (Wilson, 1989). This is shown in Equation E-9, where C_L is the concentration of the element of interest in the melt, C_0 is the concentration of the element in the original solid, F is the weight fraction of melt formed and D is the bulk partition coefficient of the element of interest.

$$\frac{C_L}{C_0} = \frac{1}{F + D - FD} \quad \text{(E-9)}$$

E-6 Decay Constants and Conversion Factors for Activities

The decay constants used in this thesis for calculating radioactive decay and isotope activities are those used by Cohen & O'Nions (1993). These are: $\lambda^{230}Th = 9.1952 \times 10^{-6}\ a^{-1}$, $\lambda^{238}U = 1.55125 \times 10^{-10}\ a^{-1}$, $\lambda^{232}Th = 4.9475 \times 10^{-11}\ a^{-1}$ and $\lambda^{226}Ra = 4.272 \times 10^{-4}\ a^{-1}$.

Activity and concentration ratios for radioactive isotopes are related by a constant value. For example if an expression for ($^{238}U/^{232}Th$) is written out in full, Equation E-10 is obtained, where A represents atomic mass and λ is the decay constant.

$$\frac{\left(^{238}U\right)}{\left(^{232}Th\right)} = \frac{\left\{[U]/A_{238}\right\}\lambda_{238}}{\left\{[Th]/A_{232}\right\}\lambda_{232}} \quad \text{(E-10)}$$

This can be rearranged to give Equation E-11,

$$\frac{(^{238}U)}{(^{232}Th)} = \left\{\frac{[U]}{[Th]}\right\}\left\{\frac{A_{Th}\lambda_{238}}{A_{U}\lambda_{232}}\right\} \quad \text{(E-11)}$$

where the expression containing the atomic masses and decay constants can be evaluated, and a single constant value determined which relates activity and concentration. This can be used to derive a number of constants for the short-lived isotope schemes of interest in this study. The values are as follows: ($^{238}U/^{232}Th$) = [U]/[[Th] x 3.043, ($^{230}Th/^{232}Th$) = [^{230}Th]/[^{232}Th] x 185885, ($^{230}Th/^{238}U$) = [^{230}Th]/[^{238}U] x 61342 and ($^{226}Ra/^{230}Th$) = [^{226}Ra]/[^{230}Th] x 47.283. These were calculated using atomic masses for the

various isotopes as follows: $A_{238} = 238.05079$, $A_{232} = 232.03805$, $A_{230} = 230.033127$, $A_{226} = 226.025403$.

E-7 Calculation of Magnesium Number (Mg#)

Magnesium number was calculated in this thesis was calculated in terms of oxide wt% as given in Equation E-12.

$$Mg\# = 100 \times \frac{MgO/40.32}{\left\{MgO/40.32 + \left(FeO/71.85 + Fe_2O_3/79.85\right)\right\}} \qquad \text{E-12}$$

E-8 Partition Coefficients used in Mass Balance Modelling

Element	$D^{ol/liq}_{element}$	$D^{cpx/liq}_{element}$	$D^{opx/liq}_{element}$	$D^{amph/liq}_{element}$	$D^{plag/liq}_{element}$
Rb	3.0E-04	4.0E-04	2.0E-04	0.023	0.008
Ba	5.0E-06	3.0E-04	6.0E-06	0.01	0.4
Th	7.0E-06	0.0021	2.0E-05	0.001	0.15
U	9.0E-06	0.001	4.0E-05	0.0012	0.05
Nb	5.0E-05	0.0089	0.003	0.08	0.008
K	2.0E-05	0.001	1.0E-05	0.22	
La	2.0E-04	0.054	0.0031	0.075	0.075
Pb	3.0E-04	0.0075	0.0014	0.019	0.2
Sr	4.0E-05	0.091	7.0E-04	0.27	1.4
P	0.01	0.03	0.03	0.2	
Nd	0.003	0.19	0.0023	0.23	0.025
Zr	0.001	0.26	0.012	0.25	0.0009
Sm	9.0E-04	0.27	0.0037	0.32	0.02
Ti	0.015	0.4	0.086	0.95	
Y	0.0082	0.47	0.015	0.54	0.01
Yb	0.024	0.43	0.038	0.5	0.004

Table E-1: Partition coefficients used for mass balance modelling in Chapter 5. Values for olivine (ol), clinopyroxene (cpx), orthopyroxene (opx), and amphibole (amph) are from Halliday et al. (1995). Partition coefficients for plagioclase (plag) are from Dunn and Sen (1994). Plagioclase values were only used for fractional crystallisation corrections, and therefore K, P and Ti values were not required.

Appendix F

Program Listings

This appendix presents the program listings for the modelling programs used in Chapter 6. All the code was written in the C programming language, and has been compiled successfully on Windows 95/98® with DJGPP 2.01 and GNU gcc 2.8.1, RedHat Linux 5.0 using GNU gcc 2.7.2.3 and on SunOS System V release 4.0 using GNU gcc 2.7.2.2.

F-1 Code for U-Th Model

The code for two files is given here. The uth.c file contains all the main program code which performs the required calculations. The file uth.h contains all the essential definitions, declarations and prototypes.

F-1.1 Code for uth.c

```
/*****************************************************************************
 *
 *  File: uth.c
 *  Author: Rob Hughes
 *  Purpose: To provide an iterative model for the behaviour of U and Th
 *           isotopes in an open system magma chamber, being able to take
 *           account of replenishment, crystallisation and assimilation
 *  Started: June 1996
 *
 *****************************************************************************/

/*
 * Include a specific header file which contains all standard includes and
 * program specific declarations, prototypes and definitions
 */

#include "uth.h"

/*****************************************************************************
 *
 *  Function: main()
 *  Purpose: Provides base program
 *  Arguments: None
 *  Return: int for exit state
 *
```

```
 ****************************************************************************/

int main( void )
{
  /*
   * Set up local variables and data structures required in the program
   */

  double cntr1, cntr2, cntr3, cntr4, cntr5;

  FILE *fp;
  int assim = FALSE;

  struct input_isotopes inp_iso, *ii;
  struct input_other inp_oth, *io;
  struct prog_data prg_dat, *pd;

  ii = &inp_iso;
  io = &inp_oth;
  pd = &prg_dat;

  /*
   * Try to open the stepdata file and results file
   */

#ifdef WIN
  system( "del results" );
  system( "del stepdata" );
#endif

#ifdef UNIX
  system( "rm results" );
  system( "rm stepdata" );
#endif

  if ( ( fp2 = fopen( "stepdata", "a+" ) ) == NULL ) {
    CLEAR;
    printf( "Cannot open stepdata - check file for errors/disk full etc. ");
    exit( 1 );
  } else if ( ( fp = fopen( "results", "a+" ) ) == NULL ) {
    CLEAR;
    printf( "Cannot open results - check file for errors/disk full etc." );
    exit( 1 );
  }

  CLEAR;

  /*
   * Get initial data and check if need to model assimilation. Write the
   * initial conditions to file and write the assimilation details to file if
   * required.
   */

  GetInitial( ii, io, pd );
  GetAssimilant( ii, pd, &assim );
  DisplayOrig( ii, io, pd, fp, assim );

  /* Main program loops to control the variables. Whilst everything can be
   * varied at once, it is recommended for the users sanity to only fiddle
   * with a couple of variables at a time.
   *
   * The factors the loops control are as follows:
   * loop 1: steps through the age range input by the user
   * loop 2: steps through the volume range input by the user
   * loop 3: steps through the 30/32 range input by the user
   * loop 4: steps through the range of iterations input by the user
   * loop 5: Performs the iterations and thus the main calculations
   */

  for ( cntr1 = io->age_min; cntr1 <= io->age_max; cntr1 += io->age_step ) {
    for ( cntr2 = io->chamber_min; cntr2 <= io->chamber_max;
```

```
        cntr2 += io->chamber_step )
    {
      for ( cntr3 = ii->th_min; cntr3 <= ii->th_max; cntr3 += ii->th_step ) {
       for ( cntr4 = io->steps_min; cntr4 <= io->steps_max;
             cntr4 += io->steps_step )
       {
          CalcOtherValues( ii, io, pd, cntr2, cntr3, cntr4, assim );
          DisplayCalcOther( pd, cntr1, cntr2, cntr3, cntr4, fp );
        check = FALSE;
        fprintf( fp2, "\n\n" );

        /*
         * Loop works out the effects of closed system processes followed
         * by a mixing event.
         */

        for ( cntr5 = 1; cntr5 <= cntr4; cntr5++ ) {
          EvolveMagma( ii, pd, cntr1, cntr3, cntr4, cntr5, assim );
          MixMagmas( ii, io, pd, cntr3, cntr2, cntr5 );
        }

         DisplayResults( pd, io, ii, fp, cntr1, cntr2, cntr3, cntr4 );
       }
      }
    }
  }

  /*
   * Close down the stepdata and results files and exit the program
   */

  fclose( fp );
  fclose( fp2 );
  exit( 0 );
}


/*****************************************************************************
 *
 *  Function: CalcOtherValues()
 *  Purpose: calculates any initial values that are required from the input
 *           conditions
 *  Arguments: pointer to structure with initial isotope data
 *             pointer to structure with other initial data
 *             pointer to structure with active data
 *             double for current value of counter 2
 *             double for current value of counter 3
 *             double for current value of counter 4
 *  Return: None
 *
 *****************************************************************************/

void CalcOtherValues( struct input_isotopes *ii, struct input_other *io,
                      struct prog_data *pd, double cntr2, double cntr3,
                     double cntr4, int assim )
{
  /*
   * Calculate 230Th conc based on Th abundance and 30/32 and set up a few
   * other values ready for use
   */

  pd->thppm_b = ( cntr3 * ii->thppm ) / THCONST;
  pd->curr_thppm_b = pd->thppm_b;
  pd->curr_thppm = ii->thppm;
  pd->th_mix = cntr3;
  pd->curr_uppm = ii->uppm;
  pd->curr_uth = ii->uth;
  pd->cmbr_vol = cntr2;

  /*
   * Rudimentary method of maintaining a volume balance - throw user out if
```

```
   * assimilation addition greater than loss through crystallisation and
   * eruption.
   */

  pd->input_vol = ( ( pd->cmbr_vol * pd->f ) + io->erupt_vol ) -
                  ( ( pd->cmbr_vol / ( 1 - ii->ass_f ) ) - pd->cmbr_vol );

  if ( pd->input_vol <= 0 ) {
    printf( "\n\n\bInput volume less than for the following conditions\n" );
    printf( "\nChamber vol: %f  Erupt Vol: %f  cryst: %.2f  assim: %.2f\n",
           pd->cmbr_vol, io->erupt_vol, pd->f, ii->ass_f );
    exit( 2 );
  }

  /*
   * Calculate some assimilation details if required
   */

  if ( assim ) {
    pd->ass_thth = ii->ass_thth;
    pd->ass_uth = ii->ass_uth;
    pd->ass_thppmb = ii->ass_thppmb;
    pd->ass_uppm = ii->ass_uppm;
    pd->ass_thppm = ii->ass_thppm;
  }
}


/*****************************************************************************
 *
 *  Function: EvolveMagma()
 *  Purpose: Deals with changes in U + Th isotopes during a closed system
 *           step. Handles radioactive decay and crystallisation
 *  Arguments: pointer to structure containing initial isotope data
 *             pointer to structure with active data
 *             double for current value of counter 1
 *             double for current value of counter 3
 *             double for current value of counter 4
 *             double for current value of counter 6
 *  Return: None
 *
 *****************************************************************************/

void EvolveMagma( struct input_isotopes *ii, struct prog_data *pd,
                  double cntr1, double cntr3, double cntr4, double cntr5,
                  int assim )
{
  /*
   * Set up local variables to handle certain calculations
   */

  double exp_tmp, exp_lamdat, f, ass_f;
  int i;

  /*
   * Calculate exp^(-LAMDA * t) value for use later in the function
   */

  exp_tmp = -LAMDA * ( ( ( cntr1 / AGECONV ) / cntr4 ) / ITERATIONS );
  exp_lamdat = exp( exp_tmp );
  f = pd->f / ITERATIONS;

  if ( assim )
    ass_f = ii->ass_f / ITERATIONS;

  /*
   * Loop first evolves the magma for the effects of radioactive decay. Then
   * crystallisation of the magma is accounted for and the concentrations of
   * 230 and the (238/232) for both the magma and the assimilant are
   * recalculated. Finally the magma and assimilant are mixed, and the
   * activity ratios recalculated
```

```
   */

  for ( i = 1; i <= ITERATIONS; i++ ) {
    pd->th_act = ( pd->curr_uth * ( 1 - exp_lamdat ) ) +
                 ( pd->th_mix * exp_lamdat );

    pd->curr_thppm *= ( pow( ( 1 - f ), ( pd->kd_th - 1 ) ) );
    pd->curr_uppm *= ( pow( ( 1 - f ), ( pd->kd_u - 1 ) ) );
    pd->curr_uth = ( pd->curr_uppm / pd->curr_thppm ) * UTHCONSTA;
    pd->curr_thppm_b = ( pd->th_act / THCONST ) * pd->curr_thppm;

    if ( assim ) {
      pd->curr_uppm = ( pd->curr_uppm * ( 1 - ass_f ) ) +
                      ( pd->ass_uppm * ass_f );
      pd->curr_thppm = ( pd->curr_thppm * ( 1 - ass_f ) ) +
                       ( pd->ass_thppm * ass_f );
      pd->curr_thppm_b = ( pd->curr_thppm_b * ( 1 - ass_f ) ) +
                         ( pd->ass_thppmb * ass_f );
    }

    pd->th_act = ( pd->curr_thppm / pd->curr_thppm_b ) * THCONST;
    pd->curr_uth = ( pd->curr_uppm / pd->curr_thppm ) * UTHCONSTA;
  }

  /*
   * Prints out data to the stepdata file
   */

  if ( check && cntr5 <= FILE2_LIMIT )
    fprintf( fp2, "  ThAct: %.3f  UThAct: %.3f ", pd->th_act, pd->curr_uth );
}


/*****************************************************************************
 *
 *  Function: MixMagmas()
 *  Purpose: Deals with input of fresh magma
 *  Arguments: pointer to structure with initial isotope data
 *             pointer to structure with other initial data
 *             pointer to structure with active data
 *             double holding current value of counter 2
 *             double holding current value of counter 3
 *             double holding current value of counter 6
 *  Return: None
 *
 *****************************************************************************/

void MixMagmas( struct input_isotopes *ii, struct input_other *io,
                struct prog_data *pd, double cntr3, double cntr2,
                double cntr5 )
{
  /*
   * Calculate the new 30/32 and 38/32 after mixing
   */

  pd->curr_thppm = ( ( pd->curr_thppm * pd->cmbr_vol ) +
                   ( ii->thppm * pd->input_vol ) ) /
                   ( pd->cmbr_vol + pd->input_vol );
  pd->curr_thppm_b = ( ( pd->curr_thppm_b * pd->cmbr_vol ) +
                     ( pd->thppm_b * pd->input_vol ) ) /
                     ( pd->cmbr_vol + pd->input_vol );
  pd->th_mix = ( pd->curr_thppm_b / pd->curr_thppm ) * THCONST;
  pd->curr_uppm = ( ( ii->uppm * pd->input_vol ) +
                  ( pd->curr_uppm * pd->cmbr_vol ) ) /
                    ( pd->cmbr_vol + pd->input_vol );
  pd->curr_uth = ( ( pd->curr_uppm / pd->curr_thppm ) * UTHCONSTA );

  if ( ( check ) && ( cntr5 <= FILE2_LIMIT ) ) {
    check = FALSE;
    fprintf( fp2, "%.3f\n", pd->th_mix );
  } else if ( check == FALSE )
```

```
    check = TRUE;

}


/*****************************************************************************
 *
 *  Function: GetAssimilant()
 *  Purpose: Gets details of the assimilant from the user
 *  Arguments: pointer to structure containing initial isotope data
 *             pointer to structure containing active data
 *             pointer to int holding assimilation flag
 *  Return: None
 *
 *****************************************************************************/

void GetAssimilant( struct input_isotopes *ii, struct prog_data *pd,
                    int *assim )
{
  CLEAR;
  printf( "\n\nModel assimilation [y/n]?: " );

  if ( GetYesNo() )
    *assim = TRUE;
  else {
    *assim = FALSE;
    return;
  }

  printf( "\nEnter U concentration of assimilant: " );
  ii->ass_uppm = GetDouble();
  printf( "\nEnter Th concentration of assimilant: " );
  ii->ass_thppm = GetDouble();
  printf( "\nEnter the weight fraction of assimilation per step: " );
  ii->ass_f = GetDouble();

  while ( ii->ass_f <= 0 || ii->ass_f >= 1 ) {
    printf( "\b\nThe fraction must be 0 < f < 1 - reenter: " );
    ii->ass_f = GetDouble();
  }

  printf( "\nEnter the (230/232) of the assimilant (eqm = %.3f): ",
         ( ii->ass_uppm / ii->ass_thppm ) * UTHCONSTA );
  ii->ass_thth = GetDouble();
  ii->ass_uth = ( ii->ass_uppm / ii->ass_thppm * UTHCONSTA );
  ii->ass_thppmb = ( ii->ass_thth / THCONST ) * ii->ass_thppm;
}


/*****************************************************************************
 *
 *  Function: DisplayOrig()
 *  Purpose: Writes the initial conditions to the file results
 *  Arguments: pointer to structure containing initial isotope data
 *             pointer to structure containing other initial data
 *             pointer to structure containing active data
 *             pointer to results file
 *  Return: None
 *
 *****************************************************************************/

void DisplayOrig( struct input_isotopes *ii, struct input_other *io,
                  struct prog_data *pd, FILE *fp, int assim )
{
  DrawHashLine( fp );
  fprintf( fp, "\n\nORIGINAL CONDITIONS\n" );
  fprintf( fp, "~~~~~~~~~~~~~~~~~~~\n\n" );
  fprintf( fp, "(230/232)min: %.3f  (230/232)max: %.3f  (230/232)step: %.3f\n",
          ii->th_min, ii->th_max, ii->th_step );
  fprintf( fp, "[Th]: %.2f  [U]: %.2f  (238/232): %.3f\n", ii->thppm,
          ii->uppm, ii->uth );
```

```
  fprintf( fp, "Steps Min: %.0f  Steps Max: %.0f  Steps step: %.0f\n",
          io->steps_min, io->steps_max, io->steps_step );
  fprintf( fp, "Chamber Age min: %.0f  CAge Max: %.0f  CAge Steps: %.0f\n",
          io->age_min / AGECONV, io->age_max / AGECONV,
          io->age_step / AGECONV );
  fprintf( fp, "Chamber Vol min: %.1f  CVol max: %.1f  CVol Steps: %.1f\n",
          io->chamber_min / VOLCONV, io->chamber_max / VOLCONV,
          io->chamber_step / VOLCONV );

  if ( var_kd )
    fprintf( fp, "\nUSING VARIABLE Kd VALUES OF U: %.3f  Th: %.3f\n",
            pd->kd_u, pd->kd_th );

  if ( assim ) {
    fprintf( fp, "\nAssimilant Details:\n" );
    fprintf( fp, "\n[Th]ppm: %.2f  [U]ppm: %.2f  [230]ppt: %.1f\n",
            ii->ass_thppm, ii->ass_uppm, ii->ass_thppmb * 1E6 );
    fprintf( fp, "(230/232)i: %.3f  (238/232): %.3f  f: %.2f\n",
            ii->ass_thth, ii->ass_uth, ii->ass_f );
  }

  fprintf( fp, "\n" );
  DrawHashLine( fp );
  fprintf( fp, "\n\n" );
}


/*****************************************************************************
 *
 *  Function: DisplayCalcOther()
 *  Purpose: Writes info from CalcOther() to results file
 *  Arguments: pointer to structure containing active data
 *             double holding value of counter 1
 *             double holding value of counter 2
 *             double holding value of counter 3
 *             double holding value of counter 4
 *             pointer to results file
 *  Return: None
 *
 *****************************************************************************/

void DisplayCalcOther( struct prog_data *pd, double cntr1, double cntr2,
                       double cntr3, double cntr4, FILE *fp )
{
  fprintf( fp, "\n" );
  DrawHashLine( fp );
  fprintf( fp, "\n\nCURRENT RUN DETAILS\n" );
  fprintf( fp, "~~~~~~~~~~~~~~~~~~~\n\n" );
  fprintf( fp, "Chamber Vol: %.1f  230ppt(init): %.1f\n",
          cntr2 / VOLCONV, pd->thppm_b * 1E6 );
  fprintf( fp, "Chamber Age: %.0f  Steps: %.0f  (230/232)init: %.3f  \n\n",
          cntr1 / AGECONV, cntr4, cntr3 );
  DrawHashLine( fp );
  fprintf( fp, "\n\n" );
}


/*****************************************************************************
 *
 *  Function: DisplayResults()
 *  Purpose: Writes results to the results file as they occur
 *  Arguments: pointer to structure containing active data
 *             pointer to structure containing other input data
 *             pointer to structure containing intial isotope data
 *             pointer to results file
 *             double holding value of counter 1
 *             double holding value of counter 2
 *             double holding value of counter 3
 *             double holding value of counter 4
 *  Return: None
 *
```

```
 ****************************************************************************/

void DisplayResults( struct prog_data *pd, struct input_other *io,
                     struct input_isotopes *ii, FILE *fp, double cntr1,
                     double cntr2, double cntr3, double cntr4 )
{
  DrawHashLine( fp );
  fprintf( fp, "\n\nRESULTS\n" );
  fprintf( fp, "~~~~~~~\n\n" );
  fprintf( fp, "(230/232)(erupt)\tTot_Erupt_Vol\tInput Vol\n" );
  fprintf( fp, "%.3f\t\t\t%.1f\t\t%.1f\n", pd->th_mix,
          ( io->erupt_vol * cntr4 ) / VOLCONV, pd->input_vol / VOLCONV );
  fprintf( fp, "[Th]\t[U]\t(238/232)\n" );
  fprintf( fp, "%.2f\t%.2f\t%.3f\n", pd->curr_thppm, pd->curr_uppm,
          pd->curr_uth );
  fprintf( fp, "Turnover Time\t\tCalcAge (Post-mix)\tCalc Age (Pre-mix)\n" );
  fprintf( fp, "%.1f\t\t\t%.1f\t\t\t%.1f\n",
          ( ( pd->cmbr_vol / pd->input_vol ) *
            ( ( cntr1 / AGECONV ) / cntr4 ) ),
          log( ( ( pd->th_mix - ii->uth ) / ( cntr3 - ii->uth ) ) ) / -LAMDA,
          log( ( ( pd->th_act - ii->uth ) /
               ( cntr3 - ii->uth ) ) ) / -LAMDA );
  fprintf( fp, "\n" );
  DrawHashLine( fp );
  fprintf( fp, "\n\n" );
}


/****************************************************************************
 *
 *  Function: GetInitial()
 *  Purpose: Gets initial conditions from the user
 *  Arguments: pointer to structure containing the initial isotope data
 *             pointer to structure containing other initial data
 *             pointer to structure containing active data
 *  Return: None
 *
 ****************************************************************************/

void GetInitial( struct input_isotopes *ii, struct input_other *io,
                 struct prog_data *pd )
{
  CLEAR;
  /* Gets Th abundance and activity values */
  printf( "Th Input Values\n" );
  printf( "~~~~~~~~~~~~~~~\n" );
  printf( "\n\n\n" );
  printf( "Th abundance (ppm): " );
  ii->thppm = GetDouble();
  printf( "\n(230)/(232) minimum value: " );
  ii->th_min = GetDouble();
  printf( "\n(230)/(232) maximum value: " );
  ii->th_max = GetDouble();
  printf( "\n(230)/(232) step value: " );
  ii->th_step = GetDouble();
  CLEAR;

  /* Gets 238/232 activity ratio */
  printf( "U-Th values\n" );
  printf( "~~~~~~~~~~\n" );
  printf( "\n\n\n" );
  printf( "(238)/(232) value: " );
  ii->uth = GetDouble();
  printf( "\nDo you want to use different U and Th Kd values? [y/n]: " );

  if ( GetYesNo( ) ) {
    var_kd = TRUE;
    printf( "\nEnter Kd for Th: " );
    pd->kd_th = GetDouble( );
    printf( "\nEnter Kd for U: " );
    pd->kd_u = GetDouble( );
```

```
  } else {
    var_kd = FALSE;
    pd->kd_th = pd->kd_u = DTH;
  }

  ii->uppm = ii->thppm * ( ii->uth / UTHCONSTA );

  CLEAR;

  /* Gets data on number of input steps required */
  printf( "Step Info\n" );
  printf( "~~~~~~~~~\n" );
  printf( "\n\n\n" );
  printf( "Minimum number of steps: " );
  io->steps_min = GetDouble();
  printf( "\nMaximum number of steps: " );
  io->steps_max = GetDouble();
  printf( "\nIncrease in steps per cycle: " );
  io->steps_step = GetDouble();
  CLEAR;

  /* Gets data on chamber age (time over which inputs occur) */
  printf( "Chamber Age Info\n" );
  printf( "~~~~~~~~~~~~~~~~\n" );
  printf( "\n\n\n" );
  printf( "Minimum Age (years): " );
  io->age_min = GetDouble();
  printf( "\nMaximum Age (years): " );
  io->age_max = GetDouble();
  printf( "\nAge step length (years): " );
  io->age_step = GetDouble();
  CLEAR;

  /* Gets constraints for chamber volume and erupted volume */
  printf( "Volume Info\n" );
  printf( "~~~~~~~~~~~\n" );
  printf( "\n\n\n" );
  printf( "Erupted volume per step (km3): " );
  io->erupt_vol = GetDouble();
  printf( "\nMinimum chamber volume (km3): " );
  io->chamber_min = GetDouble();
  printf( "\nMaximum chamber volume (km3): " );
  io->chamber_max = GetDouble();
  printf( "\nChamber volume step size (km3): " );
  io->chamber_step = GetDouble();
  CLEAR;

  /* Get crystallization percentage from user */
  printf( "\nCrystallization fraction per step (as fraction, not %%): " );
  pd->f = GetDouble();

  while ( pd->f <= 0 || pd->f >= 1 ) {
    printf( "\n\n\bValue of f must be 0 < f < 1 - reenter: " );
    pd->f = GetDouble();
  }

  CLEAR;

  /* code to set chamber/erupted volumes to metres cubed */
  io->chamber_max *= 1000000000;
  io->chamber_min *= 1000000000;
  io->chamber_step *= 1000000000;

  io->erupt_vol *= 1000000000;

  /* code to conver times to seconds */
  io->age_min *= 31557600;
  io->age_max *= 31557600;
  io->age_step *= 31557600;
}
```

```
/*************************************************************************
 *
 *  Function: GetDouble()
 *  Purpose: Gets a double value from the user
 *  Arguments: None
 *  Return: double with the value obtained from the user
 *
 *************************************************************************/

double GetDouble( void )
{
  char buf[ BUFSIZE ];
  int i;
  double j;

  while ( TRUE ) {
    for ( i = 0; i <= ( BUFSIZE - 1 ); i++ )
      buf[ i ] = '\0';

    fgets( buf, BUFSIZE, stdin );

    if ( 1 != sscanf( buf, "%lf", &j ) )
      printf( "\a\n" );
    else
      break;
  }

  return j;
}


/*************************************************************************
 *
 *  Function: GetYesNo()
 *  Purpose: Gets a yes/no response from the user
 *  Arguments: None
 *  Return: int - TRUE for yes, FALSE for no
 *
 *************************************************************************/

int GetYesNo( void )
{
  char buf[ BUFSIZE ];
  char ch;
  int i;

  while ( 1 ) {
    for ( i = 0; i <= ( BUFSIZE - 1 ); i++ )
      buf[ i ] = '\0';

    fgets( buf, BUFSIZE, stdin );

    if ( ( 1 == sscanf( buf, "%c", &ch ) ) &&
       ( ch == 'Y' || ch == 'y' || ch == 'N' || ch == 'n' ) )
      break;
    else
      printf( "\n\a" );
  }

  if ( ch == 'Y' || ch == 'y' )
    return TRUE;

  return FALSE;
}


/*************************************************************************
 *
 *  Function: DrawHashLine()
 *  Purpose: Draws a line of hashes across the output file
```

```
 *  Arguments: Pointer to file to write in
 *  Return: None
 *
 ******************************************************************************/

void DrawHashLine( FILE *fd )
{
  int i;

  for ( i = 1; i <= 80; i++ )
    fprintf( fd, "#" );
}
```

F-1.2 Code for uth.h

```
/*****************************************************************************
 *
 *  File: uth.h
 *  Author: Rob Hughes
 *  Purpose: Header file for program to model the behaviour of U and Th
 *           isotopes in open system magma chambers
 *  Started: June 1996
 *
 *****************************************************************************/

/*
 * Include header files
 */

#include <stdio.h>
#include <stdlib.h>
#include <math.h>
#include <unistd.h>

/*
 * Definition of symbolics and macros
 */

#define LAMDA 9.1952E-6      /* decay constant for 230Th */
#define THCONST 185885       /* constant for activity-abundance conversion */
#define UTHCONSTA 3.034      /* 238-232 activity-abundance conversion */
#define CRYSSTEP 0.02        /* step for crystallization % */
#define VOLCONV 1000000000   /* conversion between volume units */
#define AGECONV 31536000     /* age conversion factor */
#define BUFSIZE 20
#define FILE2_LIMIT 100      /* number of entries that should be put into
                                stepres file */
#define ITERATIONS 20        /* Iterations in closed system step */
#define DTH 0.05
#define TRUE 1
#define FALSE 0
#define WIN

#ifdef UNIX
#define CLEAR system( "clear" )
#define DELAY(X) sleep( X*1000 )
#endif

#ifdef WIN
#define CLEAR system( "cls" )
#define DELAY(X) sleep(X)
#endif

/*
 * Define structures for use in the main program
 */

struct input_isotopes {
  double thppm;
  double uppm;
```

```
  double th_min;
  double th_max;
  double th_step;
  double uth;
  double ass_uppm;
  double ass_thppm;
  double ass_f;
  double ass_thth;
  double ass_uth;
  double ass_thppmb;
};

struct input_other {
  double steps_min;
  double steps_max;
  double steps_step;
  double age_min;
  double age_max;
  double age_step;
  double chamber_min;
  double chamber_max;
  double chamber_step;
  double erupt_vol;
};

struct prog_data {
  double kd_th;
  double kd_u;
  double curr_uth;
  double curr_uppm;
  double input_vol;
  double th_act;
  double th_mix;
  double cmbr_vol;
  double thppm_b;
  double curr_thppm;
  double curr_thppm_b;
  double f;
  double ass_thppm;
  double ass_uppm;
  double ass_uth;
  double ass_thth;
  double ass_thppmb;
  double last_pre_mix;
  double last_post_mix;
};

/*
 * Prototype functions
 */

void GetInitial( struct input_isotopes *ii, struct input_other *io,
                 struct prog_data *pd );
void CalcOtherValues( struct input_isotopes *ii, struct input_other *io,
                      struct prog_data *pd, double cntr2, double cntr3,
                      double cntr4, int assim );
void EvolveMagma( struct input_isotopes *ii, struct prog_data *pd,
                  double cntr1, double cntr3, double cntr4, double cntr6,
                  int assim );
void MixMagmas( struct input_isotopes *ii, struct input_other *io,
                struct prog_data *pd, double cntr3, double cntr2,
                double cntr6 );
void GetAssimilant( struct input_isotopes *ii, struct prog_data *pd,
                    int *assim );
void DisplayOrig( struct input_isotopes *ii, struct input_other *io,
                  struct prog_data *pd, FILE *fp, int assim );
void DisplayCalcOther( struct prog_data *pd, double cntr1, double cntr2,
                       double cntr3, double cntr4, FILE *fp );
void DisplayResults( struct prog_data *pd, struct input_other *io,
                     struct input_isotopes *ii, FILE *fp, double cntr1,
                     double cntr2, double cntr3, double cntr4 );
```

```
double GetDouble( void );
int GetYesNo( void );
void DrawHashLine( FILE *fd );

/*
 * Declare global variables
 */

FILE *fp2;
int check;
int var_kd = FALSE;
```

F-2 Code for U-Th-Ra-Ba Model

The code for two files is given here. The radium.c file contains all the main program code, and radium.h contains all the essential definitions, declarations and prototypes.

F-2.1 Code for radium.c

```
/*****************************************************************************
 *
 *  File: radium.c
 *  Author: Rob Hughes
 *  Purpose: Provides an iterative model for the behaviour of U-Th-Ra-Ba
 *           in magma chamber processes
 *  Started: April 1998
 *
 *****************************************************************************/

/* Include single header which contains all definitions/includes */

#include "radium.h"

/*****************************************************************************
 *
 *  Function: main()
 *  Purpose: Core of program
 *  Arguments: None
 *  Return: int
 *
 *****************************************************************************/

int main( void )
{
  /*
   * Initialise local variables and data structures to hold all info
   */

  int i;

  struct InitialData initial;
  struct InitialData *init = &initial;
  struct ProgramData program_data;
  struct ProgramData *data = &program_data;

  /*
   * Read in the initial user data from file radium.in
   * Set up required initial values that can be calculated from initial data
   * Write header for output file with the starting values
```

```
   */

  ReadInputFile( init );
  InitialCalcs( init, data );
  WriteOutputFile( init, data, DO_HEADER, 0 );

  /*
   * The main control loop. This steps through the number of refilling
   * iterations indicated in radium.in. The iterations within the closed
   * system step are controlled elsewhere. The first thing to do is to go
   * through a closed system decay and crystallisation calculation, and output
   * the data if indicated by the user. Next comes the replenishment step and
   * data output if indicated. This is repeated until all replenishments are
   * done.
   */

  for ( i = 1; i <= init->freq; i++ ) {
    EvolveAllValues( init, data );

    if ( init->evolve_flag )
      WriteOutputFile( init, data, DO_EVOLVE, i * data->interval );

    MixingCalcs( init, data );

    if ( init->mix_flag )
      WriteOutputFile( init, data, DO_MIX, i * data->interval );
  }

  exit( 0 );
}


/*****************************************************************************
 *
 *  Function: EvolveAllValues()
 *  Purpose: Iterates a user-defined number of times during a closed system
 *           step to allow for radioactive decay and crystallisation
 *  Arguments: pointer to structure containing initial data
 *             pointer to structure containing active data
 *  Return: None
 *
 *****************************************************************************/

void EvolveAllValues( struct InitialData *init, struct ProgramData *data )
{
  /*
   * Set up a local counter
   */

  int i;

  /*
   * Second control loop to perform the indicated number of iterations per
   * step to simulate the effects of simultaneous crystallisation and decay.
   * Experimentation that 10-20 iterations per closed system step are required
   * to make this a reasonable approximation, although this is somewhat
   * dependant on the length of the closed system step.
   */

  for ( i = 1; i <= ( init->integrations + 1 ) ; i++ ) {

    /*
     * Radioactive decay is calculated first, although this is arbitary, and
     * performing crystallisation first would produce the same results if a
     * reasonable number of iterations had been chosen.
     */

    data->th_iso_chamb = IsotopeEvolveCalc( data->th_iso_chamb,
                                            data->uth_iso_chamb, LAMBDATH,
                                            init->integration_time );
    data->raba_iso_chamb = IsotopeEvolveCalc( data->raba_iso_chamb,
```

```
                                        data->thba_iso_chamb, LAMBDARA,
                                        init->integration_time );

    /*
     * Certain other values such as concentrations need to be recalculated
     * following radioactive decay prior to crystallisation calculations
     */

    data->ra_act_chamb = data->raba_iso_chamb *
                         ( data->ba_conc_chamb / 1000000 );
    data->ra_conc_chamb = ( ( data->ra_act_chamb / LAMBDARA ) *
                          ATMASSRA ) * 1000000;
    data->th230_conc_chamb = ( data->th_iso_chamb / THCONST ) *
                             data->th_conc_chamb;
    data->th230_act_chamb = ( ( data->th230_conc_chamb / 1000000 ) /
                            ATMASSTH ) * LAMBDATH;

    /*
     * Work out crystallisation effects with the updated values after
     * decay.
     */

    data->u_conc_chamb = FracCrystalCalc( data->u_conc_chamb, init->u_kd,
                                          ( init->f / init->integrations ) );
    data->th_conc_chamb = FracCrystalCalc( data->th_conc_chamb, init->th_kd,
                                           ( init->f / init->integrations ) );
    data->ra_conc_chamb = FracCrystalCalc( data->ra_conc_chamb, init->ra_kd,
                                           ( init->f / init->integrations ) );
    data->ba_conc_chamb = FracCrystalCalc( data->ba_conc_chamb, init->ba_kd,
                                           ( init->f / init->integrations ) );
    data->th230_conc_chamb = FracCrystalCalc( data->th230_conc_chamb,
                                              init->th_kd,
                                              ( init->f /
                                                init->integrations ) );

    /*
     * Recalculate other values as required once crystallisation is
     * accounted for.
     */

    data->ra_act_chamb = ( ( data->ra_conc_chamb / 1000000 ) / ATMASSRA ) *
                         LAMBDARA;
    data->th230_act_chamb = ( ( data->th230_conc_chamb / 1000000 ) /
                            ATMASSTH ) * LAMBDATH;
    data->raba_iso_chamb = data->ra_act_chamb /
                           ( data->ba_conc_chamb / 1000000 );
    data->thba_iso_chamb = data->th230_act_chamb /
                           ( data->ba_conc_chamb / 1000000 );
    data->uth_iso_chamb = ( data->u_conc_chamb / data->th_conc_chamb ) *
                          UTHCONST;

    /*
     * Write the iteration data to the chosen output file if the iteration
     * flag is set.
     */

    if ( init->integrate_flag )
      WriteOutputFile( init, data, DO_INTEGRATE, i );
  }
}


/*****************************************************************************
 *
 *  Function: MixingCalcs()
 *  Purpose: Allows for an open system mixing step which introduces fresh
 *           magma into the system
 *  Arguments: pointer to structure containing the initial data
 *             pointer to structure containing the active data
 *  Return: None
 *
```

```
 ***************************************************************************/

void MixingCalcs( struct InitialData *init, struct ProgramData *data )
{
  /*
   * Mix U+Th isotopes according to their abundances and then recalculate
   * the activities etc.
   */

  data->th230_conc_chamb = ( ( init->th230_conc * init->ivol ) +
                           ( data->th230_conc_chamb * init->cvol ) ) /
                           ( init->cvol + init->ivol );
  data->th_conc_chamb = ( ( init->th_conc * init->ivol ) +
                        ( data->th_conc_chamb * init->cvol ) ) /
                        ( init->cvol + init->ivol );
  data->u_conc_chamb = ( ( init->u_conc * init->ivol ) +
                       ( data->u_conc_chamb * init->cvol ) ) /
                       ( init->ivol + init->cvol );
  data->th_iso_chamb = ( data->th230_conc_chamb / data->th_conc_chamb ) *
                         THCONST;
  data->th230_act_chamb = ( ( data->th230_conc_chamb / 1000000 ) /
                          ATMASSTH ) * LAMBDATH;
  data->uth_iso_chamb = ( data->u_conc_chamb / data->th_conc_chamb ) *
                          UTHCONST;

  /*
   * Mix radium and barium according to their abundances and recalculate
   * activities and activity/concentration ratios.
   */

  data->ra_conc_chamb = ( ( init->ra_conc * init->ivol ) +
                        ( data->ra_conc_chamb * init->cvol ) ) /
                        ( init->cvol + init->ivol );
  data->ra_act_chamb = ( ( data->ra_conc_chamb / 1000000 ) / ATMASSRA ) *
                         LAMBDARA;
  data->ba_conc_chamb = ( ( init->ba_conc * init->ivol ) +
                        ( data->ba_conc_chamb * init->cvol ) ) /
                            ( init->cvol + init->ivol );
  data->thba_iso_chamb = data->th230_act_chamb /
                           ( data->ba_conc_chamb / 1000000 );
  data->raba_iso_chamb = data->ra_act_chamb /
                           ( data->ba_conc_chamb / 1000000 );
}


/***************************************************************************
 *
 *  Function: ReadInputFile()
 *  Purpose: Reads the radium.in input file to get starting conditions and
 *           flags
 *  Arguments: pointer to structure containing the initial data
 *  Return: None
 *
 ***************************************************************************/

void ReadInputFile( struct InitialData *init )
{
  /*
   * Set up local file pointers and buffers for reading data from radium.in
   */

  FILE *fd;
  char buf [ BUFSIZE ];
  char garbage[ 50 ];

  /*
   * Open file, and read data line by line, extracting the required numerical
   * values. Ensure file closes cleanly at the end of the function.
   */

  if ( !( fd = fopen( "radium.in", "r" ) ) ) {
```

```
    printf( "\n\n\aError opening radium.in\n" );
    exit( 1 );
  }

  fgets( buf, BUFSIZE, fd );

  if ( 8 != ( sscanf( buf, "%s %lf %s %lf %s %lf %s %lf", garbage,
                  &init->th_conc, garbage, &init->u_conc, garbage,
                  &init->ra_conc, garbage, &init->ba_conc ) ) ) {
    printf( "\n\aError reading concentrations from file\n" );
    exit( 1 );
  }

  fgets( buf, BUFSIZE, fd );

  if ( 8 != ( sscanf( buf, "%s %lf %s %lf %s %lf %s %lf", garbage,
                  &init->th_kd, garbage, &init->u_kd, garbage,
                  &init->ra_kd, garbage, &init->ba_kd ) ) ) {
    printf( "\n\aError reading kd's from file\n" );
    exit( 1 );
  }

  fgets( buf, BUFSIZE, fd );

  if ( 4 != ( sscanf( buf, "%s %lf %s %lf", garbage, &init->uth_iso,
                    garbage, &init->th_iso_init ) ) ) {
    printf( "\n\aError reading initial isotopic ratios from file\n" );
    exit( 1 );
  }

  fgets( buf, BUFSIZE, fd );

  if ( 6 != ( sscanf( buf, "%s %d %s %d %s %lf", garbage, &init->cvol,
                  garbage, &init->ivol, garbage, &init->f ) ) ) {
    printf( "\n\aError reading volumes from file\n" );
    exit( 1 );
  }

  fgets( buf, BUFSIZE, fd );

  if ( 6 != ( sscanf( buf, "%s %d %s %d %s %d", garbage, &init->freq,
                  garbage, &init->ttr, garbage, &init->integrations ) ) ) {
    printf( "\n\aError reading frequency and ttr from file\n" );
    exit( 1 );
  }

  fgets( buf, BUFSIZE, fd );

  if ( 8 != ( sscanf( buf, "%s %d %s %d %s %d %s %d", garbage,
                  &init->integrate_flag, garbage, &init->mix_flag,
                  garbage, &init->evolve_flag, garbage,
                  &init->age_calc_flag ) ) ) {
    printf( "\n\aError reading integrate flag from file\n" );
    exit( 1 );
  }

  fgets( buf, BUFSIZE, fd );

  if ( 2 != ( sscanf( buf, "%s %d", garbage, &init->time_since_run ) ) ) {
    printf( "\n\aError reading time since run from file\n" );
    exit( 1 );
  }

  fgets( buf, BUFSIZE, fd );

  if ( 1 != ( sscanf( buf, "%s", init->file_out ) ) ) {
    printf( "\n\aError reading output filename from file\n" );
    exit( 1 );
  }

  fgets( buf, BUFSIZE, fd );
```

```
  if ( 1 != ( sscanf( buf, "%s", init->file_out2 ) ) ) {
    printf( "\n\aError reading output filename from file\n" );
    exit( 1 );
  }

  fclose( fd );
}


/*****************************************************************************
 *
 *  Function: InitialCalcs()
 *  Purpose: Sets up a few values initially based on the input data
 *  Arguments: pointer to structure containing the initial data
 *             pointer to structure containing the active data
 *  Return: None
 *
 *****************************************************************************/

void InitialCalcs( struct InitialData *init, struct ProgramData *data )
{
  /*
   * Set up a local character buffer.
   */

  char buf[ 80 ];

  /*
   * Transfer starting conditions to the structure containing active data,
   * calculate activities and ratios etc. based on the starting conditions.
   * Remove a pre-existing output file if one exists
   */

  data->u_conc_chamb = init->u_conc;
  data->th_conc_chamb = init->th_conc;
  data->ra_conc_chamb = init->ra_conc;
  data->ba_conc_chamb = init->ba_conc;
  data->th_iso_chamb = init->th_iso_init;
  data->uth_iso_chamb = init->uth_iso;

  init->ra_act = ( ( init->ra_conc / 1000000 ) / ATMASSRA ) * LAMBDARA;
  data->ra_act_chamb = init->ra_act;
  init->raba_iso = init->ra_act / ( init->ba_conc / 1000000 );
  data->raba_iso_chamb = init->raba_iso;

  init->th230_conc = ( init->th_iso_init / THCONST ) * init->th_conc;
  data->th230_conc_chamb = init->th230_conc;
  init->th230_act = ( ( init->th230_conc / 1000000 ) / ATMASSTH ) * LAMBDATH;
  data->th230_act_chamb = init->th230_act;
  init->thba_iso = init->th230_act / ( init->ba_conc / 1000000 );
  data->thba_iso_chamb = init->thba_iso;

  data->interval = (double)init->ttr / (double)init->freq;
  init->integration_time = data->interval / (double)init->integrations;

#ifdef UNIX
  sprintf( buf, "rm -rf %s", init->file_out );
  system( buf );
  sprintf( buf, "rm -rf %s", init->file_out2 );
  system( buf );
#endif

#ifdef WIN
  sprintf( buf, "del %s", init->file_out );
  system( buf );
  sprintf( buf, "del %s", init->file_out2 );
  system( buf );
#endif
}
```

```
/*****************************************************************************
 *
 *  Function: WriteOutputFile
 *  Purpose: Writes details to the chosen output file according to the flags
 *           set in radium.in
 *  Arguments: pointer to structure containing the initial data
 *             pointer to structure containing the active data
 *             int indicating which type of output is required
 *             int indicating which step/iteration that has just finished
 *  Return: None
 *
 *****************************************************************************/

void WriteOutputFile( struct InitialData *init, struct ProgramData *data,
                      int flag, int step_num )
{
  /*
   * Set up a local file pointer and buffer so that file doesn't have to be
   * held open on a global scope.
   */

  FILE *fd, *fd2;
  char buf[ 80 ];

  /*
   * Open the files and move to the end so that preceding output isn't lost.
   */

  if ( !( fd = fopen( init->file_out, "a+" ) ) ) {
    printf( "\n\aError opening output file\n" );
    exit( 1 );
  } else if ( !( fd2 = fopen( init->file_out2, "a+" ) ) ) {
    printf( "\n\aError opening output file 2\n" );
    exit( 1 );
  }

  fseek( fd, 0L, SEEK_END );
  fseek( fd2, 0L, SEEK_END );

  /*
   * According to where the function is called there are four possible output
   * options which allows for user customisation of the output according to
   * need. Each option outputs all relevant data.
   */

  switch ( flag ) {
    case DO_EVOLVE :
      fprintf( fd, "\n" );
      DoHashLine( fd );
      fprintf( fd, "\n" );
      sprintf( buf, "Evolved values after %d years", step_num );
      CentreText( fd, buf );
      fprintf( fd, "\n\n" );
      fprintf( fd, "[Th]: %.3f  [230Th]: %.3g  [U]: %.3f  [Ba]: %.3f  "
              "[Ra]:%.3g\n", data->th_conc_chamb, data->th230_conc_chamb,
              data->u_conc_chamb, data->ba_conc_chamb, data->ra_conc_chamb );
      fprintf( fd, "N.B. Units for concentrations: ug g-1\n" );
      fprintf( fd, "(230/232)i: %.3f  (238/232): %.3f  (226)/[Ba]: %.2g"
              "  (230)/[Ba]: %.2g\n", data->th_iso_chamb, data->uth_iso_chamb,
              data->raba_iso_chamb * 1E15,
              data->thba_iso_chamb * 1E15 );
      fprintf( fd, "N.B. Activity/Concentration units: fmol g-1 yr-1\n" );
      fprintf( fd, "(230): %g  (226): %g\n",
              data->th230_act_chamb * 1E15,
              data->ra_act_chamb * 1E15 );
      fprintf( fd, "N.B. activities in units of: fmol g-1 yr-1\n" );
      fprintf( fd, "\n" );
      DoHashLine( fd );
      fprintf( fd, "\n" );
      fprintf( fd2, "EVOLVE: (38/32): %g (30/32): %g (30)/[Ba]: %g "
```

```
            "(26)/[Ba]: %g\n", data->uth_iso_chamb, data->th_iso_chamb,
            data->thba_iso_chamb * 1E15, data->raba_iso_chamb * 1E15 );
    break;

  case DO_MIX :
    fprintf( fd, "\n" );
    DoHashLine( fd );
    fprintf( fd, "\n" );
    sprintf( buf, "Mixed values after %d years", step_num );
    CentreText( fd, buf );
    fprintf( fd, "\n\n" );
    fprintf( fd, "[Th]: %.3f  [230Th]: %.3g  [U]: %.3f  [Ba]: %.3f  "
            "[Ra]:%.3g\n", data->th_conc_chamb, data->th230_conc_chamb,
            data->u_conc_chamb, data->ba_conc_chamb, data->ra_conc_chamb );
    fprintf( fd, "N.B. Units for concentrations: ug g-1\n" );
    fprintf( fd, "(230/232)i: %.3f  (238/232): %.3f  (226)/[Ba]: %.2g"
            "  (230)/[Ba]: %.2g\n", data->th_iso_chamb, data->uth_iso_chamb,
            data->raba_iso_chamb * 1E15,
            data->thba_iso_chamb * 1E15 );
    fprintf( fd, "N.B. Activity/Concentration units: fmol g-1 yr-1\n" );
    fprintf( fd, "(230): %g  (226): %g\n",
            data->th230_act_chamb * 1E15,
            data->ra_act_chamb * 1E15 );
    fprintf( fd, "N.B. activities in units of: fmol g-1 yr-1\n" );
    fprintf( fd, "\n" );
    DoHashLine( fd );
    fprintf( fd, "\n" );
    fprintf( fd2, "MIX: (38/32): %g (30/32): %g (30)/[Ba]: %g "
            "(26)/[Ba]: %g\n", data->uth_iso_chamb, data->th_iso_chamb,
            data->thba_iso_chamb * 1E15, data->raba_iso_chamb * 1E15 );
    break;

  case DO_HEADER :
    DoHashLine( fd );
    fprintf( fd, "\n" );
    CentreText( fd, "Starting Conditions" );
    fprintf( fd, "\n" );
    CentreText( fd, "~~~~~~~~~~~~~~~~~~~" );
    fprintf( fd, "\n\n" );
    fprintf( fd, "[Th]: %.3f  [230Th]: %.3g  [U]: %.3f  [Ba]: %.3f  "
            "[Ra]:%.3g\n", init->th_conc, init->th230_conc, init->u_conc,
            init->ba_conc, init->ra_conc );
    fprintf( fd, "N.B. Units for concentrations: ug g-1\n" );
    fprintf( fd, "(230/232)i: %.3f  (238/232): %.3f\n", init->th_iso_init,
            init->uth_iso );
    fprintf( fd, "(226)/[Ba]: %.4g  (230)/[Ba]: %.4g\n",
            init->raba_iso, init->thba_iso );
    fprintf( fd, "N.B. Activity/Concentration units: mol g-1 yr-1\n" );
    fprintf( fd, "(230): %g  (226): %g\n", init->th230_act, init->ra_act );
    fprintf( fd, "N.B. activities in units of: mol g-1 yr-1\n" );
    fprintf( fd, "Kd Th: %.3f  Kd U: %.3f  Kd Ba: %.3f  Kd Ra: %.3f\n",
            init->th_kd, init->u_kd, init->ba_kd, init->ra_kd );
    fprintf( fd, "Chamber Vol: %d km3  Input Volume: %d km3\n",
            init->cvol, init->ivol );
    fprintf( fd, "Crystallisation: %.0f%%  Input Period: %.1g years"
            "  TTR: %d years\n", init->f * 100, data->interval, init->ttr );
    fprintf( fd, "\n" );
    DoHashLine( fd );
    fprintf( fd2, "START: (38/32): %g (30/32): %g (30)/[Ba]: %g "
            "(26)/[Ba]: %g\n", data->uth_iso_chamb, data->th_iso_chamb,
            data->thba_iso_chamb * 1E15, data->raba_iso_chamb * 1E15 );
    break;

  case DO_INTEGRATE :
    fprintf( fd, "\n" );
    DoHashLine( fd );
    fprintf( fd, "\n" );
    sprintf( buf, "Integrated values after %d integrations", step_num );
    CentreText( fd, buf );
    fprintf( fd, "\n\n" );
    fprintf( fd, "[Th]: %.3f  [230Th]: %.3g  [U]: %.3f  [Ba]: %.3f  "
```

```
            "[Ra]:%.3g\n", data->th_conc_chamb, data->th230_conc_chamb,
            data->u_conc_chamb, data->ba_conc_chamb, data->ra_conc_chamb );
      fprintf( fd, "N.B. Units for concentrations: ug g-1\n" );
      fprintf( fd, "(230/232): %.3f  (238/232): %.3f\n", data->th_iso_chamb,
            data->uth_iso_chamb );
      fprintf( fd, "(226)/[Ba]: %.4g  (230)/[Ba]: %.4g\n",
            data->raba_iso_chamb * 1E15,
            data->thba_iso_chamb * 1E15 );
      fprintf( fd, "N.B. Activity/Concentration units: fmol g-1 yr-1\n" );
      fprintf( fd, "(230): %g  (226): %g\n",
            data->th230_act_chamb * 1E15,
            data->ra_act_chamb * 1E15 );
      fprintf( fd, "N.B. activities in units of: fmol g-1 yr-1\n" );

      if ( init->age_calc_flag ) {
       fprintf( fd, "Present (226)/[Ba]: %.4g\n",
              IsotopeEvolveCalc( data->raba_iso_chamb, data->thba_iso_chamb,
                                 LAMBDARA,
                                 ( init->ttr -
                                 ( step_num * init->integration_time ) ) +
                                 init->time_since_run ) * 1E15 );
      }

      fprintf( fd, "\n" );
      DoHashLine( fd );
      fprintf( fd, "\n" );
      fprintf( fd2, "INTEG: (38/32): %g (30/32): %g (30)/[Ba]: %g "
            "(26)/[Ba]: %g\n", data->uth_iso_chamb, data->th_iso_chamb,
            data->thba_iso_chamb * 1E15, data->raba_iso_chamb * 1E15 );
      break;

    default :
      printf( "\n\aError in WriteOutputFile()\n" );
      fclose( fd );
      exit( 1 );
      break;
  }

  fclose( fd );
  fclose( fd2 );
}


/*****************************************************************************
 *
 *  Function: FracCrystalCalc()
 *  Purpose: Performs Rayleigh fractional crystallisation calculations
 *  Arguments: double for the initial concentration
 *             double for the partition coefficient
 *             double for the crystallisation fraction
 *  Return: double for the new concentration
 *
 *****************************************************************************/

double FracCrystalCalc( double conc, double kd, double f )
{
  conc *= pow( ( 1 - f ), ( kd - 1 ) );
  return conc;
}


/*****************************************************************************
 *
 *  Function: IsotopeEvolveCalc()
 *  Purpose: Calculates shortlived isotope evolution according to the
 *           standard Bateman equation
 *  Arguments: double for the daughter activity
 *             double for the parent activity
 *             double for the decay constant
 *             double for the time
 *  Return: double for the new daughter activity
```

```
 *
 ****************************************************************************/

double IsotopeEvolveCalc(double daughter, double parent, double lambda,
                         double t)
{
  double e_lambda_t;

  e_lambda_t = exp( ( -1 * lambda * t ) );

  daughter = ( parent * ( 1 - e_lambda_t ) ) + ( daughter * e_lambda_t );
  return daughter;
}


/****************************************************************************
 *
 *  Function: DoHashLine()
 *  Purpose: Draws a line of hashes across the output file
 *  Arguments: pointer to the open output file
 *  Return: None
 *
 ****************************************************************************/

void DoHashLine( FILE *fd )
{
  int i;

  for ( i = 1; i <= 80; i++ )
    fprintf( fd, "#" );
}


/****************************************************************************
 *
 *  Function: CentreText()
 *  Purpose: Centres text in the output file (assumes 80 column page width)
 *  Arguments: pointer to the open file
 *             pointer to the text string
 *  Return: None
 *
 ****************************************************************************/

void CentreText( FILE *fd, char *text )
{
  int i;

  for ( i = 1; i <= ( 80 - strlen( text ) ) / 2 ; i++ )
    fprintf( fd, " " );

  fprintf( fd, text );
}
```

F-2.2 Code for radium.h

```
/****************************************************************************
 *
 *  File: radium.h
 *  Author: Rob Hughes
 *  Purpose: Provides includes/declarations/definitions for radium modelling
 *  Started: April 1998
 *
 ****************************************************************************/

/*
 * Include system header files
```

```
 */

#include <stdio.h>
#include <stdlib.h>
#include <unistd.h>
#include <ctype.h>
#include <math.h>

/*
 * Platform definition
 * If running on UNIX platforms, delete the comments on the second line and
 * comment out the definition for WIN
 */

#define WIN
/* #define UNIX */

/*
 * Symbolic constant definition
 */

#define BUFSIZE 80
#define LAMBDATH 9.1952E-6
#define LAMBDARA 4.272E-4
#define DO_EVOLVE 0
#define DO_MIX 1
#define DO_HEADER 2
#define DO_INTEGRATE 3
#define THCONST 185885
#define UTHCONST 3.034
#define ATMASSTH 230.03
#define ATMASSRA 226.025403

/*
 * Structures
 */

struct InitialData {
  double th_conc;
  double u_conc;
  double ra_conc;
  double ba_conc;
  double th_kd;
  double u_kd;
  double ra_kd;
  double ba_kd;
  double uth_iso;
  double th_iso_init;
  double raba_iso;
  double thba_iso;
  double ra_act;
  double th230_conc;
  double th230_act;
  double f;
  int cvol;
  int ivol;
  int freq;
  int ttr;
  int time_since_run;
  int integrations;
  int integrate_flag;
  int evolve_flag;
  int age_calc_flag;
  int mix_flag;
  double integration_time;
  char file_out[ BUFSIZE ];
  char file_out2[ BUFSIZE ];
};

struct ProgramData {
  double th_conc_chamb;
```

```
  double u_conc_chamb;
  double ra_conc_chamb;
  double ba_conc_chamb;
  double th_iso_chamb;
  double uth_iso_chamb;
  double raba_iso_chamb;
  double thba_iso_chamb;
  double th230_conc_chamb;
  double th230_act_chamb;
  double ra_act_chamb;
  double interval;
};

/*
 * Function Prototypes
 */

void EvolveAllValues( struct InitialData *init, struct ProgramData *data );
void ReadInputFile( struct InitialData *init );
void InitialCalcs( struct InitialData *init, struct ProgramData *data );
void WriteOutputFile( struct InitialData *init, struct ProgramData *data,
                      int flag, int step_num );
double FracCrystalCalc( double conc, double kd, double f );
double IsotopeEvolveCalc( double daughter, double parent, double lambda,
                          double t );
void MixingCalcs( struct InitialData *init, struct ProgramData *data );
void DoHashLine( FILE *fd );
void CentreText( FILE *fd, char *text );
```

F-2.3 Example of a radium.in file

The radium model uses an input file which contains the running conditions. An example of this file is given below.

```
[Th]: 1.0 [U]: 0.32959789 [Ra]: 0.000000150 [Ba]: 200
Kd-Th: 0.05 Kd-U: 0.05 Kd-Ra: 0.25 Kd-Ba: 0.25
U/Th_initial_activity: 1.0 Th_initial_activity: 0.75
Chamber_Vol: 30 Input_Vol: 5 Crystallisation_fraction: 0.2
Iteration_Frequency: 20 Time_to_Run: 100000 Integrations: 5
Integrate_Flag: 1 Mix_Flag: 1 Evolve_Flag: 0 Age_Calc_Flag: 0
Time_Since_Run: 0
radium.out
radium.stp

## N.B. Altering any of the spacing in the lines above, or removing any of
## the above lines will cause the program to fail with various errors...
##
## Description of fields:
##
## [xx] - concentration field for element xx. All concentrations are in ppm
##        (ug g-1). Note also that the program calculates its own initial
##        230Th concentration from the (230/232) and [Th] assuming all the
##        Th is 232Th.
##
## Kd-xx - partition coefficient for the specified element xx.
##
## Activity Ratios: Standard activity ratios. Note that the program will
##                  calculate (226)/[Ba] so that the units maintain
##                  internal consistency.
##
## Volumes: These are in km3
##
## Crystal Fraction: This is the percentage of the liquid which crystallizes
##                   in each evolution step. Essentially 1 - f from the
##                   Rayleigh crystallisation formula. Note that this is
##                   expressed as a fraction rather than as a percentage, so
##                   5% would be 0.05.
##
```

```
## Iteration Frequency: This is the number of new inputs in a given run.
##
## Time to Run: The time for the model to run for in years. The program
##              calculates the length of each step by dividing time to run by
##              the iteration frequency.
##
## Integrations: The number of integrations in between each new input. This
##               is required so that an approximation for the counter
##               behaviour of fractionation and decay can be achieved in
##               radium space.
##
## Flags: Each flag can be set on or off. To set a flag on, any value +ve
##        non-zero integer can be used. The evolve, mix and integrate flags
##        control whether details are printed after each evolve step,
##        mix step and integration respectively. The age calc flag, allows
##        the user to enter a time since the end of the run, essentially
##        allowing calculation of what the current values would look like.
##        This calculation is done on output, and so therefore values can
##        be generated for mix, evolve and integrate outputs.
##
## Time since run: This is the time used if the age calc flag is set. If the
##                 flag isn't set, this value is ignored by the program.
##
## Filename: This is the filename for the output file. Eventually I will get
##           around to adding a filename flag as well, so that you can choose
##           if you wish to be prompted for a filename during the program
##           run.
##
## Filename: This is the filename for the output file which contains the data
##           in a nice form to import into excel.
```

Appendix G

Conference Abstracts

Parts of this thesis have been presented at various conferences during the course of the study. The abstracts for these presentations given below.

Modelling of Uranium Series Disequilibria in Open-System Magma Chambers

R.D.Hughes, C.J.Hawkesworth and N.W.Rogers

Poster presented at the Annual Meeting of the Volcanic Studies Group, University of Cambridge, January 1997.

Some recent studies of U-Th isotopes in young volcanic rocks have yielded surprisingly old ages which may result from frequent mixing events in crustal magma chambers. Short lived isotopes have been modelled in well mixed, open-system magma chambers, with periodic injections and withdrawal of magma and a constant reservoir volume through time. Iterative calculations of the effects new magma injections allow insights into magmatic residence times in crustal reservoirs and show ages based on simple whole-rock isochrons suggests that apparent U-Th age can be significantly greater than the actual magmatic residence time. Constraining residence times makes it possible to obtain better data on rates of magma generation and transport.

Eruption rates are not required to be constant in order for a near-constant Th isotopic composition to persist. A change in the eruption rate is assumed to result from a perturbation in conditions in the magma chamber, which will alter or eradicate the steady-state isotopic composition. By varying the volume of new injections and their periodicity, the model can simulate a wide range of magmatic systems and also has potential application in systems that are not steady-state.

U-Series Disequilibrium Constraints on Magmatic Processes at an Andesitic Arc Volcano: Mt. Ruapehu, New Zealand

Rob Hughes, C. Hawkesworth and N. Rogers

Talk given at the Annual Meeting of the Volcanic and Magmatic Studies Group, University of Leicester, January 1998.

The application of short-lived isotope systematics to understanding rates of magmatic processes are investigated for a composite andesite volcano, Mt. Ruapehu, New Zealand. The edifice is at least 300,000 years old and represents four identifiable cone building episodes. The last major eruptive event was approximately 10-14 ka, with subsequent minor phreatic and phreatomagmatic activity.

Historical lavas from four eruptions this century (1945, 1971, 1995 and 1996 A.D.) and older samples belonging to coherent sequences from the Whangaehu and Ohinepango valleys (eastern Ruapehu), have been studied. All the analysed lavas show U excesses of 2-15%, consistent with other arc volcanics and usually ascribed to mobilisation of U in slab-derived fluids.

The data from the three main sequences analysed fall on well constrained linear trends. The array for the historical eruptions has the same range of ($^{238}U/^{232}Th$) values, but lower ($^{230}Th/^{232}Th$) ratios than the older lavas. If treated as isochrons, ages of 64±8 ka, 162±6 ka and 147±17 ka are obtained for the historical lavas, the Ohinepango and Whangaehu sequences respectively. Assuming fractionation of U from Th occurred during melt generation, the isochron age for the eruptions this century represents a total transport and residence time. Eruption ages of ~80-100 ka are obtained for the older sequences if this time is assumed to be invariant.

Data for the more primitive oceanic arcs (e.g. Tonga, Marianas) show arrays that suggest a total transport time of 30,000 years. This is consistent with the proposed 50-60 ka for magmas which have required a longer crustal residence time to evolve to the observed compositions.

Crystallisation and late-stage fluid alteration as mechanisms for U-Th fractionation have been ruled out for these data. Small degrees of assimilation are considered important in generating conventional isotope signatures observed in Ruapehu lavas and cannot be overlooked as a source of the U/Th and Th isotopic variation. Independent age constraints are required to determine the importance of the identified trends, and further disequilibrium data from mineral separates will help resolve the 55 ka ages into transport and crustal residence time components.

U-Series Disequilibrium Constraints on Magmatic Processes at an Andesitic Arc Volcano: Mt. Ruapehu, New Zealand

Rob Hughes, Chris Hawkesworth and Nick Rogers

Poster presented at Rates and Timescales of Magmatic Processes at Burlington House, November 1997.

How fast subduction related magmas can be formed and what happens during their pre-eruptive history is critical to an overall understanding of destructive plate margin magmatism. The application of short-lived isotope systematics to understanding rates of magmatic processes are investigated for a composite andesitic volcano, Mt. Ruapehu, New Zealand. The edifice is at least 300,000 years old and represents four identifiable cone building episodes. The last major eruptive event was approximately 10-14 ka, with subsequent minor phreatic and phreatomagmatic activity continuing into modern times.

Historical lavas from four eruptions this century (1945, 1971, 1995 and 1996) and older samples belonging to coherent sequences from the Whangaehu and Ohinepango valleys (eastern Ruapehu), have been studied. Ruapehu shows a very restricted range in compositions (53-63% SiO_2) and is dominated by calc-alkaline andesites with very minor basaltic andesites and dacites. All the analysed lavas show uranium excesses of 2-15%, consistent with other arc volcanics and usually ascribed to mobilisation of uranium in slab-derived fluids.

The data from the three main sequences analysed fall on well constrained linear trends. The array for the historical eruptions has the same range of ($^{238}U/^{232}Th$) values, but lower ($^{230}Th/^{232}Th$) ratios than the older lavas. If treated as isochrons, ages of 64±8 ka, 162±6 ka and 147±17 ka are obtained for the historical lavas, the Ohinepango and Whangaehu sequences respectively. Assuming fractionation of uranium from thorium occurred during melt generation, the isochron age for the eruptions this century represents a total transport plus residence time. Eruption ages of ~80-100 ka are obtained for the older sequences if this time is assumed to be invariant. Samples from two young satellite vents have ages calculated from the historical eruption data array that are in agreement with tephrachronological dates and glacial evidence.

Data for the more primitive oceanic arcs (e.g. Tonga, Marianas) show arrays that suggest a total transport time of 30,000 years. This is consistent with the proposed 50-60 ka for magmas which have required a longer crustal residence time to evolve to the observed compositions.

Data for the more primitive oceanic arcs (e.g. Tonga, Marianas) show arrays that suggest a total transport time of 30,000 years. This is consistent with the proposed 50-60 ka for magmas which have required a longer crustal residence time to evolve to the observed compositions.

Crystallisation and late-stage fluid alteration as mechanisms for U-Th fractionation have been ruled out for these data. Small degrees of assimilation are considered important in generating conventional isotope signatures observed in Ruapehu lavas and cannot be overlooked as a source of the U/Th and Th isotopic variation. Independent age constraints are required to determine the importance of the identified trends, and further disequilibrium data from mineral separates will help resolve the 55 ka ages into transport and crustal residence time components.

The Application of U-series Systematics in Understanding the Rates and Timescales of Magmatic Processes at a Composite Andesite Volcano, Mount Ruapehu, New Zealand.

R.D. Hughes, C.J. Hawkesworth, N.W. Rogers.

Talk given at the Annual V.M. Goldschmidt Conference, Toulouse, France, September 1998.

The application of U-Th disequilibria in investigating the timescales of recent magmatic processes is well established. Processes which fractionate U and Th and hence disturb secular equilibrium are detectable for ~350 ka. Whilst there appears to be an increased understanding of the behaviour of these isotopes in young arc rocks from ocean-ocean collision zones (e.g. Elliott et al., 1997; Turner et al., 1997), early work on continental arcs has demonstrated that the additional complexity of magma ascent through and residence in continental crust can make interpretation of U-Th data difficult (e.g. Volpe, 1992). This work is a detailed, high-precision study of a single volcano over at least 100 ka, looking at how U-Th data can aid investigation of magma fluxes and crustal residence times over a significant time span.

Mount Ruapehu is a composite andesite cone, with a history of volcanism for at least 250-300 ka. It forms the most southerly and largest volcanic edifice in the Taupo Volcanic Zone (TVZ), a zone of extension, high heat flow and volcanism related to the westward subduction of the Pacific Plate beneath the Indian Plate along the Hikurangi Margin. The volcano lies ~175 km behind the Hikurangi Trough, and 100 km above the subducting slab. The present day surface geology is dominated by sector collapse structures and glacier-related erosion, which has exposed a number of excellent vertical sequences on which this study concentrates.

Compositionally, Ruapehu has been remarkably consistent throughout its known eruption history. Lavas range from 53-63 wt.% SiO_2, but analysed material from this study and others (Graham and Hackett, 1987) is largely dominated by andesitic compositions (55-60 wt% SiO_2). U-Th isotope data has been obtained for samples from four eruptions this century (1945, 1971, 1995 and 1996), older samples belonging to coherent sequences from the Whangaehu and Ohinepango valleys (Tukino, eastern Ruapehu), and from three parasitic cones.

All of the lavas analysed show uranium excesses of 3-12%, and have relatively constant U/Th ratios of 0.26-0.3. The data for each set of contemporaneous samples plot along well constrained linear arrays (Fig. 1), with each array having a similar range in ($^{238}U/^{232}Th$), but different ($^{230}Th/^{232}Th$). The arrays are progressively closer to the equiline with increasing eruption age from a rough stratigraphy based on field evidence. Three explanations can be proposed to explain these arrays, (i) mixing with an assimilant or magma, (ii) crystallisation induced fractionation of U and Th, and/or (iii) source related variations.

Significant fractionation of U and Th during crystallisation is most likely to reflect crystallisation of an accessory phase such as apatite or zircon. There is no geochemical or petrographic evidence for such a phase, and no correlation exists between U/Th ratio and indexes of fractionation such as Mg number or Zr. Both P_2O_5 and Zr behave incompatibly throughout the full range of erupted compositions.

Traditional petrogenetic models for Ruapehu require that assimilation has played an important role in generating some of the observed geochemical signatures (Graham et al.,

1992). Mixing may also have taken place between rhyolitic magmas which dominate the central TVZ and more primitive basaltic or basaltic andesite compositions. ON the ($^{230}Th/^{232}Th$)-($^{238}U/^{232}Th$) diagram, both crustal and rhyolitic components plot on the equiline near the extrapolation of the data arrays from this study. Trace element data suggests however, that mixing between primitive Ruapehu compositions and rhyolites from Taupo (the nearest rhyolite centre) would not produce the trends observed (Fig. 2). Radiogenic isotopes have commonly been used to identify assimilation trends between basaltic melts and local Torlesse basement. However, U/Th ratio does not vary in any coherent fashion with either Sr or Nd isotopes and so at present there is no evidence that crustal contamination has significantly affected U-Th isotopes.

The lack of correlation between assimilation tracers and U-Th systematics implies that the observed variations are related to source processes. Treating the linear arrays as pseudo-isochrons yields ages of 64±8 ka, 147±17 ka and 162±6 ka for the recent eruptions, lower Whangaehu and Ohinepango sequences respectively. By using the age from the array of data for this century as an average total transport and residence time, approximate eruption ages for the older sequences can be calculated. This yields approximate eruption ages of 85 ka and 98 ka for the Whangaehu and Ohinepango sections. If estimated wedge transport times of ~30-50 ka from intra-oceanic arcs (Elliott et al., 1997; Turner et al., 1997) are assumed to be relatively constant regardless of tectonic setting, crustal residence times of 15-35 ka are implied from the total transport and residence time.

And finally for my examiners in particular...,

Si non confectvs, non reficiat

and perhaps the following,

Non svmet nvllvs pro respondo

The mottoes of the Vetinari and Ramkin Families.

from 'The concife and possibly even accuratte Mapp' and 'Discworld Companion' – Terry Pratchett & Stephen Briggs.